# THE INTERNATIONAL HYDROCOIN PROJECT

## GROUNDWATER HYDROLOGY MODELLING STRATEGIES FOR PERFORMANCE ASSESSMENT OF NUCLEAR WASTE DISPOSAL

## SUMMARY REPORT

The Coordinating Group of the HYDROCOIN Project
Swedish Nuclear Power Inspectorate (SKI)

NUCLEAR ENERGY AGENCY
ORGANISATION FOR ECONOMIC CO-OPERATION AND DEVELOPMENT

# ORGANISATION FOR ECONOMIC CO-OPERATION AND DEVELOPMENT

Pursuant to Article 1 of the Convention signed in Paris on 14th December 1960, and which came into force on 30th September 1961, the Organisation for Economic Co-operation and Development (OECD) shall promote policies designed:

- to achieve the highest sustainable economic growth and employment and a rising standard of living in Member countries, while maintaining financial stability, and thus to contribute to the development of the world economy;
- to contribute to sound economic expansion in Member as well as non-member countries in the process of economic development; and
- to contribute to the expansion of world trade on a multilateral, non-discriminatory basis in accordance with international obligations.

The original Member countries of the OECD are Austria, Belgium,Canada, Denmark, France, Germany, Greece, Iceland, Ireland, Italy, Luxembourg, the Netherlands, Norway, Portugal, Spain, Sweden, Switzerland, Turkey, the United Kingdom and the United States. The following countries became Members subsequently through accession at the dates indicated hereafter: Japan (28th April 1964), Finland (28th January 1969), Australia (7th June 1971) and New Zealand (29th May 1973). The Commission of the European Communities takes part in the work of the OECD (Article 13 of the OECD Convention). Yugoslavia has a special status at OECD (agreement of 28th October 1961).

## *NUCLEAR ENERGY AGENCY*

*The OECD Nuclear Energy Agency (NEA) was established on 1st February 1958 under the name of the OEEC European Nuclear Energy Agency. It received its present designation on 20th April 1972, when Japan became its first non-European full Member. NEA membership today consists of all European Member countries of OECD as well as Australia, Canada, Japan and the United States. The Commission of the European Communities takes part in the work of the Agency.*

*The primary objective of NEA is to promote co-operation among the governments of its participating countries in furthering the development of nuclear power as a safe, environmentally acceptable and economic energy source.*

*This is achieved by:*

- *encouraging harmonization of national regulatory policies and practices, with particular reference to the safety of nuclear installations, protection of man against ionising radiation and preservation of the environment, radioactive waste management, and nuclear third party liability and insurance;*
- *assessing the contribution of nuclear power to the overall energy supply by keeping under review the technical and economic aspects of nuclear power growth and forecasting demand and supply for the different phases of the nuclear fuel cycle;*
- *developing exchanges of scientific and technical information particularly through participation in common services;*
- *setting up international research and development programmes and joint undertakings.*

*In these and related tasks, NEA works in close collaboration with the International Atomic Energy Agency in Vienna, with which it has concluded a Co-operation Agreement, as well as with other international organisations in the nuclear field.*

# Abstract

In 1984 the Swedish Nuclear Power Inspectorate, SKI, initiated the international cooperation project HYDROCOIN for the study of groundwater flow modelling in the context of radioactive waste disposal. Thirteen organisations from ten countries and two international organisations participated in the project which was managed by the SKI.

The three levels of the project have been reported in separate publications by SKI-OECD/NEA. This report gives an overview and summary of the three reports.

The objective of HYDROCOIN as formulated in the Agreement between the parties was to improve knowledge of the influence of various strategies for groundwater flow modelling for the safety assessment of final repositories for nuclear waste. The study comprised:

— the impact on the groundwater flow calculations of different solution algorithms,
— the capabilities of different models to describe field and laboratory experiments, and
— the impact on the groundwater flow calculations of incorporating various physical phenomena.

The work was conducted at three levels addressing code verification (Level 1), model validation (Level 2), and sensitivity and uncertainty analysis of groundwater flow calculations (Level 3).

The Swedish Nuclear Power Inspectorate, SKI, acted as Managing Participant. Each Party organised one or several Project Teams that were responsible for performing calculations and evaluations associated with the test cases approved by the Coordinating Group.

The test cases of HYDROCOIN Level 1 were primarily designed for testing codes. All the seven test cases presumed that the conceptual porous medium model was valid. In the test cases giving rise to linear equations, the primary field entities calculated by the Project Teams were in good agreement and agreed with analytical solutions, where those were known. Velocity fields and trajectories showed reasonable agreement. The results illustrated the importance of post-processing procedures. It was concluded that HYDROCOIN Level 1 met its objectives to test the numerical accuracy of the codes. Results indicated that appropriate numerical methods are available to solve linear or mildly non-linear problems.

HYDROCOIN Level 2 addressed the issue of validation of groundwater flow models. Five test cases were selected based on data sets that to some degree met the requirement of the availability of independent data sets. They covered a number of processes relevant for the analysis of radioactive waste disposal in different media.

From the analyses performed it was concluded that the intended use of a particular model strongly affects the validation process and especially determines the level of detail required in the model, the performance measure that should be correctly predicted by the model, and the criteria for the goodness-of-fit function or qualitative judgement used to assess, whether the appropriate level of confidence or validation has been achieved.

The analyses gave substantial experience in the application of the framework for validation. It was demonstrated that experiments for model validation purposes need to be designed and

conducted over a range of conditions that, when possible, brackets the expected conditions for which the model will be applied. Experiments performed at a series of spatial and temporal scales are needed in order to demonstrate that there is an adequate understanding of scaling and averaging processes. Selection of an appropriate performance measure is an important part of model validation. Statistical methods and inverse modelling techniques proved beneficial in the model calibration as well as in the model validation process.

The validation process was identified to be iterative. In many of the analyses a need for further experiments to determine parameters or to investigate the cause of certain features of the data sets was identified. The participants felt that HYDROCOIN Level 2 had contributed to an increased confidence in the applicability of groundwater flow models to situations relevant for radioactive waste disposal. They concluded that model validation is an interdisciplinary exercise and that the process requires substantial interaction between experimentalists and modellers.

As an introduction to HYDROCOIN Level 3 an overview was given on the methodologies used in uncertainty and sensitivity analysis. Seven test cases were selected to illustrate the importance of sensitivity and uncertainty analyses in groundwater flow modelling representing four different media. It was concluded that several performance measures should be used in order to fully explain the system, as different techniques applied for the analyses can lead to different conclusions. The need for automated procedures for sensitivity and uncertainty analyses of non-linear problems to check the quality of numerical solutions for all sets of parameters was stressed. Parameter estimation results must be carefully examined for instability and insensitivity problems. Different performance measures such as pathlines with their associated path lengths and travel times and point values of the flow rates give different possibilities to judge the sensitivity of a system.

The analyses of the cases clearly demonstrated the importance of having a good understanding of the effects of uncertainties and sensitivities in the performance assessment of a nuclear waste repository. It was concluded that the choice of conceptual model can have a great influence on the outcome of an assessment.

A particular test case of HYDROCOIN Level 3 was devoted to the difficulties of calculating flow paths. This case evoked particularly great interest from the participants. The general consensus was that particle tracking at present is much of an art which is still developing. In order to model accurately a pathline that passes over a stagnation point on a flow divide or has high curvature, or crosses an interface between media of very different permabilities, it is necessary to take considerable care in numerical modelling and use a sufficiently fine discretisation. Examination of particle trajectories is, however, a necessary part in getting a good understanding of the hydrogeology of a nuclear waste repository.

Although HYDROCOIN Level 3 was restricted to geohydrology, the methods used in the study may have a more general application in other fields.

# Preface

HYDROCOIN was initiated in May 1984 by the Swedish Nuclear Power Inspectorate, SKI, as an international cooperation project for studying groundwater hydrology modelling strategies. The work was performed in three stages. The report from the first stage, Level 1, was published in 1988, the second stage, Level 2, was reported in 1990 and the third stage, Level 3, in 1991.

In response to a demand from the participants in the study the present Summary Report has been prepared. It contains principal points of interest from all three main reports as well as a summary of their contents. The Summary Report does not include any references, nor does it contain any mathematics. The reader must therefore consult the main reports to get references and also to obtain details on specific items, as the present report of necessity is a subjective compilation of facts from the main reports.

The following organisations participated in the study:

| | |
|---|---|
| Atomic Energy of Canada Ltd | CANADA |
| British Geological Survey | UNITED KINGDOM |
| Commissariat à l'Energie Atomique/ Institut de Protection et de Sûreté Nucléaire | FRANCE |
| Gesellschaft für Strahlen- und Umweltforschung | FEDERAL REPUBLIC OF GERMANY |
| Japan Atomic Energy Research Institute | JAPAN |
| Nationale Genossenschaft für die Lagerung radioaktiver Abfälle | SWIZERLAND |
| Nordic Liaison Committee for Atomic Energy | NKA |
| Organisation for Economic Cooperation and Development/Nuclear Energy Agency | OECD/NEA |
| Rijksinstituut voor Volksgezondheid en Milieuhygiëne | NETHERLANDS |
| Swedish Nuclear Fuel and Waste Management Co. | SWEDEN |
| Swedish Nuclear Power Inspectorate (Managing Participant) | SWEDEN |
| Technical Research Centre of Finland | FINLAND |
| U.K. Atomic Energy Authority/Harwell Laboratory | UNITED KINGDOM |
| U.S. Department of Energy | USA |
| U.S. Nuclear Regulatory Commission | USA |

This report was prepared by the Project Secretariat and is being published after approval by the Coordinating Group. Neither the Coordinating Group nor the Project Secretariat take any legal responsibility for results presented in this report or for their use.

# Table of Contents

# HYDROCOIN
# A Summary Report

## 1. Introduction

### 1.1 Background

All countries in the world in which there are operating nuclear reactors are today confronted with the problem of finding solutions for final disposal of the radioactive wastes that are produced from their nuclear power generation. Of special concern is the disposal of high-level waste arising from the reprocessing of spent nuclear fuel, as well as the disposal of spent fuel itself, if regarded as waste.

Several concepts have been considered for the disposal of high-level wastes. Today, the main effort is directed towards finding sites for disposal in deep geological formations, as this method has the potential for creating safe repositories which will effectively isolate the waste for very long time periods.

For site selection purposes, as well as for the evaluation of the safety of a chosen site, it is essential that adequate data are acquired on the geological and other properties of the host medium. Appropriate conceptual, physical, and mathematical models have to be developed as components of the safety evaluation of the disposal system.

Assessment of the groundwater flow through a repository and the host rock to the accessible environment forms an important part of the safety analysis of a disposal system. Normally, mathematical models and corresponding computer codes have to be employed to describe the flow mechanisms involved. Such models and codes are being developed by many organisations in different countries.

As a result of discussions among specialists involved in hydrologic flow modelling, an international project, HYDROCOIN (*Hydro*logic *Co*de *In*tercomparison Study), was initiated in 1984 by the Swedish Nuclear Power Inspectorate, SKI. The overall objective was to improve the understanding of the effect of groundwater flow modelling strategies on the safety analysis of nuclear waste repositories. Participating organisations included implementing organisations as well as governmental safety authorities.

The first workshop and Coordinating Group meeting took place in Stockholm, Sweden in October 1984. During the period 1984 to 1987 seven meetings were held, the last in Paris, France in November 1987.

Interest in the HYDROCOIN project grew over time and the project finally comprised 13 Parties and 25 Project Teams, in addition to the OECD/NEA and the Nordic Liaison Committee for Atomic Energy Matters which took part in the Secretariat.

## 1.2. Hydrology as Part of Performance Assessment of Nuclear Waste Repositories

Performance assessment is a procedure that is used in evaluation of the safety of a repository for radioactive waste. In order to use this tool in an accurate manner, it is essential to have a good knowledge of the properties of the environment, i.e., the rock in which the packages of radioactive waste are to be emplaced, the hydrology, and the long and short term processes affecting the waste packages and the rock. Furthermore, it is necessary to understand the natural long term processes which change the surface and the conditions in the vicinity of the repository. Some of these processes are of a stochastic nature, while others are bound to happen, though it might be difficult or impossible to determine exactly when.

In principle, the processes directly affecting the waste packages and the surrounding rock can be recognised and evaluated. In practice, however, many difficulties arise. The processes are often complex and the spatial and temporal scales are not easy to incorporate in a correct manner. In a real case, simplifying assumptions have to be made and it is important to estimate any errors introduced as a consequence of these simplifications.

Water movement plays a critical role in the evaluation of the safety of a waste repository. In typical cases, temperatures in repositories will stay well below those causing evaporation of radioactive substances, excluding tritium and gaseous fission products. Thus, water flowing from the repository to the surface waters is the principal vehicle available for carrying radioactivity from the repository to the biosphere.

The interest in acquiring knowledge about water movements in low permeability rock and partially saturated rock is fairly new and mainly related to the assessment of repositories for radioactive waste. The technique employed for estimation of the water movements at a repository site is basically the same as is being used in other hydrological fields. For practical applications in the waste disposal field, however, the technique has been subject to considerable refinement.

In 1980 the Swedish Nuclear Power Inspectorate (SKI) initiated an international project, INTRACOIN (*I*nternational *N*uclide *Tra*nsport *Co*de *In*tercomparison Study). For the study, comparisons were made between different computational codes describing transport of radionuclides in geologic media. The study started in 1981 and was finalised in 1984. At an early stage of the INTRACOIN project, SKI explored the interest among the participants to take part in a complementary study on an intercomparison of hydrological codes applied in modelling water movements at a waste repository. As there turned out to be a substantial interest in such a project, SKI sent out an invitation for participation in the HYDROCOIN study in January 1984 as a follow up to INTRACOIN.

# 2. The HYDROCOIN Agreement and Organisation

## 2.1 Agreement

The Agreement for participation in the HYDROCOIN project was signed by the participating organisations during the first half of 1984. The objectives, as formulated in the Agreement, were to obtain improved knowledge of the influence of various strategies for groundwater flow modelling for the safety assessment of final repositories for nuclear waste. To this end calculations were to be made by applying different mathematical models used by the participating organisations. The project would comprise:

- study of the impact on the ground water flow calculations of different solution algorithms
- study of the capabilities of different models to describe field measurements
- study of the impact on the groundwater flow calculations of incorporating various physical phenomena

## 2.2 Organisation

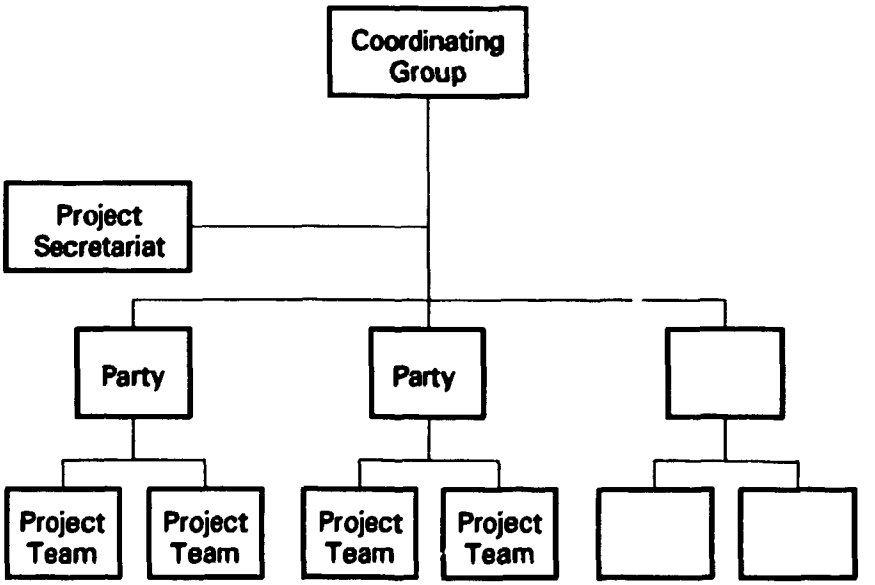


Figure 2.1. Organisational chart for HYDROCOIN.

The organisation of the project was basically the same as for the preceding INTRACOIN study.The project was directed by a Coordinating Group consisting of one representative from each participating organisation (Party). The Swedish Nuclear Power Inspectorate (SKI) acted as Managing Participant. Each Party organised one or several Project Teams that were responsible for performing calculations related to defined test cases approved by the Coordinating Group.

A Project Secretariat was set up by SKI in cooperation with the U.K. Atomic Energy Authority/Harwell, the OECD/Nuclear Energy Agency and the Nordic Liaison Group for Atomic Energy. KEMAKTA Consultants Co., Sweden, served as Principal Investigator for HYDROCOIN and had the main responsibility for the technical work within the Project Secretariat. KEMAKTA furthermore compiled the results from the Project Teams and gave general support to SKI.

Each Party covered the costs for its participation and provided the funding for its Project Team or Teams. The administrative costs associated with the Project Secretariat and the costs for the Principal Investigator were covered by SKI.

A list of the participants and the Coordinating Group members is given in Appendix 1.

The organisation of workshops formed an essential part of the project. The workshops provided the participants with excellent opportunities to discuss their results and to exchange ideas in an informal manner. A total of seven Progress Reports were issued during the study.

# 3. Project Outline

Three levels of realisation were proposed for the the HYDROCOIN study treating different parts of the subject. The intent was to have the different levels of the study following each other in time but not necessarily so that a previous level would serve as an input to the next. A period of three years was foreseen for the main part of the project, the time needed for publication of the final reports not being included.

The primary objective of *Level 1* was to check the numerical accuracy of the codes, by intercomparison or by comparison with analytical solutions. Secondary objectives were the development of discretisation strategies and the exchange of ideas on pre- and post-processing techniques. The objective of *Level 2* was to deal with validation of models using field or laboratory experiments. *Level 3* concerned sensitivity and uncertainty analyses.

Different cases, generic or based upon laboratory and field experiments, were defined for the three levels. Sometimes a single experiment could serve as input to more than one level. The initial definitions of the cases were usually made by "pilot groups" and then commented upon by the Project Teams. After decisions by the Coordinating Group, the Secretariat sent descriptions covering the final definitions of the test cases with supporting documentation to the Project Teams as basic material for their calculations.

Preliminary results were presented at workshops. Often the presentations gave rise to discussions among the participants following which revised calculations were made by the Project Teams, sometimes involving revision of the codes being used in the modelling exercises.

Final results from the calculations of the Project Teams were sent to the Secretariat, ordinarily in form of magnetic tapes with accompanying notes and Project Team reports. The results are contained in three reports covering the three levels of the study. The main content of the three reports is condensed in this Summary Report.

# 4. HYDROCOIN Level 1

## 4.1 General

The primary objective of Level 1 was to verify the numerical accuracy of groundwater flow codes. The numerical accuracy of the codes would be determined by comparing the computational results with analytical solutions, if available, and by intercomparing results from the application of different codes. A secondary objective was the exchange of experience from the use of methods for cost-effective and accurate computer code calculations and techniques for the further processing and presentation of the results. A total of seven cases were designed to yield sensitive tests of the codes. They can briefly be described as follows:

*Case 1:* *Comparison of numerical solutions with an analytical solution to a problem involving transient flow from a borehole in a permeable medium containing a single fracture.*

*Case 2:* *Simulation of steady-state flow in a rock mass intersected by permeable fracture zones.*

*Case 3:* *Simulation of partially saturated flow through a sequence of alternating high and low permeability sedimentary rocks.*

*Case 4:* *Comparison of analytical and numerical solutions of thermal convection where the heat is evolved from a spherical source with a decaying heat output.*

*Case 5:* *Simulation of water flow and salt transport in a two-dimensional domain in which the fluid density depends on the salt concentration.*

*Case 6:* *Simulation of steady-state flow in a three-dimensional domain representing a generic bedded-salt geological setting.*

*Case 7:* *Simulation of steady-state flow through a shallow land-burial site in argillaceous media.*

Over twenty groups from eleven countries participated in the calculations. Most of the results were discussed at workshops before they were submitted to the Secretariat for processing and publication.

## 4.2 Case 1. Transient Flow from a Borehole in a Fractured Permeable Medium

Case 1 concerned the transient flow of water from a vertical borehole which was assumed to penetrate a saturated permeable layer of rock underlain by a horizontal fracture and confined between impermeable horizontal boundaries (Figure 4.1).

Analytical solutions to many related cases have been published in the literature. However, none of these appeared to be entirely satisfactory from the point of view of model verification. One reason for this is that the analytical solutions almost always assume that the borehole is a line

source, i.e. it has a zero radius. This assumption creates a number of problems for the numerical codes in a modelling attempt.

The case 1 problem was formulated with the indicated difficulties in mind. It involved transient flow from a finite-radius borehole in a finite cylindrical region of permeable rock with a single fissure. Also, the hydraulic head in the borehole was assumed to change continuously from its initial to its final value. A prescribed time dependent head relative to a fixed hydraulic head at a defined radial distance was maintained in the borehole. The pressure field induced in the matrix and fracture could in principle be monitored using piezometers.

It was assumed that the flow in the rock matrix as well as in the fracture could be described by Darcy's law. The matrix was taken to be homogeneous and isotropic and characterised by a hydraulic conductivity and a specific storage. It was further assumed that no vertical hydraulic gradient existed in the fracture.

The required outputs were the hydraulic head relative to the steady-state hydraulic head in the borehole as a function of time and space. The analytical solutions were submitted to the participants for comparison with their model results. As time dependent flow rates into the rock matrix and fracture could provide a more stringent test for some of the numerical models, the analytical solution for these quantities were also calculated and circulated to the participants. Additionally, the analytical solution for a fracture having a transmissivity ten times larger than the standard case was evaluated (Figure 4.2) to provide further checks on the algorithms.

*Results from Case 1*

The results of the calculations were provided: hydraulic head as a function of time, hydraulic head as a function of radial distance, flow rates into the matrix, and flow rates into the fracture. In addition to calculations for the base case, some Project Teams performed calculations for an optional case with increased fracture transmissivity.

The results were presented in common plot frames together with the relevant analytical solution, indicated as a narrow cross-hatched area spanning $\pm 2\%$ around the analytical solution.

For the base case Figures 4.3 and 4.4 show the relative head (i.e. hydraulic head divided by the head applied in the injection well) as a function of time at a point in the middle of the aquifer matrix and at a point in the fracture. In the matrix the pressure rise starts to be visible after about 100 s. Steady-state conditions are reached after about 4000 s. The corresponding transient in the fracture occurs during the first 2500 s. The figures show a high degree of congruence between the fourteen superimposed curves as well as with the analytical solution. Only for one calculation of the transient simulation in the fracture the transient appears to arrive too early by a factor of about 0.6. Also for an optional case with the fracture transmissivity increased by a factor of ten, the results were within $\pm 2\%$ of the analytical solution, except for the first part of the curve.

Figure 4.5 shows results for the relative hydraulic head at a radial distance of 4 m. Also here the results agree well with the analytical solution. Only one Project Team obtained results 30% higher than the analytical solution, a result in conformity with the previously mentioned early arrival of the pressure transient.

Six teams made calculations of the flow rate from the injection well into the aquifer matrix and the fracture as a function of time. The results for times after 1 s (Figure 4.6) seem to be in fair agreement with the analytical solution with only one team getting results falling slightly outside the ±2% band.

The spread of the calculated results for the relative flow rates into the fracture (Figure 4.7) was less pronounced than the spread of the relative flow rates into the matrix.

The results from Case 1 generally showed good agreement, i.e. falling within ±2% of the given analytical solution, both for the hydraulic head and flow rates from the well into the aquifer and the fracture. A team using 1-D elements to simulate the fracture reported results that agreed well with the results from the teams employing 2-D elements.

No obvious difference was observed comparing the results from calculations with finite-element codes and finite-difference codes. A possible explanation could be that the domain, being axis parallel, caused no problem in the discretisation with any of the two types of codes.

Evaluation of fluxes into the matrix and the fracture apparently requires a much finer discretisation than is needed for the calculation of the pressure distribution. One team showed that only 95% of the steady-state flux could be reached, despite the fact that they employed a mesh size of the order of a few centimetres close to the well.

The general conclusion that could be drawn from the calculations for test case 1 was that the results were fairly similar, probably because the analytical solutions provided a means for tuning the calculations. Furthermore, the case proved to be easier than was initially anticipated.

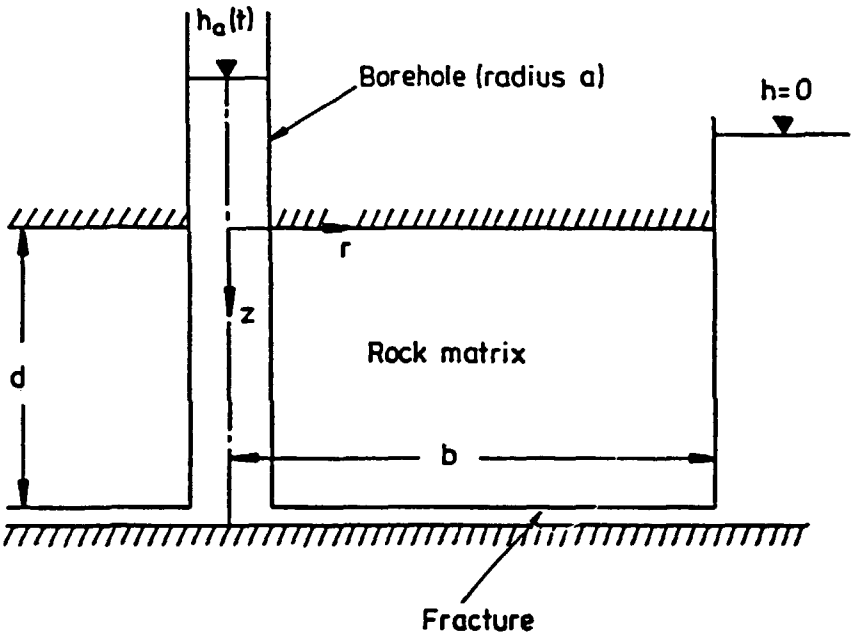


*Figure 4.1. Schematic diagram of the test problem Case 1.*

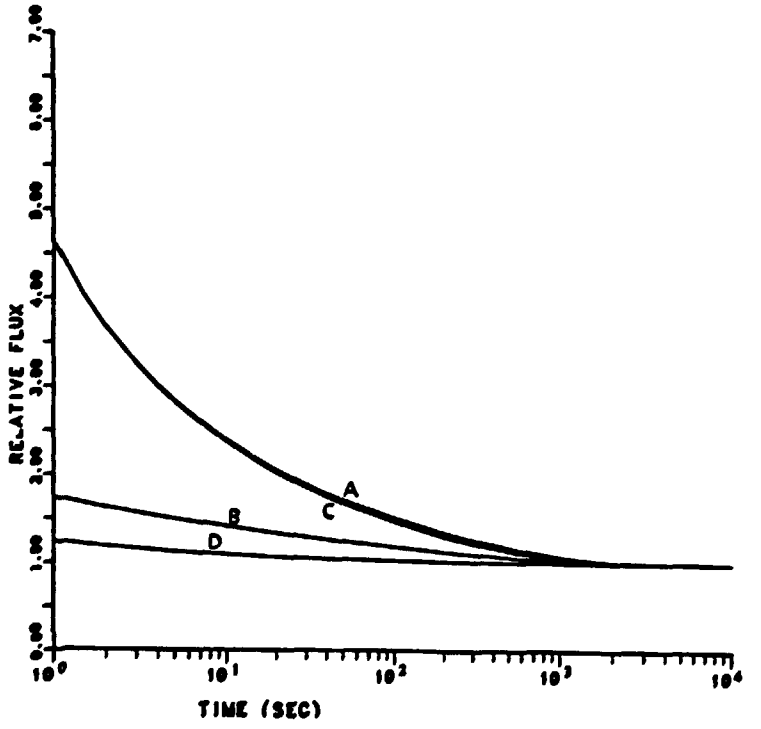


*Figure 4.2. Analytical solutions for the relative flow rates as a function of time. Curves A and C represent flow rates into the matrix and curves B and D represent the flow rates into the fracture zone. Curves C and D correspond to the case with increased transmissivity in the fracture zone.*

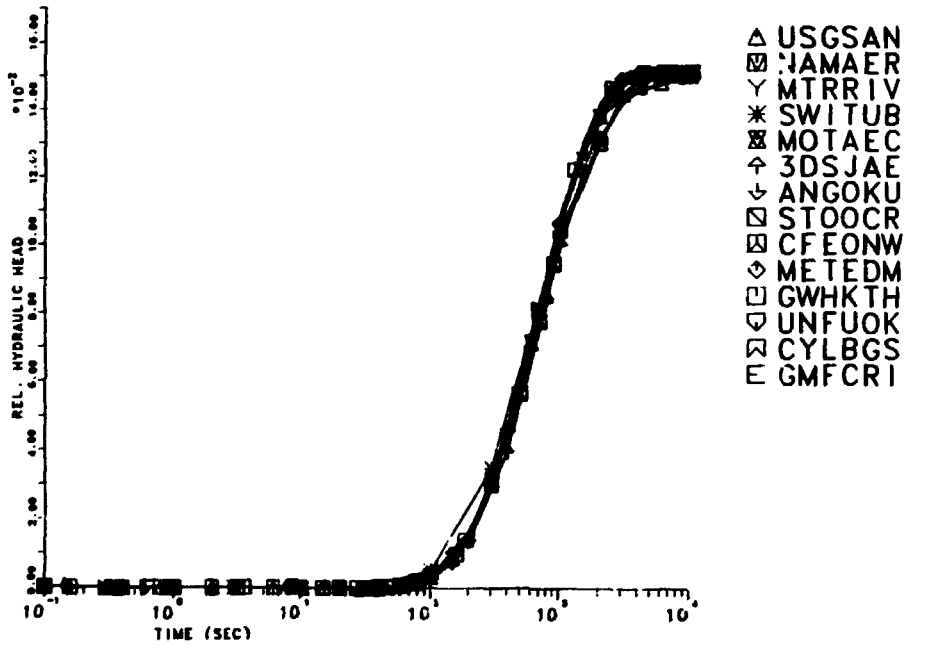


*Figure 4.3. Calculated relative hydraulic head as a function of time at r =5.0 m and z =2.5 m.*

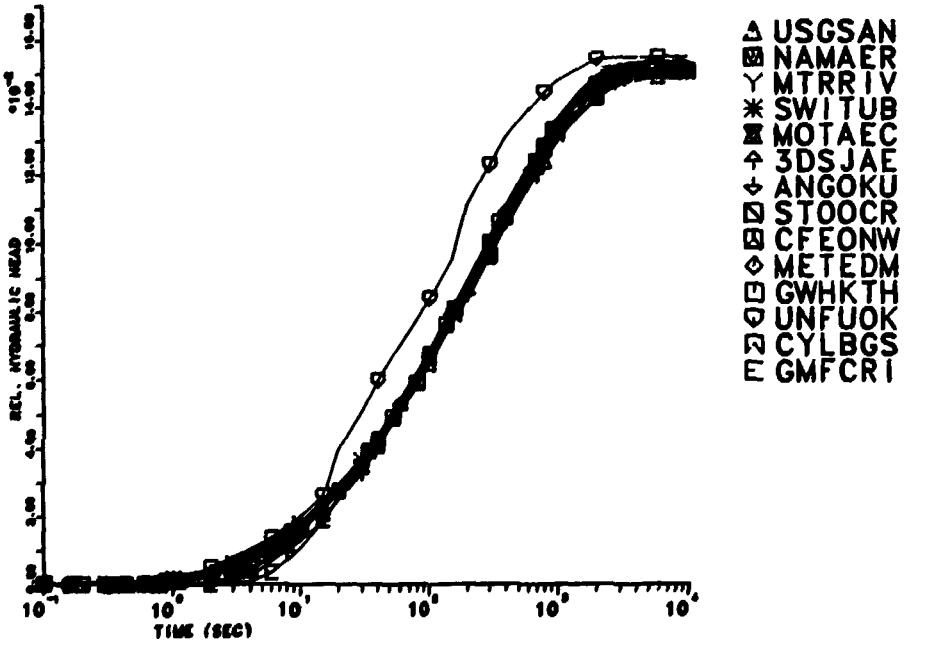


*Figure 4.4. Calculated relative hydraulic head as a function of time at r =5.0 m and z =5.0 m.*

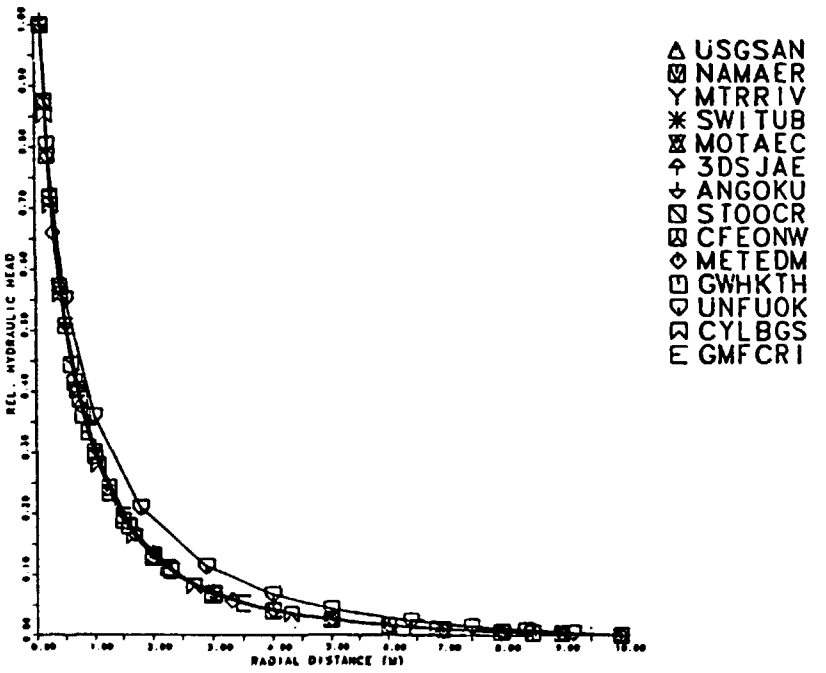


*Figure 4.5. Calculated relative hydraulic head as a function of radial distance at z = 4.0 m and t = 100 s.*

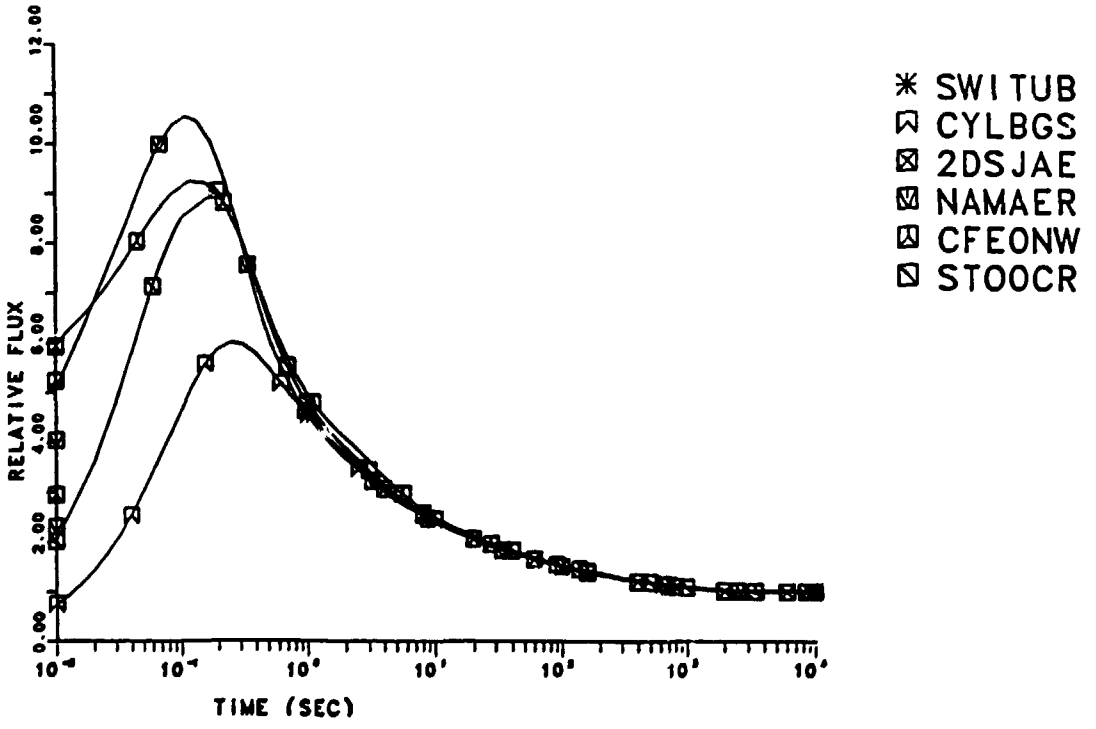


*Figure 4.6. Calculated relative flow rates into the matrix as a function of time. Note that values for the analytical solution have not been calculated for t <1.0 s.*

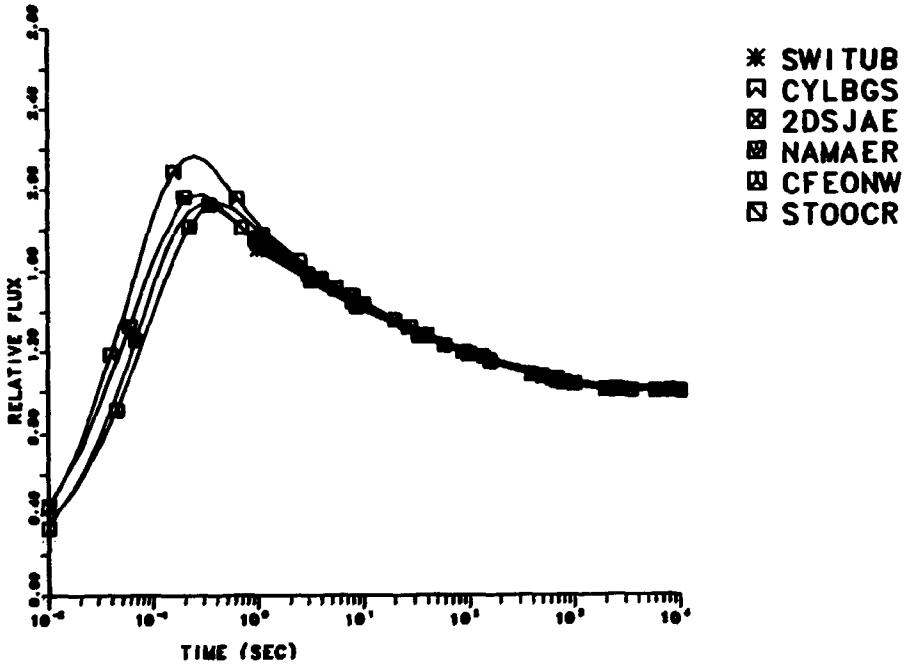


*Figure 4.7. Calculated relative flow rates into the fracture as a function of time. Note that values for the analytical solution have not been calculated for t < 1.0 s.*

## 4.3 Case 2. Steady-State Flow in a Rock Mass Intersected by Permeable Fracture Zones

The purpose of the problem was to test the capabilities of different codes to treat large permeability contrasts. The case concerned steady-state flow in a two-dimensional vertical slice of a fractured rock. A two-dimensional cross-section of a fractured rock mass was supposed to be intersected by two fracture zones (Figure 4.8). The zones, having different widths and inclinations, intersected at depth within the modelled region. The region containing the two inclined fracture zones had a higher permeability than the surrounding rock.

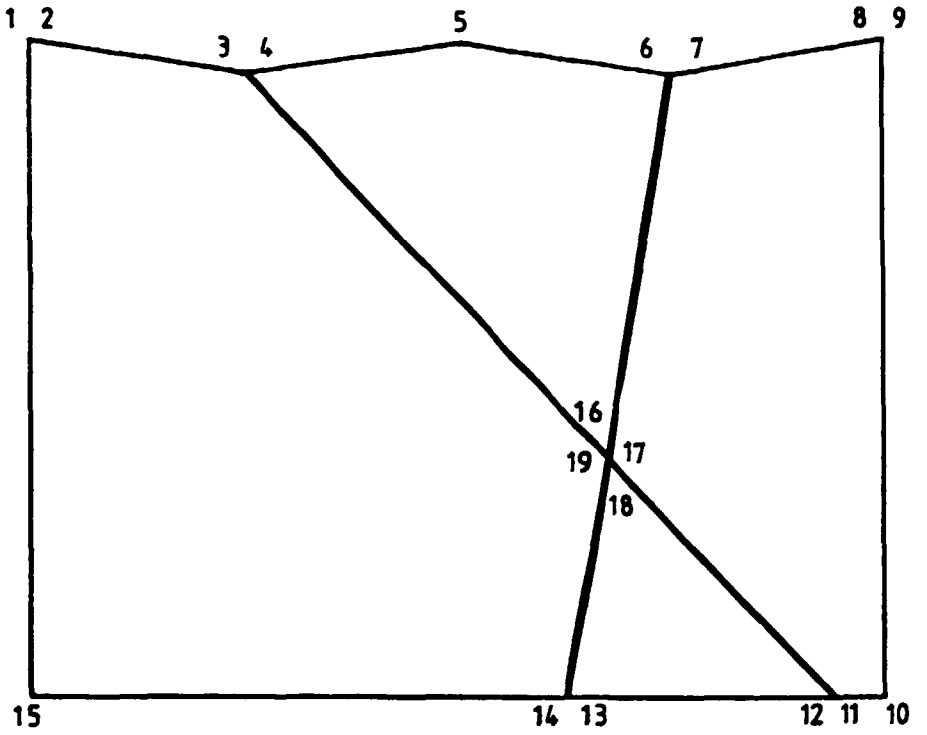


*Figure 4.8. Geometry of the modelled domain in Case 2.*

Two valleys were assumed to be located where the fracture zones met the surface. The surface was taken to be horizontal near the lateral boundaries in order to avoid singularities in the top outer corners of the domain. Although the surface topography was supposed to be symmetric, the flow would be influenced by the asymmetry of the fracture zones due to differences in their width and inclination.

Darcy's law was considered to be applicable to both the fracture zones and the rock mass. Moreover, both units were assumed to be homogeneous and isotropic media. The rainfall was considered to be sufficient to cause the water table to be coincident with the surface. The remaining boundaries were assumed to be impermeable to water flow.

In view of the complicated geometry, no attempt was made to find an analytical solution. The accuracy of the solutions was to be judged by examining the convergence with respect to spatial discretisation.

The teams were asked to provide the piezometric head distribution along five horizontal lines through the modelled domain. In addition they were supposed to check the accuracy to which water flow paths could be calculated, since this was assumed to be a more relevant performance assessment measure for radionuclide migration problems. The starting points for the pathline calculations were given in the problem definition.

*Results from Case 2*

One objective of Case 2 was to study the effect of the discretisation density. The Project Teams used between one and four different meshes. The meshes were classified as being coarse (<200 nodes), medium (200—500 nodes), fine (500—1600 nodes), or superfine >1600 nodes.

Generally, the spread of results was widest for the coarse meshes. The results that departed most significantly from the bulk were either results from calculations using a comparatively low discretisation density or results from finite-difference modelling. The deviations in the latter case were due to the presence of slanted fracture zones creating difficulties in describing the domain with axis-parallel blocks. It was demonstrated that this problem could be partly circumvented, e.g. by tilting the mesh so that the fracture zones were located along the diagonals of the grid blocks. However, the effective transmissivity of the fracture zones then became dependent on the grid-block sizes.

The results for the distribution of hydraulic head along horizontal lines, specified to cross the domain at certain levels, agreed fairly well among the different teams. As can be expected, the spread of results was greater for the coarse meshes than for the medium and fine ones. Also, the spread was smaller for the lines at greater than at more shallow depths. The effect of the discretisation is illustrated by the Figures 4.9, 4.10 and 4.11, giving the results for hydraulic heads for the coarse, medium and fine mesh for one line at 200 m depth. Four curves are off by more than 1 m head for the coarse mesh, whereas only one curve is off by more than 1 m for the medium and fine mesh. From the figures it is can be noticed that the curve representing a finite-difference solution deviates from the bulk of the solutions. Since the domain had features that were not axis parallel, the number of finite-difference grid blocks needed to approximate the geometry of the domain had to be rather large.

The Project Teams were also requested to present trajectories starting at four different points in the domain. The results from one of the trajectories are shown in Figures 4.12, 4.13 and 4.14 for three different discretisation densities. It is apparent that the coarse discretisation, as illustrated by the wide spread in Figure 4.12, is not sufficient to describe the flow field. Several Teams found the particles to exit through the left fracture and the application of one code resulted in a "kick-back" (return of the particle). Two Teams experienced similar problems with the medium discretisation, but for the fine mesh all Project Teams got the particles to exit through the rightmost fracture zone.

To illustrate the convergence of the solutions using different discretisation densities five teams were selected representing the different discretisation strategies used to solve the test case, one team applying a finite-difference code and four teams using finite-element codes. As the trajectories are influenced by the tracking algorithm, their application in the convergence test became somewhat uncertain.

With regard to the head distribution, the difference between coarse and medium mesh was generally greater than between medium and fine mesh. The difference in head between the different discretisation levels decreased with an increasing number of nodes per element.

The trajectories exited from the domain for all five codes. For quadratic elements the medium mesh trajectory also exited through the right-hand fracture zone. The increase in discretisation density caused by the use of quadratic interpolation elements instead of linear elements

increased the rate of convergence. When using finite-difference codes, the effective width of the fracture zones decreased when the discretisation density increased, implying that in a strict sense the convergence test would only be valid far away from the fracture zones, although the effect was not pronounced in the actual case.

Two teams showed that the use of one-dimensional elements in the fracture zones seems to be a feasible method to reduce the number of nodal points. However, it remains to develop a particle tracking algorithm that is applicable to this approach.

One Project Team demonstrated that it is essential to pay special attention to cases in which schemes to smooth the flow field from a finite-element calculation are used, since these algorithms affect the pathlines, the integrated pathlengths and the travel times.

The difference between the results from coarse and medium meshes was usually greater than the difference between medium and fine meshes and, for Case 2, it may not be worthwhile to increase the discretisation beyond the medium mesh. On the other hand the coarse discretisations used in the test case were inadequate to solve the problem. The calculated particle tracks showed that different results represented qualitatively different flow fields.

A final conclusion that can be drawn from exercise within Case 2 is that the spread between pathlines is greater than between the heads. This implies that the tracking algorithms have a significant influence when used on the calculated flow fields.

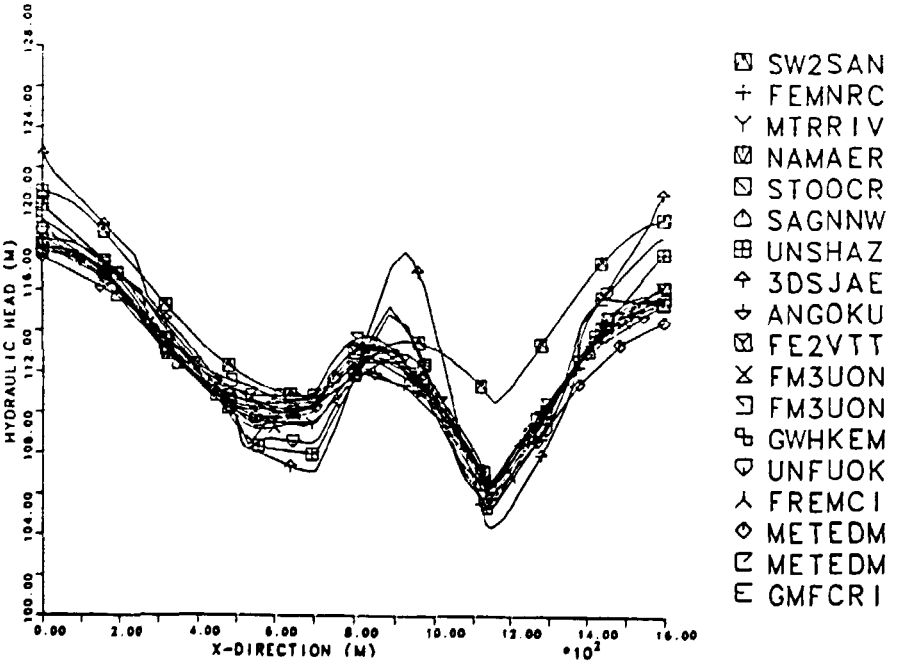


*Figure 4.9. Distribution of hydraulic head at a level of -200 m with coarse meshes. The second set of results for FM3UON and METEDM corresponds to calculations with 1D fracture elements.*

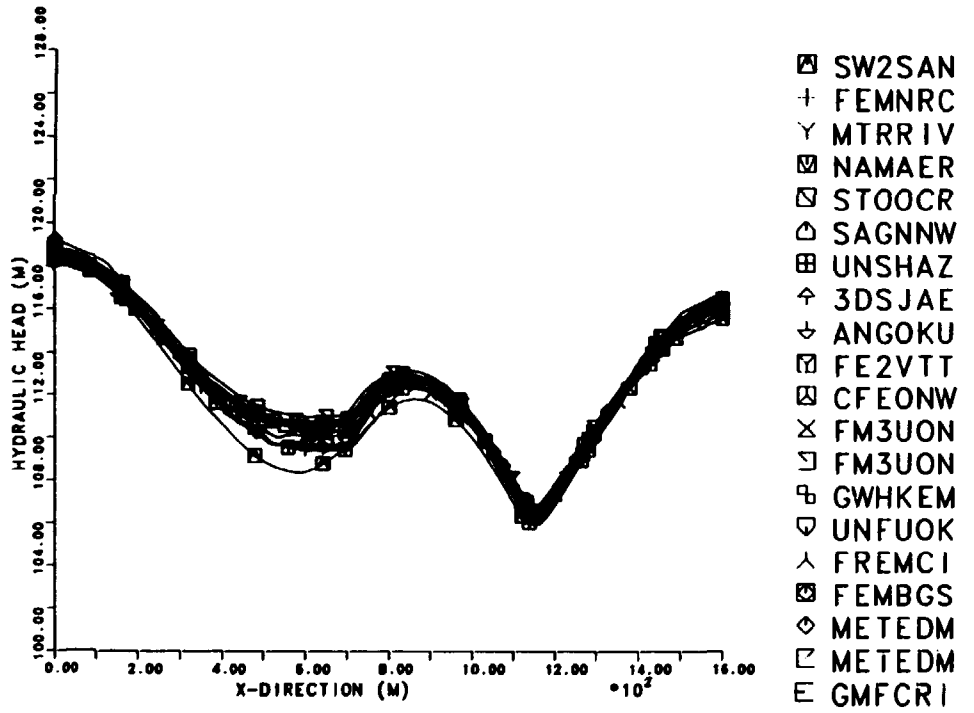


*Figure 4.10. Distribution of hydraulic head at a level of -200 m with medium meshes.*

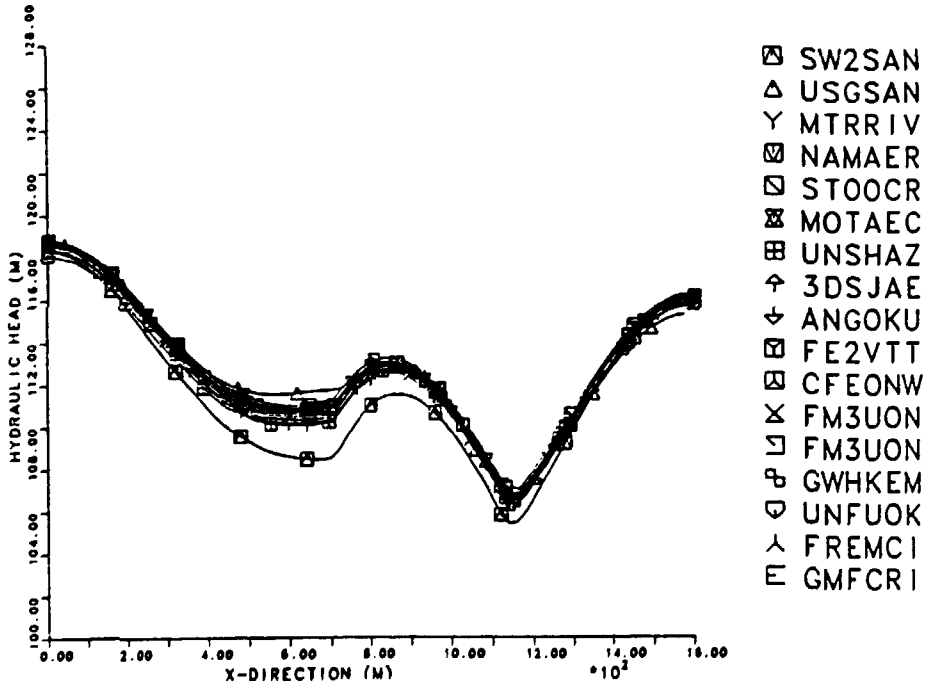


*Figure 4.11. Distribution of hydraulic head at a level of -200 m with fine meshes.*

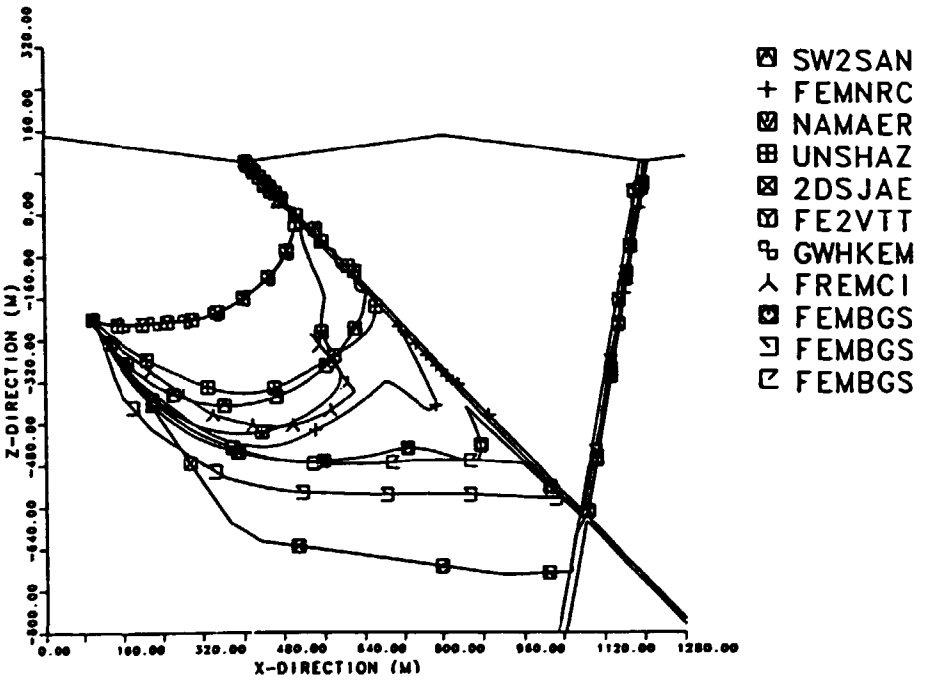


*Figure 4.12. Trajectory 2 as calculated by the various Project Teams using coarse meshes. The different solutions obtained with FEMBGS correspond to calculations with different tracking algorithms. Note the "kickback" effects introduced by the FEM-code.*

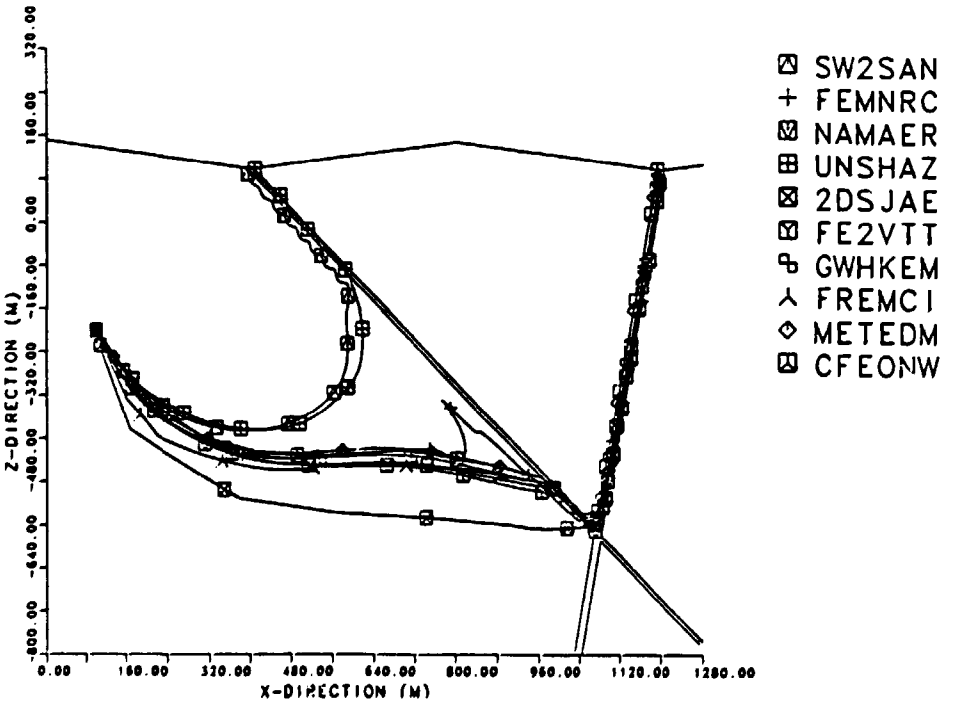


*Figure 4.13. Trajectory 2 calculated with medium meshes.*

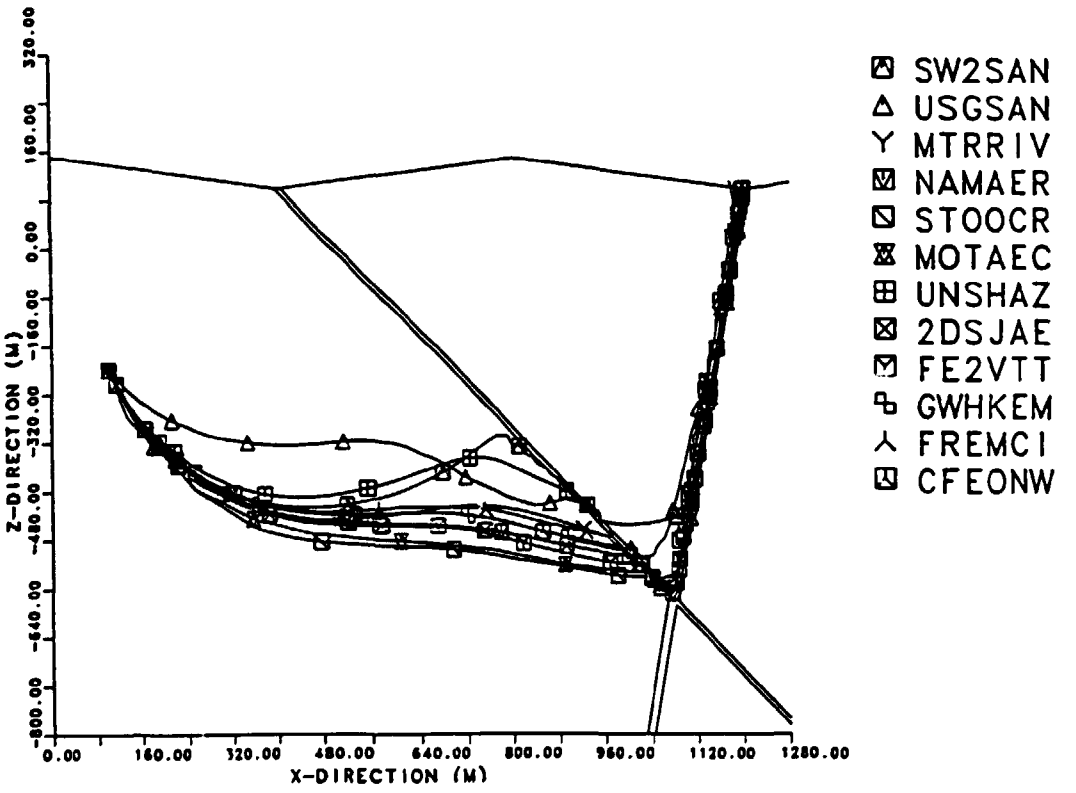


*Figure 4.14. Trajectory 2 calculated with fine meshes.*

## 4.4 Case 3. Saturated-Unsaturated Flow through a Layered Sequence of Sedimentary Rocks

The host rock of a waste repository may be covered by layered sedimentary rocks having different hydraulic properties. The objective of Case 3 was to compute the transient position of the groundwater table in a layered, partially saturated system (Figure 4.15).

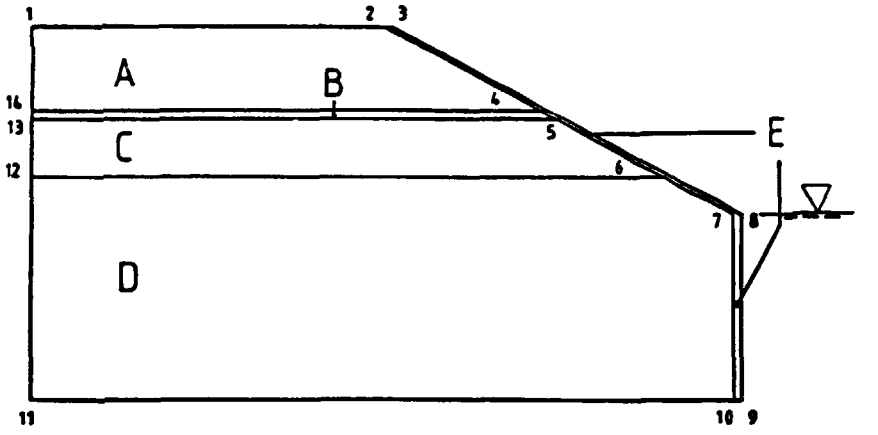


*Figure 4.15. Geometry of the modelled domain in Case 3. Medium D is the host rock, media A and C are permeable relative to the host rock, medium B is an aquitard between A and C, medium E is a pervious layer of loose material acting as a seepage face on the right flank.*

For the problem a two-dimensional cross-section with five media was to be modelled. The flow through the system was to be considered as saturated-unsaturated. The upper layer was fed with water from above by groundwater infiltration. The right-hand part of the host rock was located beneath a lake. The hydrostatic pressure of the lake defines the boundary conditions at the eastern flank of the host rock. All other boundaries were assumed to be no-flow. All media were considered to be homogeneous and isotropic.

The system was initially supposed to be in hydrostatic equilibrium. At a given point in time a water flow was imposed across the top surface of the modelled domain. The development of the groundwater table was to be followed as a function of time.

A mathematical model was supplied for the case by the Secretariat as well as input parameters comprising the geometry, rock properties and fluid properties (capillary pressure as a function of saturation and relative permeability as a function of saturation). The required output was the location of the groundwater table at successive time steps and at steady-state.

### *Results from Case 3*

The case proved to be a difficult test for the models. The difficulty arose mainly from the characteristic curves of the material properties, i.e. the capillary pressure versus saturation and the relative permeability versus saturation. None of the six Project Teams that tackled the case obtained a converged solution using the parameters specified in the original case definition.

Several attempts were made to obtain solutions by modifying the characteristic curves, however.

Three teams submitted transient solutions using different assumptions regarding the minimum value for the relative permeability. One team produced results with the values 0 (Figure 4.16), 0.0003 and 0.01, another team used 0.0003 (Figure 4.17) and a third team used 0.1. None of the first two teams appeared to have obtained converged solutions, although for the second team the solution for the first time-steps seemed to behave reasonably well. The reason for the deterioration at later time-steps is obviously the very large permeability contrasts created by the small pressure changes, when the relative permeability is allowed to drop to near-zero values for low saturations. Thus it seems sensible that the team that used a minimum value for the relative permeability of 0.1 should get the best converged solution.

No team submitted steady-state solutions with characteristic curves according to the problem specification, although four teams gave steady-state solutions with modified curves.

Two teams assigned a very high capillary pressure for low saturation. They thus effectively set the specific storage and moisture capacity to zero, causing the relative permeability to be high in the whole domain and, accordingly, avoided the high permeability contrasts (Figure 4.18). One team made attempts selecting different minimum values for the relative permeability ranging from 0.0025 to 0.01 (Figure 4.19). They found that the higher the minimum value for the relative permeability, the lower the position of the steady-state groundwater table. This appears to imply that a high permeability facilitates drainage of water to the seepage face. That conclusion was seemingly contradicted, however, by the results of another team.

Due to the difficult formulation of the test case, no team succeed in getting a converged solution without modifying either the data for capillary pressure versus saturation or the relative permeability versus saturation. No consensus could be reached regarding the position of the groundwater table at steady-state. There appears to be contradictory results as to the effect of changes in the minimum value of the relative permeability upon the groundwater table.

It was pointed out at the workshops that, although taken from the literature, the data given for the test case 3 were unrealistic. As a consequence, another test case was formulated for Level 3 of the HYDROCOIN study in order to address some of the anomalies experienced by the teams.

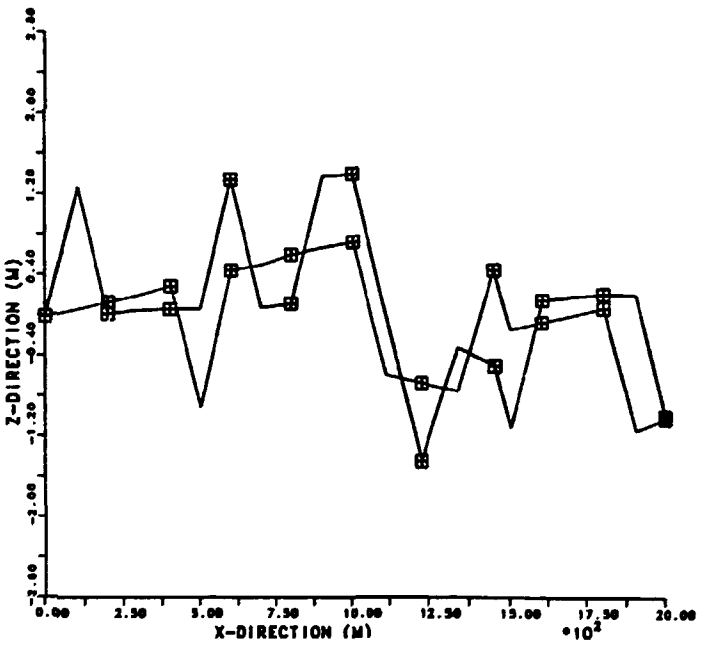


*Figure 4.16. Transient solution as calculated by UNSHAZ. A minimum value of 0.0 is used for the relative permeability. Six time steps are calculated. The results of the five last time-steps are identical.*

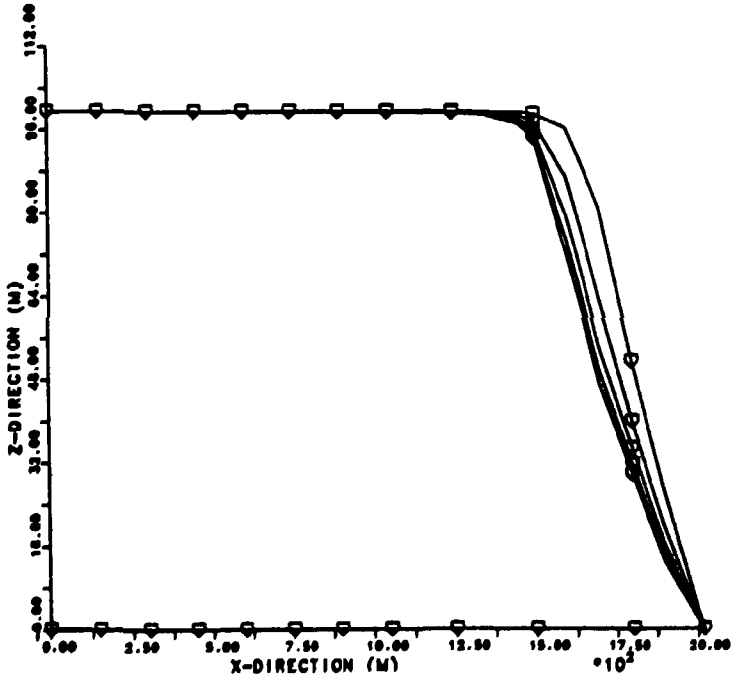


*Figure 4.17. Transient solution as calculated by UNFUOK. A minimum value of 0.003 is used for the relative permeability. Six time steps are calculated. The last coincides with the x-axis.*

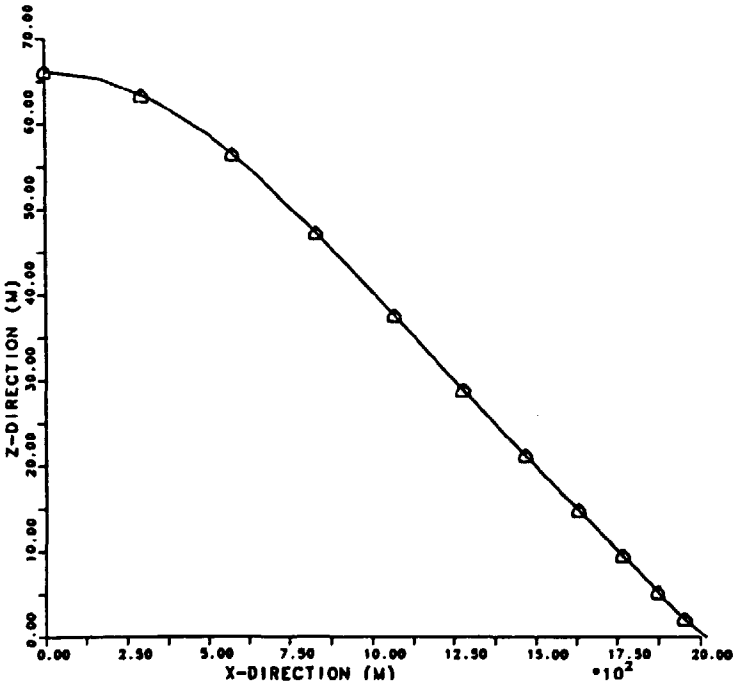


*Figure 4.18. Steady-state solution as calculated by SAGNNW. By applying a high capillary pressure, the non-linearity is circumvented and the problem turns into a nonlinear steady-state case, sharp interface approach.*

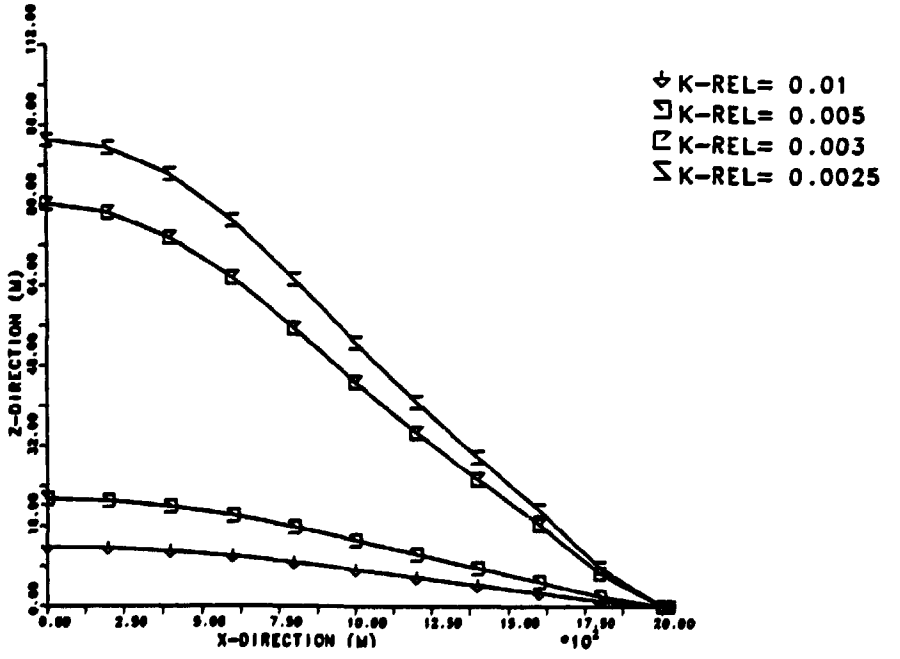


*Figure 4.19. Four different steady-state solutions as calculated by ANGOKU. The minimum values of the relative permeability range from 0.01 to 0.0025.*

## 4.5 Case 4. Transient Thermal Convection in a Saturated Permeable Medium

Heat output from a repository containing high-level waste can induce regional groundwater flows. Since these flows are predominantly vertical, they could shorten the leakage paths and transit times of water-born radionuclides. The purpose of case 4 was to test the accuracy with which numerical codes can treat time-dependent buoyancy driven flow.

For the test case the rock-mass was assumed to be a homogeneous, isotropic, permeable medium of infinite extent, with constant physical properties. The repository was idealised as a uniform spherical heat source with the same physical properties as the surrounding rock and a power output which decayed exponentially with time. The model assumed that the dominant heat transfer mechanism was conduction through the rock, rather than convective transfer due to the flow of groundwater. Flow transients were neglected, due to their short duration compared to the evolution of the regional temperature field. The flow was assumed to be governed by Darcy's law. No other driving forces than thermal buoyancy were assumed.

A mathematical model was provided by the Secretariat. Furthermore, analytical values of the required outputs were given as well as analytical solutions for temperature rise as a function of time, pressure rise as a function of time, temperature rise as a function of distance, pressure rise as a function of distance and trajectories for different starting positions in time and space. Figure 4.20 gives an example of the analytical solution for the trajectories. Table 4.1 gives the coordinates for the starting points.

*Table 4.1. Analytical solutions for travel times and final radial coordinates for pathlines starting at $t = t_0$ and $r = r_0$ in the mid-plane of the repository ($z = 0$ m) and ending on the plane $z = 1000$ m.*

| Pathline no | $t_0$ (years) | $r_0$ (m) | $t_0$ (years) | $r_0$ (m) |
|---|---|---|---|---|
| 1 | 100 | 0 | $1.5135 \cdot 10^3$ | 0.0000 |
| 2 | 100 | 125 | $2.1135 \cdot 10^4$ | $1.1050 \cdot 10^3$ |
| 3 | 100 | 250 | $2.4586 \cdot 10^4$ | $9.4772 \cdot 10^2$ |
| 4 | 1000 | 0 | $2.2972 \cdot 10^3$ | 0.0000 |
| 5 | 1000 | 125 | $2.9057 \cdot 10^3$ | $3.2284 \cdot 10^3$ |
| 6 | 1000 | 250 | $5.5446 \cdot 10^3$ | $6.3361 \cdot 10^2$ |
| 7 | 10000 | 0 | $7.8234 \cdot 10^4$ | 0.0000 |
| 8 | 10000 | 125 | $8.0396 \cdot 10^4$ | $1.3429 \cdot 10^2$ |
| 9 | 10000 | 500 | $8.7346 \cdot 10^4$ | $2.6811 \cdot 10^2$ |

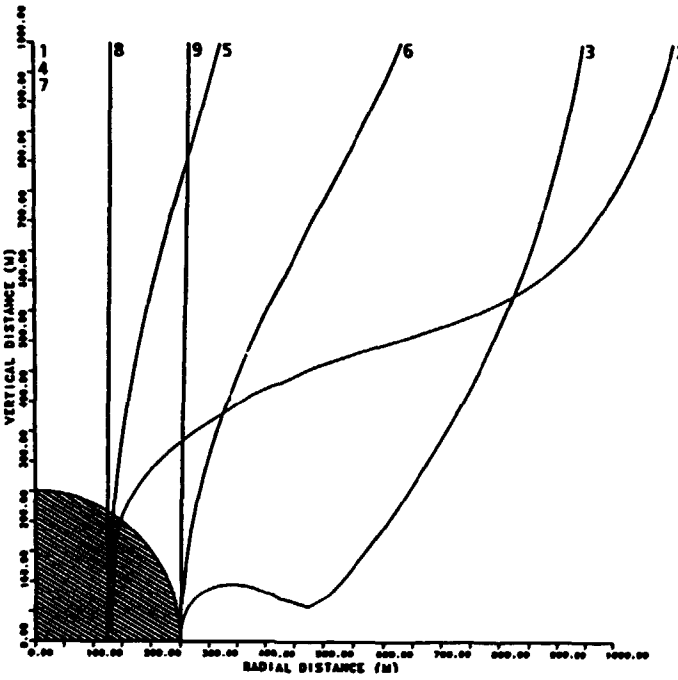


*Figure 4.20 Analytical solution for trajectories 1—9 for different starting positions in time and space given in Table 4.1.*

The required outputs were temperature and dynamic pressure rises on the centreline as a function of time and space, temperature and dynamic pressure rises as a function of distance from the centreline at specified time intervals and in addition, participants were requested to calculate pathlines from the mid-plane of the repository from different starting points.

Analytical values of the required results were given as well as analytical solutions for pathlines.

*Results from Case 4*

Ten teams tackled the problem. The calculated profiles of temperature as a function of time agreed particularly well with the given analytical solution (Figure 4.21). Also the dynamic pressure as a function of time generally agreed satisfactorily with the analytical solution, though some teams got deviating results for the vertical distance equal to zero (Figure 4.22).

Calculated results for temperature as a function of distance also agreed excellently with the analytical solution, with only one team being off by about 6% for radial distances between 0 and 200 m (Figures 4.23 and 4.24).

Calculated profiles of dynamic pressure as a function of distance matched satisfactorily the analytical solution.

Five Project Teams presented results for the pathlines. Here the spread between the results was much greater. In general, the positions of the calculated pathlines agree well with the analytical

solutions. This shows that there was reasonable conformity in the flow fields. However, there was a very wide spread in travel times, attributable to the varying algorithms in use for tracking pathlines. A couple of figures illustrate this point (Figures 4.25 and 4.26).

Both finite-element and finite-difference codes showed their ability to model time-dependent buoyancy-induced flows extremely well. There seems to be no significant difference between results obtained with the various finite-element models used by the different teams.

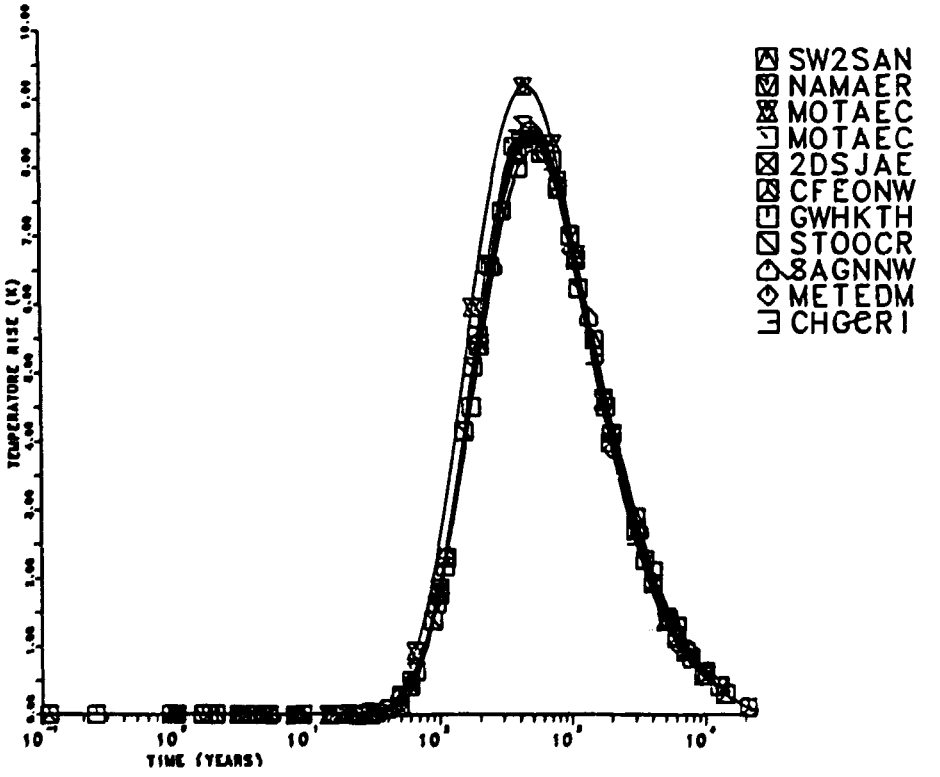


*Figure 4.21. Temperature rise at z = 375 m as a function of time.*

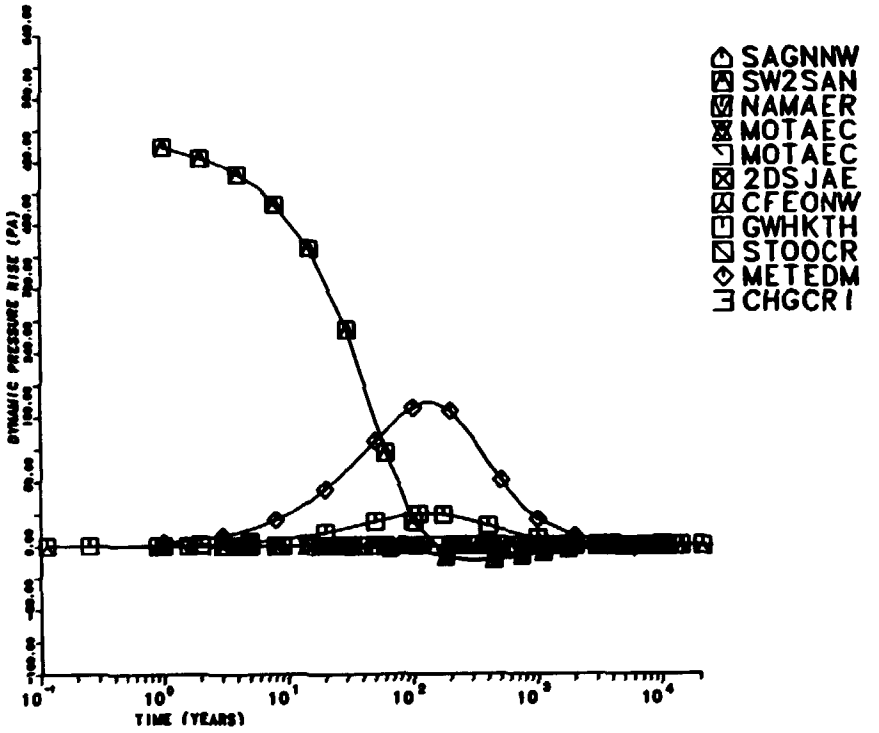


*Figure 4.22. Pressure rise at $z = 0$ m as a function of time.*

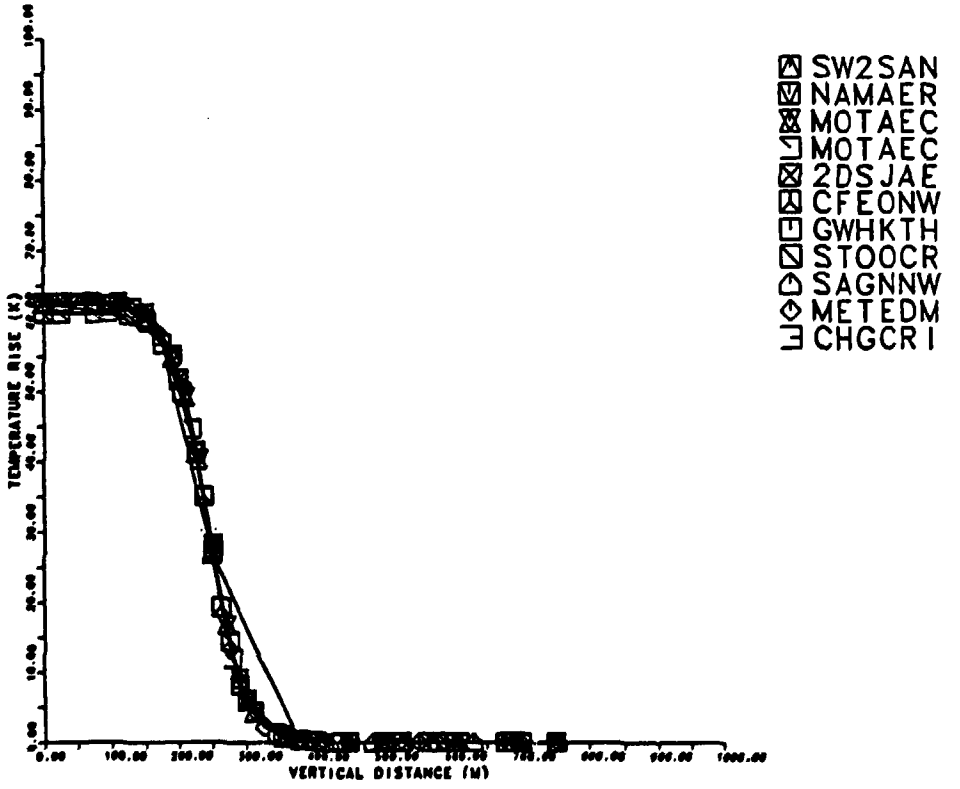


*Figure 4.23. Temperature rise at $t = 50$ years as a function of distance.*

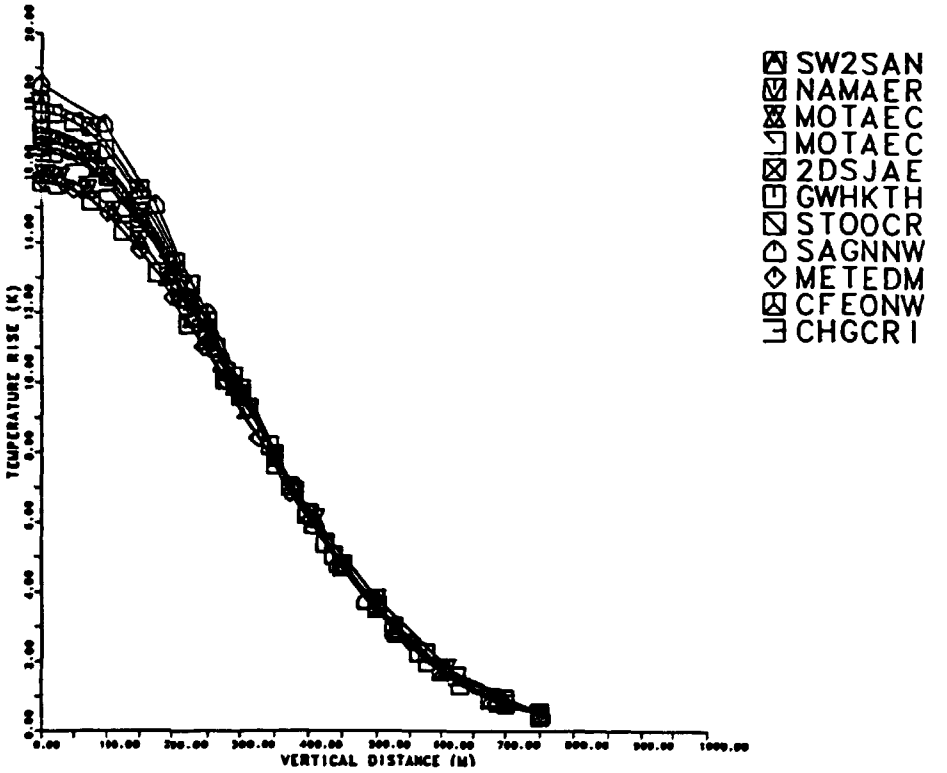


*Figure 4.24. Temperature rise at t = 1000 years as a function of distance.*

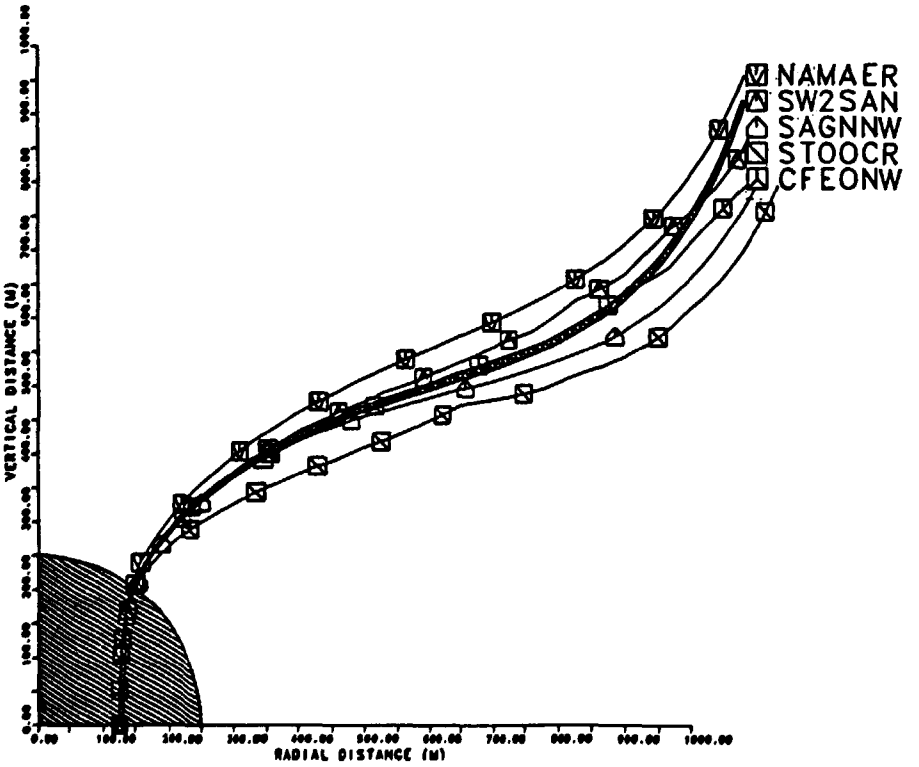


*Figure 4.25. Trajectory starting at r = 125 m and 7 = 100 years.*

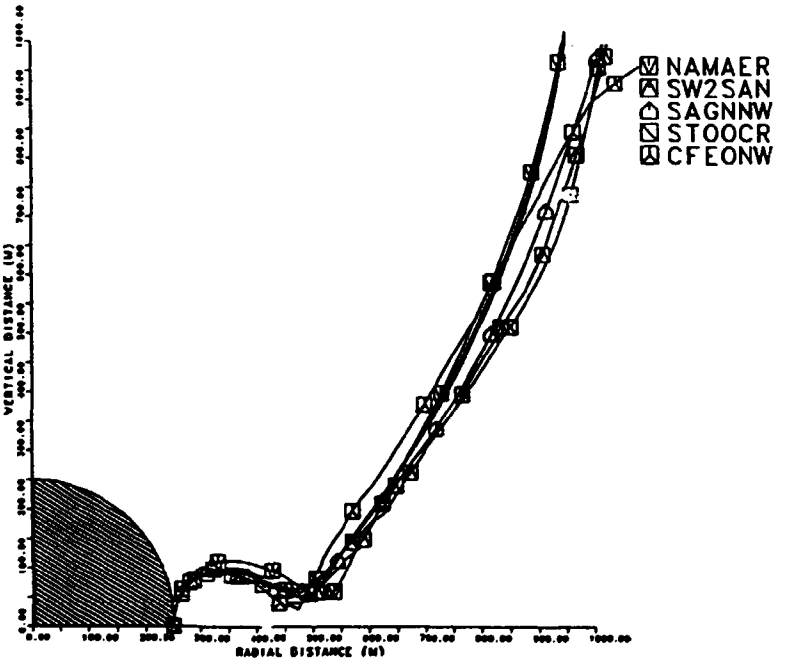


*Figure 4.26. Trajectory starting at r = 250 m and t = 100 years.*

## 4.6 Case 5. Salt Water Distribution in a Saturated Porous Medium

There are a number of important situations in which groundwater flow is influenced by density and viscosity variations due to the presence of dissolved salt. The most notable of these situations concerns flow in regions surrounding salt domes or bedded salt deposits which may be used for the disposal of radioactive waste. However, such considerations may also be important for repositories at coastal sites.

Case 5 is an idealisation of the situation found in the rocks overlying the Gorleben salt dome in the Federal Republic of Germany. The uppermost Quaternary aquifer at the site contains fresh water. At a depth of 300 m the groundwater is saturated with salt.

In the idealised example, the porous sedimentary rock was assumed to have homogeneous and isotropic properties. Since the example was intended for a verification exercise, it was assumed sufficient to consider a two-dimensional vertical cross-section.

The flow was considered to be isothermal and governed by Darcy's law using an appropriately mass-averaged velocity. In the interest of simplicity, the viscosity was considered to be independent of the brine concentration.

The anticipated physical behaviour could briefly be described as follows. The pressure head should decrease from left to right across the domain, and also decrease from the bottom to the top of the domain. The salt should form a plume flowing upwards and to the right from the part

of the bottom of the domain representing the salt dome. The pathlines starting at the prescribed points should descend towards the bottom of the domain, then move across the domain, and finally move upwards and out of the domain. A mathematical model of the flow situation was provided to the participating teams.

The required outputs were the pressure distribution and steady-state salt concentration distribution along seven horizontal lines through the domain, trajectories with calculated travel times, and the vertical velocity calculated along the top boundary (Table 4.2 and 4.3).

*Table 4.2. Coordinates of the evaluation lines.*

| Line no | Starting position | | Ending position | |
|---|---|---|---|---|
| | x (m) | z (m) | x (m) | z (m) |
| 1 | 0 | 0 | 900 | 0 |
| 2 | 0 | - 50 | 900 | - 50 |
| 3 | 0 | -100 | 900 | -100 |
| 4 | 0 | -150 | 900 | -150 |
| 5 | 0 | -200 | 900 | -200 |
| 6 | 0 | -250 | 900 | -250 |
| 7 | 0 | -300 | 900 | -300 |

*Table 4.3. Starting positions for trajectory calculations*

| Trajectory no | x (m) | z (m) |
|---|---|---|
| 1 | 10 | -10 |
| 2 | 50 | -10 |
| 3 | 100 | -10 |
| 4 | 150 | -10 |
| 5 | 200 | -10 |

***Results from Case 5***

The case presented a very severe challenge to the various codes. It was highly non-linear and the balance between gravity, convection and dispersion varied throughout the domain. The solution, therefore, could not be calculated analytically. Hence, the results of the various Project Teams could only be compared with one another and with the expected physical behaviour of the system.

Results from five code-team combinations were submitted. Some of the teams had to use grids which were very refined near the sides and the base of the domain, as well as near the limits of the hypothetical salt dome in order to obtain numerically stable and converging solutions.

The teams had to use, and in some cases develop, special methods to handle various aspects of the problem. Initial results presented by some of the teams differed markedly from their final results, which were obtained in the light of discussions at the workshops and at a special meeting held to discuss the case.

Much of the discussion was devoted to the physical representation of the system. Thus, the existence of convection cells was much debated, as such cells would have a marked influence on the solutions to the problem. There was finally general agreement that the flow consisted of the main cell driven by the imposed pressure gradient at the top surface, a small weak convection cell in the bottom left corner of the domain driven by the salt source, and a weak convection cell in the bottom right corner driven by the salt source. The left hand convection cell was dragged up to the right by the main flow cell.

The calculated pressures showed a consistent pattern. They agreed, as might be expected, on line 1, which is where the pressure was specified, but the differences between the results increased towards the bottom of the domain. The pressure field was dominated by the gravitational component and the results were readily explained in terms of variations in concentration. (Figures 4.27 and 4.28).

The results from three of the codes for the salt concentration along specified lines showed a band of significant salt concentration across the bottom of the domain and a plume of moderate concentration rising towards the top right corner. This was illustrated most clearly when the results were presented in terms of concentration contours. On line 6 one code always showed extremely small concentrations, whereas another code demonstrated quite large concentrations due to the coarser grid used, and the results from three other codes fell in between (Figure 4.29).

The pathlines followed the same pattern as pressure and concentration. Here, two of the codes deviated from the three others. The greatest difference was about 50 m (Figure 4.30).

Due to the difficulty in understanding the complicated flow field from the pressure profiles, all Project Teams calculated representations of the flow. These took the form either of vector plots of the velocity field or of streamline plots. Flow fields obtained by three of the Project Teams and for one external code were very similar. Figure 4.31 shows an example of a streamline plot.

The definition of this case was much discussed at the workshops, expecially the absence of molecular diffusion in the salt transport equation. Since dispersion in a porous medium to some extent is a consequence of molecular diffusion on the scale of the pores, molecular diffusion should also be present if there is dispersion. In principle, the absence of molecular diffusion could present serious problems, because, if the velocity is zero in a finite region, the salt transport equation becomes meaningless in that region. The absence of molecular diffusion did cause problems for some codes.

Also the choice of boundary conditions for the groundwater flow caused difficulties, as the no-flux conditions on the sides of the domain were inconsistent with the specified pressure condition on the top surface. This led to singularities in the pressure at the two top corners.

The problem served to illustrate some of the difficulties that would occur in simulating more realistic scenarios and stimulated discussions on the correct form of the equations that should be used to model salt transport.

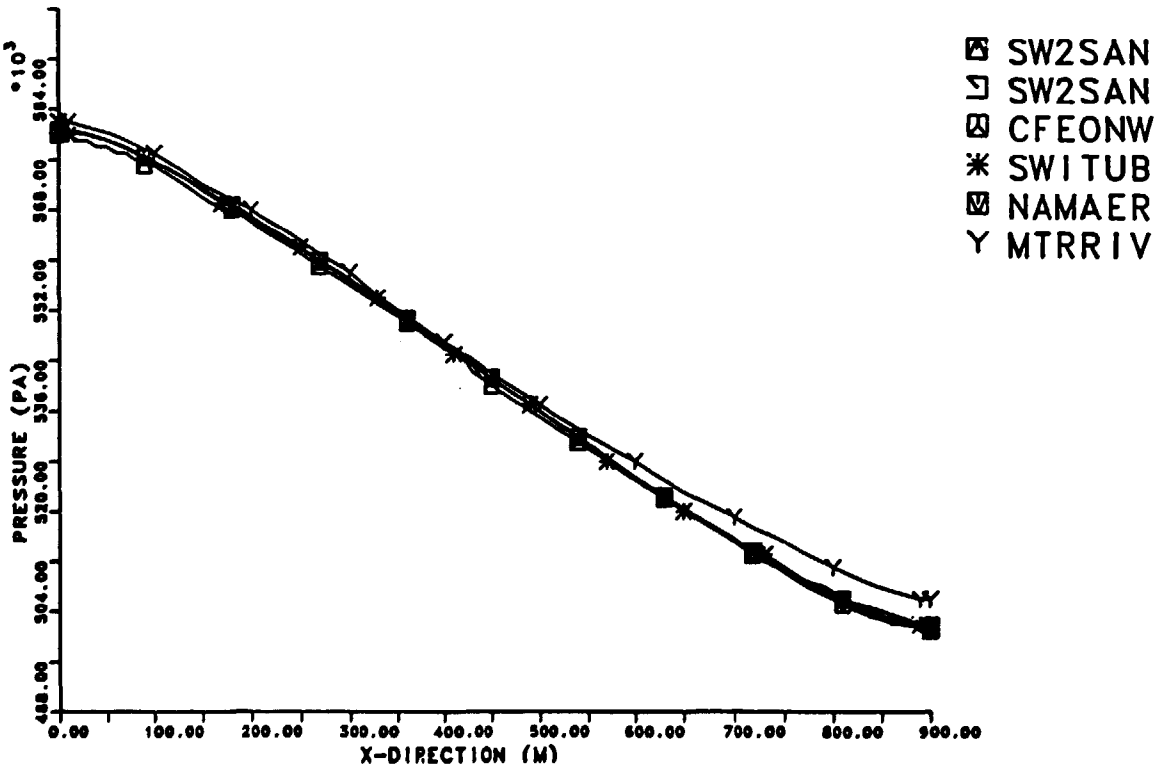


*Figure 4.27. Pressure distribution on line 2.*

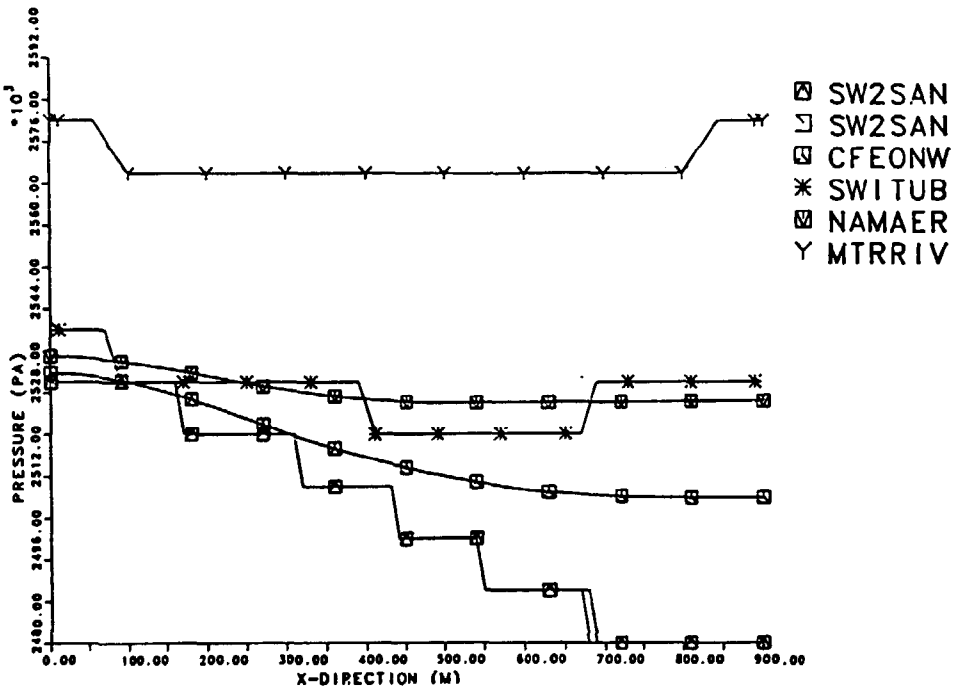


*Figure 4.28. Pressure distribution on Line 6.*

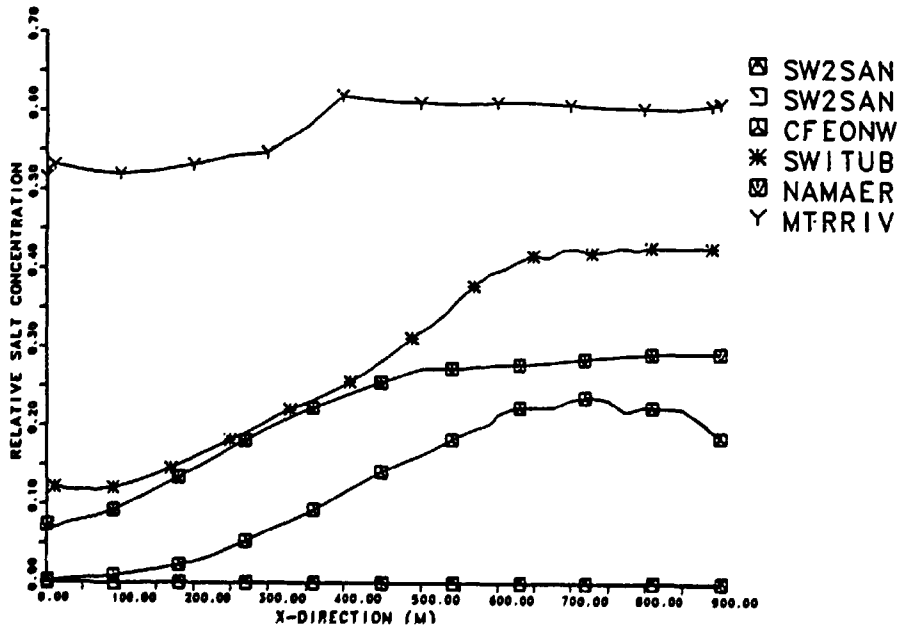


*Figure 4.29. Concentration distribution on Line 6.*

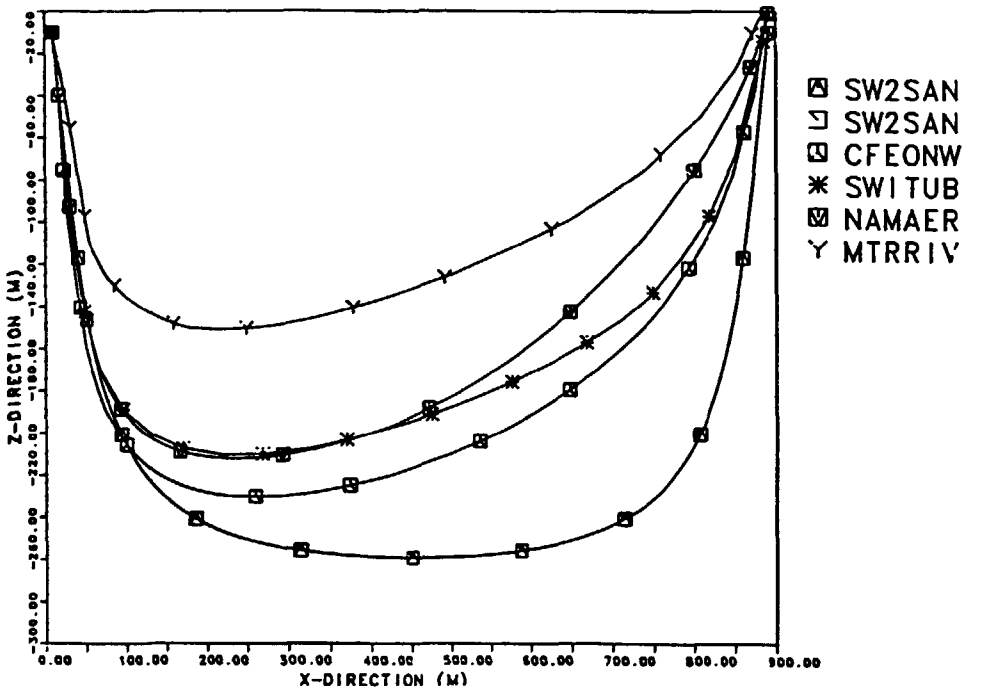


*Figure 4.30. Pathline 1.*

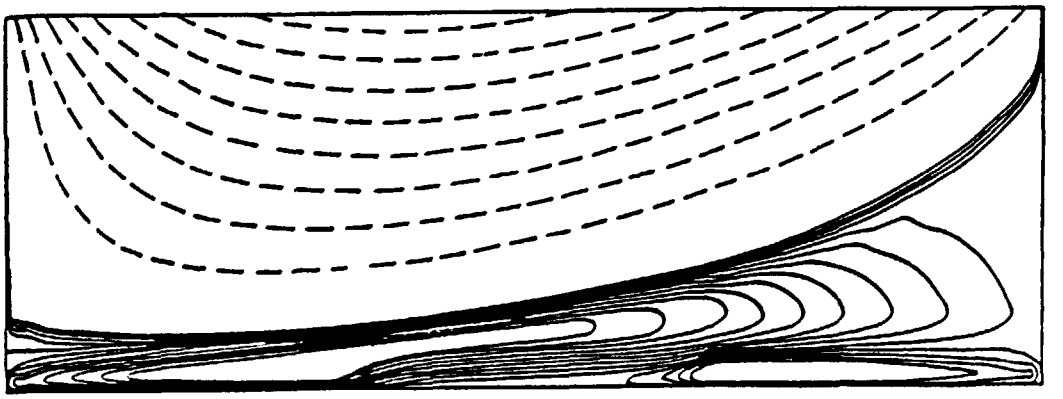

*Figure 4.31. Streamline plot representation of the flow field obtained by NAMAER. Solid lines correspond to streamfunction contours at regular intervals between $-2.0 \cdot 10^{-4}$ and $1.0 \cdot 10^{-4}$; dashed lines correspond to streamfunction contours at regular intervals between $2.5 \cdot 10^{-3}$ and $2 \cdot 10^{-2}$.*

## 4.7 Case 6. Three dimensional Steady-State Flow in a Regional Aquifer

The test case was designed to test the ability of computer codes to model steady-state, three-dimensional fluid flow. The case represented a regional groundwater system with rock layers of highly contrasting hydraulic conductivity, typical of bedded salt sites.

The hydrological system consisted of essentially five material layers: a layer of a low hydraulic conductivity overlain by two aquifer layers and underlain by two additional aquifer units. These five layers degraded into one material in the recharge areas where the salt-shale strata truncated. (Figure 4.32).

The problem was designed to simulate groundwater flow under the following assumptions:

- The groundwater in the hydrological systems would have the same constant density and temperature.
- Darcy's law associated with the porous media continuum approach would apply.
- The system being simulated would be confined and fully saturated.
- The hydrological system would be in steady state and boundary conditions would be constant over time, so that only the steady state solution for the hydrological system would need to be considered.
- No significant hydrological flow would take place in the basement rock underneath the modelled domain.

The required outputs were hydraulic heads along eight evaluation lines with given starting and ending points, eight trajectories to be generated with given starting points and, the magnitude of fluxes at given points within a specified rectangle in the salt-shale system.

### *Results from Case 6*

Eight Project Teams tackled the case. Three teams used finite-difference codes, whereas five employed finite-element codes. As the case involved a large domain (400×150× 3.8 km) with high permeability contrasts and anisotropic permeability, the discretisation of the domain constituted a challenge to most Project Teams, particularly in view of the limited computer storage available and the budget constraints.

The results for distribution of hydraulic head along one of eight requested lines is seen in Figure 4.33. The boundary conditions specified for the top surface were found to be unrealistic for that part of the domain lying east of the river running north-south. Here, the specified infiltration rate exceeded the infiltration capacity of the fluvial-lacustrine system which resulted in calculated potentials exceeding the elevation of the ground surface. This effect was more pronounced for the finite-difference codes due to their restrictions in terms of axis-parallel grids. For other lines the discrepancies were less apparent. One team used a fixed-head boundary condition on the top instead of the specified infiltration and another team applied a free-surface boundary condition, resulting in physically more reasonable values of the hydraulic head. The effect of the unrealistic infiltration rate was strongly reduced as the depth increased (Figure 4.34).

Figure 4.35 illustrates of the results from the particle tracking exercise for trajectory 2. The teams all agreed that the discharge should be to the north-south running river, although the path to get there varied between the different calculations. Differences in pathlines can derive either from differences in the calculated groundwater pressure field or from differences in the trajectory-generating procedure used. For trajectory 3 (Figure 4.36) the spread was wider than that for trajectory 2 and there was no definite agreement as to the point of discharge.

Despite the high permeability contrast between the salt-shale system and the surrounding media, the spread between the lowest (Figure 4.37) and the highest (Figure 4.38) calculated flow rates in the specified horizontal domain was only a factor of 2.3. The pattern in Figure 4.37 was followed by most of the teams. In general, the results showing a high hydraulic head in the fluvial-lacustrine system had higher fluxes in the leftmost part of the salt-shale system than in the rightmost part.

In addition to the base case, some teams made calculations using modified boundary conditions and different particle-tracking algorithms. Furthermore, one team applied a two-dimensional model, realising that the domain as specified only gave a three-dimensional flow field to a limited extent. They also imposed a held potential boundary condition along the top surface instead of a specified infiltration rate. The results are illustrated in the Figures 4.39 and 4.40.

The results of the exercise showed a considerable spread both in hydraulic head and pathlines. The spread was most pronounced close to the top surface, where the influence from the boundary conditions was greatest. It was shown that an adjustment of the infiltration rate would cause a significant change to the results close to the surface, whereas the effect was less apparent at greater depths. Despite the high permeability contrasts and the demonstrated variability of the calculated pressure distributions, the fluxes calculated in the salt-shale system agreed within a factor of about two.

The divergence in the calculated trajectories were due to the choice of different particle tracking algorithms. Smoothing of the velocity field led to unreliable particle tracks close to permeability contrasts.

The complex geometry and large variance in hydraulic properties in combination with the three-dimensionality of the problem required a rather finely discretisised mesh. Inadequate spatial discretisation was probably the cause of some of the anomalies occurring in the solutions.

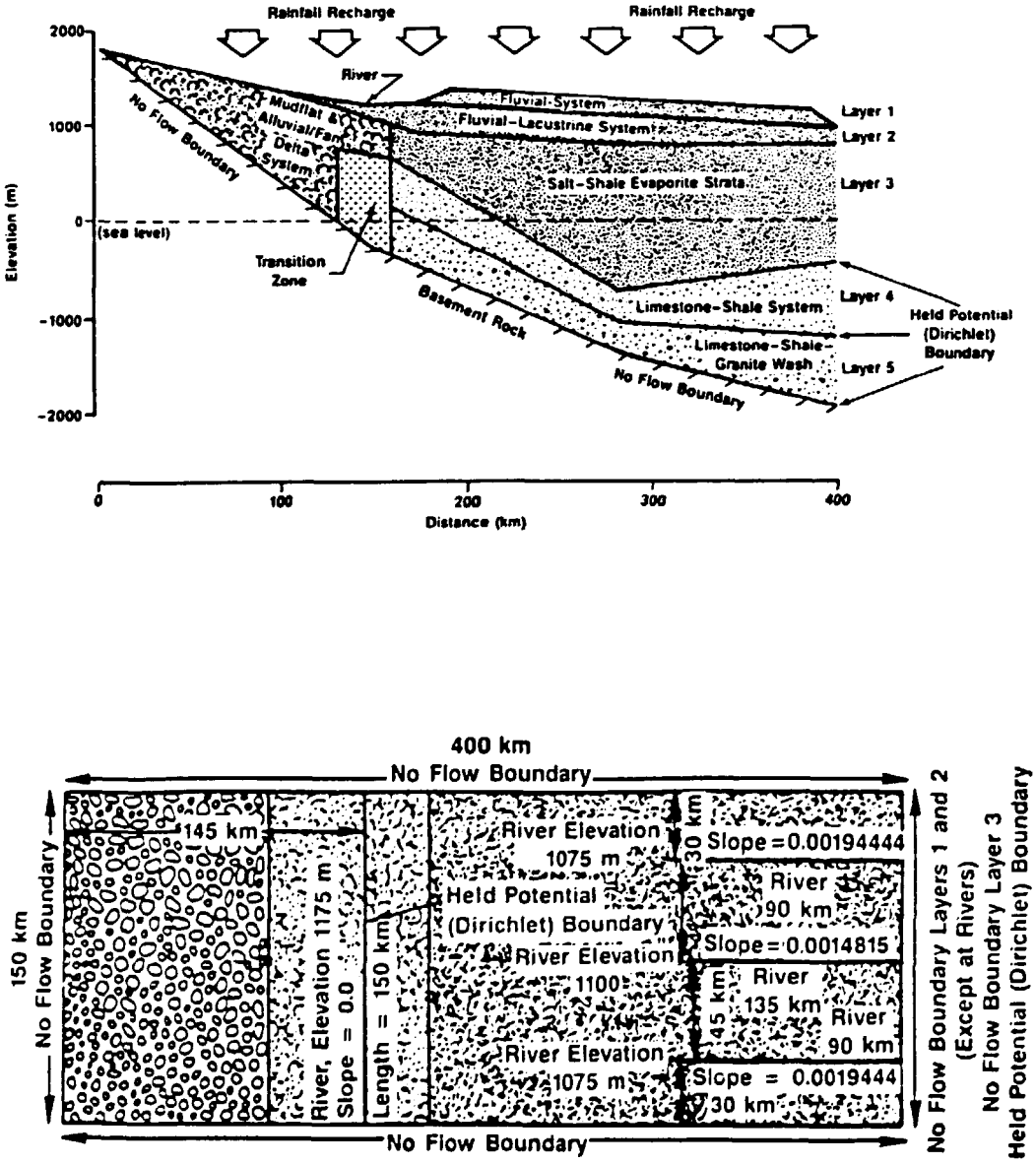


*Figure 4.32. Schematic view of the modelled domain indicating the geological system and boundary conditions. Upper: vertical cross-sectional view. Lower: plan view showing surface drainage and outcrops.*

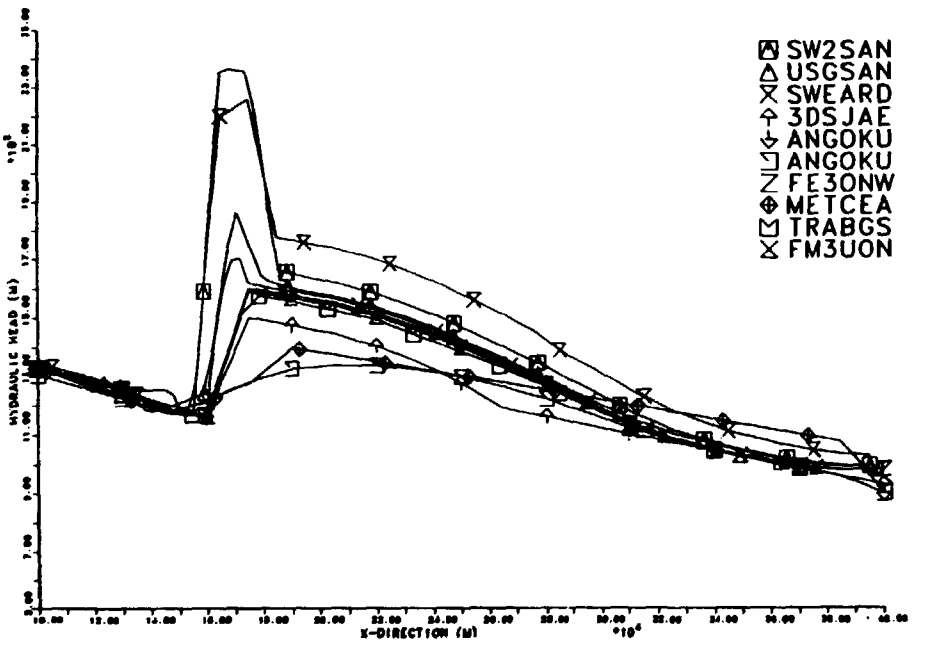


*Figure 4.33. Distribution of hydraulic head along evaluation line 1.*

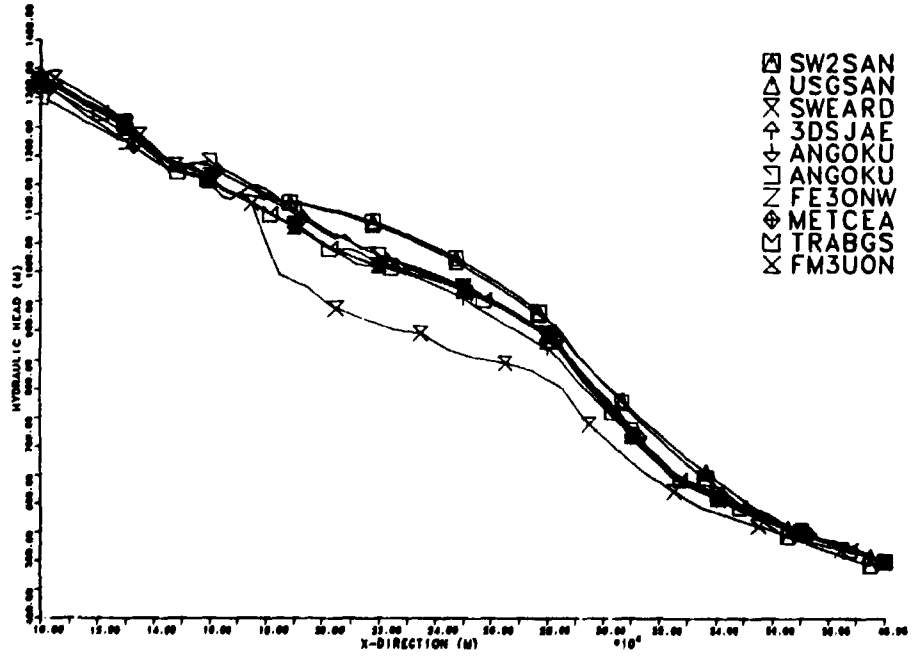


*Figure 4.34. Distribution of hydraulic head along evaluation line 3.*

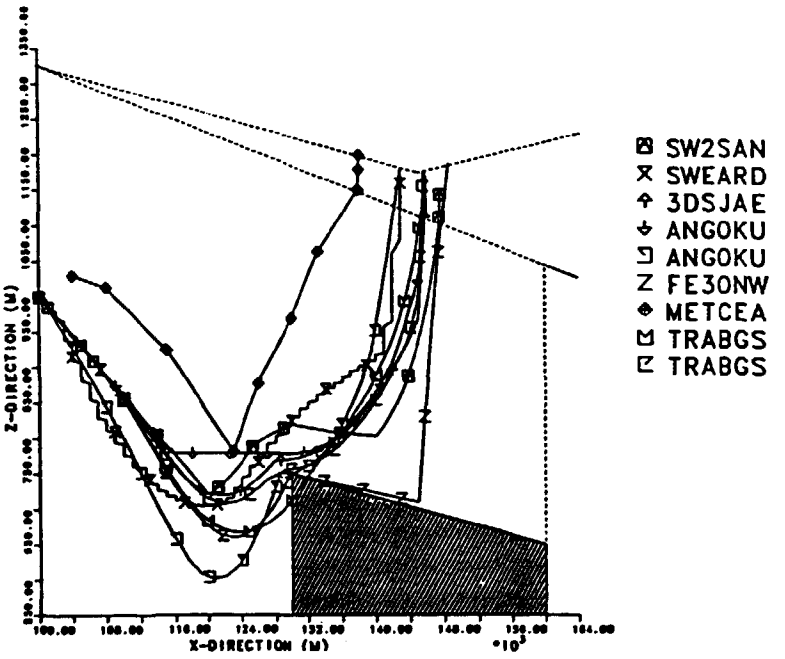


*Figure 4.35. Pathline 2 projected onto the xz-plane. Two sets of boundary conditions were applied by the OKU-team and two different tracking algorithms were tested by FEMBGS.*

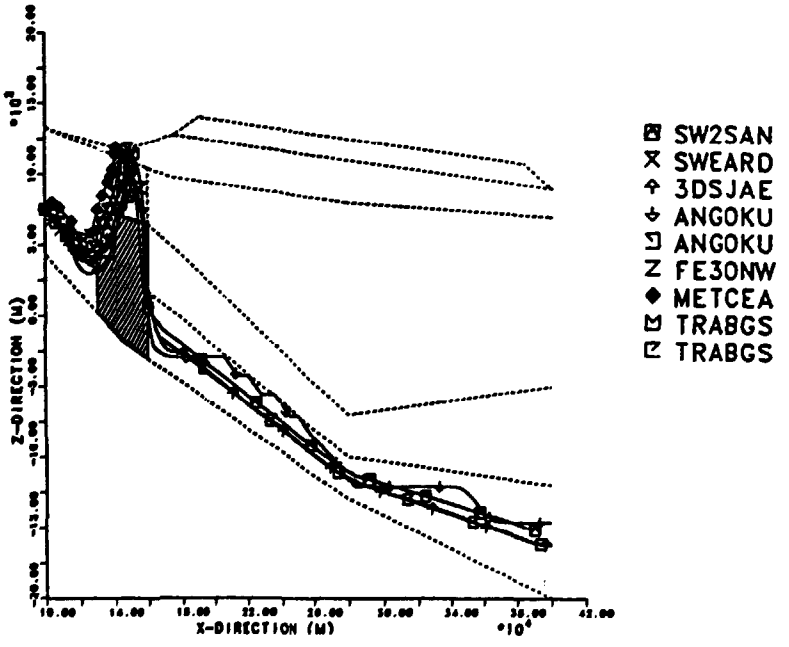


*Figure 4.36. Pathline 3 projected onto the xz-plane.*

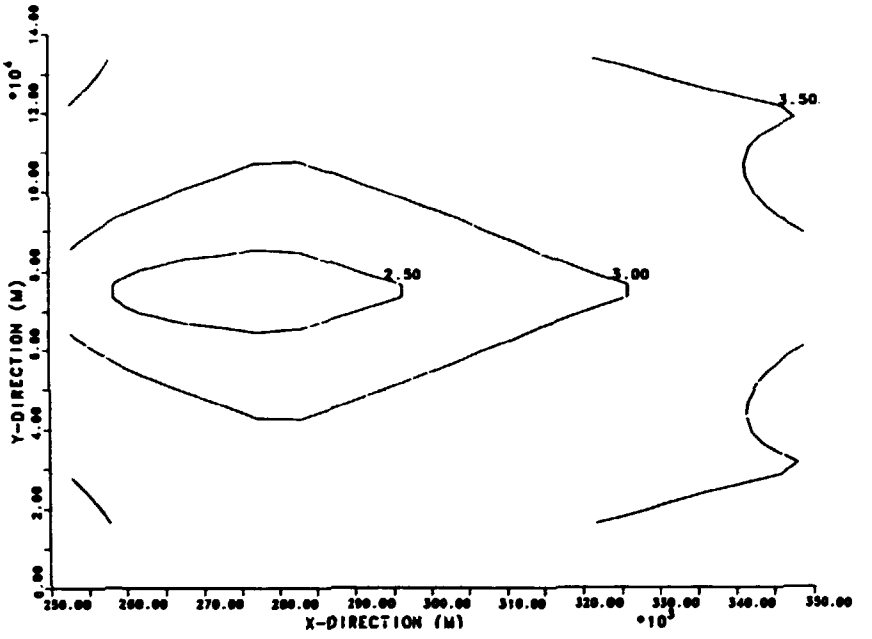


*Figure 4.37. Distribution of flux in the salt-shale system as reported by ANGOKU. This calculation corresponds to an infiltration rate adjusted to the capacity of the top soil layer. The values on the contours should be multiplied by a factor of $10^{-17}$ to get the value in $m \cdot s^{-1}$.*

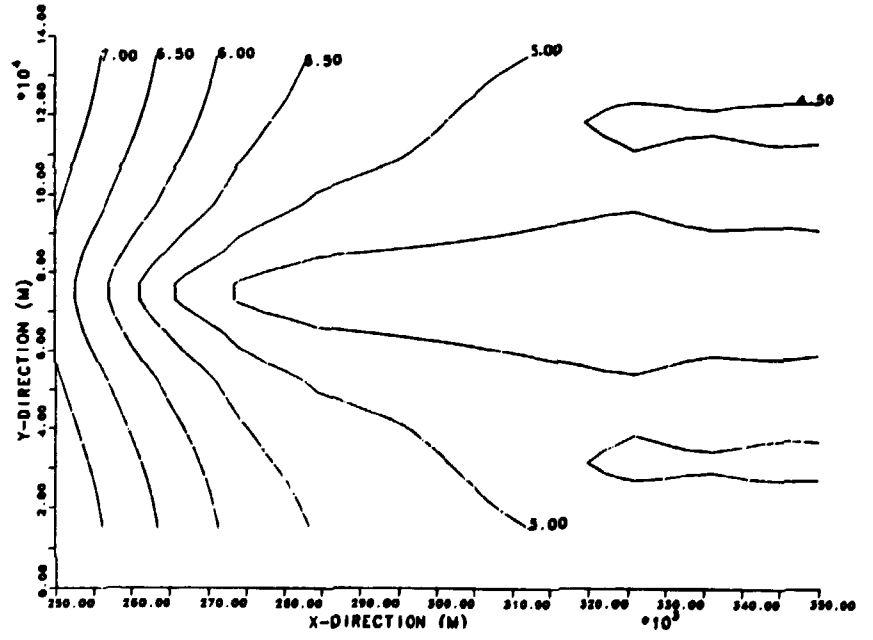


*Figure 4.38. Distribution of flux in the salt-shale system as reported by SWEARD. The results correspond to an infiltration rate in agreement with the case definition. The values on the contours should be multiplied by a factor of $10^{-17}$ to get the value in $m \cdot s^{-1}$.*

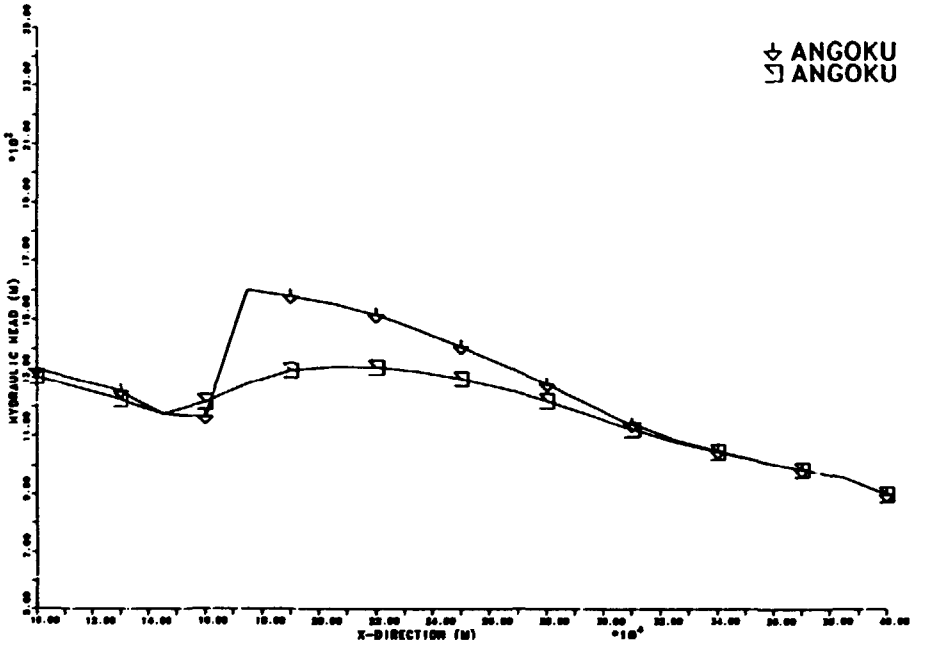


*Figure 4.39. Distribution of hydraulic heads along line 1 for the two formulations of boundary conditions as reported by ANGOKU. The first set of results corresponds to calculations with boundary conditions according to the case definition, whereas the second set corresponds to an infiltration rate adjusted to the capacity of the top soil layer.*

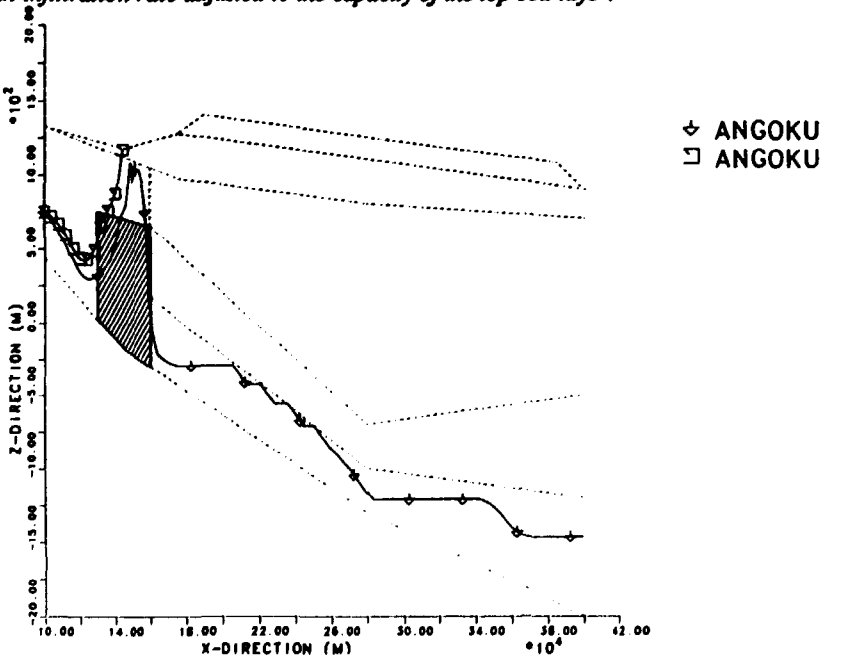


*Figure 4.40. Trajectory 3 as calculated by ANGOKU with two different infiltration rates, to be compared with Figure 4.39. The second set of results corresponds to the case with decreased infiltration.*

## 4.8 Case 7. Saturated Two-Dimensional Flow Through a Shallow Land Disposal Facility in Argillaceous Media

This case was set up to study the groundwater flow around a shallow land-disposal facility for low and intermediate level waste in an argillaceous medium.

For the case the waste was envisaged as being disposed of in parallel trenches about ten metres below the surface. Each trench was assumed to be protected by a concrete anti-intrusion shield, above which were layers of rolled clay and soil (Figures 4.41 and 4.42). The site consisted of horizontally bedded clay resting conformably on a 3 m thick aquifer. The aquifer overlaid an low-permeable clay formation and the boundary between them was abrupt. The clay had a hydraulic conductivity that varied continuously with depth. Two homogeneous and isotropic concrete boxes and their associated caps were embedded within the clay medium.

In the interest of simplicity, a two-dimensional fully saturated medium with idealised boundary conditions was chosen to enable a maximum number of codes to participate. The specified boundary conditions would impose a hydraulic gradient across the domain. The water table coincided with the sloping ground surface. A flooded clay pit was supposed to be located at the left of the domain, whilst at the right an empty clay pit was assumed with water seeping out of the vertical face.

For the case, a two-dimensional section perpendicular to the trenches and parallel to the direction of flow was to be modelled. The seepage face boundary condition on the right-hand end of the domain was simplified by assuming the medium to be fully saturated all along this end and at atmospheric pressure. Flow through the clay and rock was assumed to be fully saturated and to obey Darcy's law.

Two variants of the case were proposed in which the hydraulic conductivity of the concrete structures was substantially different, a low conductivity corresponding to poor quality concrete which may have resulted from physical, chemical or biological degradation and a higher conductivity equal to good quality intact concrete.

A mathematical model and input parameters were provided to the Project Teams. For the outputs the vertical velocity was required along three horizontal lines. Furthermore, twelve particle trajectories were to be calculated. Calculations were to be made for the two conductivities of the concrete blocks.

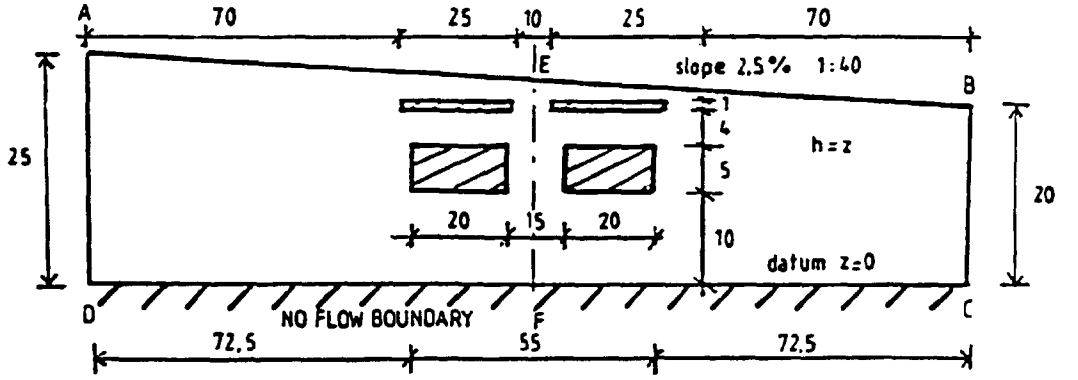


*Figure 4.41. Geometrical description of the domain.*

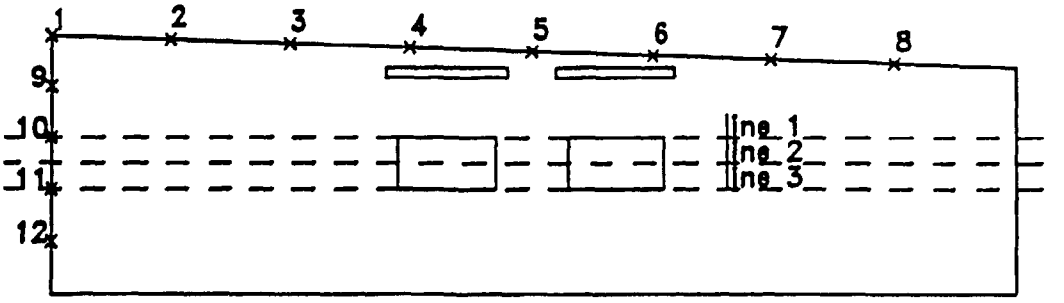


*Figure 4.42. Schematic view of the modelled area. Points 1—12 indicate starting positions for pathlines. Lines 1, 2 and 3 are lines along which the vertical velocities should be calculated.*

*Results from Case 7*

Thirteen teams tackled the case with a total of 15 codes, three of finite-difference type and the remainder finite-element codes. No analytical solution was provided for the case and the exercise consisted of intercomparing numerical results.

The permeability of the concrete blocks affected the velocity primarily within the blocks. An example of the vertical velocity for line 1 is given in (Figure 4.43). The spread of the results was reasonably small with only two codes deviating significantly. For one of these, the quality of the solution was probably affected by the use of triangular elements, for the second, the deviation in the results in the low permeability concrete blocks appeared to derive from the algorithm used to evaluate the velocity.

There was a general tendency that the spread of the trajectories was less pronounced with the high permeability blocks than with low permeability blocks (Figure 4.44). The spread with low permeability blocks was particularly pronounced for pathline 3, especially where the permeability contrasts appeared.(Figure 4.45). Due to numerical difficulties near the boundaries of the domain, some pathlines either went in the wrong direction or showed flutter close to the boundary.

In Test Case 7 the velocity field was evaluated in a situation with varying permeability and porosity. Principal difficulties in solving the case were related to the variation of the hydraulic conductivity and the porosity with depth, and the vertical seepage face at the right hand boundary. In general, the presented results agreed reasonably well. However, some significantly deviating results could be seen, mainly depending on differences in velocity evaluation procedures and the level of discretisation. The particle-tracking exercise revealed numerical difficulties near the boundaries. Indeed, one Project Team found that a pathline exited upstream from the release point.

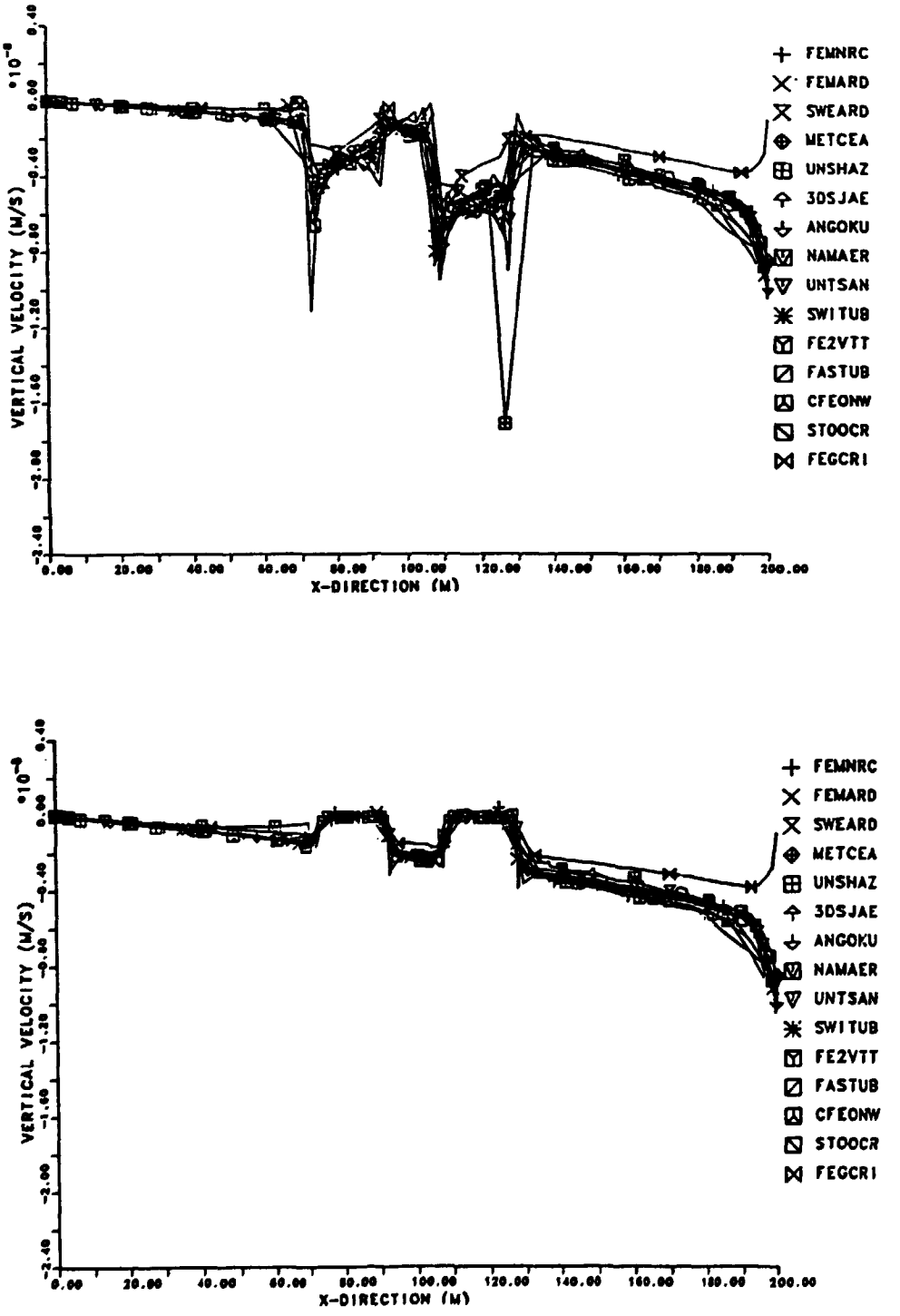


*Figure 4.43. Vertical velocities along line 1. Upper: high permeable concrete blocks. Lower: low permeable concrete blocks.*

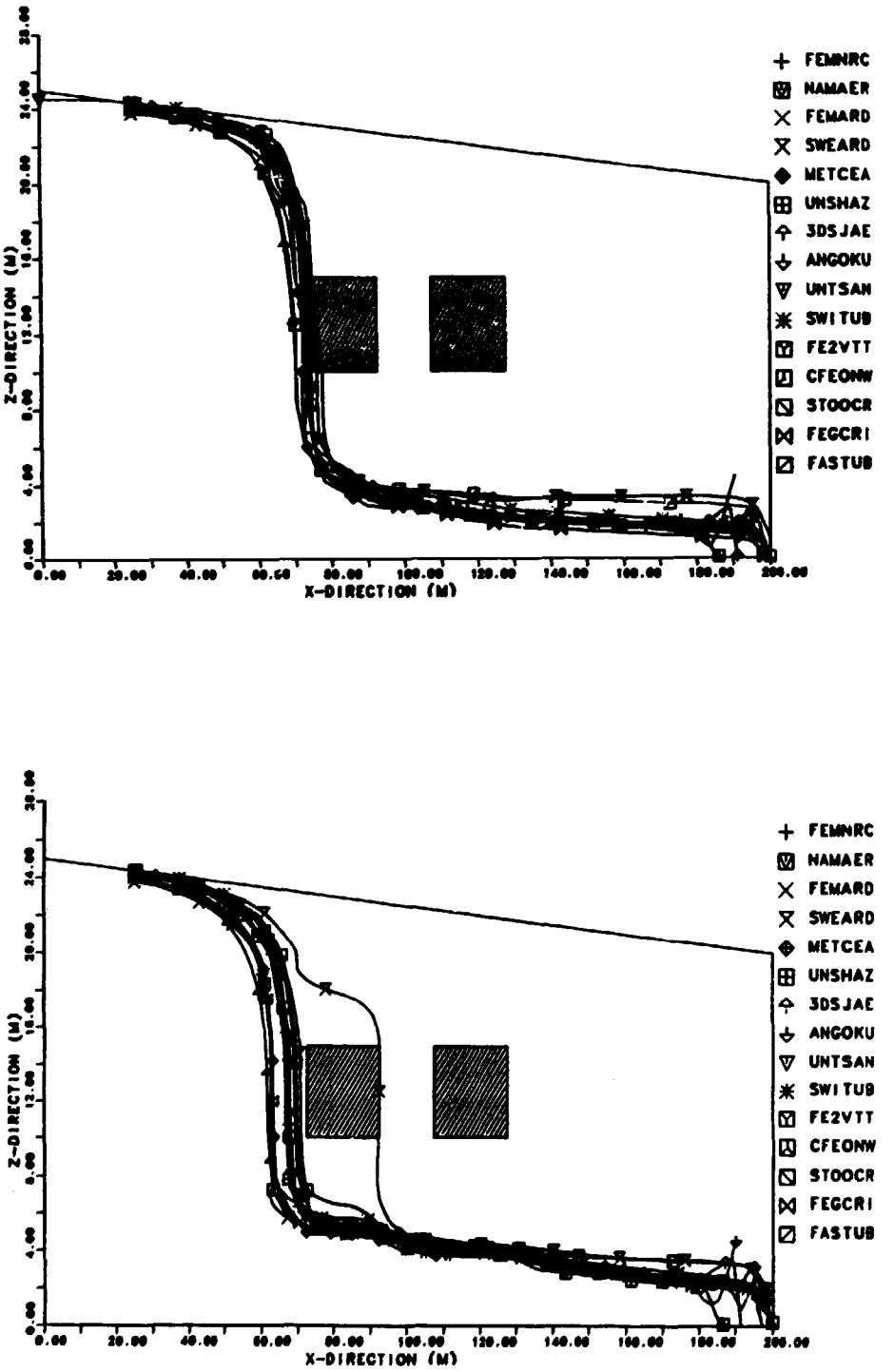


*Figure 4.44. Tracking of pathline 2. Upper: high permeable concrete blocks. Lower: low permeable concrete blocks.*

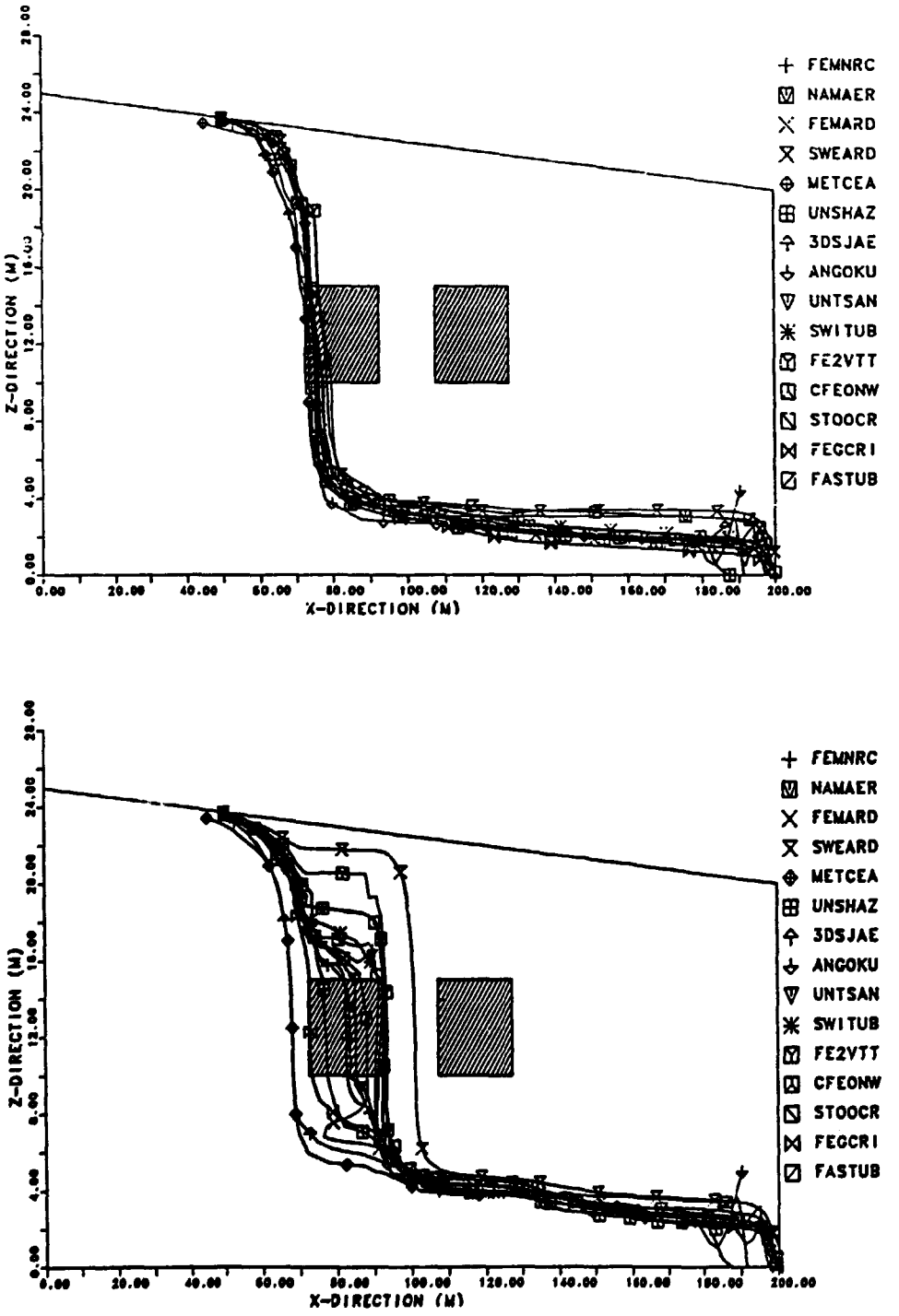


*Figure 4.45. Tracking of pathline 3. Upper: high permeable concrete blocks. Lower: low permeable concrete blocks.*

# 5. HYDROCOIN Level 2

## 5.1 Case Definitions. General

In Level 2 of the HYDROCOIN study, aspects of validation of groundwater flow models were analysed. In the context of groundwater flow modelling, the term model validation usually refers to the process of demonstrating the adequacy of models to describe natural hydrogeological systems, both structures and processes. Here, adequacy means adequate for the intended usage and does not imply absolute truth or accuracy, since even the most complex models are simplifications of the true systems.

Several organisations have formulated definitions of model validation in the context of nuclear waste management. The definitions generally indicate that the ability of the models to describe the real system must be tested by comparing modelling results with experimental data or other empirical observations. This process is complex and may include several steps, e.g.:

- formulation of an appropriate conceptual model (or suite of alternative conceptual models) based on available experimental evidence and field observations
- translation of the conceptual model/models and available data on the system being modelled into appropriate mathematical and numerical models of the system
- identification of appropriate goodness-of-fit functions for use in model calibration and validation, with due care taken to assure that the goodness-of-fit function is an appropriate measure of model adequacy for a given purpose
- calibration of the models with observations and experimental data
- development of model validation criteria
- calculation of the goodness-of fit functions from model predictions for a variety of conditions and data sets that are independent of the data sets and conditions used during the model calibration process
- assessment of the acceptability of the model or suite of alternative models using the values of the goodness-of-fit functions and other model results

Experiments and models are designed and tested iteratively with successive refinements until confidence is reached that an adequate level of understanding has been achieved. Although one attempts to reduce the subjective elements in the validation process, it is important to realise that the process always to some extent will be subjective.

There are particular problems in validation of models for repository performance assessments. Nuclear waste repositories are often associated with complex spatial variation of material properties, such as permeability and there is a need to make predictions which extrapolate the behaviour of the models over very long time periods, in general much greater than those over which the models have been tested. Furthermore, there will always be limitations in the level of detail with which a site can be described. The interpretation of site data for the modelling as well as the modelling strategies themselves also introduce uncertainties into the site assessment and are as such part of the validation problem. The handling of uncertainties are treated in Level 3 of HYDROCOIN.

In Level 2 of the study, the quality of the predicted results as compared to measured experimental values is expressed as goodness-of-fit measures. These measures were defined by individual

Project Teams analysing the test case in question, or formed part of the test case specification. In addition to the quantitative goodness-of-fit measures, more qualitative measures, such as visual inspection of results, were used.

Five test cases were defined for Level 2 based on experimental results which were available to the group. The criteria for selecting the experiments were:

— The physical flow situation studied in the experiment should be relevant to the performance assessment of radioactive waste repositories. The experiments should represent different types of media and cover a variety of spatial as well as temporal scales.

— The experiment should be the 'best available' of its kind.

The choice of experiments was based on the knowledge of the HYDROCOIN participants. Complex problems, in terms of data manipulation and simulation, were avoided due to the time and resource constraints of the study.

Due to availability of data, experiments which were not primarily designed for model validation had to be accepted as test cases. This implied that measured quantities might not always be those that were most relevant to model validation. Additionally, there were in most cases a lack of independent data sets for use in model calibration and assessment of model predictions. The characteristics of the Level 2 test cases are given in Table 5.1.

*Table 5.1 Summary of characteristics of the Level 2 test cases.*

| Case no | Physical processes addressed | Spatial scale | Temporal scale | Pilot Group |
|---|---|---|---|---|
| 1 | Coupled groundwater flow and heat transport | 3×15 m | 5.5 yrs | Harwell |
| 2 | Variable density flow and salt transport by analogy with heat transport | 150×600 m | 10 yrs | GSF |
| 3 | Groundwater flow in a crystalline rock | 200×150×50 m | <10 days/ steady-state | KEMAKTA AECL |
| 4 | Regional groundwater flow in low permeability rock | 80×80× 0.5 km | steady-state | SANDIA |
| 5 | Groundwater flow in an unsaturated soil | <10 m | 75 days | U.S. NRC |

## 5.2 Case 1. Thermal Convection and Conduction around a Field Heat Transfer Experiment

Heat generated by radioactive waste placed in a repository will lead to an increase in the temperature of the rock in and around the repository which varies in time. The governing processes are thermal conduction and convection. Conduction will be the dominant process for a repository in a low permeability rock.

Heat may also be transferred either by forced convection arising from groundwater flow generated by external pressure gradients, or by free convection arising from flow driven by buoyancy forces. The temperature rise will lead to buoyancy driven flow. This has important implications for radioactive waste disposal, since buoyancy driven flow is predominantly vertical near a repository. Hence, it could shorten the migration path and travel times from a repository to the biosphere or alter flow rates.

The objective of the test case was to test models for coupled groundwater flow and heat transport. The mathematical problem is non-linear, and in the test case both free and forced convection may be important.

The heat transfer experiment which formed the basis for the validation exercise was performed in a disused granite quarry. An electrical heater was located in a cased borehole. The temperatures in the surrounding rock were recorded at regular intervals. The equivalent permeability of the fractured granite was considerably greater in the vicinity of the heater than at greater depths. While the flow through the rock mass took place in discrete fractures, it was assumed for the test case, that the fractures were sufficiently closely spaced and interconnected for the rock to be reasonably approximated as a permeable porous medium (Figure 5.1).

The purpose of the experiment was to determine the heat transfer properties of rock. Due to the fact that most data consisted of temperature measurements, while there were only a few measurements of pressure head, the database was not ideal for validation of models for coupled groundwater and heat transport. Despite the obvious limitations, the test case was included in the study because of its general value in confidence-building.

The time-dependent temperatures were recorded with resistance thermometers in contact with the rock in the heater hole and in sixteen surrounding boreholes. In all, the temperature was sampled at 48 points located throughout a sphere with a radius of about 20 m around the heater.

Much of the collected data did not appear reliable enough for the test case. However, one of the boreholes seemed to give dependable results between 80 and 1900 days. Data from that borehole were then chosen as the primary data set for the validation exercise within HYDROCOIN.

One notable feature of the data was a marked temperature asymmetry between the top and bottom thermometers. The fact that the rock above the heater was significantly hotter than that below indicated that some thermal convection was taking place.

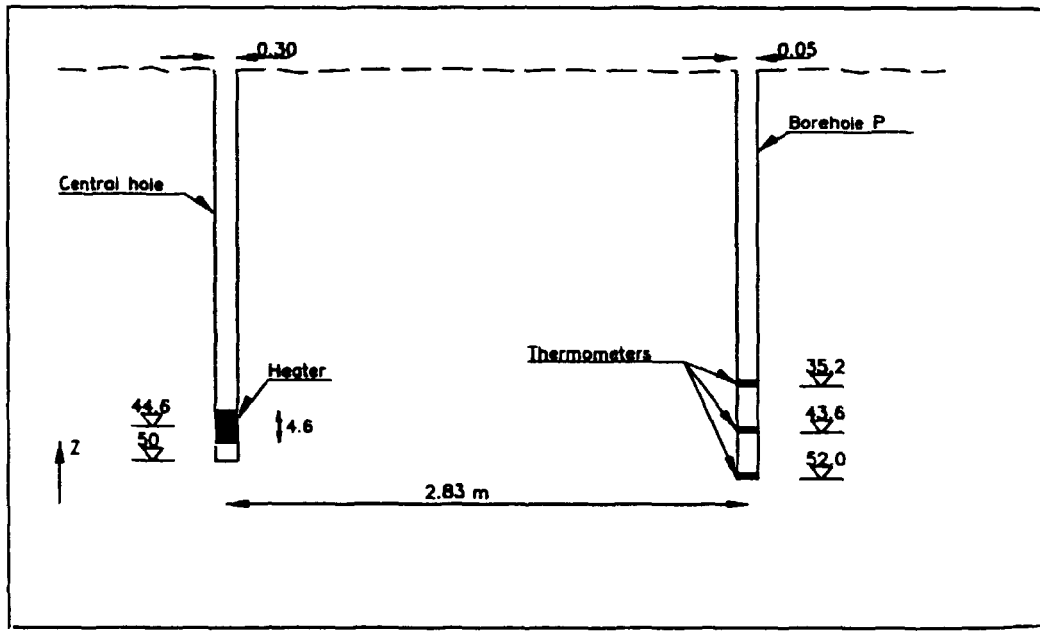


*Figure 5.1. Schematic of the geometry of the heater and borehole P.*

The data could be analysed to give in-situ values for the heat transfer properties of the rock mass such as the thermal conductivity and the effective permeability. In order to be able to judge whether such values were reasonable, they were to be compared with independent measurements. To this end, laboratory measurements were made of the density, specific heat and thermal conductivity of the rock. Furthermore, single hole permeability tests were performed. Unfortunately, no measured values of the specific storage or porosity were available.

For the conceptual model of the test case, the major flow paths through the rock mass were assumed to be approximately planar fractures intersecting one another to form a three-dimensional network. The complex system of intersecting flow paths was to be treated as an equivalent saturated porous medium, although a free interpretation was included as an option for the case.

Heat was considered to be transported by conduction through the rock and by convection of water. In addition, the following assumptions were made:

- The water and rock would have a common temperature field.
- In the absence of the heat source, the temperature was taken to be constant everywhere and the flow was vertically upwards, governed by the natural pressure gradient.
- The physical properties of the water and the rock were independent of pressure.
- The physical properties of the water and the rock were assumed to be independent of temperature except for the density and viscosity of water.

In the test case, the physical parameters derived from fitting a model to the experiment were to be assessed for consistency with other independent data. If two sets of parameter determinations agreed with one another within expected uncertainty bounds, then the model could be assumed

to have some degree of validity. This approach should be used in conjunction with the data to validate models of coupled heat transfer and groundwater flow.

Three levels of participation with increasing complexity were envisaged. The first two levels concerned validating the porous permeable medium model for the steady-state (*Subcase 1a*) or time-dependent (*Subcase 1b*) situation.

In *Subcase 1a*, the thermal conductivity and the permeability were to be fitted to "steady-state" data and compared with independent measurements to see if the fitted parameters were reasonable.

*Subcase 1b* was to be conducted as *Subcase 1a*, but in addition it was requested to fit the model to time-dependent data for a time-dependent power output.

*Subcase 1c* allowed free interpretation of the data.

### *Results from Case 1*

The case was analysed by seven Project Teams. Most of the calculations were made for *Subcase 1a*. Values of thermal conductivity and permeability were to be chosen to fit the pseudo steady-state vertical temperature profile in one of the boreholes and the chosen values were then to be compared with measurements. Three teams performed extensive parameter variations, including the introduction of additional physical concepts, such as anisotropic hydraulic and thermal conductivities. One team used adjoint sensitivity analysis as a guidance for adjusting the model parameters to obtain an improvement of the fit between the computed and the experimental results.

Two teams also made calculations for the transient *Subcase 1 b*, and two teams also tried to use alternative conceptual models within the framework of the free interpretation in *Subcase 1c*.

For the steady-state simulations, most of Project Teams used both qualitative and quantitative methods to assess the agreement between the measured and calculated temperatures in order to calibrate the model. They compared temperature profiles "by eye", and also used quantitative goodness-of-fit measures to make more quantitative comparisons. Usually, they compared their computed results with the temperature profile measured in one of the boreholes after 1470 days. The measured temperatures in holes at similar radial distances to the selected one were averaged in order to remove the traces of radial asymmetry in the experiment. The best-fit parameter values obtained by the Project Teams are listed in Table 5.2.

*Table 5.2. Best-fit values of thermal conductivity, permeability, and hydraulic gradients*

| Project Team | Thermal cond. ($W \cdot m^{-1} \cdot K^{-1}$) | Permeability ($m^{2)}$ | Gradient (m/m) |
|---|---|---|---|
| GWHKTH | 3.0 | $4.0 \cdot 10^{-13}$ | 0.025 |
| SW2NRC | 3.6 | $1.8 \cdot 10^{-13}$ | 0.025 |
| NAMHAR | 4.5 | $1.1 \cdot 10^{-12}$ | 0.0 |
| CHGCRI | 4.4 | $1.6 \cdot 10^{-12}$ | |
| 2DSJAE | 3.9 | $1.4 \cdot 10^{-12}$ | 0.0 |
| METEDM | 2.9 | $1.5 \cdot 10^{-13}$ | 0.075 |
| STOOCR | 4.0[a] | $2.0 \cdot 10^{-12}$ | 0.0 |

[a] The value in the table is the vertical component. The horizontal component is 3.6 $W \cdot m^{-1} \cdot K^{-1}$

Examples of the fits obtained are found in Figures 5.2 and 5.3.

Three of the teams got their best fits with a zero hydraulic gradient. These teams also reported significantly higher values for hydraulic and thermal conductivity than the other teams and the values were also higher than the measured data. One team, however, reported a high value for the hydraulic gradient and comparatively low values for the thermal and hydraulic conductivity. This illustrates the possibility that a unique calibration of the given model to a particular experiment may not exist. There may be several combinations of parameter values that can be judged to be acceptable. In the present case, the different best fits obtained by the Project Teams showed that conduction is inadequate to describe the experimental results and that significant quantities of heat are being transferred by convection. The difference between the teams is in the balance between free and forced convection.

One team performed a local sensitivity analysis with respect to rock porosity, vertical hydraulic gradient, hydraulic conductivity of rock, and thermal conductivity. The results proved to be fairly insensitive to variations of the porosity over three orders of magnitude, whereas a variation of the thermal conductivity with a factor of two caused significant changes in the computed temperature profiles (Table 5.3).

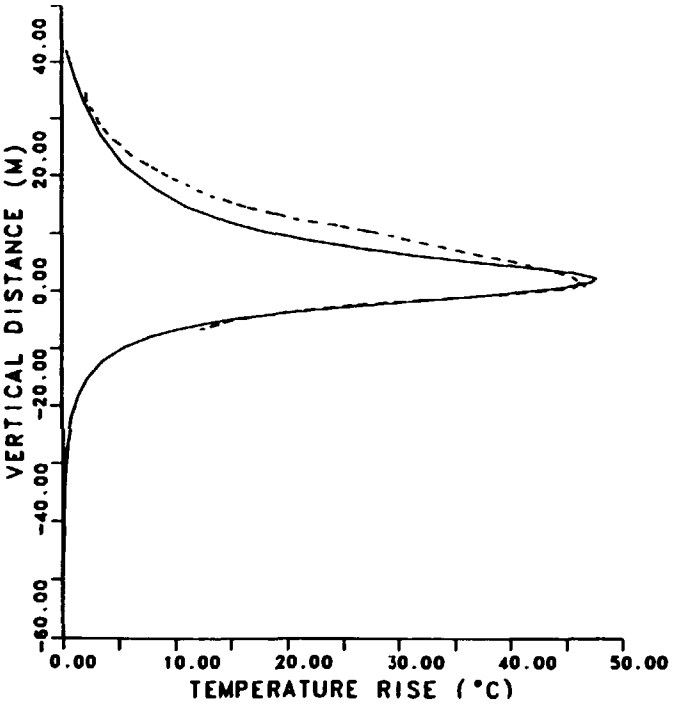


*Figure 5.2.Steady-state temperature profile in borehole P as calculated by SW2NRC. Dashed line corresponds to measured field data.*

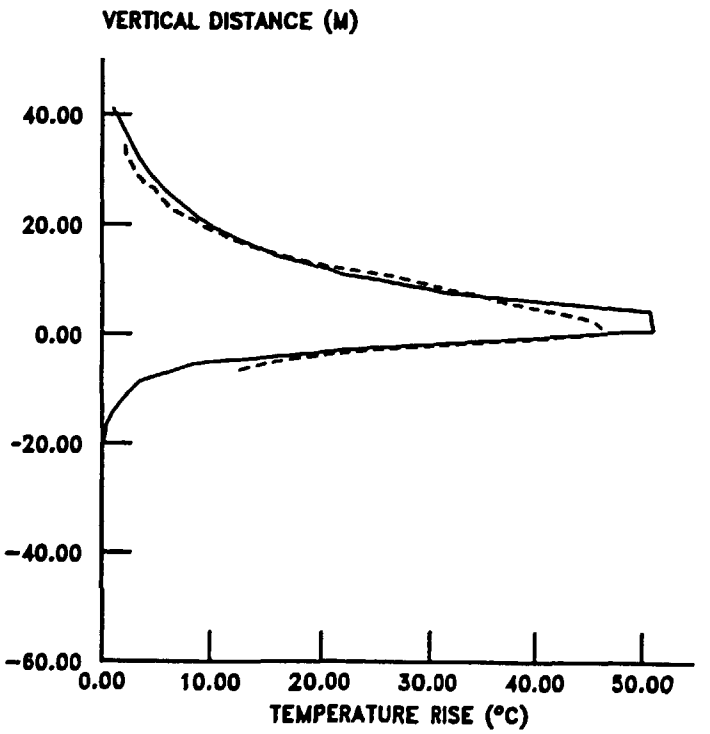


*Figure 5.3.Steady state temperature rise profile in borehole P as calculated by GWHKTH. Dashed line corresponds to measured field data.*

*Table 5.3. Relative importance of parameters as evaluated by stepwise and rank regression on 20 Latin Hypercube samples using three different performance measures.*

| Parameter | Squared temperature differences | | Peak temperature differences | | Vert. location of temperature peak | |
|---|---|---|---|---|---|---|
| | Linear | Rank | Linear | Rank | Linear | Rank |
| Hydraulic gradient | 0.42 | 0.08 | 0.30 | 0.22 | 0.18 | 0.15 |
| Thermal conductivity | 0.15 | 0.29 | 0.10 | 0.10 | 0.23 | 0.15 |
| Hydraulic conductivity (vert.) | 0.0 | 0.0 | 0.31 | 0.30 | 0.32 | 0.50 |
| Dispersion length | 0.14 | 0.12 | 0.19 | 0.25 | 0.08 | 0.09 |
| Thermal expansion | 0.0 | 0.18 | 0.0 | 0.08 | 0.0 | 0.01 |
| Heat capacity | 0.0 | 0.0 | 0.0 | 0.0 | 0.04 | 0.03 |
| Porosity | 0.0 | 0.05 | 0.0 | 0.0 | 0.0 | 0.0 |
| Hydraulic conductivity (isotr.) | 0.0 | 0.0 | 0.0 | 0.0 | 0.0 | 0.01 |

The Project Teams were asked to pass a judgement on the degree of validation obtained in Subcase 1 and answer the question to what extent the case for the model would be regarded asestablished. The answers are compiled in Table 5.4.

*Table 5.4. Approaches to model validation and conclusions regarding the degree of validation achieved. E denotes comparison of experimental and measured temperatures by eye and G denotes use of a quantitative goodness-of-fit function.*

| Project Team | Approaches | Conclusions |
|---|---|---|
| GWHKTH | E | probably proven |
| SW2NRC | E, G | not proven |
| NAMHAR | E, G | not proven |
| CHGCRI | G | |
| 2DSJAE | G | probably proven |
| METEDM | E | not proven |
| STOOCR | G | not proven |

Calculations for the time-dependent *Subcase 1b*, using the best estimates of thermal conductivity and permeability obtained from *Subcase 1a*, and comparing by eye the calculated evolution of the temperature at the three main measurement locations with the measured evolution showed that the general behaviour of the calculated and measured evolution was similar, but also that the fit was poorer than for the steady-state case. This result casts some doubts on the validity of the quasi steady-state assumption used for calibrating the model.

Variations taking into account a heater breakdown and a later incurred stepwise increase in heater power resulted in a better fit between the calculated temperature responses and the measured temperatures. The time for recovery of the temperature field after heater disturbances seemed to be fairly well represented by the model, whereas the calculated temperatures for the top and bottom thermometers were systematically lower than the measured temperatures (Figure 5.4).

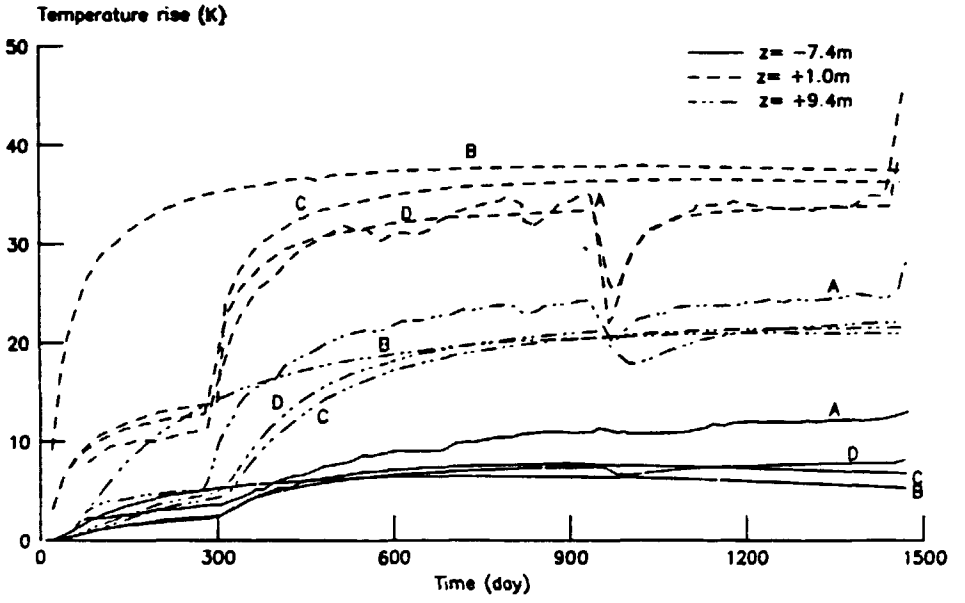


*Figure 5.4. Transient temperature rise in borehole P for top, middle and bottom thermometers as calculated by METEDM. Three different representations of the temporal variation of the heater power output was used. A: experimental results; B: 8 kW for 1470 days; C: 3 kW for 280 days and 8.5 kW for days 281—1470; D 3 kW for days 0—280, 8.5 kW for days 281—940, 0 kW for days 941—968, 8.5 kW for days 969—1446, 14 kW for days 1447—1470.*

As for alternative interpretations of the experiment (*Subcase 1c*), one team made several calculations in an attempt to find an improved agreement between calculated and experimental results. They examined such effects as:

- anisotropy of permeability
- alternative equations of state for the groundwater
- conduction in the steel casing in the heater borehole
- possible heat-pipe effect in the granular packing between the casing and the borehole wall
- damaged zone of altered permeability near the borehole
- variation of permeability with depth

None of the attempts gave significantly better agreement between the model and the experiment. It was also concluded that a pure heat conduction model could be ruled out, since the results obtained from such models were considerably poorer than the convective models.

As a result of studying Test Case 1 the Project Teams gained a degree of confidence, both in the ability of the given mathematical model to generally represent the processes of groundwater flow and heat transport in geological media, and to apply the model to the specific experimental site. The model proposed in the definition of the test case could represent many of the features of the experiment. However, the discrepancies remaining between measurements and the results of the model were sufficiently large to imply that the model could not give a complete description of the experiment. Furthermore, the fact that the database is limited, also limited the degree of support provided for the model.

The agreement between the model and the experiment provided some support for the use of porous medium models when analysing heat transport in fractured crystalline rocks.

The Project Teams agreed that the model of coupled groundwater flow and heat transport could not be validated using the data presented in this case, the main reason being that under the circumstances of the experiment there appeared to exist an important, albeit small effect that was not included in the model.

The inability of the model to predict at the same time both peak temperature and skewness was taken as an indication of incomplete description of the physical features of the experiment. It is clearly desirable that features which are considered important in repository performance assessment should be adequately modelled. At the same time, it is also necessary to show that all available data can be adequately explained. Thus, the goodness-of-fit function should be chosen to assess the adequacy of the model for all the data, bearing in mind the quantities likely to be particularly important for repository performance assessment.

The database from the experiments was not ideal for validating models of coupled groundwater flow and heat transport, since it consisted almost entirely of temperature measurements. However, the test case proved extremely valuable as an example exercise for validation with limited data. The test case is a good illustration of the need for careful design of experiments for validation and the fact that validation is inherently an iterative process. Initial experiments will ordinarily provide some support for a model or possibly rule it out. Additional experiments are then required to provide more confidence in the model.

## 5.3 Case 2. Model for Variable Density Fluid Flow Based on a Laboratory Experiment with Thermal Convection

The test case addresses validation of variable density groundwater flow models. Initial results obtained during the verification exercise of Case 5 in Level 1, which included the modelling of idealised groundwater flow over a salt formation influenced by density variation, varied considerably between the different Project Teams. The case proved to be very complex with the presence of both free and forced convection. Convection cells appeared within the flow domain.

The present test case, which represents a less complex problem involving only free convection, was proposed to study the behaviour of the convection cells in detail. The basis for the case was a laboratory experiment published by Elder in 1967. In that study, transient heat convection in a Hele-Shaw cell was investigated. In the definition of the test case, an analogy between heat and brine transport was assumed to be valid. The physics of the original Elder experiment,

involving a fluid heated from below, was transformed into an equivalent situation involving dissolution of salt at the top boundary of the domain. The form in which the experimental data were represented in the original report did not allow a quantitative comparison between the calculations and the experiment. Instead, two photographs of the convection cells, published in the experimental report, could be used for qualitative judgement of the results of the validation exercise.

For the conceptual model, a two-dimensional vertical flow domain of saturated homogeneous porous medium was contemplated. The flow was supposed to be driven by density variations caused by differences in salt concentration. The flow was assumed to be isothermal and governed by Darcy's law. To preserve as much correspondence with the heater experiment as possible, velocity dependent hydrodynamic dispersion was neglected and only a constant molecular diffusion coefficient was considered.

In addition to a set of dimensionless parameters chosen by Elder for both the laboratory and numerical experiment, a set of physical input parameters were supplied, which matched the dimensionless parameters used by Elder but for an enlarged model domain.

The requested output was restricted to a qualitative comparison of the results of numerical models with that of the laboratory experiment. Stream-function and concentration distributions at six different times were sought.

### *Results from Case 2*

The case was attempted by three Project Teams using four computer codes. For comparison, the results of the numerical model of Elder (NUMELD) was also considered. Two of the models used the Boussinesq approximation to simplify the set of governing equations. Examples of the results for stream-function distributions are given in Figures 5.5 and 5.6.

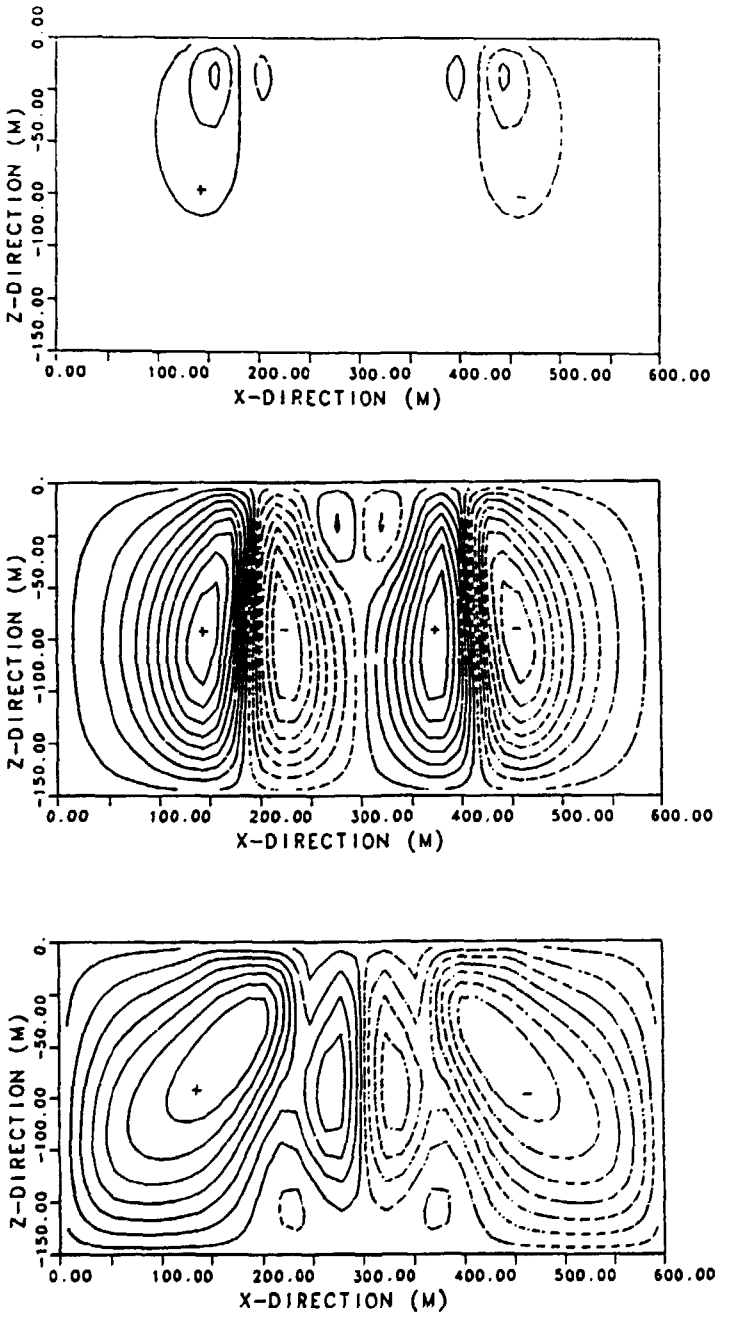


*Figure 5.5. Stream-function distributions calculated by FASGSF at times of 1 year (upper), 4 years (middle), and 10 years (lower). The plus and minus signs indicate the rational direction of the convection cells such that plus corresponds to a counter-clockwise rotation and minus to a clockwise rotation.*

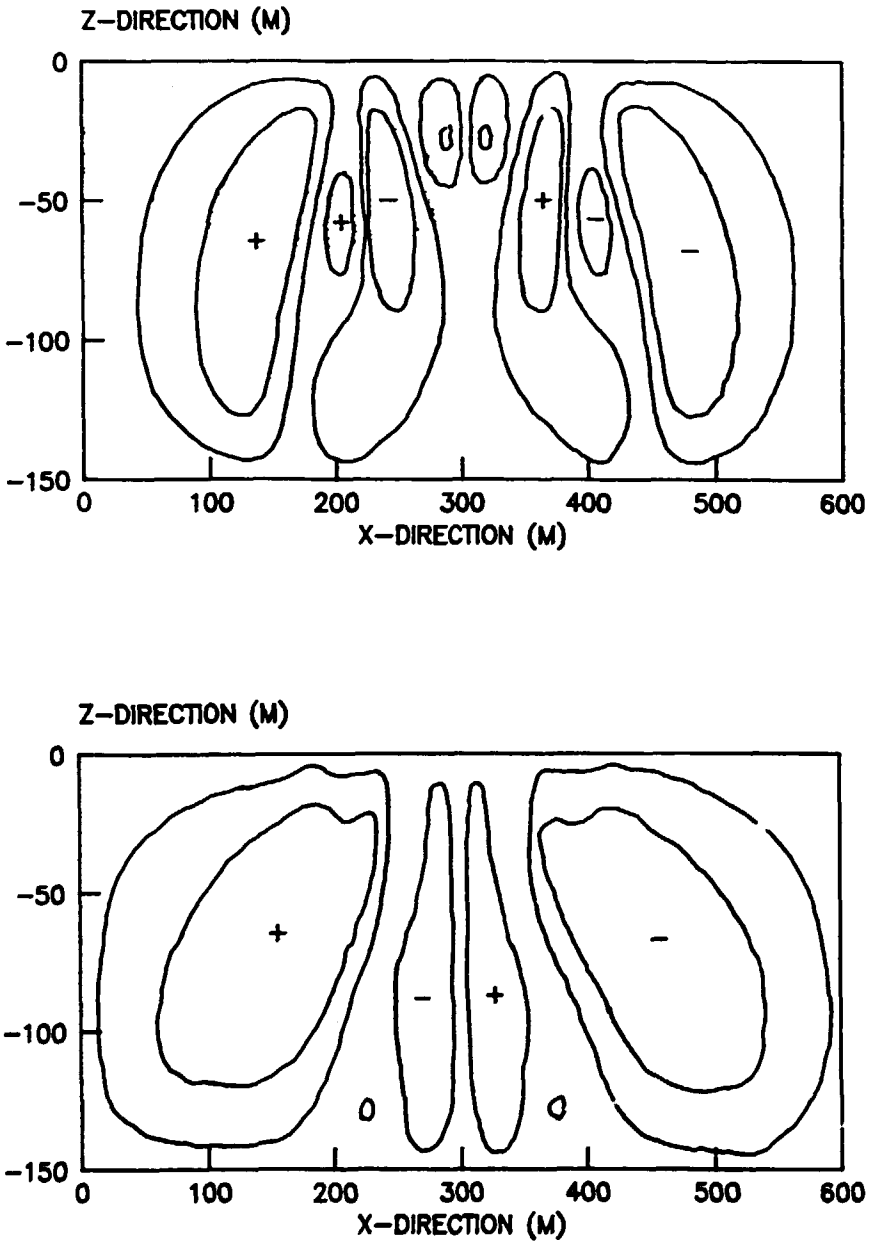


*Figure 5.6. Stream-function distributions calculated by NUMELD. The plus and minus signs indicate the rational direction of the convection cells such that plus corresponds to a counter-clockwise rotation and minus to a clock-wise rotation. Upper: dimensionless time 0.025 (5 years); lower: dimensionless time 0.05 (10 years).*

The results at the time of 1 year show very modest development of the stream-function for the reported results, while at 4 years, in all the calculations, a total number of six cells of different sizes are present. This is in agreement with Elder's experimental photograph. At 10 years four cells are present, also in conformity with Elder. The results from one team indicate that the discretisation apparently has some influence on the calculated results, a finer grid giving smoother curves and removing a pair of eddies at the base of the domain.

Examples of calculated concentration contours are shown at 1, 4, and 10 years in Figures 5.7 and 5.8. This contributes to further confidence in the ability to solve the governing equations for the assumed mathematical model. It should be pointed out, however, that the model of variable density fluid flow used in the test case could not be properly validated due to lack of well established experimental data. Further, the test case assumed the validity of an analogy between heat and salt transport, which is probably true for low concentrations but not for high concentration differences, because the Boussinesq approximation not being applicable to the high concentration situation.

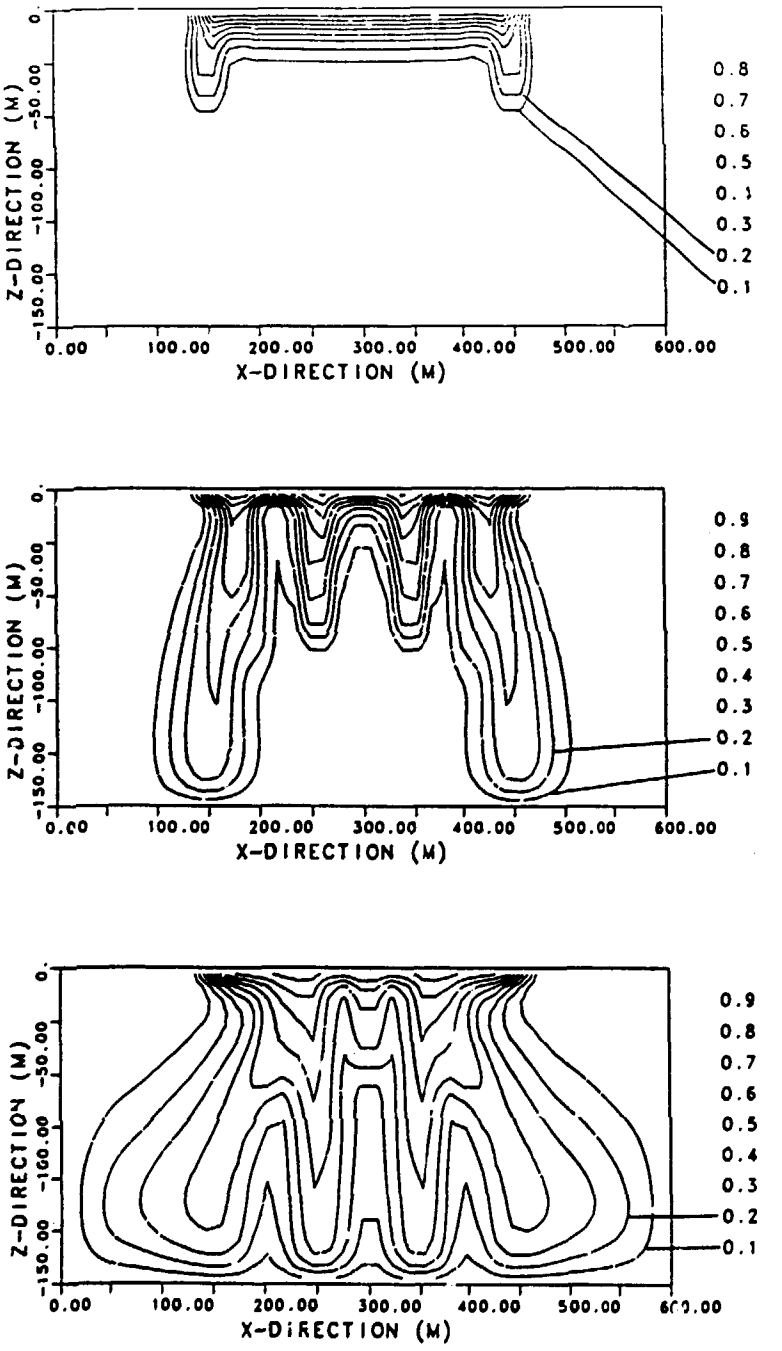


*Figure 5.7. Concentration distributions as calculated by MTRRIV at times of 1 year (upper), 4 years (middle), and 10 years (lower). The spacing between the contours is 0.1.*

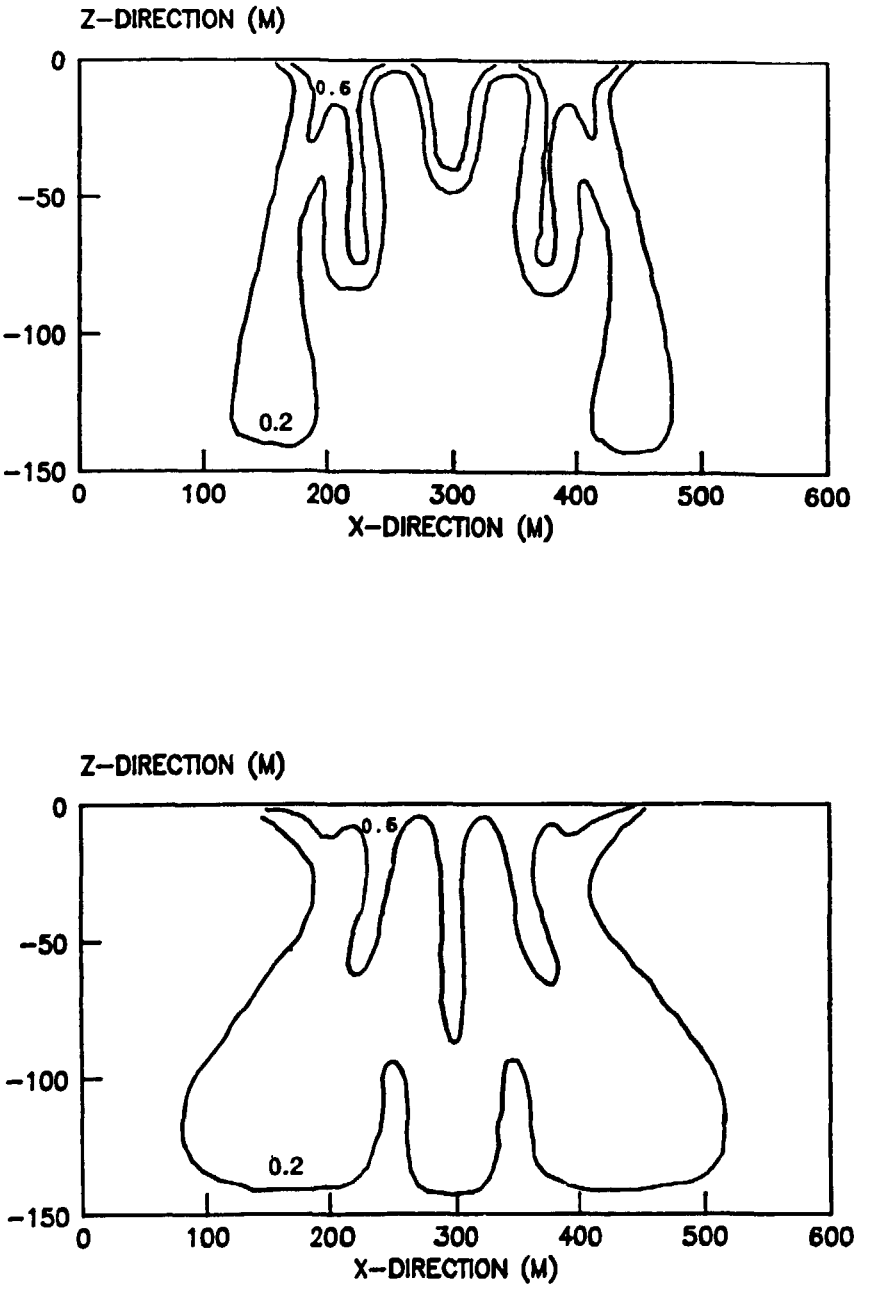


*Figure 5.8. Concentration distributions calculated by NUMELD. Contours are shown for the concentrations 0.2 and 0.6. Upper: dimensionless time 0.025 (5 years); lower: dimensionless time 0.05 (10 years).*

## 5A Case 3. A Small Groundwater Flow System in Fractured Monzonitic Gneiss at AECL's Chalk River Research Area

Test Case 3 concerned validation of models for groundwater flow in fractured crystalline rock on a 100 m scale. The case was a three-dimensional problem providing data sets for both steady-state and transient modelling. The site and data were judged well fitted for the validation of the site-specific aspects of model validation (model calibration).

The case was based on investigations at the Chalk River Nuclear Laboratories (CRNL), which were performed to define the hydrogeology of a small groundwater flow system in fractured monzonitic gneiss. The site, located about 200 kilometres northwest of Ottawa, Ontario, consisted of a 200 m by 150 m area of predominantly quartz monzonite, overlain and underlain by paragneiss with inclusions of other rock types.

The experimental programme on the site comprised:

- fracture system characterisation
- injection tests
- hydraulic interference tests
- hydraulic head monitoring

17 boreholes were drilled. Vertical and lateral hydraulic interference tests, tracer tests, groundwater sampling and long-term hydraulic head monitoring were made during the investigations at CRNL.

Results from fracture system characterisation, injection tests, hydraulic interference tests, hydraulic conductivity tensor evaluation and hydraulic head monitoring were combined and interpreted to provide a three-dimensional picture of the groundwater flow system at the site. Four major fracture zones were identified by the injection tests and their existence was confirmed by the results from the interference tests. Two of the fracture zones were oriented subhorizontally, one was inclined and one was vertical (Figure 5.9).

The equivalent single-fracture apertures and storativities of the fracture zones were evaluated from injection and interference tests. A typical value of the storativity was about $10^{-5}$ and a typical value of the fracture aperture was about 100–900 $\mu$m. The drawdown responses were also used to determine the vertical hydraulic diffusivity in the rock mass giving an average value of about $2 \cdot 10^{-4}$ m·s$^{-1}$.

Hydrographs of borehole test intervals were used to identify periods with minimal hydraulic head fluctuations for determination of equilibrium hydraulic head distributions. The tests indicated a relatively simple recharging groundwater flow system directed north and northwest. The horizontal component of flow was governed by surface topography. Vertical and horizontal hydraulic gradients at the site averaged 0.15 and 0.02 respectively.

For the conceptual model, it was assumed that it would probably be necessary to model the site in three dimensions in order to simulate the general flow pattern. The boundary condition on the top could be approximated with a constant head equal to the ground elevation. As no flux measurements or measurements of the groundwater infiltration rate were available at the time

of the pumping tests, the constant head approximation was also recommended for transient modelling.

The bottom boundary condition was proposed to be a constant head in the horizontal fracture zone. The vertical boundaries in the south, west and east were proposed to be no-flow boundaries, and the virtually impermeable diabase dyke seemed to form a natural boundary to the south. For the case, it was also proposed that the density and viscosity of the groundwater would be constant over the entire site and that it was appropriate to apply linear potential flow models.

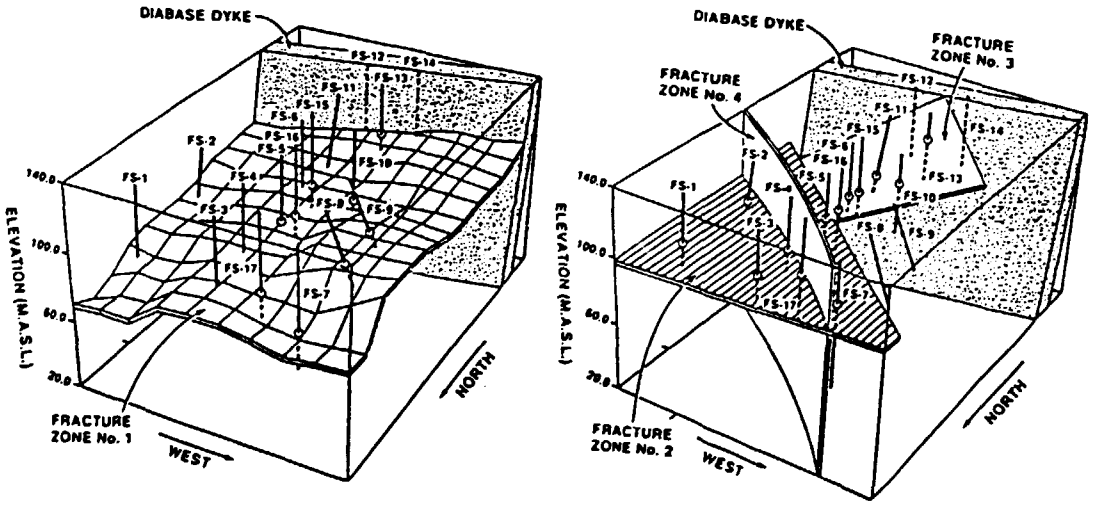


*Figure 5.9. Isometric sketch of the test site showing the locations of boreholes, diabase dyke, fracture zone 1 (left) and fracture zones 2, 3 and 4 (right).*

Three levels of effort were proposed for simulations:

a) prediction of steady-state hydraulic heads using evaluated hydraulic conductivity tensors or scalars, assuming a porous medium model

b) prediction of the transient responses to a set of pumping test responses assuming the same hydraulic properties as in a) and the storativities and hydraulic diffusivities evaluated from the hydraulic interference tests

c) free interpretation of the reported data to predict the measured piezometric heads and, optionally, a set of pumping test responses

*Results from Case 3*

The case was analyzed by seven Project Teams. All but one applied equivalent porous media models of the finite-element type. One team used a stochastic network model.

An unbiased evaluation of the case would have involved a substantial effort both in terms of manpower and computer resources. Four teams therefore restricted their approach to tackle only the steady-state hydraulic head simulation. One team complemented the steady-state calibration with one simulation of a transient pumping test, whereas another team concentrated on the transient data after having showed that the steady-state data contained too little information for a proper model calibration and that the proposed boundary conditions led to an identifiability problem.

In order to evaluate the fit between calculated and observed values, the Project Teams used different strategies, including visual comparisons and comparison by means of quantitative goodness-of-fit functions.

The extensive data base for this test case was thought to be particularly valuable, since it included data from independent measurements and from measurements at different locations and times. Consequently, independent data sets could be used for model calibration and prediction. Due to cost and time constraints, this possibility was only exploited to a limited extent. Most teams, therefore, restricted their efforts to the steady-state hydraulic head analyses part of the test case and the modelling results presented for the test case were calibration exercises based on the steady-state hydraulic heads measured. The results were presented in terms of calculated head profiles along the boreholes. The calculated heads were then compared with the measured. Figure 5.10 illustrates the type of head profiles for one of the boreholes computed with a porous media code. The result shown represents the best-fit obtained after manual trial-and-error calibration.

One team made an attempt to predict a transient pumping test using a fully three-dimensional model, whereas another team used a quasi three-dimensional model, in which the fracture zones were two-dimensional elements and the rock between the zones was described with one-dimensional elements. By using this later approach, the team could afford model calibration using transient data and automatic inverse modelling. As part of a model development process, one of the teams applied a fracture network model in which the rock matrix was either not represented at all or represented only by a network of randomly oriented fractures.

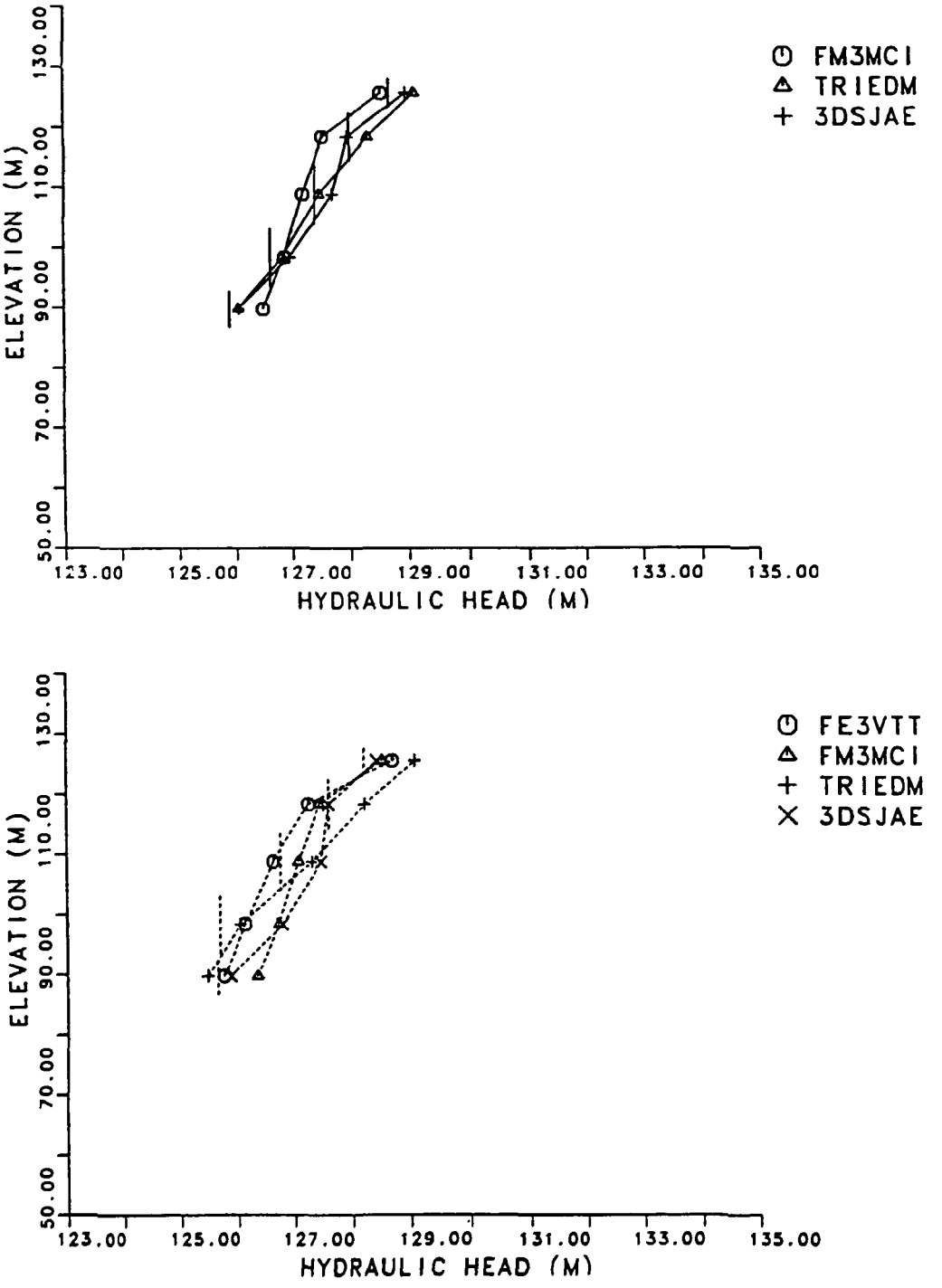


*Figure 5.10. Computed hydraulic head profiles along borehole FS 1 compared with experimental values with FS 10 closed (top) and open (bottom). Solid and dashed vertical bars correspond to borehole test intervals.*

Since most of the teams varied only the hydraulic conductivity of the various units, it was possible to compare the selected best-fit values of these parameters, as is shown in Table 5.5. In addition to the porous-media model parameters, also the fracture network model parameters used by one team and the quasi 3-D data obtained by another team are shown in the table.

*Table 5.5 Best-fit hydraulic parameters.*

| Parameter | FE3VTT | FM3MCI | NAPHAR | TRIEDM | 3DSJAE |
|---|---|---|---|---|---|
| **Hydraulic conductivity of rock mass ($m \cdot s^{-1}$):** | | | | | |
| *Upper part* | | | | | |
| $K_x = K_y$ | $10^{-9}$ | $10^{-8}$ | NA | $10^{-10}$ | $1 \cdot 10^{-8}$ |
| $K_z$ | $10^{-10}$ | $10^{-9}$ | NA | $10^{-10}$ | $2 \cdot 10^{-9}$ |
| *Lower part* | | | | | |
| $K_x = K_y$ | $10^{-9}$ | $10^{-9}$ | NA | $10^{-10}$ | $1 \cdot 10^{-9}$ |
| $K_z$ | $10^{-10}$ | $10^{-10}$ | NA | $10^{-10}$ | $1 \cdot 10^{-10}$ |
| **Transmissivities of fracture zones ($m^2 \cdot s^{-1}$):** | | | | | |
| Zone 1 | $10^{-7}$ | $10^{-5}$ | $4.5 \cdot 10^{-5}$ | $10^{-5}$ | $3 \cdot 10^{-6}$ |
| Zone 2 | $10^{-7}$ | $10^{-7}$ | $5.7 \cdot 10^{-6}$ | $10^{-5}$ | $3 \cdot 10^{-6}$ |
| Zone 3 | $10^{-7}$ | $10^{-7}$ | $1.1 \cdot 10^{-8}$ | $10^{-5}$ | $1 \cdot 10^{-8}$ |
| Zone 4 | $10^{-8}$ | $10^{-7}$ | $7.1 \cdot 10^{-7}$ | $10^{-6}$ | $2 \cdot 10^{-7}$ |

There was a reasonably good agreement between the best-fit rock mass conductivities reported by the Project Teams and the experimental data. The fitted values were in general somewhat lower than the experimental data. The Project Teams that used a tensor representation all obtained a factor of 10 as the best-fit ratio between the horizontal and vertical conductivity components. This appears to be in fair agreement with the experimental results.

The best-fit values of the fracture zone transmissivities tended to be lower than the experimental data. It was shown by one team that despite the good overall fit between measured and computed hydraulic heads (see Figure 5.11), the models failed to represent the very flat piezometric surface observed in this zone in the field, due to the low best-fit transmissivities in zone 1. It was concluded that the zone was likely to be heterogeneous with highly permeable areas which efficiently transmit pressures, while the average transmissivity, as evaluated from the aquifer tests, are lowered by the presence of low-conductivity areas.

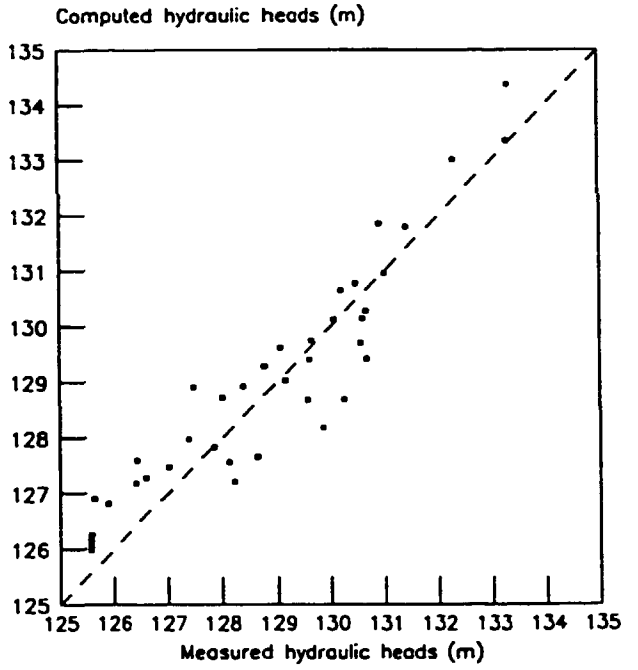


*Figure 5.11. Comparison between measured and computed hydraulic heads as obtained from INVUPC by automatic calibration of the steady-state model. The conceptual model used was model 1 (the simplest).*

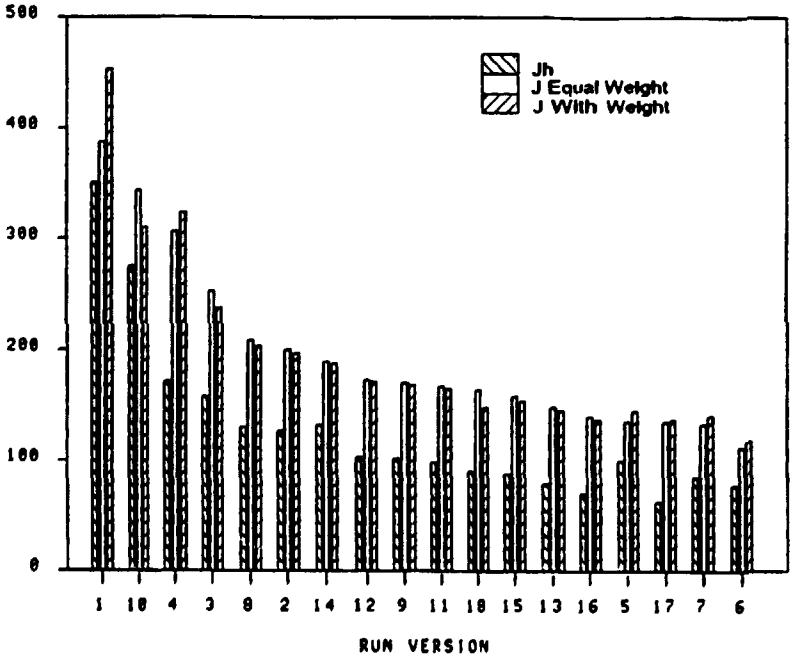


*Figure 5.12. Calibration simulations by FM3MCI sorted in order of decreasing value of the goodness-of-fit function. Three different types of functions have been used.*

The geometries of the fracture zones were poorly specified in the test case description, since the modelled domain extended outside the bounds of the study site. In fact, results from one team employing steady-state model calibration indicated that the amount of information available in the head measurements was insufficient for a proper model calibration.

Generally, the best-fit values seemed to be lower than the experimental data, although the uncertainty, as evaluated from the spread of results, was a factor of 10 or more. TRIEDM used the model parameters obtained in steady-state calibration in simulating the transient pumping test performed in one of the boreholes. The resulting drawdown as a function of time shows little resemblance to the measured data, except for single borehole sections (see Figure 5.19). The Project Team concluded that this indicates an uncertainty regarding the fracture zone geometry applied.

The various Project Teams obtained slightly different solutions. Since all teams used similar boundary conditions and grid densities, the differences in the shape of the predicted hydraulic responses are likely to derive from a combination of differences in permeability distributions and fracture zone geometries. As the geometries of the fracture zones were poorly specified in the test case description, the distribution of hydraulic properties over the site was either too complex to be handled in a reasonably sized numerical model or poorly laid down by the experimental observations.

It was thus concluded that none of the best-fit hydraulic conductivity distributions in table 5.5 was more valid than the others. All teams concluded that the predominant feature is the downward flow caused by fracture zone "1". FM3MCI seemed to more correctly identify the structural features of the site. This team also applied goodness-of-fit functions which included penalty criteria for deviation of the fitted hydraulic properties from their prior estimates. A demonstration of the influence of these penalty criteria is shown in Figure 5.12. Obviously, the choice of a goodness-of-fit function has an effect on the ranking of the simulations. It was concluded by the Project Team that a firmer theoretical background for the selection of penalty criteria is needed. The exercise shows, however, that a trial-and-error procedure combined with an appropriate goodness-of-fit function is a valuable tool for model calibration in the absence of an inverse model. Such a model was employed by INVUPC for calibrating transient pumping tests.

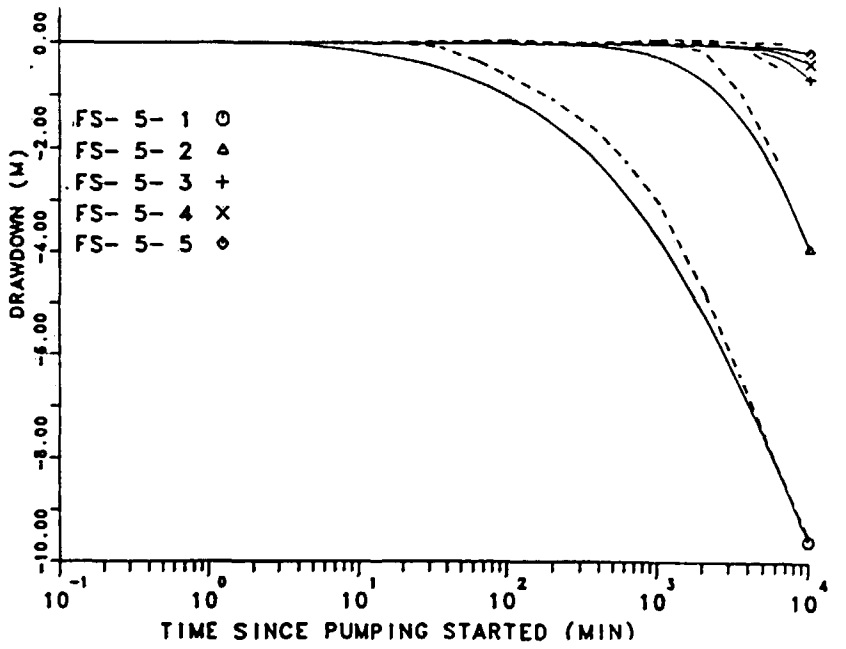


*Figure 5.13. Best fit obtained by INVUPC during calibration of model 4. Dashed lines are measured drawdowns in FS 5 as response to pumping in FS 10 and solid lines are computed responses.*

As opposed to the Project Teams employing equivalent porous medium models the Project Team NAPHAR applied a fracture network model to this test case. Examples of results obtained by using a best-fit five-zone model are shown in Figure 5.13. The Project Team did not find that the five-zone model explained the experimental results. The inclusion of 1500 randomly oriented fractures of a uniform size and uniform aperture did not change the situation. However, the inclusion of two extra fracture zones not mentioned in the reported experiment improved significantly the overall results. The team also observed that head values very easily can be distorted by local influences and believed flux measurements to be a better means for validating these types of models.

It was noted that model calibration based only on heads is ambiguous, if also the boundary conditions are expressed as heads. Since scaling of all hydraulic conductivities in the domain with a constant factor still would yield the same field of hydraulic heads, flux data are also needed to define the system adequately.

The degree of agreement between computed and measured data was judged to be fair, although with some local discrepancies. All teams identified the main flow mechanisms. Once the flow pattern had been established, the models were moderately insensitive to variations in other parameters.

The experiment at Chalk River constitutes one of the few available experimental programmes originally designed to help in the validation of groundwater flow models. Despite the extensive data base available, the Project Teams suggested additional experiments to make the data even

more valuable for validating groundwater flow models. To this end, it was emphasised that it was essential to get measured flux data to complement the piezometric data of hydraulic heads.

## 5.5 Case 4. Three Dimensional Regional Groundwater Flow in Low Permeability Rocks

Many repository concepts involve host rocks which have low permeability as a principal safety feature. This test case was selected as an example of such characteristics. The objective was validation of models by using the data from a regional field study which may be regarded as typical in terms of data density. The participating teams were asked to compare parameters and results of a calibrated model with prior estimates of hydraulic parameters and results of other applied models.

As for any regional flow system, there is for this case a large degree of uncertainty in the prior estimates of hydraulic parameters. The data base for the case includes assigned ranges to prior estimates of parameters. These ranges should be regarded as an expression of the uncertainty introduced by the generalisations made on a regional scale rather than as uncertainties inherent in the measurements.

The area to be simulated for the problem was the Piceance Basin located in the northwestern part of Colorado, United States. The Basin is a structural depression within the Rocky Mountains physiographic province. The bedding of sedimentary deposits within the basin generally dips gently inwards and towards the northeast margin. The Uinta and Green River Formations, the youngest regionally continuous geological units within the basin, contained the hydrostratigraphical units to be simulated. The Parachute Creek Member of the Green River Formation was subdivided into four hydrostratigraphical units. The Uinta Formation, extending from the top of the Green River Formation to the surface, was included as a single unit (Figure 5.14 and Table 5.6). Zone 3, the principal oil shale horizon, might be viewed as a confining unit dividing the sequence into two aquifers, the lower comprising zones 1 and 2 and the upper comprising zones 4 and 5.

Groundwater flow within the low-permeability rocks of the basin is probably dominated by flow within fractures. However, the fractures were considered to be sufficiently frequent to allow the use of Darcy's law on the regional scale. Horizontal flow within the basin is generally from south to north, except in the extreme southern part, where flow is directed towards the canyons in the south. As the boundaries of the groundwater system were well defined, the edges of the units could be treated as no-flow boundaries. The same conditions applied also for the zone underneath the Parachute Creek Member.

Recharge to the Piceance Basin originates from the infiltration of snow-melt. The annual rate of precipitation is generally highest at high elevations on the south, east and west margins of the basin. Discharge from the basin occurs at seepage faces on the southwest margin as base flow to the principal streams draining the central part of the basin.

The purpose of the test case was to test the ability of the computer codes to simulate large-scale, three-dimensional flow in low-permeable, anisotropic rocks. The scope of the problem was limited by the method of parameter specification. Thus, issues such as spatial correlation of hydraulic parameters could not be addressed.

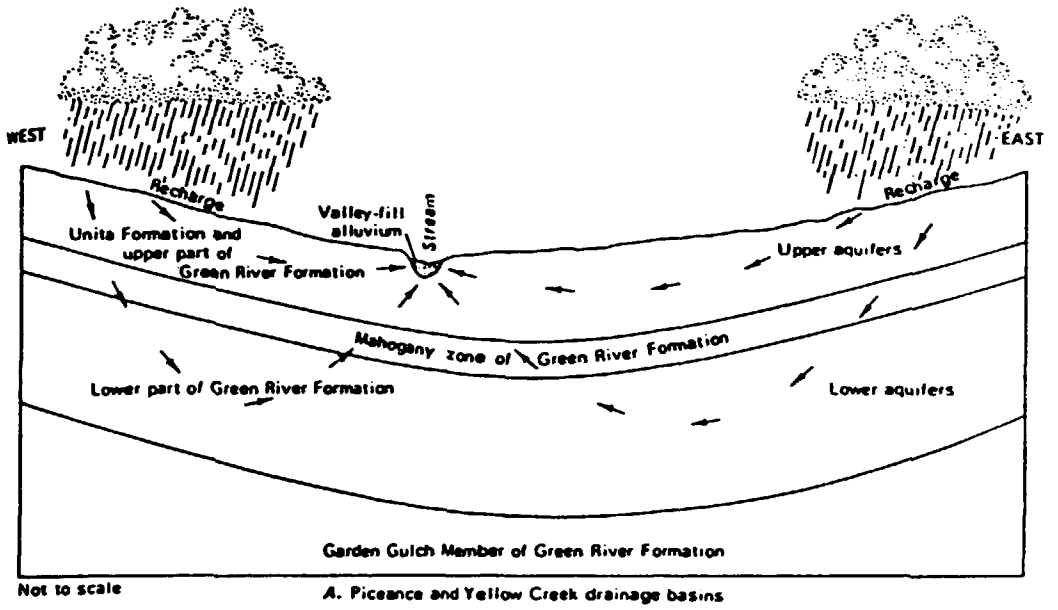


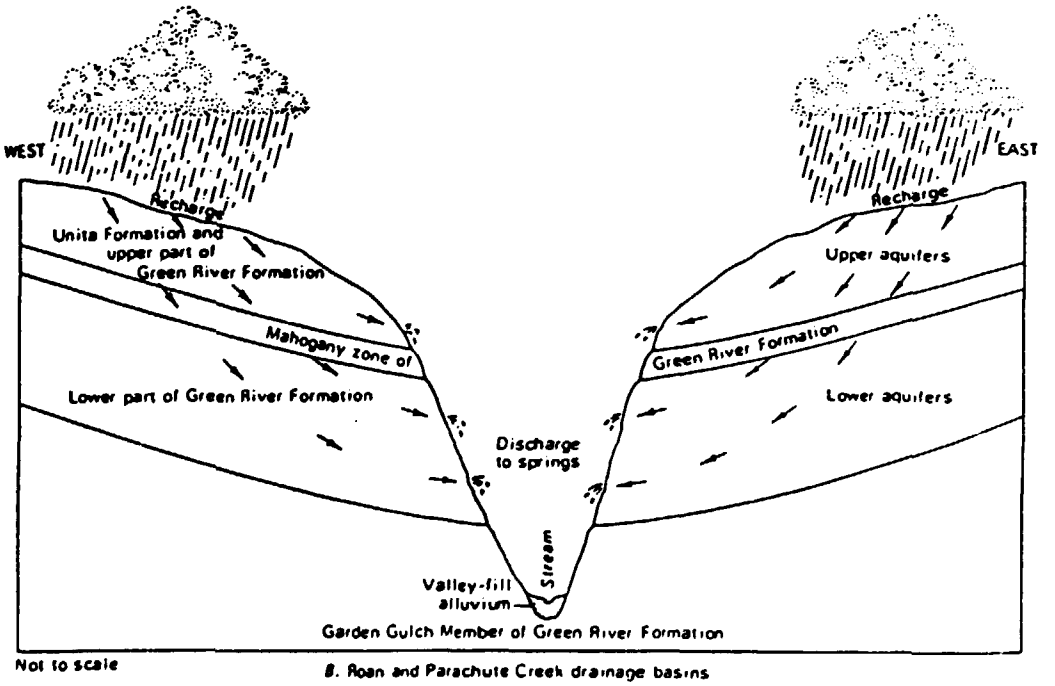


*Figure 5.14. Idealised cross-sections of the Piceance Basin illustrating the concept of groundwater flow in the basin.*

*Table 5.6. Stratigraphical and hydrostratigraphical units in the Piceance Basein.*

| Formation | Member | Lithology | Zone |
|---|---|---|---|
| Uinta Formation | | Fractured Sandstone, Marlstone and Siltstone | 5 |
| Green River Formation | Parachute Creek | Fractured Marlstone | 4 |
| | | Oil Shale | 3 |
| | | Fractured Marlstone | 2 |
| | | | 1 |
| | Garden Gulch | Shale and Marlstone | |

The input data to the test case consisted of prior estimates of hydrological quantities, such as distribution and range of transmissivity for horizontal flow in four of the hydrostratigraphical units, vertical hydraulic conductivity in Zone 3, average vertical hydraulic conductivity of four units and of the average transmissivity of Zone 3, range and distribution of recharge to the basin, and discharge to springs and seepage faces. A constant effective porosity of 0.10 was assumed for all units. The transmissivity data did not include estimates of measurement uncertainty.

The results of simulations of the problem were to be evaluated by comparing results from several models by means of a goodness-of-fit measure for calculated hydraulic heads and by inspection of particle paths and travel times of particles released at twelve points within the basin. The goodness-of-fit measure was defined in terms of differences between measured and model calculated hydraulic heads along the lines shown in Figure 5.15. Line 1 is the north-south section and line 2 is the east-west section. The figure also shows the particle release points.

The regional nature of the case and the inherent complications that accompany the use of prior estimates of hydraulic parameters in a regional setting emphasises the importance of subjective decision making in the formulation and calibration of a groundwater flow model.

### *Results from Case 4*

Five sets of results were submitted for Test Case 4. One team used a finite-difference code, whereas the other analyses involved finite-element codes. Generally, the teams applied the same set of boundary conditions consisting of a fixed infiltration rate distribution over the top surface except for the rivers and springs. Fixed head boundary conditions were used at river locations and at springs in the canyons along the southern vertical boundary. No-flow boundary conditions were used for the rest of the vertical boundaries and the bottom boundary.

The teams employed manual trial-and-error procedures in order to arrive at a calibrated model by adjusting the parameters of recharge rate and hydraulic conductivity distribution.

Because of the high horizontal-to-vertical aspect ratio of the domain, the discretisation might have influenced the results. In particular, the vertical discretisation had an impact on the capability of describing the vertical flow velocity component. The results of one team were produced using a seven-layer mesh, whereas the other teams described the domain with one element/block layer per unit, or five elements/block layers in all.

Most teams simulated confined conditions, i.e. the topographic variations were irrelevant. However, in the seven-layer-approach the mesh was adjusted so that the elevations of the springs at the southern boundary were explicitly represented.

The teams managed to calibrate their models with respect to the kriged head profiles to a reasonable degree of fit in the northern part of the domain. It was evident that the fixed-head boundary conditions applied to the rivers in this part of the region constrained the solutions, so that the sensitivity to permeability variations became relatively low. Due to this circumstance, the best-fit permeabilities were determined with a limited degree of confidence.

For the southern part, it was much more difficult to obtain a reasonable fit because of a combination of uncertain boundary condition descriptions and a possible lack of resolution in the hydrogeological characterisation.

Figure 5.16 shows an example of computed calibration errors for the north-south (top) and east-west (bottom) profiles in Layer 1 compared to the standard deviation of the kriging error.

The diagrams show some patterns which are common to most of the submitted results. Apparently, the fits are not as good in the southern part of the domain as in the northern. A possible explanation is the uncertainty in the description of the springs in the canyons in the southern part, whereas the fixed head boundary conditions at the rivers in the northern part decreases the sensitivity to errors in the hydraulic conductivity.

No team managed to calibrate the model to the extent that the goodness-of-fit measure was less that 1.0 everywhere along the profiles.

Figure 5.17 presents horizontal projections of pathlines of particles released at four locations in layer 1. The results from the different teams were qualitatively similar. Thus, pathline 1 discharged to a stream in the central part of the domain, pathlines 2 and 3 exited at the northern boundary, and pathline 4 went to a canyon in the southeastern part of the domain. The exception of one pathline 4 which moved towards the north might be explained by a too coarse discretisation.

The most sensitive parameter in the fitting procedure involving manual trial-and-error type methods was apparently the recharge rate and the permeability close to the canyons in the south. The anisotropy ratio had also a strong influence and, because of the sparsity of data, it introduced a significant element of uncertainty in the model calibration.

The data used to calibrate the models consisted of hydraulic heads kriged from a sparse set of data measured in wells distributed over the domain. The uncertainty introduced by the application of the kriging procedure was not evaluated in this test case. There is a need, however,

The setting of the basin in combination with the large horizontal to vertical aspect ratio made the evaluation of the vertical flux component very uncertain. The model results were described by one Project Team as almost two-dimensional.

Most teams judged their fits to be reasonable considering the uncertainties present in the definition of the case. Since no independent data set existed for comparison with model prediction, it was difficult to make statements about the validity of the models.

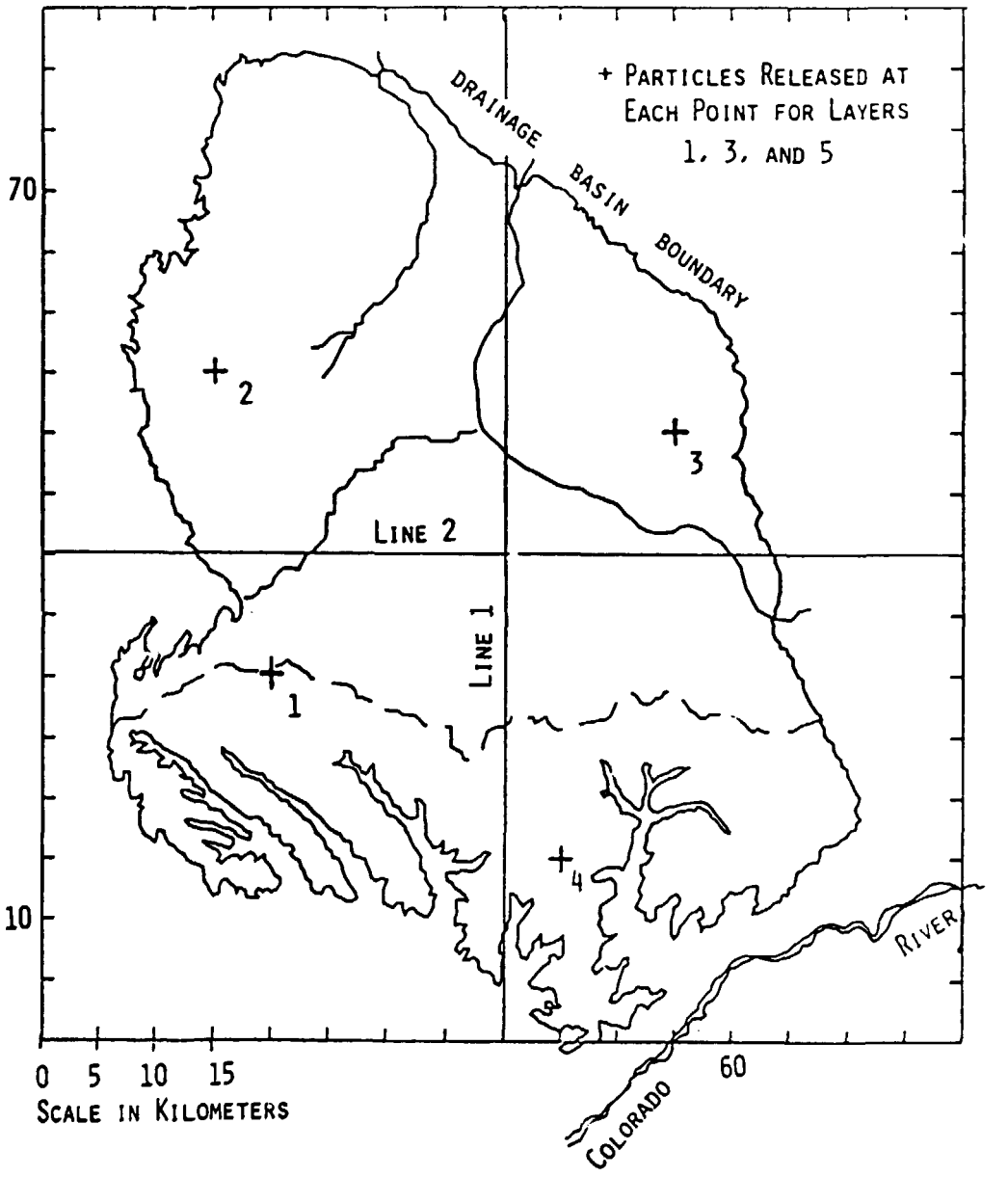


*Figure 5.15. Location of cross-section lines and particle release points for problem evaluation.*

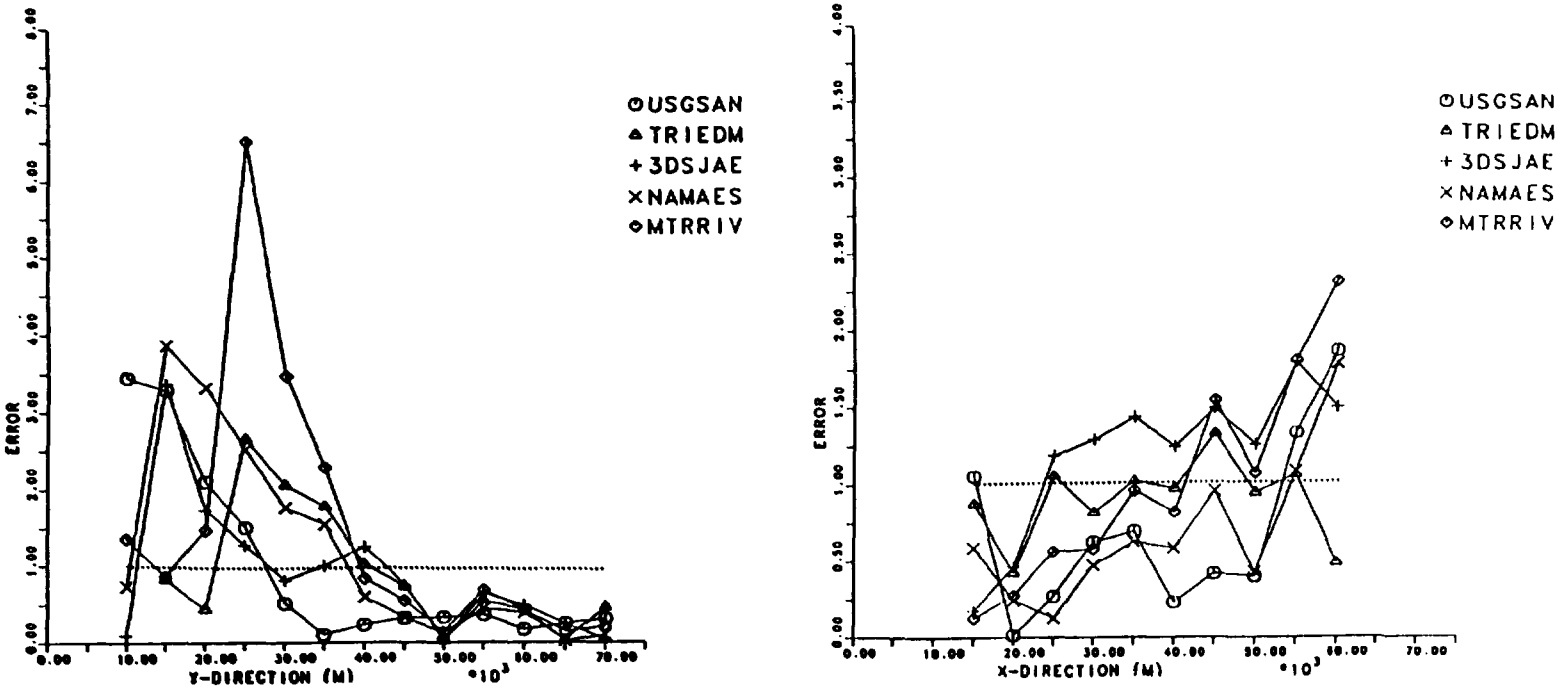


*Figure 5.16. Computed calibration errors for the north-south (right) and east-west (left) profiles in layer 1. The dotted line (error = 1) corresponds to the standard deviation of the kriging.*

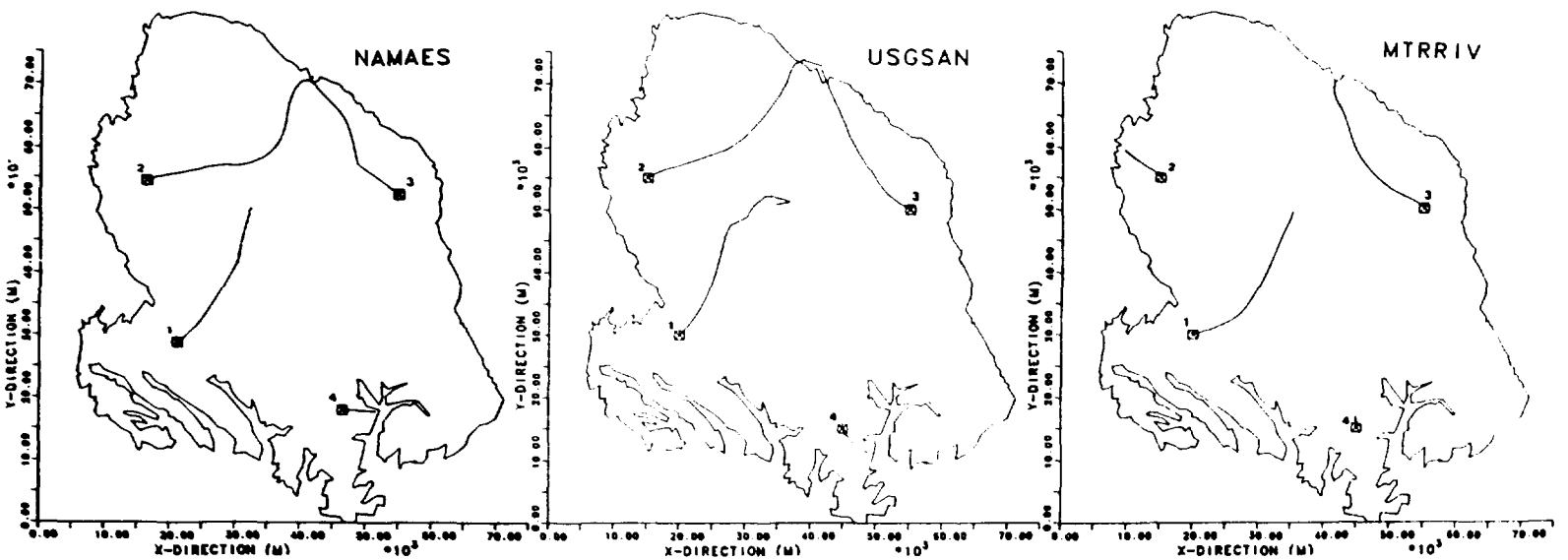


*Figure 5.17. Horizontal projections of pathlines originating in layer 1.*

## 5.6 Case 5. Soil-Water Redistribution Near the Surface at a Field Site

Flow in partially saturated porous media is an important process that may need to be considered in the development of repository conceptual models, either for the evaluation of the boundary conditions or as a principal mechanism for initial saturation or resaturation of a repository. In the present Test Case 5, the redistribution of soil moisture through partially saturated soils was studied to determine, whether the models could simulate the movement of soil-water through partially saturated media.

The case was based upon a soil-physics field experiment at the field experimental site "West Side Field Station" of the University of California at Davis, Cal., a highly researched and well-documented test facility for soil science studies. The objective of that experiment was to collect an extensive database from 20 test plots located in a fairly uniform soil in order to examine the spatial variability of field measured soil-water properties and the possibility of using averaged values in characterising the hydraulic properties of the soil (Figure 5.18).

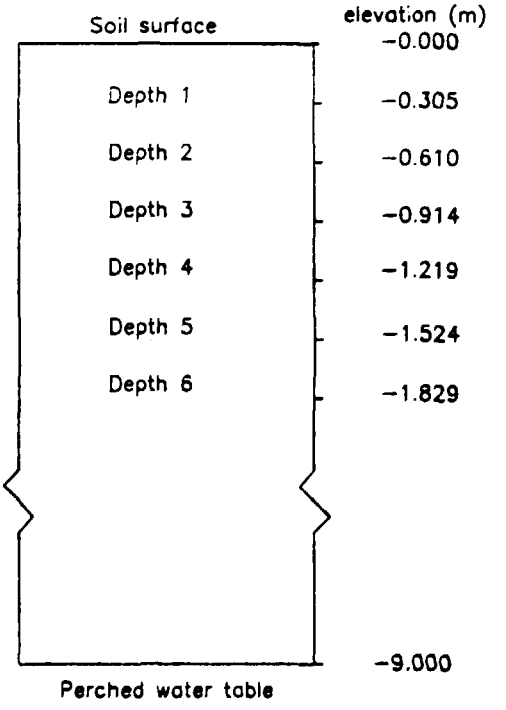


*Figure 5.18 Schematic view of the soil profile with the locations of the tensiometers indicated.*

The test case, using a limited subset from the data base, was designed to evaluate the capabilities of various codes to simulate soil-water redistribution for partially saturated media under slightly heterogeneous field conditions. The computer codes were thus required to solve a non-linear transient problem.

The direct measurements used for the test case consisted of field tensiometer readings and laboratory data of moisture content as a function of tension (pressure). The remaining data contained indirect measurements or calculated property values based upon analysis of directly obtained field and laboratory measurements.

At the experimental site the soil properties were considered to be fairly uniform with some small-scale variability. The water table was located at approximately 900 cm below ground surface with natural infiltration and recharge occurring as gentle rains during the winter months. Twenty 6.5 $m^2$ plots were randomly established over a 150 hectare site and tensiometers were placed at six depths down to 183 cm below ground surface to follow soil-water pressure changes. Infiltration was initiated by ponding water on each plot until steady-state flow was established down to the 183 cm level. The lower boundary was defined as the local water table at 900 cm.

Once steady-state conditions were established, the ponding of water was terminated and the plots were covered with plastic sheets and a thin layer of soil to minimise evapotranspiration losses, extreme temperature fluctuations, and natural recharge.

Soil-water redistribution was monitored at various depths. The interpretation of the experimental results assumed that during the measurement period:

— evapotranspiration losses were negligible,
— groundwater flow was only taking place in the vertical direction, and
— the infiltration did not cause fluctuations in the local water table elevation.

Core and soil samples were collected for laboratory analysis to determine soil-water characteristic curves and the bulk density of the soil.

The data base for the test case used data from one test plot. The data were originally organised corresponding to the depths where the tensiometer measurements were made with no intention to define distinct hydrostratigraphical units. The Project Teams were free to use any interpretation of the data to characterise the hydrology, however.

The data base for the test case comprised the following data from the experiment:

— soil-water characteristic curves (moisture content versus pressure head)
— soil-water content (storage) versus time for each soil depth (i.e., tensiometer levels)
— effective hydraulic conductivity at each soil depth versus time
— values for the data as result of direct field and laboratory measurements and derivations based on analyses of those measurements

The Project Teams were requested to report the variation with time of both the moisture content and the total head at the six tensiometer locations over a period of 30 days.

*Results from Case 5*

Six sets of results were reported, all produced assuming one-dimensional vertical flow with a zero-flux boundary at the surface and a zero pressure boundary at the 900 cm depth. Although the Project Teams were allowed to decide how to use the hydraulic conductivity values given for the six tensiometer emplacement depths, all teams used six layers corresponding to the tensiometer locations. Due to the difficulties encountered in the corresponding test case in Level 1, special attention was paid to the problem of numerical convergence. Two Project Teams considered solution convergence for the case.

Figures 5.19 and 5.20 show the calculated moisture content profiles and the experimental profile for two of the six tensiometer depths. The results of the various teams were in very close agreement and agreed also quite well with the experimental data, particularly in the upper layers. As the test case was well defined and focused on a single process, namely drainage of a test plot, it left little possibility of variation in conceptual models between the Project Teams. The close agreement in results is furthermore an indication of similarity between the applied computer codes.

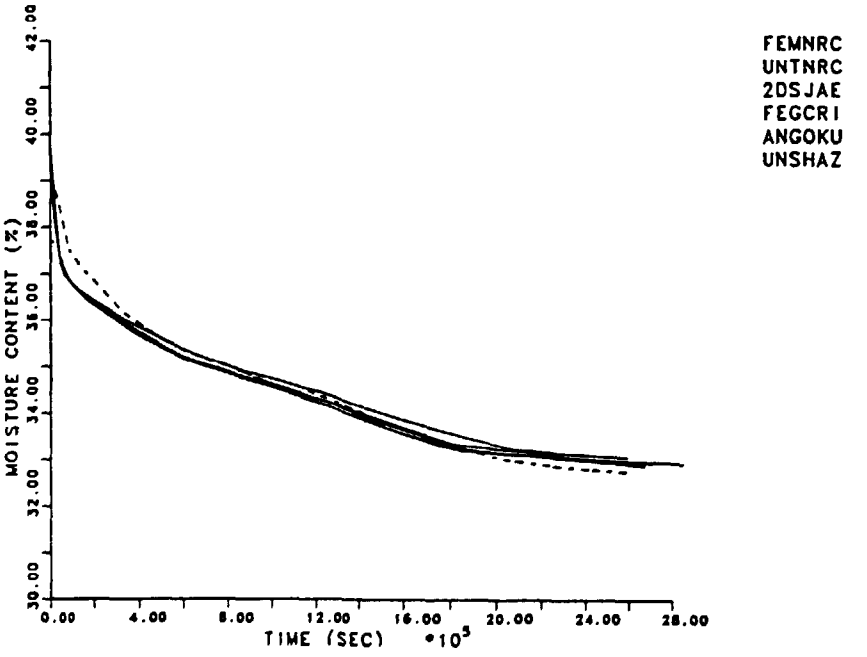


*Figure 5.19. Moisture content versus time at a depth of 30.5 cm as calculated by six Project Teams. The experimental curve is shown as a dashed line.*

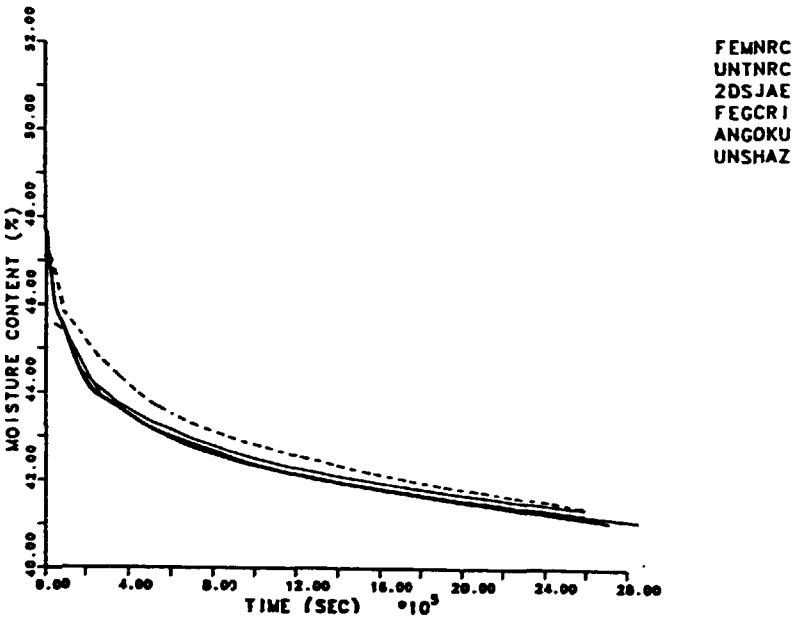


*Figure 5.20. Moisture content versus time at a depth of 121.9 cm as calculated by six Project Teams. The experimental curve is shown as a dashed line.*

The simulation results showed, however, an increased deviation from experimental data with increasing depth. There are several possible explanations for this. The lack of measurement points between 183 cm and 900 cm contributes to a low resolution of property variability, i.e. vertical heterogeneity, below a depth of 2 m. This could lead to a larger error in moisture redistribution predictions at lower tensiometer locations. Another explanation is a possible change in soil property due to initial saturation conditions, since the effect of variable moisture content may cause the hydraulic properties to change in a different manner to that described by the moisture-retention curves outlined in the test case setup. There may also be variations in flow propagation with depth due to lateral and vertical heterogeneities.

The current database did not allow for a distinction between the proposed explanations.

The Project Teams attempting the case concluded that the fit between simulated and experimental results was satisfactory in spite of the observed deviations. Test Case 5 has increased the confidence in the ability to partially saturated flow models to simulate the drainage flow regime and slightly heterogeneous site characteristics. A claim of validation for partially saturated flow could not be made due to the limitations of the database and the limited range of site characteristics and flow conditions.

# 6. HYDROCOIN Level 3

## 6.1 General

The behaviour of a radioactive waste repository is affected by many complex physical and chemical processes acting over very long times. Mathematical and numerical models are normally used to assess the performance of a repository. However, the parameters which are introduced in these models are generally not well known. The main goal of Level 3 of HYDROCOIN was to study different methods for treating such uncertainties and examining the sensitivity of the results of models to changes in the parameters. An overview of metods used or considered in the Level 3 study is given below.

The objective of *uncertainty analysis* is to estimate the uncertainty in the performance of a system (the consequence) from the uncertainties in the parameters of the model. In this context uncertainty means lack of knowledge. Thus one speaks of uncertainty in a model, meaning lack of knowledge as to exactly which model and model parameters that correspond to the natural world. Uncertainties in a model can be broadly classified as uncertainties in conceptual model or as uncertainties in parameters. Uncertainties in simple readily quantified parameters can usually be quantified to some extent. On the basis of the available information a probability density can be defined, which gives the probability that the parameters have given values. It should be born in mind that this density is just a measure of one's ignorance. It is thus very subjective and dependent upon expert opinions. By its nature uncertainty can only be reduced by gaining additional information, which can only derive from measurements on the physical system. It should be noted that there will always be measurement errors, although they may be insignificant, and the probability density function that describes the system after the results of the measurements are known must take account of the these errors.

It is the uncertainty in the consequence of a model or performance measure that is important rather than the uncertainty in the model. Typical consequences measures are the groundwater travel time from a repository or the flux through the repository. Uncertainty analysis aims to determine the uncertainty in the consequence from the uncertainty in the model. In principle, the handling of uncertainties in parameters is easy. The approach is to calculate the probability density function of the consequence using the model together with the probability distribution for the parameters of the model. In practice, it may be necessary to evaluate several consequences or performance measures.

Parameter estimation plays an important role in uncertainty analyses. Often the quantities that can be readily measured are not the parameters of the model but quantities that depend on these in a complicated fashion. For example, groundwater heads are readily measured, but the primary parameter in normal groundwater flow models is the permeability field, and the head depends in a complex manner on the permeability distribution. In such cases the parameters can be estimated by choosing the values that give the best fit to the data in some sense.

*Sensitivity analyses* provide answers to questions, such as "What happens if such and such a parameter is changed by so much?" and "Which parameters are important?". The simplest way to approach sensitivity analysis is to make calculations for different combinations of parameters and compare the corresponding consequences. Generally, the parameter combinations will be selected on the basis of expert judgement in the attempt to elucidate the behaviour of the system.

Another possibility is to calculate local sensitivities for various parameters, defined as the derivative of the consequence with respect to a given parameter.

The response surface technique can also be used. In this technique, the consequence is approximated as a simple function of the parameters. Sensitivities can then be obtained by differentiating the response surface function. Often a response surface in the form of a simple polynomial in the parameters is sought. Regression analysis can then be applied to determine the coefficients of the chosen terms. One way in which to assess the relative importance of the parameters is to calculate measures of the correlations between the parameters and the consequence.

Models are often used to determine many primary quantities, from which are calculated a few performance measures that are complicated functions of the primary quantities. This is particularly likely for finite-difference or finite-element discretisations of continuum groundwater flow models. In these models, the head is calculated at many nodes, but the only quantity of interest may be the travel time from a potential repository site. In such cases considerable computational savings may be made in calculating local sensitivities by using a technique called the adjoint method.

Both uncertainty and sensitivity analysis require the selection of combinations of parameter values from the parameter space. Various approaches can be used, such as Expert Choice Sampling, Point Estimate Sampling, Simple Random Sampling, Latin Hypercube Sampling and Importance Sampling. The first two approaches are deterministic, whereas the last three are random sampling techniques that can be used in Monte-Carlo studies. In such studies, the required samples are chosen randomly on the basis of suitable probability density functions.

A major source of uncertainty in groundwater flow modelling arises, because the permeability usually varies in space in an irregular, unpredictable fashion, even within a single rock type. Other hydrogeological properties exhibit similar behaviour. The treatment of the effects of spatial variation on the consequences of a groundwater flow model is more complicated than the treatment of uncertainty in simple parameters. Whereas one accurate measurement of a homogeneous parameter suffices to eliminate the uncertainty associated with the parameter, many accurate measurements of a spatially-varying quantity may be needed to reduce the associated uncertainty significantly. Geostatistics is an interesting approach to handling spatial variation. It should be noted,however, that geostatistics requires various assumptions to be made which may not be applicable on a specific case.

A possibility to undertake uncertainty and sensitivity analyses that takes spatial variation into account is to generate realisations of the spatially varying fields. The Turning Bands Method is one way of doing this. It produces realisations of a random field with important statistic properties in agreement with the estimated statistic properties of the investigated region. The generated fields do not match the measured values at the measurement locations but may be conditioned to do so.

It is usually necessary to estimate the value of the field at locations other than the measurement points. One method for interpolating from the measured values is kriging. The kriged interpolate of a spatially varying field at a point is the best unbiased linear estimate of the field. Kriging has the benefit that it provides an estimate of the error in the interpolate, namely the variance of the estimator. The kriged estimator is exact at the measurement points.

## 6.2 Case definitions

Seven Test Cases were treated in HYDROCOIN Level 3 representing a variety of flow situations ranging from three-dimensional, saturated flow on a regional scale to two-dimensional flow in an unsaturated situation on a metre scale (Table 6.1).

*Table 6.1. Cases in HYDROCOIN Level 3.*

| Case no | Medium | Features studied | Spatial scale | Temporal scale |
|---|---|---|---|---|
| 1 | argillaceous | partial saturation, layering | 20 - 200m | 50 - 150 years |
| 2 | fractured tuff | high nonlinearity, partial saturation | 500 - 1000 m | 1 - $10^6$ years |
| 3 | salt | uncertainties in the interpretation of field data | 2 - 400 km | steady-state |
| 4 | brine transport | saturated brine, convection cells | 300 - 900 m | 500 years |
| 5 | crystalline rock | spatial distribution of hydraulic conductivity | 200 - 2000 m | steady-state |
| 6 | low permeability rock | spatial variability | 80 km | steady-state |
| 7 | | accuracy of particle tracking | 300 m | steady-state |

## 6.3 Case 1. Near Surface Disposal in Argillaceous Media

Case 1 was set up as an extension of Case 7 of HYDROCOIN Level 1. It treated sensitivity and uncertainty analysis of groundwater flow in an argillaceous medium. A sensitivity study should ideally allow for the freedom to formulate different conceptual models of a given site from the available experimental information. This view was incorporated into the case by defining two base case scenarios, one for a *saturated medium* and one for an *unsaturated*. The secenarios were defined by conceptual and mathematical models, and base case parameters were given as well as a description of possible variations consisting of parameter ranges and alternative site attributes. The primary purpose of the exercise was to determine the most important hydrogeological attributes and parameters.

For the *saturated medium scenario*, the radioactive waste was assumed to be deposited in trenches excavated from the surface. The concrete lined trenches were filled with concrete encapsulated waste and the trenches were grouted with cement. For the purpose of the study, the trenches were treated as a homogeneous mass of concrete. The region above the trenches was assumed to be backfilled with compacted clay. As an option, a concrete anti-intrusion shield was assumed to be placed above each trench within the clay backfill.

The site consisted of horizontally bedded clay, 17 m to 22 m in thickness, resting conformably on a 3 m thick aquifer overlying an impermeable clay formation. The hydraulic conductivity of the clay varied vertically as a result of weathering, compaction and textural variation. The modelled domain was limited to a two-dimensional cross-section, perpendicular to the back-filled trenches and parallel to the major flow direction.

The geometry of the modelled domain is shown in Figure 6.1

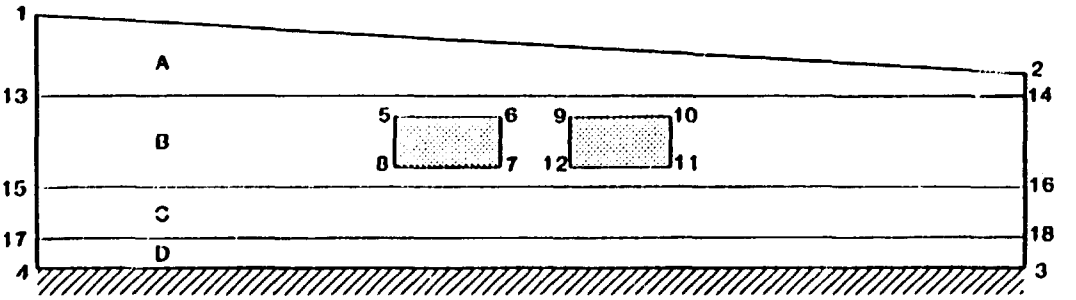


*Figure 6.1. Geometry of the modelled domain for the saturated medium scenario.*

The overall length of the region was 200 m, over which distance the height of the surface fell linearly from 25 m to 20 m between the left and right hand edges. The clay had an isotropic hydraulic conductivity varying continuously with depth, while the hydraulic conductivity of concrete was assumed to be homogeneous and isotropic.

The selected boundary conditions imposed a hydraulic gradient across the domain. The water table was coincident with the sloping ground surface and reinforced the hydraulic gradient. A flooded clay pit was located at the left of the domain, whereas water seeped out of the vertical face of an empty clay pit at the right hand side.

Flow through the clay and concrete was assumed to be fully saturated and to obey Darcy's law. The seepage face boundary condition at the right end of the domain was considerably simplified for the test case by assuming the medium to be fully saturated and at atmospheric pressure all along this end.

For the base case calculations, the hydraulic conductivity of the rock was assumed to be isotropic and to vary continuously with depth.

The first performance measure was taken to be the shortest water travel time between any part of the concrete vaults and a boundary of the modelled region. The second measure was the volumetric flow rate of water passing through the vaults.

A number of variations to the case were proposed. They are shortly described below.

The hydraulic conductivity of the argillaceous medium was uncertain. This uncertainty could be systematic or a statistical variation with position. Both of these could be addressed by suitable variations. Instead of being isotropic the conductivity of the clay could be anisotropic.

A more realistic representation than that for the base case would be to consider four or five uniform horizontal layers with the hydraulic conductivity changing discontinuously at the interfaces.

Also the presence of vertical fault zones upstream or downstream of the repository might be looked into. The hydraulic conductivity of concrete was likely to range between $10^{-10}$ and $10^{-6}$ $m \cdot s^{-1}$. The lower value would correspond to good quality intact concrete, while the higher value would be appropriate for poor quality concrete resulting from physical, chemical or biological degradation. The kinematic porosity of the argillaceous medium and concrete could be lower than defined, if the water passed preferentially through channels and cracks rather than through the interconnected pore structure.

The clay surrounding and overlaying the vaults could become altered during construction, resulting in increased permeability of the clay.

Concrete caps above the cemented waste would be used to reduce risks from human intrusion. The effects of removing the caps could be investigated.

*The unsaturated medium scenario* considered time periods before the concrete vaults had become resaturated or periods with insufficient rainfall to make the soil fully saturated. In the saturated medium scenario, the seepage face boundary condition to the right of the domain had to be drastically approximated. In the unsaturated case the media were regarded as being variably saturated and a more realistic treatment of the seepage face could be adopted.

The geometry of the modelled domain in the unsaturated case was essentially the same as in the first scenario, except that the medium was assumed to consist of four distinct sedimentary layers and that the concrete caps above the vaults were omitted (Figure 6.2).

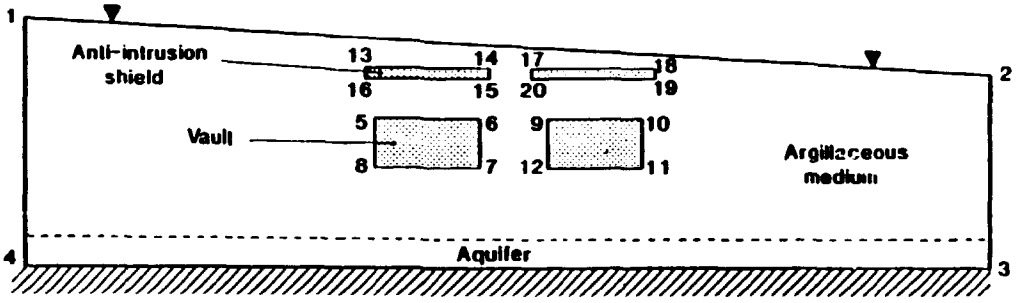


*Figure 6.2. Geometry of the modelled domain for the unsaturated medium scenario.*

The surface layer was assumed to consist of weathered material with a rather high permeability. The vaults were located in a low permeability layer underlain by a layer of intermediate permeability, and a silty sand aquifer was situated above an impermeable clay deposit. The argillaceous layers and the concrete were assumed to behave as variably saturated permeable media.

Precipitation was considered to occur uniformly over the top surface of the region and to give rise to a uniform accretion which infiltrated the medium, assuming excess water to run off at the surface. Disused clay pits were supposed to be present to the right as well as to the left hand sides of the domain and would have specified water levels, with the remainder of the vertical surfaces acting as seepage faces. For the base case scenario the left pit was assumed to be full and the right one empty, but the sensitivity to water levels in the pits might be examined. The lower boundary of the domain was supposed to be impermeable.

The base case unsaturated scenario and the variations required only a steady-state solution. However, the problem was formulated as transient, since a time-stepping procedure to reach the steady-state solution might be envisaged. The performance measured envisaged for this case were the same as for the saturated case.

The accretion was given as 20 mm/year, corresponding approximately to the average surface flux in the saturated scenario.

Many of the uncertainties in the saturated medium scenario would also apply to the unsaturated case and were to be included in the sensitivity analysis, where appropriate.

The boundary conditions to be used at the interfaces between the different media were selected so that the pressure and the normal component of the unsaturated Darcy flux were continuous. An infiltration boundary condition was assumed along the top surface. This required that either the flux into the boundary would be specified or that the pressure head would be defined to be atmospheric, if ponding occurred. These conditions gave a complicated nonlinear boundary condition.

Three levels of participation were envisaged. In *Subcase 1a* a free choice of methodology and numerical technique was allowed for performing the sensitivity analysis. Statistical sampling of the parameter values including the degree of correlation among the input parameters was thought to be adequate. Either local or global sensitivity analyses could be performed using a variety of different methodologies and numerical techniques. Extra phenomena, such as transpiration or alternative conceptual models, could also be considered.

In *Subcase 1b* a set of 15 variations was prescribed, each of which probed an important part of the parameter space. The methodology was to use the base case scenarios and subcases derived from them, and to vary a single parameter within each variation.

In *Subcase 1c* the same methodology was to be employed as in *Subcase 1b*, but the number of variations was extended in order to highlight important sensitivities. It was also suggested that combinations of the variations in *Subcase 1b* would be considered.

### *Results from Case 1*

The test case was tackled by nine Project Teams using various approaches. Nearly all the teams presented results for variations selected on the basis of expert judgement. This approach is primarily a technique for sensitivity analysis that provides information on important parameters and features of the conceptual model. The studies of parameter variations roughly corresponded to *Subcase 1b*, whereas the uncertainty analyses and local sensitivity analyses corresponded to *Subcase 1a*. The flow fields were found to be broadly similar for all the variations. The flow was predominantly from left to right with a slight downward component. The pathlines from the repository moved down and to the right and exited through the right-hand boundary. Figure 6.3 shows the flow calculated for one of the realisations in the uncertainty analyses for the unsaturated scenario.

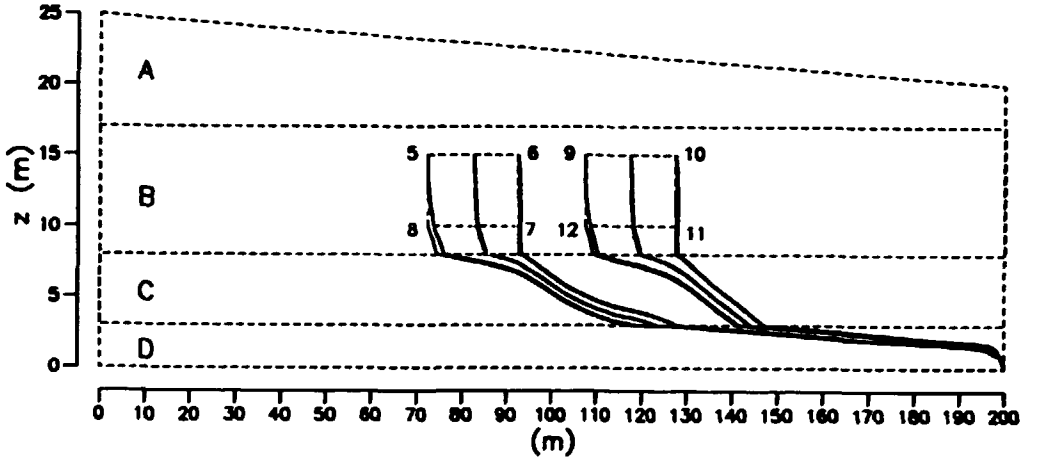


*Figure 6.3. Calculated pathlines for one of the realisations in the uncertainty analysis undertaken by the SAN-team.*

As a result of the *parameter variations* in calculations for the unsaturated scenario, it was found that the two performance measures, flux through the vaults and minimum travel time from the vaults, varied very little for head on the left hand side boundary in the range 18 to 25 m. In examination of the sensitivities of the performance measures to the saturated hydraulic conductivity of concrete for the range $10^{-10}$ m·s$^{-1}$-$10^{-6}$ m·s$^{-1}$, it was observed that the minimum travel time measure was not significantly affected, whereas the flux through the vaults was quite sensitive and increased with increasing conductivity. As expected, the flux through the vaults was limited by the hydraulic conductivity of the unit surrounding the vaults.

The flux and the travel time were sensitive to the hydraulic conductivity of a "disturbed zone" around the vaults with a conductivity in the range $10^{-9}$ m·s$^{-1}$-$10^{-7}$ m·s$^{-1}$. Both performance measures were also sensitive to the anisotropy of the hydraulic conductivities of the formations. However, they were insensitive to variations in infiltration rate.

One team presented results for the minimum water travel time from the boundary to the vaults. The value of this measure, about 110 years, was almost the same in most of the saturated variations. Figure 6.4 gives the results for variation S1. For the unsaturated variants, the measure varied between 21 and 416 years, implying that the sensitivity to the conceptual model was the most important sensitivity for this measure.

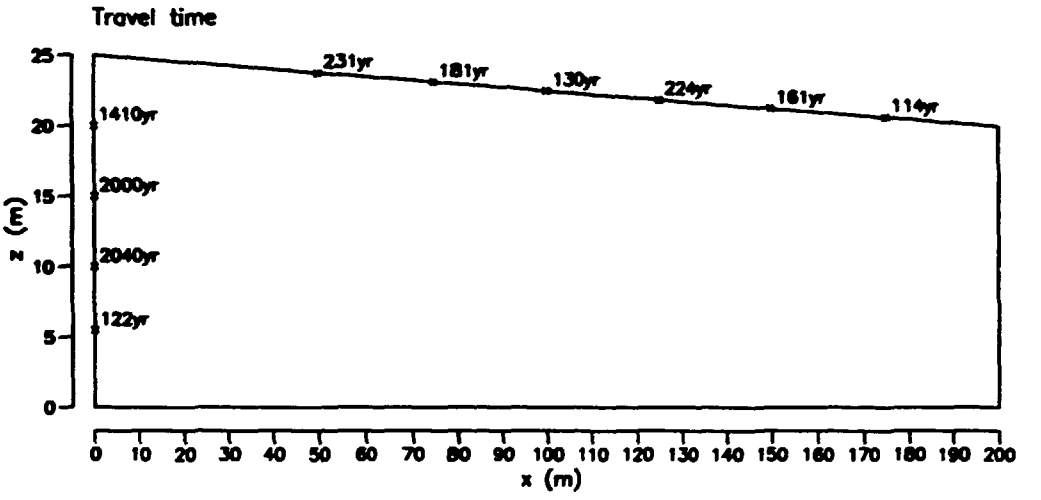


*Figure 6.4. Travel times from the boundary to the vaults calculated by the CRI-team for the S1 variation.*

One team made calculations for variations with the conductivity of the concrete $10^{-10}$ m· $s^{-1}$. For one of the variants they found a total water flux through the vaults of $1.3 \cdot 10^{-7}$ $m^3 \cdot m^{-2} \cdot s^{-1}$ and a minimum travel time of 14 years. Increasing the hydraulic conductivity of the concrete led to increased flux through the repository and slightly reduced travel time, although the flux was limited by the hydraulic conductivity of the surrounding medium. Decreasing the hydraulic conductivity of the concrete had opposite effects.

*Uncertainty analyses* were carried out by three Project Teams. Probability density functions had to be assumed for the conductivities, porosities and infiltration rate, selecting a base case value as well as a range. The results for the flux obtained by one of the teams are given in Figures 6.5 and 6.6.

The flux through the vaults was found to be most sensitive to the saturated hydraulic conductivity of the concrete and sensitive to a lesser extent to the conductivity of the unit surrounding the vaults. The most important parameter for the minimum travel time performance measure depended on whether stepwise or rank regression was used. Stepwise regression implied that the infiltration rate was the more important parameter and that the saturated hydraulic conductivities of the units surrounding and below the vaults were the next most important parameters. However, rank regression indicated that the minimum travel time was most sensitive to the saturated hydraulic conductivity of the unit below the vaults.

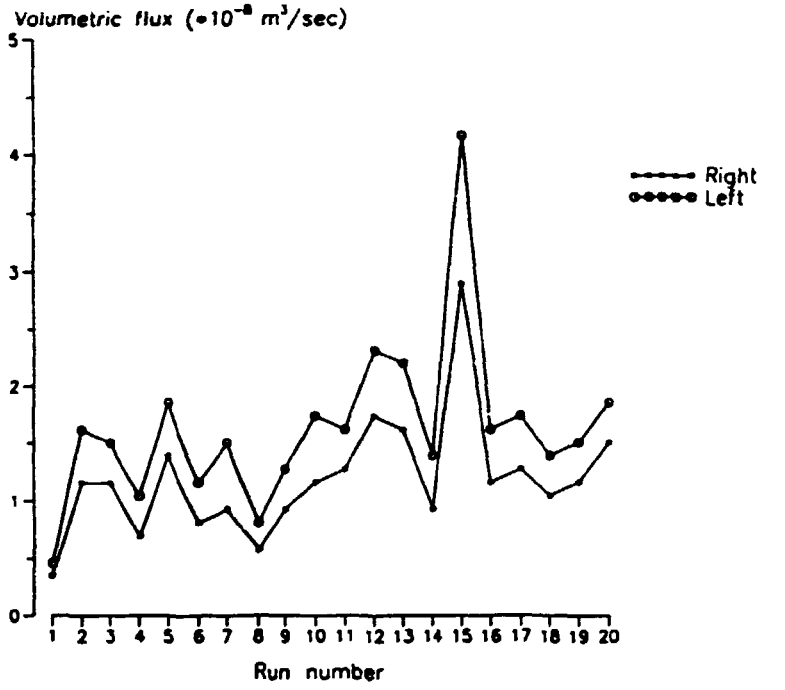


*Figure 6.5. Summary of the values for the flux performance measure for the realisations in the uncertainty analysis carried out by the NRC-team using the FEM-code.*

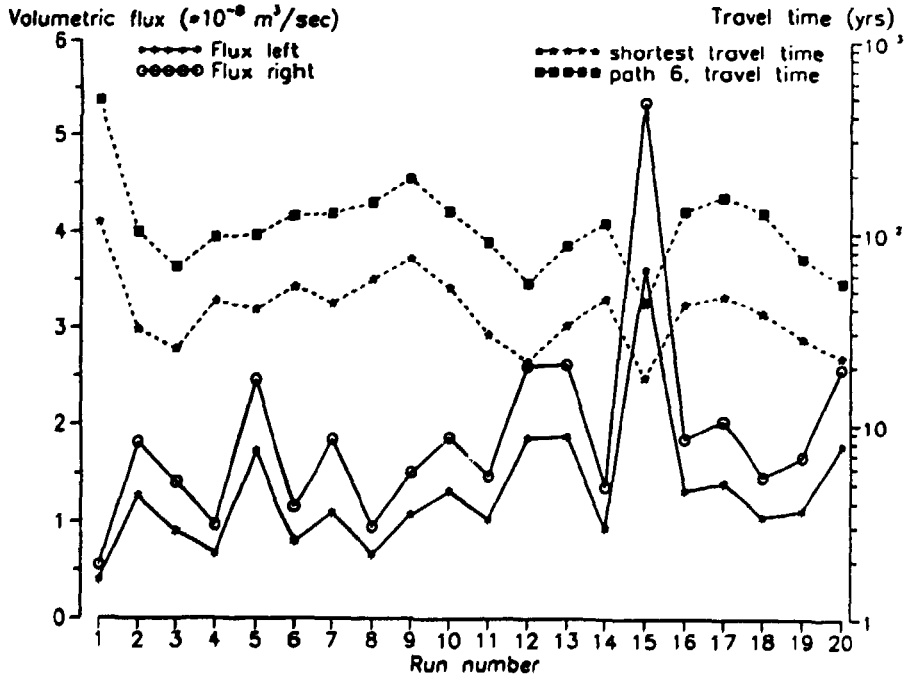


*Figure 6.6. Summary of the values for the flux performance measure for the realisations in the uncertainty analysis carried out by the SAN-team using the UNT-code.*

One team undertook uncertainty analyses for the layered variant. The sample statistics was tested for normality and stepwise regression analyses were performed for first and second order models. The flow rates and minimum travel times were found to be log-normally distributed. Regression analyses with the first order model gave some unreasonable results, albeit with a very low correlation coefficient. Regression analyses with the second order model showed that the most important parameter for the flux was the product of the hydraulic conductivities of layers B and D.

A local sensitivity analysis, varying the values of the parameters by a small fraction of their value and calculating standardised sensitivity coefficients, indicated that the conductivity of the concrete was the most important variable for the flow rate and that the porosity of layer C and the permeability of layer D were the most important parameters for the minimum travel time. It was concluded that the choice of performance measure had considerable influence on which parameters are considered be the most important. Several performance measures should therefore be used in order to get a full understanding of the total system. It is likely that the important parameters will vary over the position in the parameter space for a realistic system with a complicated hydrogeology, and therefore great care should be taken in transferring results from one system to another.

## 6.4 Case 2. Groundwater Flow in Partially Saturated, Fractured Tuff

Case 2 dealt with a potential repository site which was evaluated by the U.S. Department of Energy. It consisted of a sequence of layers of volcanic tuff. Hydrologic characteristics varied greatly between the layers because of large differences in the degree of welding, fracturing, and chemical alteration. The proposed repository horizon lied entirely within the unsaturated zone.

The test case involved a sensitivity analysis of models that could be used to describe partially saturated flow through fractured tuff. The analyses addressed modelling of nonlinearity, partially saturated flow, combined matrix and fracture flow, volcanic tuffs, layered materials with sharp layer boundaries and large material property contrasts.

The purpose of the analyses was to evaluate the sensitivity of the output from a particular mathematical model for isothermal, partially saturated flow through fractured tuff, to variations in input parameters and differences in the conceptual models that describe the hydrology and the geological structure of a tuff site. Sensitivity would be evaluated by observing the changes in performance measures based on model output.

Several base cases were defined, including both high and low flux cases of one-dimensional steady-state and transient flow as well as two-dimensional steady-state flow. The water transport was expected to be matrix dominated at low fluxes, whereas fracture dominated flow was expected at high fluxes.

The hydrogeological system is shown schematically in Figure 6.7.

The site was composed of a sequence of ash-fall and ash-flow tuffs. Fracturing in all units was dominated by two sets of nearly vertical fractures and one set of horizontal fractures. Major

fault zones cut through the entire vertical section. The water table is fairly flat beneath most of the site.

The hydrogeological units at the tuff site could be grouped into three broad categories:

- Densely welded, highly fractured tuffs. These units have low saturated matrix conductivities and high saturated fracture conductivities.
- Non-welded, vitric tuffs with few fractures. These units have high saturated matrix conductivities and relatively low saturated fracture conductivities.
- Non-welded, zeolitised tuffs with few fractures. These units have low saturated matrix conductivities and low saturated fracture conductivities.

The contacts between these units generally tend to be sharp and extreme contrasts in hydraulic conductivities can occur over very short distances.

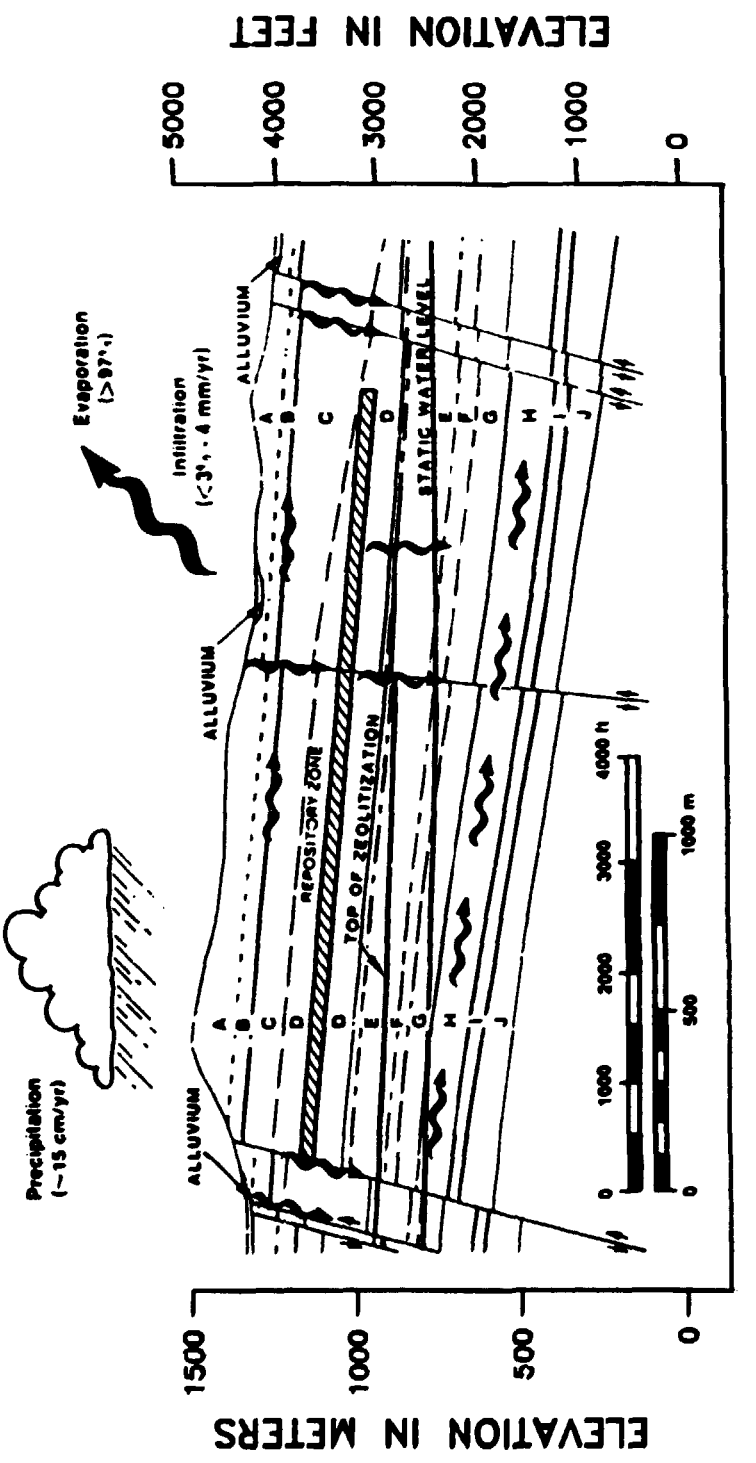


*Figure 6.7. Generalised hydrogeological system at the tuff site.*

Two conceptual models for current or possible future climatic conditions seemed possible for the site, though for different ranges of flux: a model with one-dimensional, vertical, downward flow and a model with multi-dimensional flow, in particular flow from non-welded units and layer contacts diverted laterally into major structural features of the site .

The estimate of the present average flow through the mountain is 0.1 mm/yr or less, with the flow regime being dominated by flow through the rock matrix. It could probably be represented by one-dimensional, downward in a vertical direction. In this model, as long as conditions are isothermal, all of the water that percolates past the zone where evapotranspiration occurs, ultimately passes through the repository horizon and flows down to the water table.

At fluxes 1.0 mm/yr or higher, flow in fractures begins to predominate. Existing permeability contrasts and fault zones might then cause the flow to be diverted, either above or below the repository horizon, into the fault zones. If diverted above the repository, the amount of water reaching the waste packages could be significantly less than is indicated by the recharge rate. This indicates that a multi-dimensional flow model should be used.

Six cases were defined, four one-dimensional conceptual model cases and two two-dimensional model cases. Analyses of both steady-state and transient flow were suggested for the one-dimensional base cases. Only steady-flow analyses were suggested for the two-dimensional base cases because of expected convergence problems with currently available numerical techniques.

A mathematical model was provided for partially saturated flow in a compressible, fractured tuff. The highly nonlinear model used a composite continuum approach to describe the effective hydrological properties of the fractured rock mass that represent the combined effect of the matrix and the fractures.

In the conceptual model for one-dimensional flow, it was assumed that all moisture infiltrating past the zone of evapotranspiration flowed vertically downward to the water table (Figure 6.8).

Furthermore , the following conditions would prevail at all fluxes considered:

- anisotropic hydraulic conductivities
- conductivity contrasts at contacts between hydrogeologic units
- structural tilting of the hydrogeologic units
- distortions of the flow field caused by the presence of major structural features having hydraulic properties that are different from the surrounding rock mass would not be sufficient to cause water to be diverted laterally

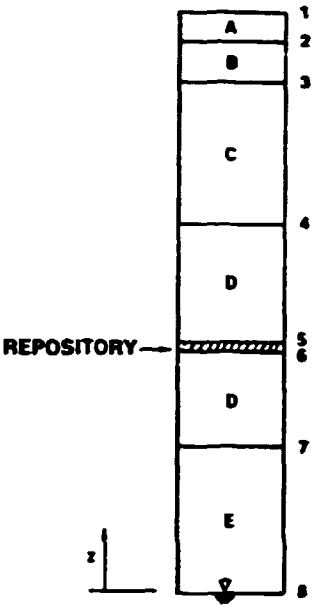


*Figure 6.8. Stratigraphy for one-dimensional base cases, Base Cases 1—4.*

Since the purpose of the analyses was to test the sensitivity of model outputs (i.e. the performance measures) to variations in the parameters for the zone of partially saturated flow, the water table was taken as the lower boundary of the modelled region. A known flux was applied at the upper boundary and temperature conditions were isothermal.

The performance measures used for the *one-dimensional, steady-flow* calculations was the shortest groundwater travel time between the base of the repository and the water table. In steady-state analyses, water travel time is a function of the flux and the effective volume of water along the flow path. The effective water volume is a nonlinear function of pressure head. The water travel time is then a nonlinear function of all the parameters that affect the distribution of moisture and pressure head in the column. The velocity was taken to be the greater of the velocity in the fractures and matrix, provided that the corresponding volumes of water proved a significant fraction of the total.

The first performance measure for the *transient flow* cases was also the shortest water-travel time. The second and third performance measures were the normalised volume of flow passing the base of the repository and the normalised volume of flow passing the water table, respectively.

Because of the extremely nonlinear nature of this problem, sensitivities were expected to be dependent on the flux chosen for the base cases. Two base cases each were proposed for steady and non-steady analyses. For steady-flow conditions, base case fluxes were:

— Base Case 1. 0.1 mm/yr for matrix dominated flow.
— Base Case 2. 1.0 mm/yr for conditions near the transition from matrix-dominated to fracture-dominated flow.

For the non-steady flow cases, it was assumed that steady-flow conditions would prevail under the initial flux, after which a step change in flux was applied. Transient flow would then be observed until a new steady-flow condition was reached. The base case flux changes were:

— Base Case 3. Flux change from 0.1 to 0.2 mm/year for transient, matrix dominated flow.
— Base Case 4. Flux change from 0.5 to 1.0 mm/year for transient flow in the transition from matrix dominated to combined matrix and fracture flow.

Base case values were given for the hydrological properties for each of the hydrological units as well as a suggested range of values to be used for sensitivity analyses for parameters to be varied.

Suggested variations included changes in flux rates, hydraulic conductivities, residual saturation, matrix and fracture porosities, height of water table, and thicknesses of vitric and zeolitised zones.

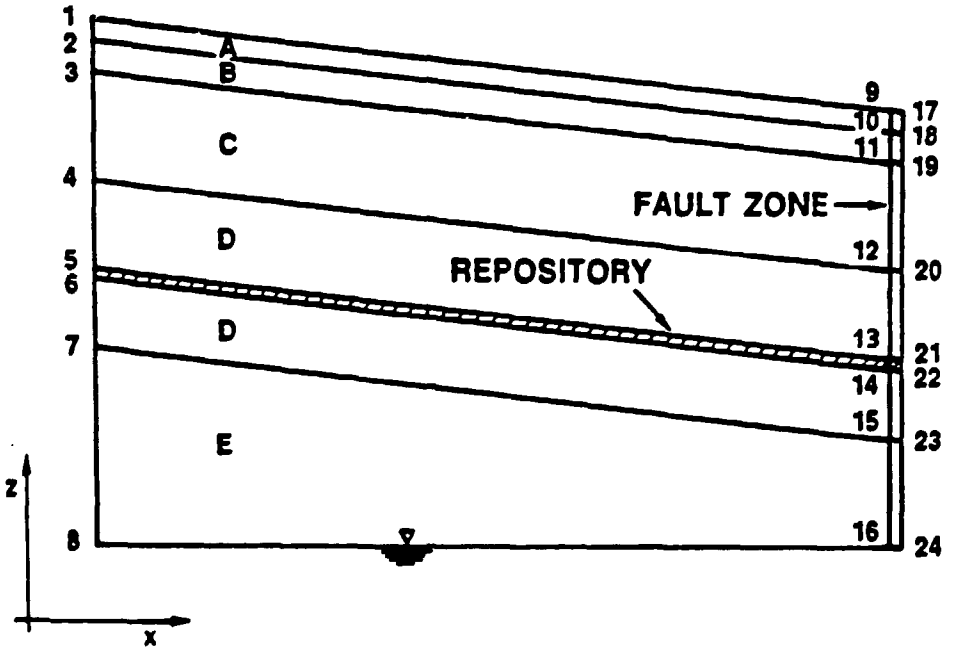


*Figure 6.9. Stratigraphy for two-dimensional base cases. Base Cases 5—6.*

In the *two-dimensional analyses*, all factors that could cause lateral flow were allowed to act. In the conceptual model for two-dimensional flow it was assumed, as in the model for one-dimensional flow, that the flux entering the top of the column had already migrated past the zone of evapotranspiration. Figure 6.9 shows the geological section for the hydrogeological units involved.

The earlier one-dimensional column was expanded to a two-dimensional section. The modelled region was bounded on the right by a fault zone and it was assumed that the repository extended across this fault zone. Each unit was supposed to be homogeneous and isotropic. A known vertical flux was applied along the upper boundary. The left boundary was a no-flow boundary. The fault zone along the right boundary was initially to be represented by a seepage face. The water table was the lower boundary of the modelled region and was assumed to be horizontal. Isothermal temperature conditions were envisaged.

Performance measures for the two-dimensional base cases were the volumetric flow rate of water passing through the repository horizon and the shortest water-travel time from any portion of the repository to the water table. It was also suggested that the magnitude of lateral diversion of flow and its impact on the performance of the repository should be examined.

Two base cases fluxes were proposed for the two-dimensional, steady-flow analyses:

- Base Case 5. 0.1 mm/year for matrix-dominated flow.
- Base Case 6. 1.0 mm/year for conditions near the transition from matrix dominated to fracture dominated flow.

Base case values for the hydrological properties for each of the hydrological units were given. No values were provided for hydrological properties of the fault zone, as the fault was treated as a seepage face.

All variations suggested for the one-dimensional flow analyses also applied to the two-dimensional cases. The two-dimensionality introduced additional sources of uncertainty. For example, the right boundary could be treated as an unfractured, porous material, whose hydraulic properties and effective width are not known, so that the flow may or may not act as a conduit for flow. The correlation between measured anisotropy in saturated conductivities and in conductivities for partially saturated flow was poorly known. Diversion of significant volumes of water above the repository from the rock mass into the fault zone would reduce the volume of water contacting the waste, if the waste was not stored close to the fault.

### *Results from Case 2*

The nonlinearities of the test case were extreme and posed a very challenging numerical problem for the Project Teams. The NNW-team used approximately 1500 hours of CPU time on a Cray X/MP 416 computer.

For the *one-dimensional steady-state flow* subcase the NNW-team performed a conditional variation of parameters, varying porosity, saturated hydraulic conductivity, residual saturation, and curve fitting parameters describing the pressure versus saturation relationship. Other

variations included input flux, water table location, and properties of Unit E (vitric or zeolitic). The performance measure used was minimum groundwater travel time from the repository to the water table. 1092 simulations were undertaken in the sensitivity analysis.

In all the simulations the most striking change in travel time was observed at the transition from matrix to fracture flow. Such a transition would occur when the matrix is near full saturation. The team demonstrated that the transition from fracture to matrix flow resulted in a nonlinear behaviour in the performance measure (Figure 6.10). In addition, they showed that as matrix conductivity was lowered, the minimum travel time also decreased (Figure 6.11).

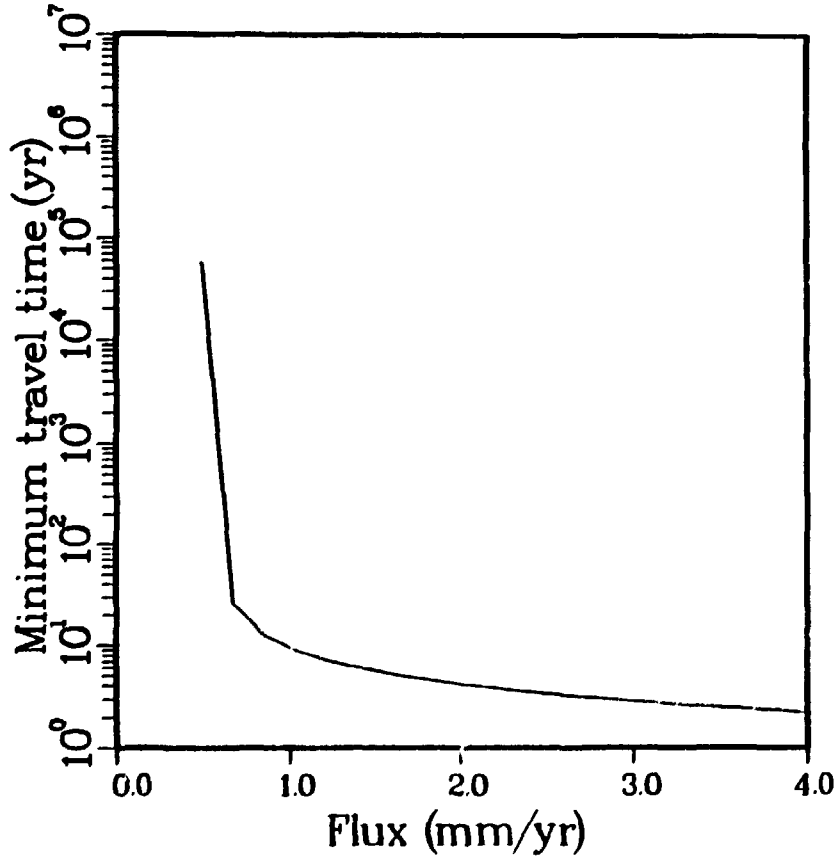


*Figure 6.10. Variation of travel time versus applied flux assuming Unit E being zeolitic (1D, steady state, using the LLU-code).*

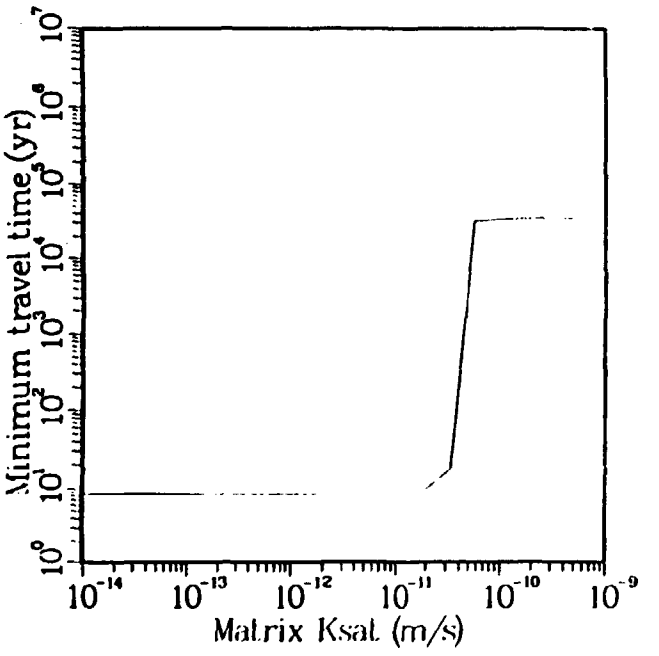


*Figure 6.11. Variation of travel time versus saturated matrix conductivity assuming Unit E being zeolitic and a flux of 1.0 mm/year (1D, steady state, using the LLU-code).*

The SAN team performed uncertainty and sensitivity analyses using both simple random sampling and a Latin Hypercube sampling technique to reduce the number of required simulations. They evaluated the regression of the values, combinations of values, and their ranks to analyse sensitivity. Results from the analyses showed a predicted range in travel times from a few years to several million years with a median value of approximately 60 000 years, and a probability that the travel time will be less than 1000 years of about 10 percent.

Given that this test case was highly nonlinear, there was concern that a Latin Hypercube sampling procedure would not adequately cover all the parameter space compared to pure random sampling. A test made to examine this possibility showed, however, that for travel times greater than about 10 000 years, the cumulative distribution functions were nearly identical for both methods, although some deviations were observed for shorter travel times.

The team also performed regression analyses on the Latin Hypercube simulations to examine parameter sensitivity. Although analyses were conducted using the sampled values, the ranks of the sampled values, and combinations of parameters, the fit was poor for all the regressions. The analyses identified recharge as the most important parameter and the saturated conductivity of the layers below the repository as the next most important parameter.

The HAR-team used the parameter-stepping technique for solving highly nonlinear steady-state problems. The technique can be automated and provides a robust method for solving highly nonlinear problems. It also affords a tool for exploring the sensitivity of the solution to the parameters. The team used a finite-element program and the results were compared against the analytical solution as a check. In exploring the sensitivity of the solution to the computation

and the grid, they found that it was necessary to use a very fine grid in regions where the solutions changed rapidly, usually at the interfaces between the different units. Coarse grids could lead to large errors. The team commented that if automated methods for sensitivity and uncertainty analysis were used, it would be necessary to check that the grid was adequate for each set of parametervalues. They suggested that automated checks on solution quality would be useful.

The NNW team performed four simulations for the *one-dimensional, transient subcase*. The performance measures were time distribution of flux at the repository and water table, and the minimum groundwater travel time. For simulations of low "normalised flux" - 0.1 to 0.2 mm/yr - whether Unit E being vitric or zeolitic had minimal effect on the fluxes at the repository or the water table and on the travel times (Figure 6.12).

For high "normalised flux" simulations, there was a significant difference in the calculated performance measures when Unit E was vitric as compared to zeolitic. When Unit E was zeolitic, (low saturated matrix conductivity) flow was fracture dominated, the flux front passed very quickly and the groundwater travel time was very short.

A *two-dimensional, steady state subcase* was defined to examine how flow diversion would affect spatial distribution of flux through the repository and groundwater travel times.

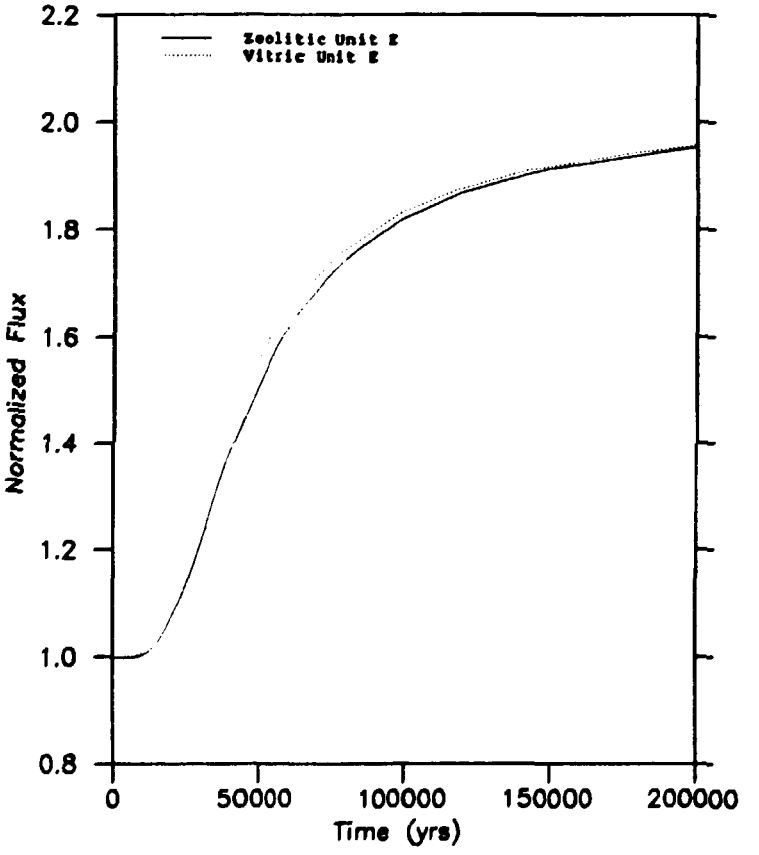


*Figure 6.12. Normalised flux versus time as calculated at the water table; the applied flux increased from 0.1 to 0.2 mm/year (1D, transient, using an unnamed code).*

The NNW team examined the following variations:

- a change of the value of a given model parameter simultaneously in all units combined with a variation of the applied flux
- a change of the values of a group of parameters in one or more units combined with a variation of the applied flux
- explicit modelling of the fault zone with a change in fault zone properties combined with a variation in the applied flux

Results were compared using four types of plots:

- particle paths between the ground surface and the water table
- spatial distribution of flux normal to the repository
- spatial distribution of flux normal to the water table
- spatial distribution of groundwater travel times for flow between the repository and the water table

As was the case for the one-dimensional analysis, the first variation showed that the two-dimensional results are very sensitive to the applied flux. For the lowest flux (0.01 mm/yr), the flow was matrix dominated and vertical in all units. As the applied flux increased, the amount of flow diverted laterally by the conductivity contrasts between Unit B and C increased. At higher fluxes, the conductivity contrasts between these units and the slope of the units combined to effectively shield most of the repository from the effects of increases in the applied flux by diverting the flow through Unit B to the fractures near the right boundary (Figure 6.13).

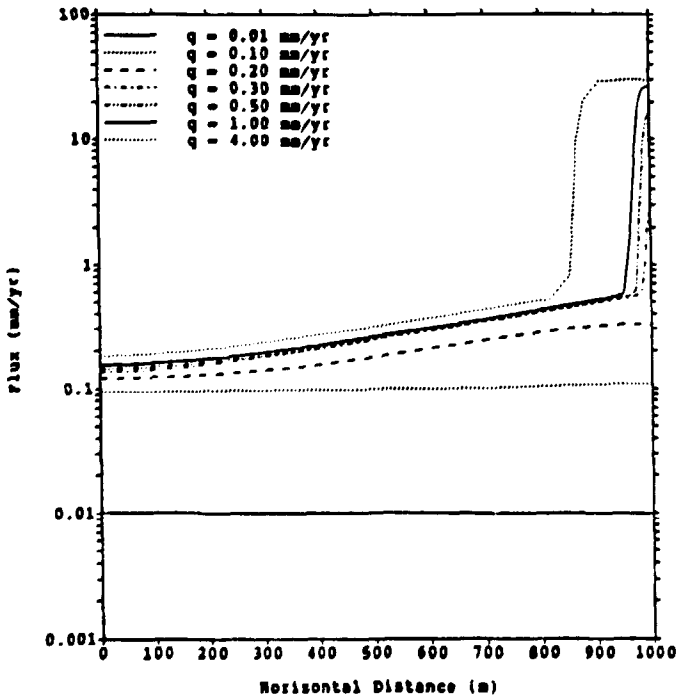


*Figure 6.13. Spatial distribution of flux at the repository level assuming base case parameter values and Unit E to be zeolitic (2D, steady state, using the NOR-code).*

Many of the variations affected the conductivity contrast between Unit B and C and therefore influenced the flow diversion above the repository. For low fluxes (less than 0.3 mm/yr), anisotropy induced a significant amount of lateral diversion as compared to the base case. For higher fluxes, the existing tendency for lateral diversion in Unit B with isotropic properties, completely masks any possible effects of anisotropy. The change of Unit E from zeolitic to vitric properties resulted in increased travel times.

The simulations addressing the properties and size of the fault zone showed that as the conductivity of the fault zone increased, its capacity to carry all of the diverted water also increased. Very small travel times occurred in the vicinity of the fault zone caused by the large fluxes and long travel times occurred over the remainder of the repository length.

The HAR-team undertook preliminary studies of the two-dimensional steady-state case using the same methodology as for the one-dimensional case. It became apparent that accurate modelling would have required a highly refined grid near the right hand edge which would have been very costly.

## 6.5 Case 3. Groundwater Flow Through a Hypothetical Salt Repository

The test case was a refined version of HYDROCOIN Level 1 Case 6, a hypothetical salt repository in a regional geological setting. The objective was to examine sensitivity and uncertainty analysis techniques and other steps, like conceptual model development and model calibration, that are important to the estimation of performance measures such as groundwater travel time from the repository to the accessible environment. In particular conceptual model development and model calibration on total regional and local scales were to be addressed.

The regional hydrologic system extended from the recharge areas in the mountains west of the Pecos River in New Mexico to major discharge areas to the east in Texas and Oklahoma (Figures 6.14 and 6.15)

The local scale model, approximately 15 km in length, enclosed a 2 km repository in the salt layer at a depth of 750 m, and a 5 km accessible environment.

22 materials were defined for the regional system. All layers were assumed to be horizontal.The following parameters for the regional model were found to be the best estimates:

- flux across the western boundary $0.37\ m^3 \cdot yr^{-1} \cdot m^{-1}$
- flux across the eastern boundary $2.4\ m^3 \cdot yr^{-1} \cdot m^{-1}$
- natural recharge to the Ogallala layer $7.5\ mm \cdot yr^{-1}$.

The geothermal gradient in the region was estimated to 2 °C/100 m and it was assumed that the ambient repository temperature was 30.5 °C. Overburden materials were considered to have a density of 2100 $kg/m^3$.

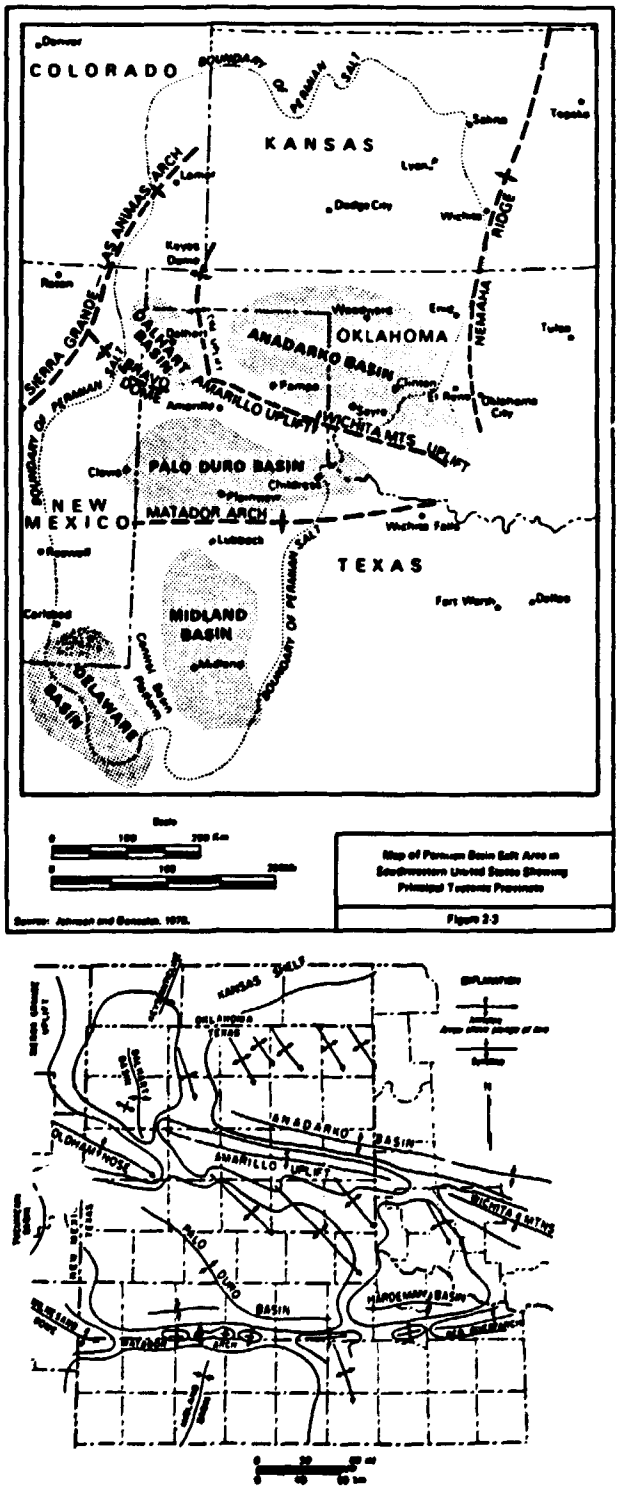


*Figure 6.14. Map showing the Permean Basin Salt Area and principal tectonic provinces (upper). Expanded map showing the major structural elements of the Texas Panhandle (lower).*

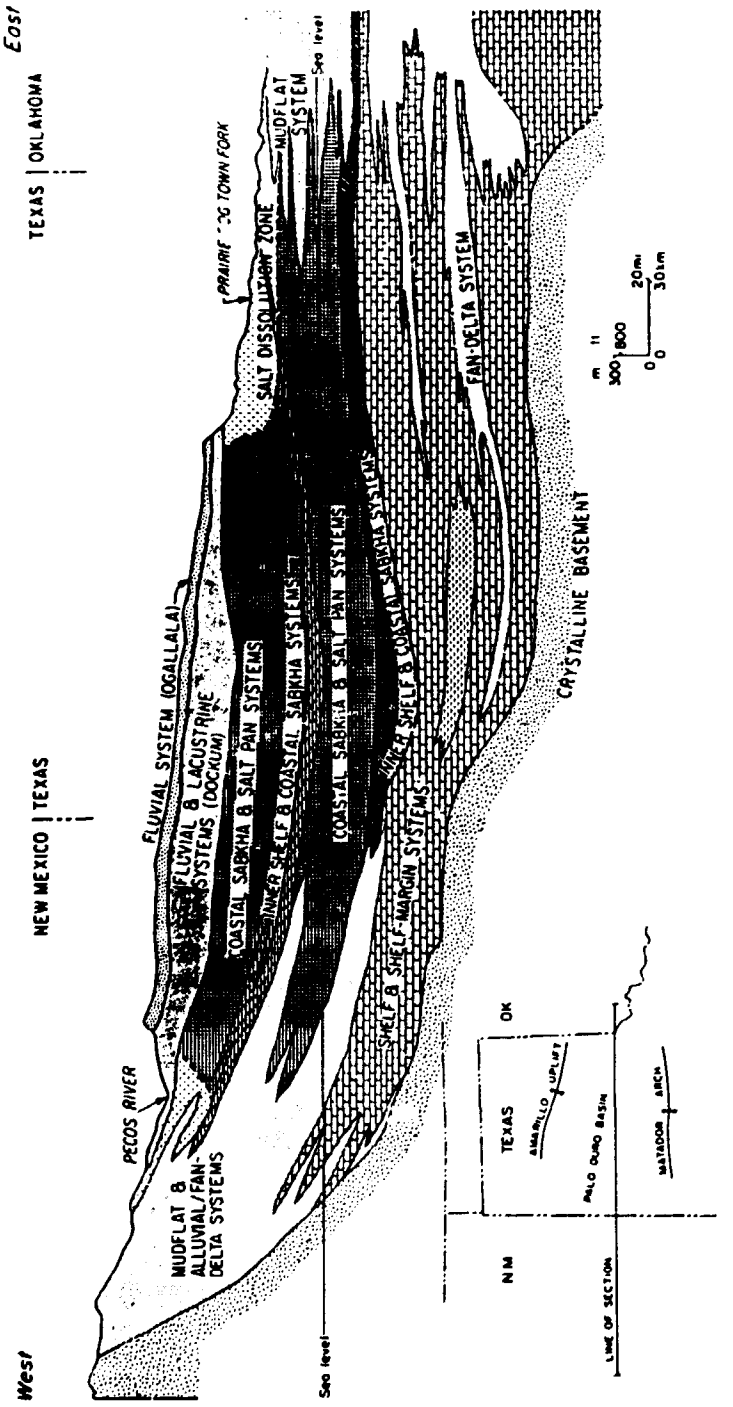


*Figure 6.15. Regional east-west cross section through eastern New Mexico and the Texas Panhandle illustrating stratigraphic relationships between major depositional systems in the Palo Duro Basin.*

Permeability distributions were given for each local scale material (Figure 6.16). For each lithology except salt, a horizontal-to-vertical permeability anisotropy of 10 to 1 was assumed. A range of salt conductivities of $9.7 \cdot 10^{-16}$ to $9.7 \cdot 10^{-11}$ $m \cdot s^{-1}$ for salt with log-normal distribution. Salt was considered to be isotropic. Sufficient data were available for some materials to deduce that the permeability distributions were log-normal and thus mean and standard deviation values were supplied. For most lithologies only parameter ranges were available and participants had to assume lognormal distributions.

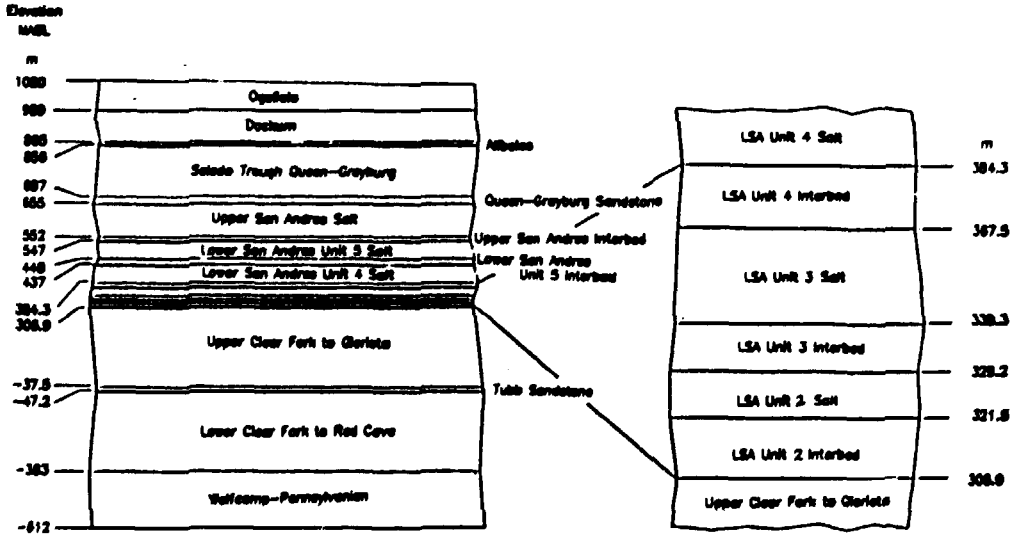


*Figure 6.16. Local model geology.*

The most likely flow mechanism for travel time assessments was assumed to be flow through porous media. In the analyses, a normal distribution of porosity was assumed with the following ranges:

— Ogalla 10 — 20%
— Sandstone 5 — 30%
— Dolomite 0.4 — 8%
— Salt 0.3 — 1.65%

Results from a drill stem test from a pumping well in the vicinity of the site gave a typical example of the pressure head versus depth relationship observed beneath the salt sequence (Table 6.2).

*Table 6.2. Results from a drill stem test (DST) from a pumping well in the vicinity of the site.*

| Formation | Midpoint of Test Interval Elev. (m) | Mean Pressure (Pa) | Pressure Range (Pa) | Standard Deviation (Pa) |
|---|---|---|---|---|
| Queen/Grayburg | 699.5 | $3.415 \cdot 10^6$ | $3.415 \cdot 10^6 — 3.949 \cdot 10^6$ | $1.72 \cdot 10^5$ |
| LSA/Interbed | 380.7 | $6.277 \cdot 10^6$ | $6.063 \cdot 10^6 — 6.490 \cdot 10^6$ | $6.9 \cdot 10^4$ |
| Wolfcamp | -564.1 | $1.176 \cdot 10^7$ | $11.23 \cdot 10^6 — 12.30 \cdot 10^6$ | $1.72 \cdot 10^5$ |

The dissolved solids of the formation waters would affect the environmental head and the flow field. Values for the salt content of the different formations were given.

***Results from Case 3***

ThisTest Case was analysed by the SRP-team and the SAN-team. The SRP-team used two finite element codes and one finite difference code, while the SAN-team used a finite difference code. In Table 6.3 participation in the test case is summarised and study identifiers (REG-1, -2, -3 and LOC-1) presented. Three of the studies involved regional analyses and one a local travel time analysis.

*Table 6.3. Summary of participation in Case 3.*

| Study Code used Team | Purpose and approach (dimensionality and scale) |
|---|---|
| REG-1<br>SW2<br>SAN | Regional model study to demonstrate deterministic sensitivity/uncertainty analysis techniques; (2D cross sectional model, appr. 700 km by 4 km) |
| REG-2<br>CFE/INV<br>SRP | Regional model travel time estimates to natural discharge areas, trial-and-error calibration and calibration using inverse methods with point estimates of equivalent freshwater heads, sensitivity to variable density driving forces, and limited uncertainty analysis; (2D cross sectional model, appr. 700 km by 4 km) |
| REG-3<br>CFE/INV<br>SRP | Regional model stochastic travel time analysis using statistical inverse model calibration using kriged freshwater heads; (2D cross sectional model, appr. 700 km by 4 km) |
| LOC-1<br>MAG<br>SRP | Assessment of uncertainty in groundwater travel time due to uncertainty in material properties using a highly refined local (possibly intermediate) scale model and a Monte Carlo stochastic analysis approach; (2D cross sectional model, appr. 20 km by 2.5 km) |

Except for one sensitivity analysis performed in the REG-2 study all the groundwater flow codes solved the steady-state, two-dimensional, continuum, mass balance equation for saturated, confined groundwater flow. The domain geometry and spatial discretisation in regional modelling studies generally corresponded to the geologic layers of the site. The parameter estimation approach to model calibration used in the REG-2 and REG-3 studies required additional discretisation, known as parameter zonation, to be developed for each parameter to be estimated.

All the regional studies used the same spatial distribution and type of boundary conditions as illustrated in Figure 6.17.

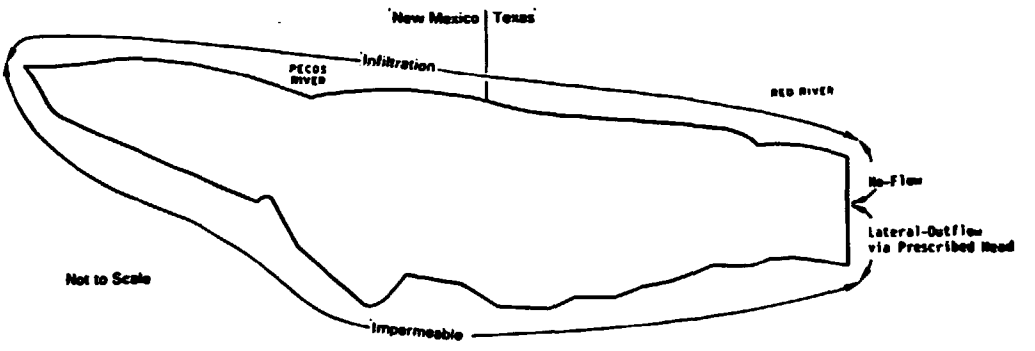


*Figure 6.17. Plot illustrating the distribution of boundary condition types being used for the regional Palo Duro cross-section models.*

The local study used a hierarchial approach to obtain boundary conditions. Permeability distributions for the major lithologic units considered in the REG-2 and REG-3 studies were derived from test case descriptions, while initial parameter values for the REG-1 study were generally computed.

REG-2 and REG-3 studies used constant effective porosities of 0.05 to calculate travel times. Only the LOC-1 study used the recommended normal distribution for porosity.

Recharge was an important calibration variable in all the regional studies. It was noted that recharge could not be varied independently from hydraulic conductivity. The REG-1 study examined a few values of the recharge distributed between 1.5 mm/yr and 20 mm/yr, whereas the REG-2 study trial-and-error part studied a range of recharge values that included values from 3.13 to 7.5 mm/yr west of the Pecos river, and values from 0.73 to 1.74 mm/yr east of the river. In the REG-3 study three recharge zones were used.

The 61 equivalent freshwater head calibration points in the problem description were used directly in the REG-1 study, but some were only used indirectly in the REG-2 study. Kriged values of head at each model node point provided the prior information used as part of the complex goodness-of-fit measure in the REG-3 study.

The root-mean-square (RMS) difference between computed and interpreted freshwater heads provided the *goodness-of-fit measure* used in the REG-1 study. In the initial phase of the REG-2 study a trial-and-error approach to model calibration was used, but the goodness-of-fit measure included both qualitative and quantitative parts. The final phase of the REG-2 study employed

a parameter estimation approach to calibration and a goodness-of-fit measure based on both prior information on aquifer parameters and observed values for hydraulic heads at the calibration points. The CFE/INV software used in the REG-3 study used a statistical inverse technique and a complex goodness-of-fit measure to automatically adjust both the hydraulic conductivity and recharge.

Time and resources for the REG-1 study precluded calibration of the model and the study limited its calibration effort to four model runs that included three variations of recharge using median hydraulic conductivities and a fourth involving simultaneous reduction of the distributed recharge and an increase in all hydraulic conductivities. Table 6.4 summarises these four runs and the RMS error values attained for the three converged solutions.

*Table 6.4. Summary of the REG-1 calibration runs and the associated RMS errors (all 61 calibration points considered).*

| Run no | Description | RMS (m) |
|---|---|---|
| 1 | Median hydraulic conductivities and uniform recharge (10.6 mm/yr) | Code failed to converge |
| 2 | Median hydraulic conductivities and distributed recharge | 17300 |
| 3 | Median hydraulic conductivities and no recharge | 200 |
| 4 | 10× (median hydraulic conductivities) and 0.1× (distributed recharge values) | 348 |

The team making trial-and-error calibration runs in the initial phase of the REG-2 study felt that the model was not satisfactorily calibrated, since the RMS was too high (149.3 m). However, they accepted the model, given the time constraints and purpose of the effort.

Eight cases were investigated in the parameter estimation part of the REG-2 study. In Table 6.5 the range of goodness-of-fit measures obtained with eight automatic calibration cases are compared as well as the trial-and-error calibration case. The best results were obtained for cases 8 and 6.

*Table 6.5. Model calibration runs completed as part of the REG-2 study (by trial-and-error (Case 0) and by an automatic calibration procedure (Cases 1 through 8)).*

| Case | Zones | Observations | Recharge considered | Errors RMS | Errors maximum |
|---|---|---|---|---|---|
| 0 | - | 51 | From trial-and-error runs | 124.6 | - |
| 1 | 99 | 51 | From trial-and-error runs | 47.0 | - |
| 2 | 105 | 51 | From trial-and-error runs | 44.0 | -117.8 |
| 3 | 105 | 70 | From trial-and-error runs | 36.3 | -106.6 |
| 4 | 105 | 70 | Minimum 1.45 mm/yr | 39.5 | 107.7 |
| 5 | 105 | 70 | Maximum 20.9 mm/yr | 38.4 | -116.4 |
| 6 | 105 | 70 | Distributed 1.45 to 20.9 mm/yr | 35.0 | 115.0 |
| 7 | 105 | 70 | Mean 0.5× (1.45+20.9) mm/yr | 38.5 | -117.5 |
| 8 | 105 | 70 | From previous studies 7.6 mm/yr | 34.9 | 114.5 |

Estimation errors were calculated for two of the cases. The magnitude of the errors indicated that the hydraulic heads were not sensitive to changes in most of the hydraulic conductivity values. The insensitivities and instabilities revealed that additional head observations and hydraulic conductivity measurements were required to reduce the uncertainty in the conductivities to reasonable levels to allow the hydrologic model to be used in the assessment of flow paths and associated travel times with acceptable uncertainty bounds.

In the REG-3 study the model was first calibrated for recharge using median values for hydraulic conductivities and then hydraulic conductivities were then calibrated once the best recharge distribution had been determined for the median hydraulic conductivity case. The calibration procedure proved to be very sensitive to the median values used for related parameters (e.g. recharge and hydraulic conductivity) and this in turn affected the order in which the calibration could be performed for the parameters. Excellent agreement between the prior and predicted hydraulic head distributions was observed for both the 11 and 22 hydraulic conductivity zone models in the region down gradient from the repository location. Lesser agreement was observed up gradient from the repository, particularly in New Mexico. Differences between prior and predicted hydraulic head distributions were well within three standard deviations of the kriging error. The Project Team noted that lack of hydraulic head data at the various stratigraphic interfaces made it difficult adequately to resolve hydraulic conductivity differences between zones.

*Sensitivity and uncertainty analyses* were performed as part of the REG-2, REG-3 and LOC-1 studies. The REG-2 study included a sensitivity analysis of 25 runs and a Monte-Carlo uncertainty analysis of 10 runs using Latin Hypercube sampling. Model boundary travel time for the calibrated equivalent freshwater head model was 15.9 million years. Groundwater travel time calculation difficulties were encountered with all variable density runs. This was attributed to poor grid resolution along the salt-bearing strata and basal formation interface, where a

high-density gradient existed and where there were sharp contrasts in material properties. Sensitivity analysis results for the equivalent freshwater head model indicated that the single run with prescribed-head boundary conditions caused the greatest change in RMS error (15.2 m), while it produced only a minor change in groundwater travel time, relative to the calibrated model. Head (or pressure) results, as judged by RMS error, were not very sensitive to the LSA4 salt unit permeability in either the freshwater or variable density model. Maximum RMS error difference for equivalent infiltration was 5.1 m for the freshwater model and 4.8 m for the variable density model. RMS error in both models became less sensitive to changes in salt unit permeability as infiltration increased. However, RMS error was somewhat more sensitive to changes in infiltration in both models. Maximum RMS error difference for equivalent salt unit permeability was 8.2 m for the freshwater model and 16.0 m for the variable density model.

RMS error, for both models, was less sensitive to changes in infiltration as salt permeability increased. Groundwater travel time estimates for the five freshwater simulations ranged from 2.3 to 404 million years, and they ranged from 7.5 to 445 million years for the four variable density simulations. This large range was attributed to the lack of realism in some realisations (as judged by their large RMS errors).

The inverse modelling approach applied in the REG-3 study for the *uncertainty and first order variance analysis* used additional information on kriged heads to constrain parameter distributions to plausible ones. This allowed prior estimates for parameter values and ranges (variances) to be modified according to the calibrated model results to form new or post estimates for parameter values and ranges.

Two Monte-Carlo Simulations were performed in the REG-3 study to determine the effect of uncertainties in hydrologic coefficient estimation on groundwater travel paths and travel times. Groundwater travel path variations for the 11- and 22-zone models were fairly similar. Histograms indicated a log-normal distribution with median values of 5.2 and 7.6 million years and minimum values of 2.9 and 2.4 million years for the two models.

Uncertainties in statistical parameters had a significant effect on the calculated groundwater travel times. Monte-Carlo and first-order analysis estimates of the lower 1-percentile, based on post hydraulic conductivity variances were a factor of 100 larger than lower 1-percentile estimates based on prior hydraulic conductivity variation alone for both the 11 and 22 zone models. This demonstrated that use of plentiful, relatively accurate, potentiometric head data in conjunction with prior hydraulic conductivity data could be combined through a statistical inverse approach to provide additional constraints that could reduce the uncertainty in computed groundwater velocity and travel time.

The Monte-Carlo uncertainty analysis in the LOC-1 study was limited to five realisations of log-permeability and porosity random heterogeneous fields generated using a Turning Bands Method. Base case simulations were run to establish the effects of intra-layer heterogeneities an additional homogeneous-layer using expected values of hydraulic conductivity and porosity for each nod in a given layer. Figure 6.18 illustrates the spatial distributions of expected values of hydraulic conductivity and porosity, contours of the resulting hydraulic head distribution, and predicted travel paths for streamlines starting at the eastern and western extent of the repository. For this base case, hydraulic conductivity was spatially uniform over each material subregion and changed abruptly at the interfaces between the 23 layers (subregions).

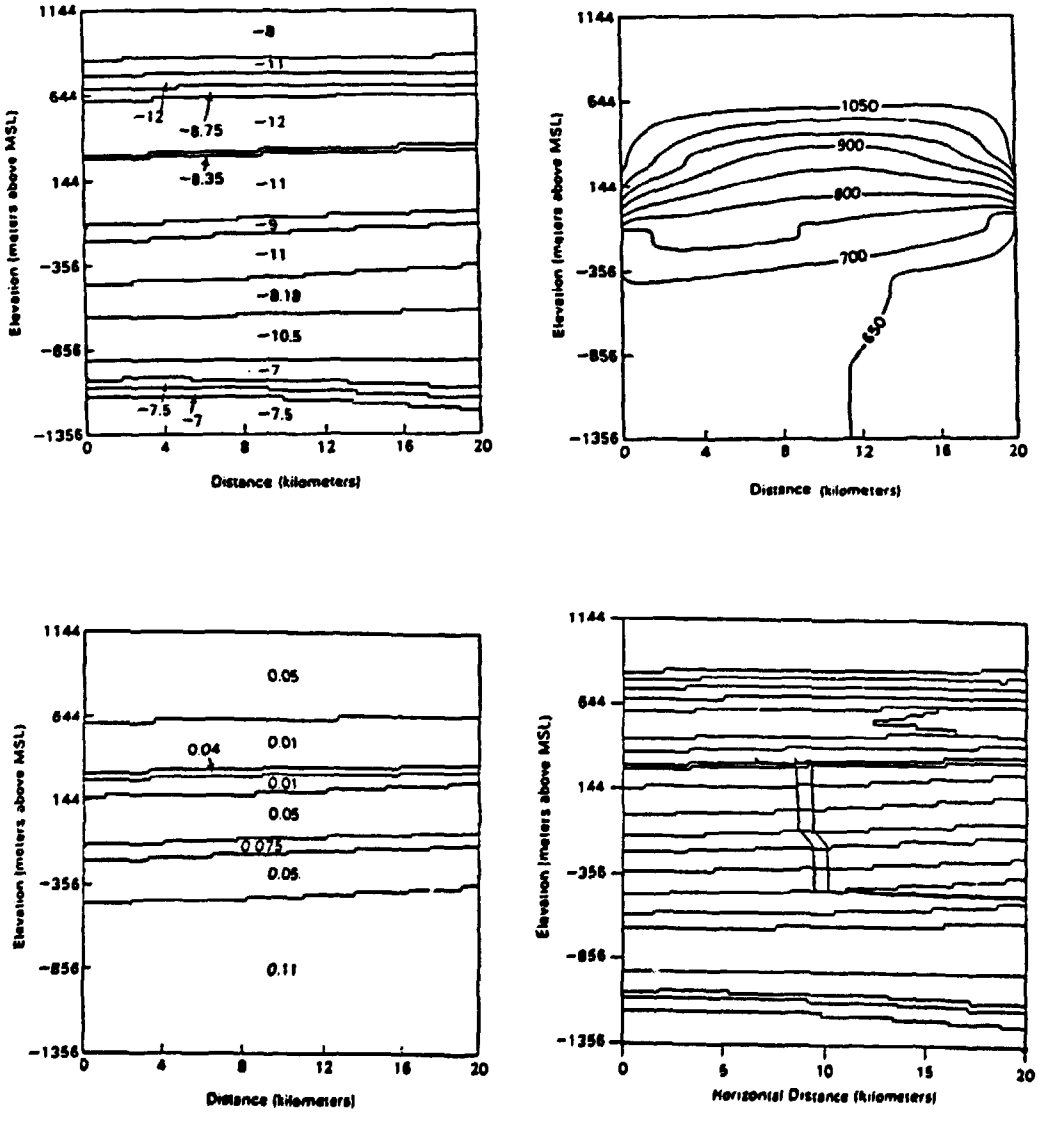


*Figure 6.18. LOC-1 study homogeneous-layer inputs and results. Contours of a) $\log_{10}$ horizontal hydraulic conductivity (m/s); b) porosity; c) head; d) calculated travel paths. Reported by the SRP-team using the MAG-code.*

The MAG-code converged for only three of the five realisations. All three hydraulic head distributions had the same gross features as for the homogeneous-layer case. Travel times to the edge of the disturbed zone varied from a minimum of 0.11 million years for realisation 1, through 2.3 million years for the homogeneous-layer case, to a maximum of 8.3 million years for realisation 2. The observed variability in travel times illustrated how travel time could be dominated by flow in high and low conductivity features.

Although the statistical model used was conditional, it was concluded that, because it explicitly incorporated available information on the locations of various hydrologic units, it was unconditional in the sense that the generated realisations of parameters did not correspond to, or were constrained by, any real data. It was felt that future stochastic modelling should incorporate conditional simulation methods and that boundary condition information for the intermediate scale should be based on regional hydrologic simulations performed conjunctively in order to explicitly incorporate geometry and effective average parameters of the intermediate-scale model in the regional modelling.

## 6.6 Case 4. Groundwater Flow over a Salt Dome

The particular problem considered here is an idealisation of the situation found in the rock overlying the Gorleben salt dome in Germany. The uppermost quaternary aquifer at the site contained fresh water. At a depth of 300 m the groundwater is saturated with salt. Geophysical measurements in boreholes revealed that the interface between fresh and salt water was usually sharp. The interface is a result of the hydrogeological situation and of diffusive/dispersive processes.

Results from HYDROCOIN Level 1 indicated that convection cells arised from the salt source along the bottom of the system as illustrated in Figure 6.19. It was not clear whether these cells were physically realistic. This Level 3 case was developed to investigate if the convection cells would be relevant for flow over salt domes. The investigation was performed by carrying out a sensitivity analysis to investigate effects of uncertainties in hydrogeological parameters, boundary conditions, and the conceptual model.

The modelled region was a two-dimensional vertical cross-section as shown in Figure 6.20.

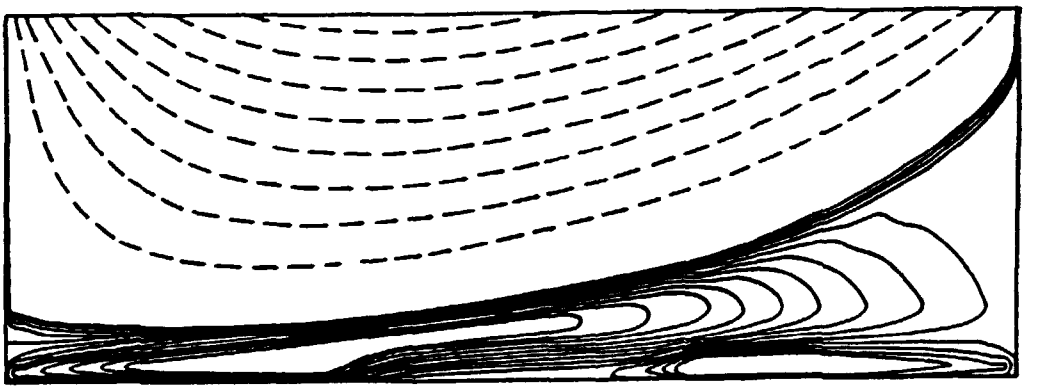

*Figure 6.19. Flow field streamlines computed by the AER Team's NAM-code illustrating predicted stratification of the system and the convection cells at salt dome edges. Solid lines are stream function contours at regular intervals between $-2.0 \cdot 10^{-4}$ and $-1.0 \cdot 10^{-3}$. Dashed lines are stream function contours at regular intervals between $-2.5 \cdot 10^{-3}$ and $-1.0 \cdot 10^{-2}$. These results were reported for Case 5 at Level 1.*

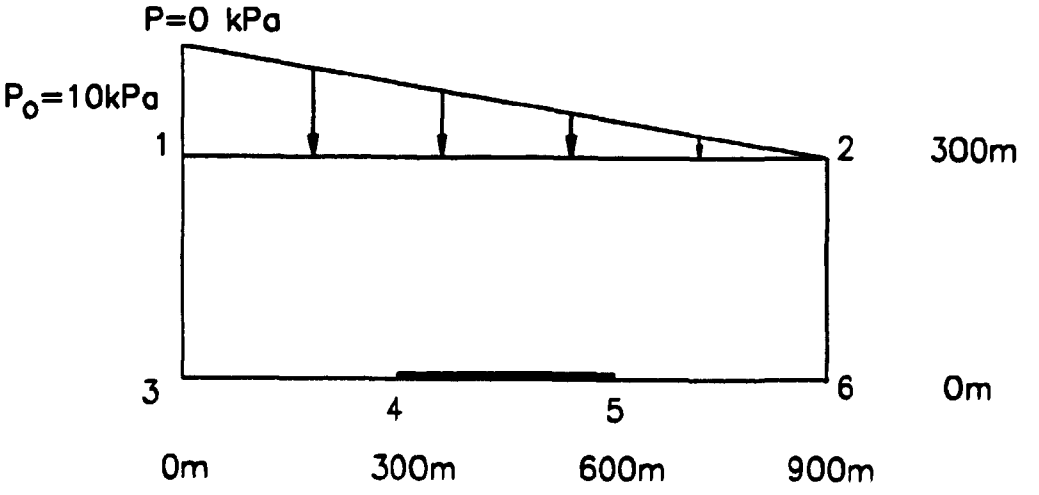


*Figure 6.20. Diagram of modelled region for Level 3 Case 4. Linear pressure variation imposed along top boundary (between points 1—2) and salt source located along bottom boundary midpoint (between points 4—5).*

Homogeneous and isotropic properties were suggested for the base case formulation. A linear variation in the pressure distribution was imposed along the top boundary with a maximum value of $p = 10^5$ Pa and a salt source was prescribed along the midpoint of the bottom boundary. The flow was assumed to be isothermal and governed by Darcy's law using an appropriately mass-averaged velocity. A mathematical model, boundary conditions, and values for base case parameters were provided to the participants.

Four basic variations were suggested, each including several additional minor variations. The basic variations included:

— 1. altered hydrogeological parameters for the homogeneous aquifer
— 2. altered conceptual model (inhomogeneous aquifer)
— 3. changes in boundary conditions, fluid properties (brine density and fluid viscosity), and geometry
— 4. sensitivity of the solution to grid density

***Results from Case 4***

Calculations on this test case were undertaken by the RIV- and the GSF-teams. All four basic variations as well as some combinations of them were studied to some extent. Additionally a new variant with a caprock boundary condition was investigated by the RIV-team.

A compilation of the studies by the GSF-team is presented in Table 6.6.

*Table 6.6. Summary descriptions of the base case and twelve variations studied by the GSF-team.*

| Variation | Description of variation | Mean recharge $l/m^2 \cdot yr$ | Maximum velocity $m \cdot yr^{-1}$ | Case realistic (y or n) | Max. change in concentration per time step at 500 years* | Case stationary (y or n) |
|---|---|---|---|---|---|---|
| | | **Homogenous Aquifer Variations** | | | | |
| Base Case | | $1.9 \cdot 10^3$ | 33.0 | n | $2.4 \cdot 10^{-4}$ | y |
| Fresh-water Case | | $1.9 \cdot 10^3$ | 31.0 | n | $2.4 \cdot 10^{-4}$ | y |
| 1.1 | only diffusion no dispersion | $1.6 \cdot 10^2$ | 3.6 | y | $6.7 \cdot 10^{-3}$ | n |
| 1.2** | only dispersion | $1.9 \cdot 10^3$ | 28.0 | n | $5.0 \cdot 10^{-5}$ | y |
| 1.3 | permeability decrease | $1.7 \cdot 10^2$ | 3.4 | y | $1.6 \cdot 10^{-2}$ | n |
| 1.4 | anisotropy | $6.5 \cdot 10^2$ | 16.0 | n | $7.7 \cdot 10^{-4}$ | y |
| | | **Inhomogeneous Aquifer Variations** | | | | |
| 2.2 | two horizontal anisotropic layers | $6.4 \cdot 10^2$ | 16.0 | n | - | n |
| 2.2(a) | anisotropic layers diffusion ($10^{-6}$ $m^2 \cdot s^{-1}$) | $4.3 \cdot 10^2$ | 17.0 | n | $9.2 \cdot 10^{-2}$ | n |
| | | **Altered Boundary Condition and Model Geometry Variations** | | | | |
| 3.1 | reduced density | $1.8 \cdot 10^3$ | 36.0 | n | $-2 \cdot 10^{-4}$ | y |
| 3.2 | max density along whole base | $9.9 \cdot 10^2$ | 32.0 | n | $1.9 \cdot 10^{-3}$ | n |
| 3.3 | reduced pressure on top boundary | $1.7 \cdot 10^2$ | 3.2 | y | $5.2 \cdot 10^{-5}$ | y |
| 3.2(a) | combination of 3.2 and 3.3 | $8.7 \cdot 10^1$ | 3.0 | y | $3.1 \cdot 10^{-4}$ | y |
| 3.2(b) | combination of 3.2 and 3.3 with diffusion ($10^{-6}$ $m^2 \cdot s^{-1}$) | - | - | - | $1.9 \cdot 10^{-2}$ | n |

* Concentration is salt mass fraction expressed in percentage.

** This case is equivalent to Level 1 Case 5.

The RIV-team used three different finite-element grids with their MTR-code, a regular grid, a fine regular grid and an irregular fine mesh designed to cope with the large salt mass fraction gradients near the salt dome boundary.

The calculated velocity vectors of the SW1-code for this case clearly showed convection cells at the bottom of the system at the edges of the salt dome. Differences in salt mass fraction contours, particle trajectories travel time and total distance supported the RIV conclusion that the MTR-solution was very sensitive to the spatial discretisation, especially in the lower part of the domain. Surprisingly, the coarse grid used by the TUB/BSF team, which was roughly equivalent to the RIV coarse grid, appeared to produce an adequate solution.

As indicated in Table 6.6, none of the *base case and homogeneous aquifer variations* which converged were judged to be realistic. Only the "diffusion only" and the "decreased permeability" cases were considered realistic. Recharge and maximum velocity were approximately one order of magnitude smaller for the realistic than for the unrealistic cases. The salt mass fraction distribution computed for the anisotropic variation after 500 years compared with the result from the RIV base-case showed that reduced vertical permeability decreased salt transport in the z-direction even for the coarse grid.

Plotted results from the *inhomogeneous aquifer variation* 2.2a shown in Figure 6.21 illustrate the presence of convection cells. Anisotropic layering appeared to enhance the formation of more clearly defined convection cells even in the presence of very high pore water diffusion. Calculational results also showed that combination of layering and anisotropy provides for an even sharper interface between the brine and freshwater parts of the system.

The GSF-team investigated five variations involving *altered boundary conditions*. The results indicated that reduced density caused the convection cells to disappear.

The RIV team examined variations of altered geometry involving an elongated domain. The salt mass fractions were reduced above the salt dome boundary and increased at the outflow boundary.

The team furthermore considered the coupling between fluid flow and salt transport specified by the salt dome boundary conditions as defined in the original case description to be physically inadmissible. They therefore examined both the simplified caprock boundary condition and the full caprock boundary condition along the salt dome boundary for the elongated domain. Results showed that the difference between the base case boundary condition and the simplified one was negligible. The small difference could partly be explained by the spatial discretisation used in the vicinity of the salt dome boundary. In contrast, the salt mass fraction for the full set of boundary conditions builds up very slowly.

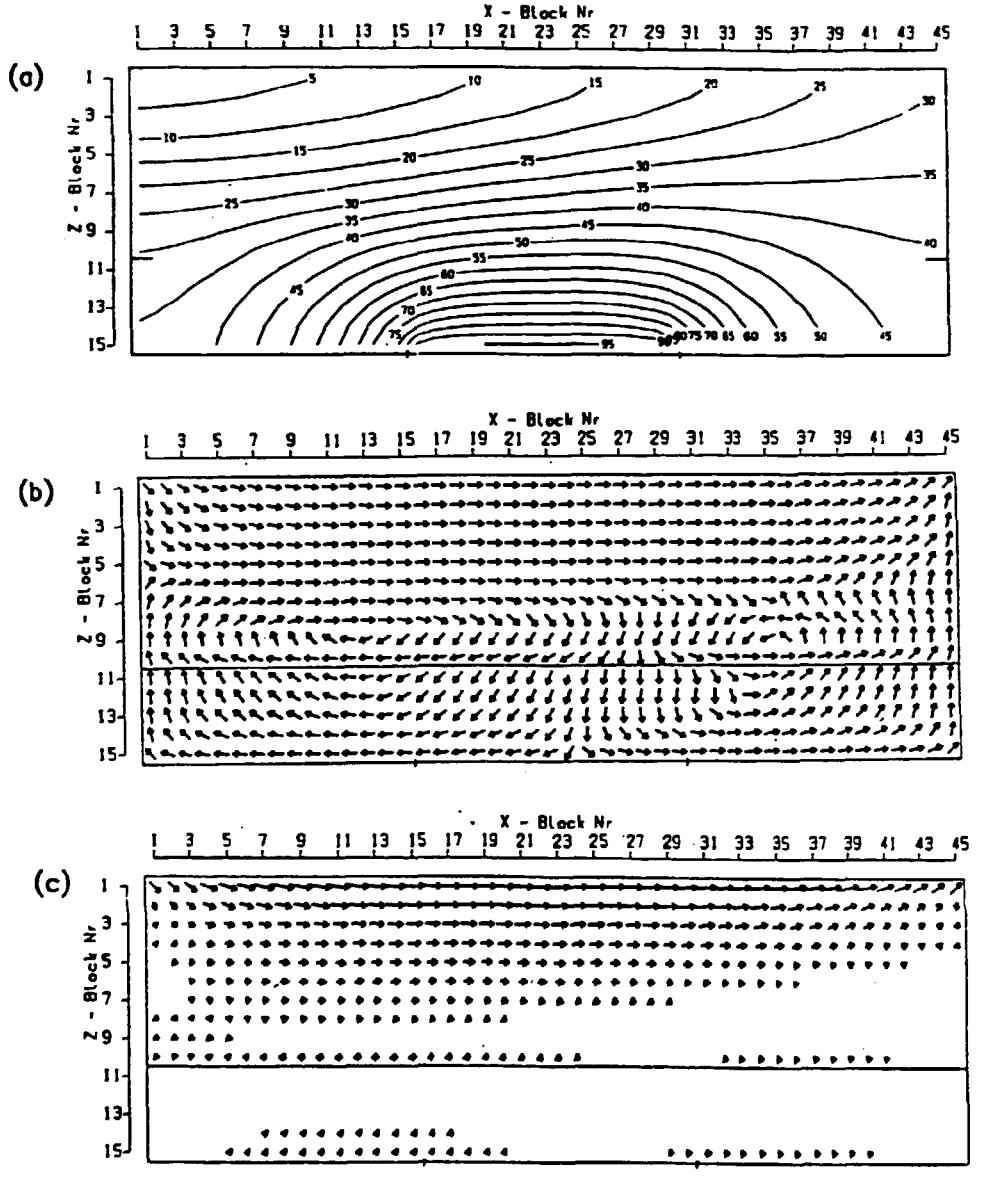


*Figure 6.21. SWI-code results for variation 2.2a (anisotropic horizontal layers and increased pore water diffusion $10^{-6}$ $m^2 \cdot s^{-1}$): (a) salt concentration contours (from 5% through 95%), (b) velocity vector field (direction only), (c) velocity vector field (small vectors not plotted). Results from the GSF-team.*

## 6.7 Case 5. Groundwater Flow in Crystalline Rocks
## Case 5a. Chalk River Nuclear Laboratory Site
## Case 5b. Fjällveden Site

The test case addressed the issue of uncertainty analyses of flow problems in crystalline rocks at the two sites Chalk River and Fjällveden. The investigations involved the uncertainty in boundary conditions, permeability distribution and numeric model. A base case scenario was formulated for each site and a number of possible variations were proposed. The flow rate at a given point and the travel time along a pathline starting at a given point were proposed as performance criteria.

### Case 5a. Chalk River

The Chalk River test case was based on the results of investigations made at the Chalk River Nuclear Laboratories (CRNL). The site consists of a 200 m by 150 m area of predominantly quartz monzonite overlain and underlain by paragneiss (Figure 6.22).

The site was judged to be of relatively uniform fracturing. An experimental programme had been performed to get information on inherent hydraulic properties governing the groundwater flow, such as

- the overall fracture geometry at the site,
- measurements of hydraulic conductivities, specific storage, natural groundwater flow and pressure boundaries, and
- the distribution of hydraulic head under undisturbed conditions.

Seventeen vertical and inclined boreholes were drilled at the study site. The location of the holes relative to the fracture zones are indicated in Figure 6.23.

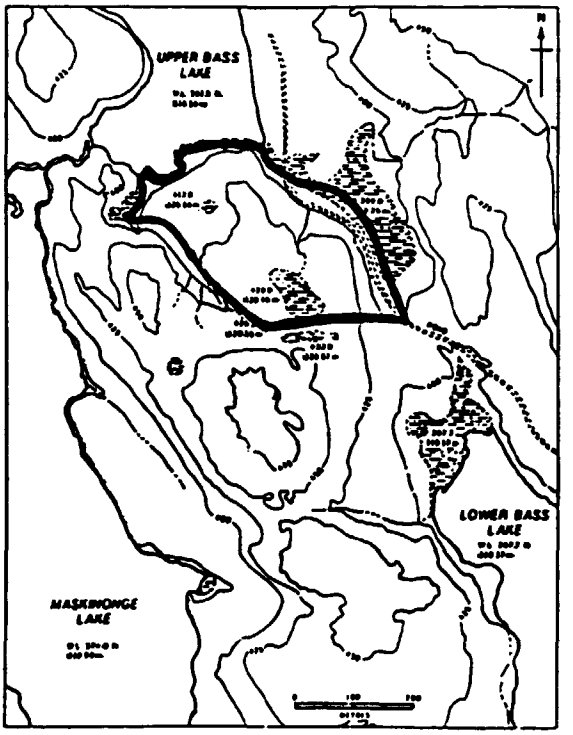


*Figure 6.22. Topographical map of the CRNL-test area. The proposed model domain is indicated with a thick line.*

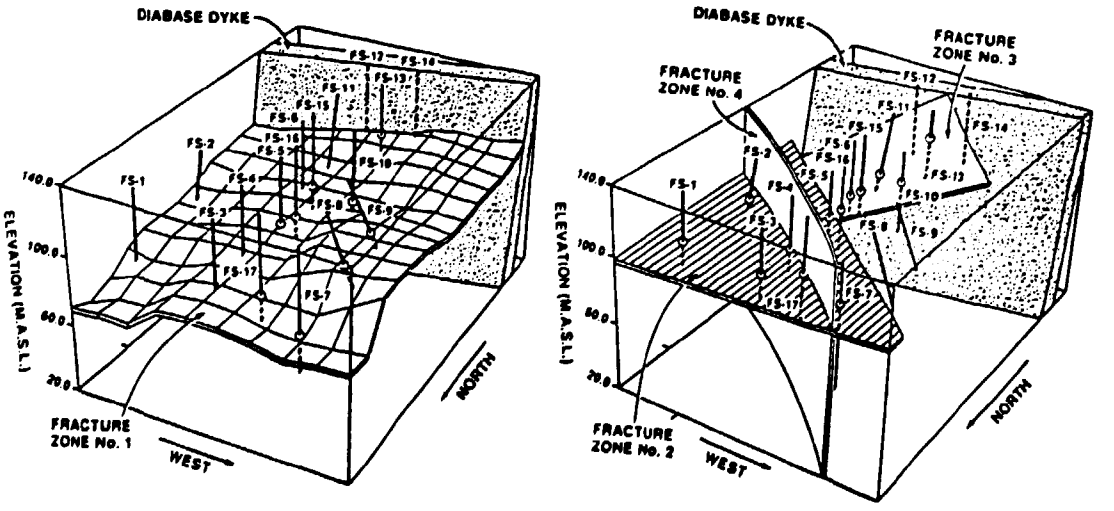


*Figure 6.23. Isometric sketch of the CRNL test site showing the locations of boreholes and hydraulic structures.*

More than 350 steady-state injection tests yielding data on flow rate per unit head have been performed. Most of the interference tests were performed at a constant flow rate, where the drawdowns were monitored at a number of positions as a function of time. In addition, the hydraulic diffusivity of the adjacent rock was evaluated.

The test case was analysed by the MCI-team using the FM3-code. The sensitivity and uncertainty analyses used 29 model runs performed for the model calibration step which was part of HYDROCOIN Level 2. The parameter sets were selected by Expert Choice in order to minimise a goodness-of-fit function and not to explore the sensitivity and uncertainty of a given performance measure.

***Results from Case 5a***

The *sensitivity analysis* was based on linear regression. The performance measure was defined as the groundwater travel time from a location at the top of hole FS-11 to fracture zone no. 1.

To allow for a comparison between the regression slopes for the various model parameters the parameters and the performance measures were normalised with their respective standard deviations. The slope of the regression curve of the normalised performance measure against a normalised parameter could then be calculated as the correlation coefficient for this parameter.

It was concluded that the chosen performance measure was more sensitive to the permeabilities in the topmost mesh layer than to the azimuth of the symmetry axis of the permeability tensor in the same mesh layer. The correlation coefficients of the individual parameters showed that the permeabilities in the topmost layers of the mesh had a strong influence on the chosen travel time. Also the inclination of the permeability tensor had a comparatively strong correlation, whereas the transmissivities in the fracture zones appeared to be of little significance for this performance measure. The analysis showed that there was no predominant influence from any single parameter. The chosen performance measure thus depended on a set of parameters.

The travel time was plotted versus the flow rate at the starting point of the path line (Figure 6.24). The correlation between the two performance measures proved to be quite good and it was concluded that the analysis could be restricted to one of the two.

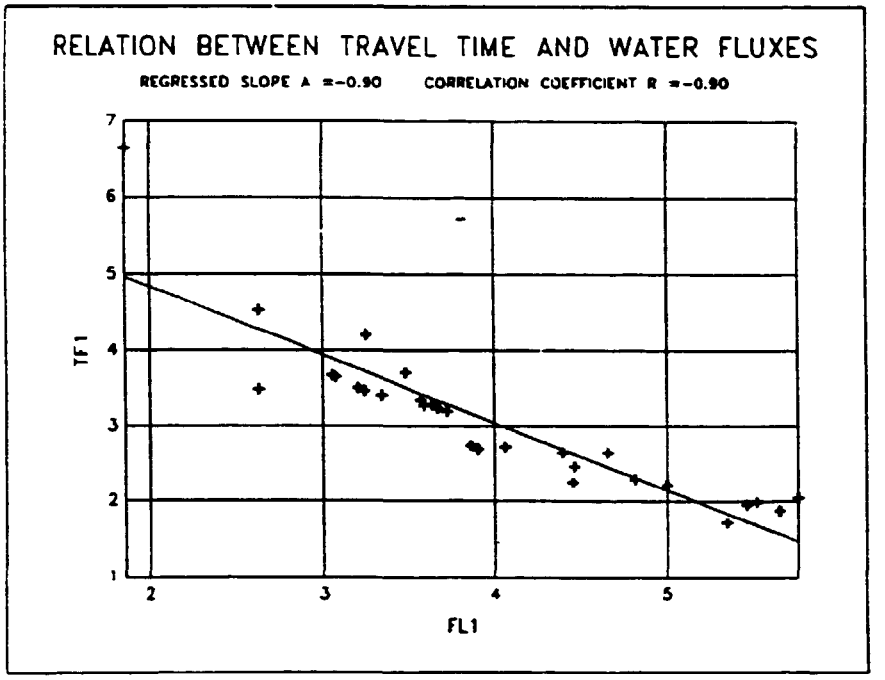


*Figure 6.24. Regression curve for normalised travel time versus normalised groundwater flow rate.*

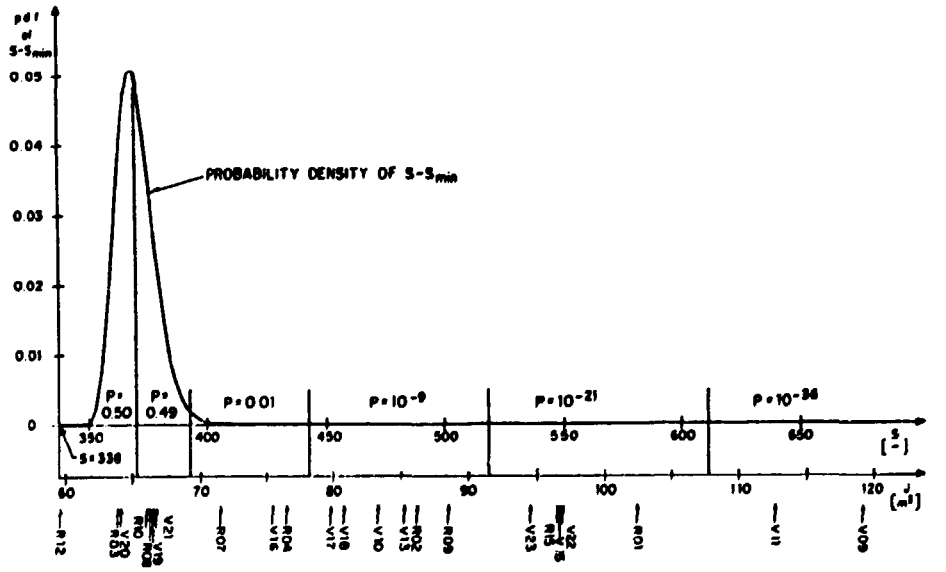


*Figure 6.25. Probability density function for the goodness-of-fit function and the probabilities of intervals of this function. The arrows under the x-axis denote the individual runs.*

Uncertainty analysis normally requires that probabilities are assigned to the parameter sets used. In the MCI-analysis the parameter values were not assigned a priori probabilities. Instead the hydraulic heads measured at the site and the calculated goodness-of-fit function for the 29 model runs were utilised to assign a posteriori probabilities to the parameter sets, and complementary probability distribution were calculated for the selected performance measure. Bayes' theorem was used to establish a relationship between the log-likelihood criterion and the goodness-of-fit function. Figure 6.25 shows the probability density function of the log-likelihood function and the calculated interval probabilities. It was commented by the Project Team that the actual probabilities of the individual runs depended strongly on the scaling factor between the goodness-of-fit function and the log-likelihood function.

## Case 5 b. Fjällveden

The Fjällveden site was investigated as part of the Swedish KBS-3 study. The area of the site is 2.7 by 3.7 km. 15 deep (> 150 m) and 49 shallow (< 150 m) boreholes have been drilled at the site. Figure 6.26 shows a map of the site and Figure 6.27 gives a conceptualisation of the linear map.

The site was modelled in three dimensions. Two hydraulic unites "rock mass" and fracture zones" were modelled in the base case scenario. They were attributed the following expressions for the variation of the hydraulic conductivity with depth:

$K = 1.5 \cdot 10^{-3} \cdot (\text{depth})^{-2.78}$ m·s$^{-1}$ for the rock mass

$K = 0.17 \cdot (\text{depth})^{-3.25}$ m·s$^{-1}$ for the fracture zones

These expressions represent the geometric mean of all the conductivity measurements at the site. A held potential corresponding to an interpreted groundwater table was applied at the top surface. Zero flux boundary conditions were imposed on the vertical and bottom boundaries.

It can be seen in Figure 6.28 that the spread of the hydraulic conductivity data was very wide.

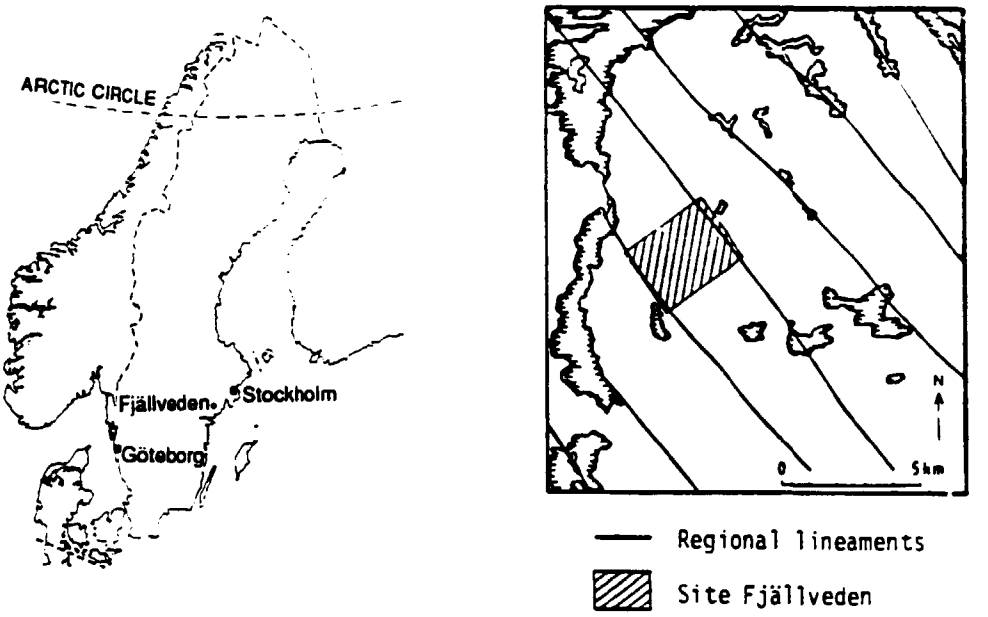


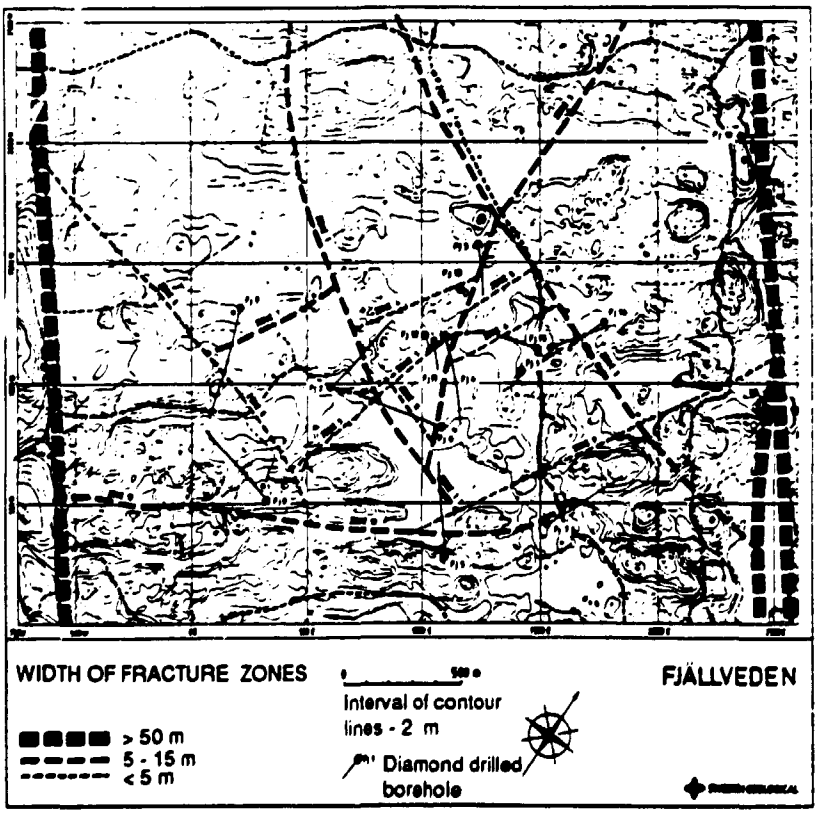


*Figure 6.26. Lineament map over the Fjällveden site.*

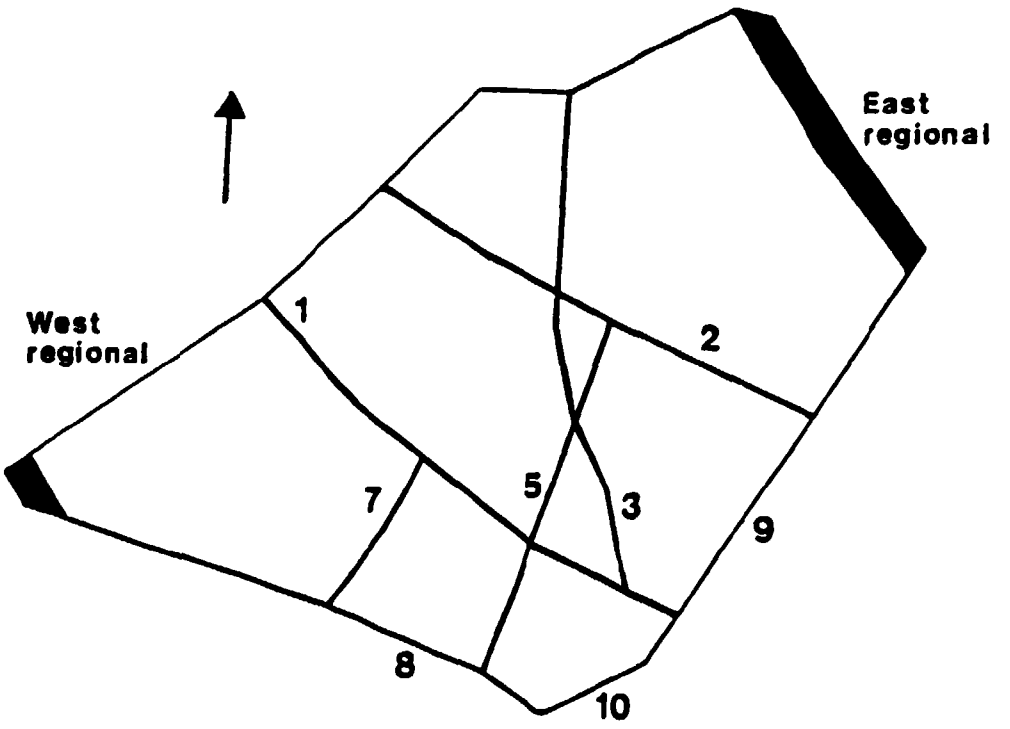


*Figure 6.27 Conceptualisation of the lineament map. This map formed the base for the mesh that was available to the Project Teams. The numbers correspond to the number of the fracture zones.*

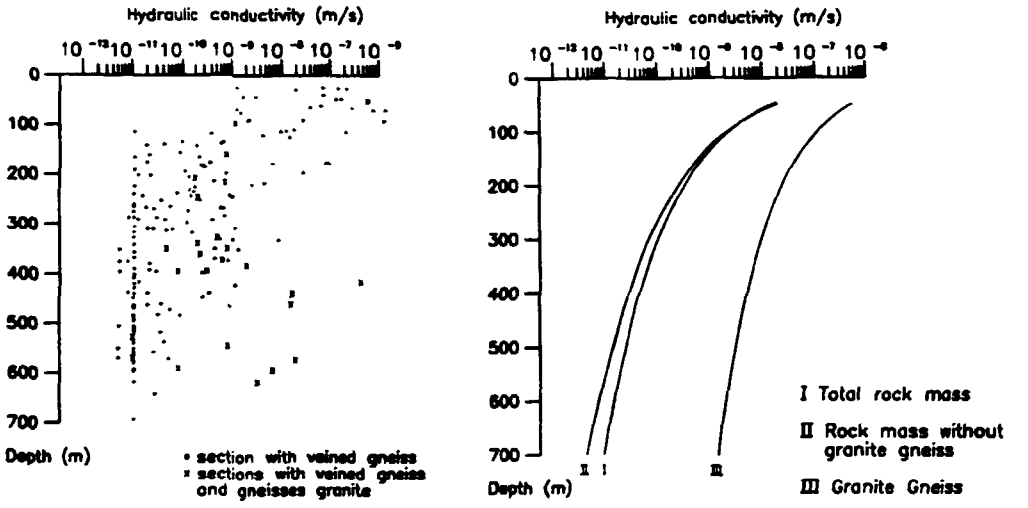


*Figure 6.28. Hydraulic conductivity vs depth for the rock mass at the Fjällveden site. The data comprises more than 200 points.*

As a variation to the base case the uncertainties caused by the regression curves and their interpretation were analysed.

The performance measures to be analysed were the flow rate at the point x =365 m, y = 60 m, z =-500 m, and the travel time for a particle released at the same point. A fictional porosity of 1.0 was assumed for convenience in comparing results, so that the particle velocity would be equal to the Darcy velocity.

### *Results from Case 5b*

The test case was attempted by the JAE and the KEM-teams. JAE used the 3DS-code, while the KEM applied the GWH-code, both codes being finite-element codes. As can be seen in Table 6.7, there are minor deviations between the approaches of the Project Teams in the modelling of the fracture zones.

*Table 6.7. Modelled geometrical properties of the fracture zones at Fjällveden.*

| Fracture zone | Width (m) JAE | Width (m) KEM | Incl. (°) JAE | Incl. (°) KEM |
|---|---|---|---|---|
| 1 | 10 | 5 | 90 | 90 |
| 2 | 10 | 20 | 80 NE | 80 NE |
| 3 | 10 | 10 | 90 | 90 |
| 4 | - | - | - | - |
| 5 | 3 | 5 | 80 NW | 80 NW |
| 6 | - | - | - | - |
| 7 | 14 | 14 | 60 NW | 60 NW |
| 8 | 5 | 5 | 90 | 90 |
| 9 | 5 | 5 | 75 SE | 75 SE |
| 10 | 5 | 5 | 70 SE | 70 SE |
| 11 | - | - | - | - |
| Regional | 90 | 100 | 75 SW | 90 |

The *JAE-team* performed 22 simulations in 3D for this test case. All simulations aimed at investigating the sensitivity of the model to changes in hydraulic conductivities of the rock mass and the fracture zones. In the analysis, the team assumed different depth dependence of either one or both hydraulic units (rock mass and fracture zones). The conductivities were treated as depth dependent according to the base case formulation obeying a power function

— (step-wise) constant
— depth dependent obeying a log-linear function
— depth-dependent according to the anisotropic formulation in the test case description

The different subcases were grouped into four classes according to the chosen strategy of assigning hydraulic conductivities:

— Group 1. Fracture zone properties were kept constant. Rock mass properties were varied.
— Group 2. Fracture zone properties were varied, rock mass properties were kept constant.
— Group 3. Fracture zone properties and rock mass properties were considered either constant with depth or log-linearly decreasing with depth.
— Group 4. Anisotropic rock mass conditions were assumed as in the base case definition. Fracture zone properties were varied.

Results for Group 1 variations showed rather small deviations from the average travel length, indicating that the flowpaths followed the regional flow pattern with only small internal deviations. On the other hand the travel times showed a rather wide spread, which reflected the ranges of conductivities assumed for the rock mass.

Of the six Group 2 simulations only two gave pathlines that exited the domain in the regional fracture zone. The deviations from the average travel time for the water particles to fracture zone 9 were relatively small. The average path was 1160 m with a range of ±15%.

In Group 3 with three subcases the pathlines appeared to have shorter travel times and travel lengths on average compared to the base case and Group 1 and 2.

Within group 4 consisting of four subcases all released particles reached the regional fracture zone, which was supposed to be the correct exit point.

The JAE-team also reported the flow rates for the 22 simulations. The variability of the results reflected the variation of the permeability assigned at the point, where the flow rate was evaluated. Although no detailed analysis was performed, the hydraulic gradient did not seem to vary to the same extent as the permeability.

The *KEM-team* performed nine simulations in three dimensions for this case. The calculations comprised variations of the hydraulic conductivities of the rock mass and the fracture zones. The assumed variations of the hydraulic conductivities for the subcases are shown in Table 6.8.

*Table 6.8. Hydraulic conductivities ($m \cdot s^{-1}$) assigned to the model for Subcases 1-9.*

| | Subcase | Rock mass | Fracture zones |
|---|---|---|---|
| 1 | | $1.5 \cdot 10^{-3} \cdot z^{-2.78}$ | $0.17 \cdot z^{-3.15}$ |
| 2 | NE & Vert | $2.8 \cdot 10^{-3} \cdot z^{-2.38}$ | = Subcase 1 |
| | NW | $3.4 \cdot 10^{-3} \cdot z^{-3.11}$ | |
| 3 | | = Subcase 1 | |
| 4 | 0-260 m | = Subcase 2 | $3.12 \cdot 10^{-7}$ |
| | >260 m | | $2.26 \cdot 10^{-9}$ |
| 5 | | = Subcase 2 | $2.29 \cdot z^{-3.15}$ |
| 6 | | = Subcase 2 | $5.12 \cdot 10^{-9}$ |
| 7 | 0-100 m | | = Subcase 1 |
| | 100-200 m | | |
| | >200 m NE & Vert | $2.9 \cdot 10^{-9} \cdot z^{-0.49}$ | |
| | NW | $3.0 \cdot 10^{-5} \cdot z^{-2.32}$ | |
| 8 | "near-zone" | $3.9 \cdot 10^{-2} \cdot z^{-3.13}$ | = Subcase 1 |
| | NE & Vert | $6.8 \cdot 10^{-4} \cdot z^{-2.53}$ | |
| | NW | $1.2 \cdot 10^{-3} \cdot z^{-2.93}$ | |
| 9 | NE & N | = Subcase 8 | $4.5 \cdot 10^{-2} \cdot z^{-3.02}$ |
| | NW | | $7.6 \cdot z^{-3.73}$ |

Note that the fracture zone properties in Subcases 4 and 5 were based on the arithmetic mean values as opposed to the geometric mean for the remainder of the cases.

For the nine subcases a water particle was released at the position specified for the test case. The results for the nine subcases were quite similar for both the travel time and the travel length. Travel times and travel lengths are summarised in Table 6.9.

*Table 6.9. Pathlines for the KEM-team; accumulated travel times and travel lengths.*

| Subcase | Travel time (years) | Travel length (m) |
|---|---|---|
| 1 | $1.3 \cdot 10^8$ | 1070 |
| 2 | $6.6 \cdot 10^7$ | 1075 |
| 3 | $1.2 \cdot 10^8$ | 1490 |
| 4 | $7.4 \cdot 10^7$ | 1345 |
| 5 | $6.6 \cdot 10^7$ | 1625 |
| 6 | $7.3 \cdot 10^7$ | 1615 |
| 7 | $4.8 \cdot 10^7$ | 1520 |
| 8 | $7.8 \cdot 10^7$ | 1500 |
| 9 | $7.5 \cdot 10^7$ | 1715 |

The results could be seen as an indication that the fracture zone properties are less important than the rock mass properties, at least for the performance measure chosen. This depends mainly on the fact that the principal part of the flow path is running in the anisotropic rock mass in a direction coinciding with the main strike of the increased conductivity.

The flow rates were calculated at the position corresponding to the release point for the calculated flow paths. The resulting flux values for the nine subcases are shown in Table 6.10.

*Table 6.10. Flow rates as reported by the KEM-team for their simulations of the Fjällveden site.*

| Subcase | Flow rate ($m \cdot s^{-1}$) |
|---|---|
| 1 | $1.27 \cdot 10^{-13}$ |
| 2 | $3.49 \cdot 10^{-13}$ |
| 3 | $9.51 \cdot 10^{-14}$ |
| 4 | $3.17 \cdot 10^{-13}$ |
| 5 | $3.49 \cdot 10^{-13}$ |
| 6 | $3.17 \cdot 10^{-13}$ |
| 7 | $7.29 \cdot 10^{-13}$ |
| 8 | $3.17 \cdot 10^{-13}$ |
| 9 | $3.17 \cdot 10^{-13}$ |

The results showed that the flow rate was relatively insensitive to the different assumptions about the hydraulic conductivities.

The KEM-team also evaluated the distribution of the flow rate over a rectangle corresponding to the location of a potential repository covering about 1 $km^2$. Figure 6.29 shows the calculated distribution of the groundwater flow rate.

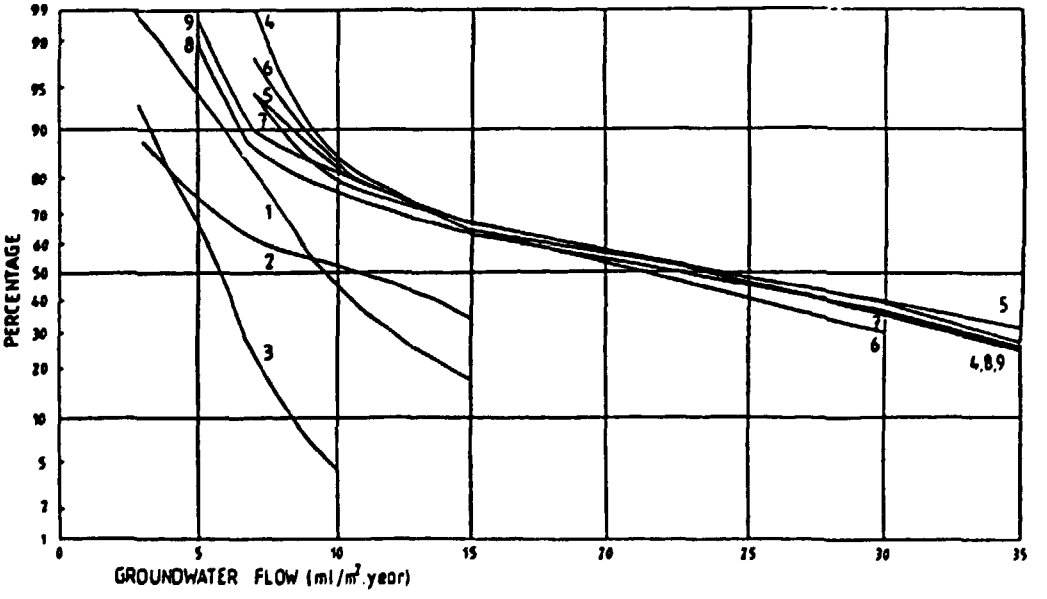


*Figure 6.29. Frequency distribution of the groundwater flow rate at z = -500 m over an area corresponding to the potential repository (reported by the KEM-team).*

## 6.8 Case 6. Three-Dimensional Regional Groundwater Flow in Low Permeability Rocks

The test case was an extension to Test Case 4 of HYDROCOIN Level 2 involving regional groundwater flow in the Piceance Basin. As for any regional flow system, there was a large degree of uncertainty in the prior estimates of hydraulic parameters for this case.

The Piceance Basin is a structural depression located in northwestern Colorado. Stratigraphical and hydrostratigraphical units are listed in Table 6.11. Major drainages along with the basin boundaries are displayed in Figure 6.30.

*Table 6.11. Stratigraphical and hydrostratigraphical units in the Piceance Basin.*

| Formation | Member | Lithology | Zone |
|---|---|---|---|
| Uinta Formation | | Fractured Sandstone, Marlstone and Siltstone | 5 |
| Green River Formation | Parachute Creek | Fractured Marlstone | 4 |
| | | Oil Shale | 3 |
| | | Fractured Marlstone | 2 |
| | | | 1 |
| | Garden Gulch | Shale and Marlstone | |

Boundaries of the groundwater system were well defined, as the "impermeable" Garden Gulch Member of the Green River Formation crops out along the entire perimeter of the basin, indicating that the basin tilts from south to north.

The conceptual model of the system is displayed in Figure 6.31.

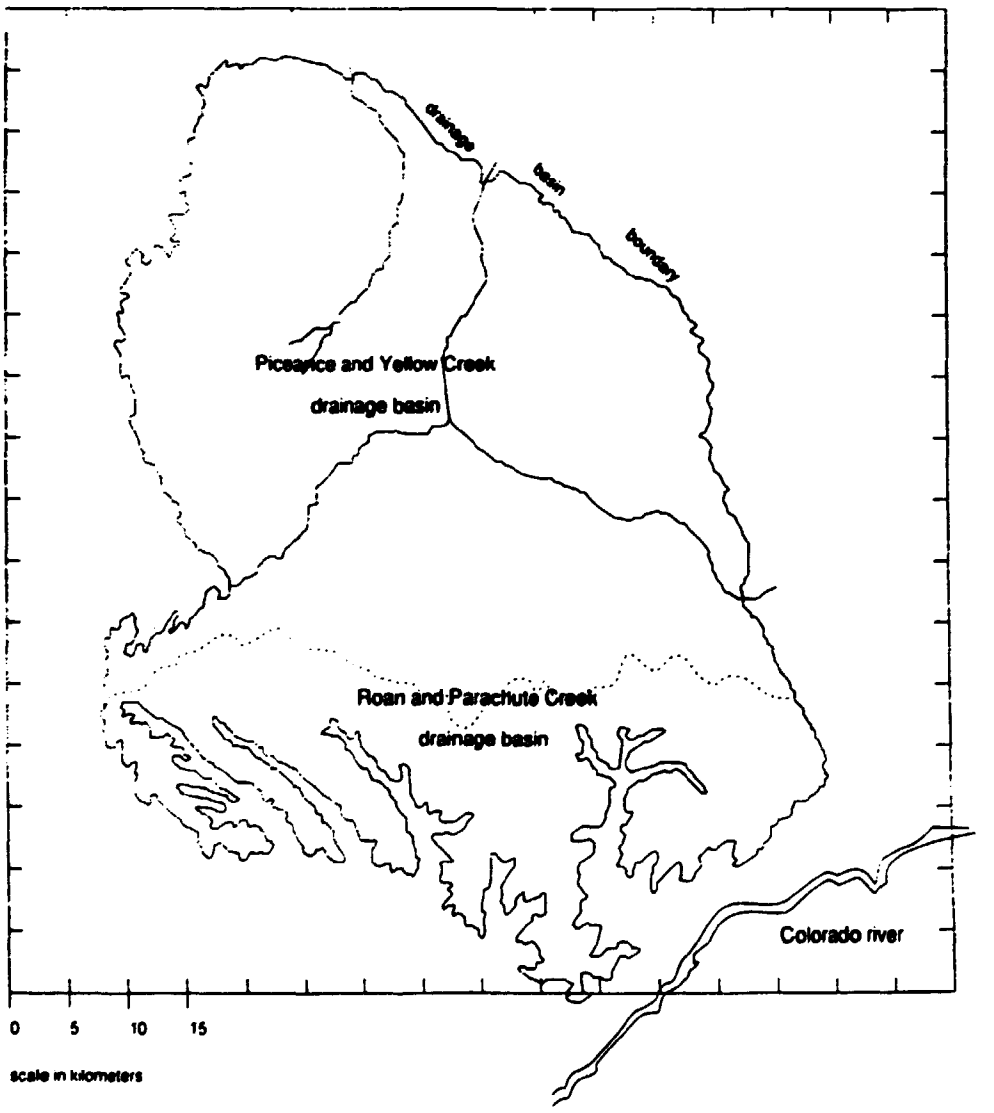


*Figure 6.30. Margins of the Piceance Basin and major streams within the basin.*

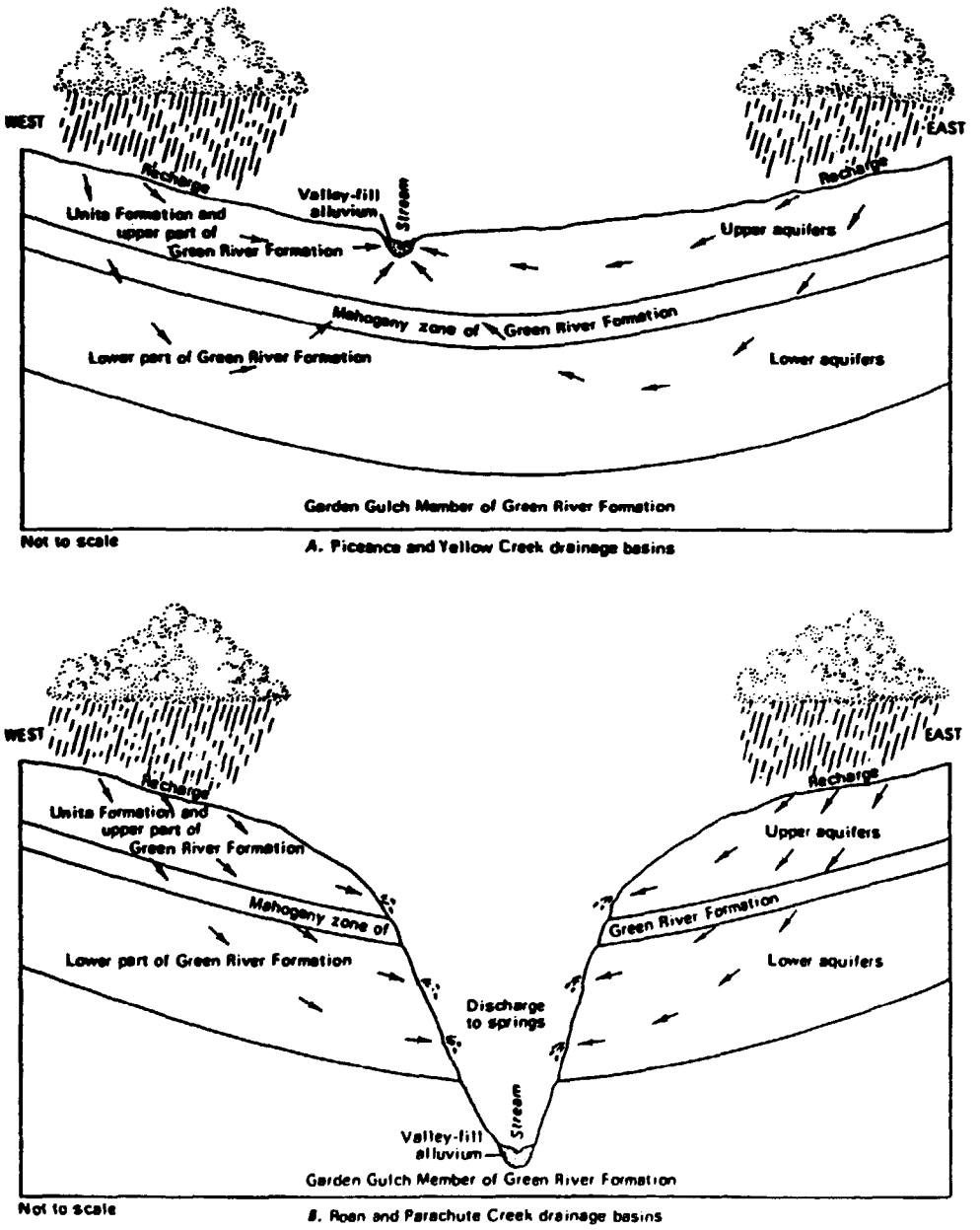


*Figure 6.31. Idealised cross-sections of the Piceance Basin illustrating the concept of groundwater flow in the basin.*

For the study, the Garden Gulch Member of the Green River Formation was taken to be an impermeable lower and lateral barrier to groundwater flow. The measured hydraulic heads and fluxes were assumed to represent steady-state conditions. The layers were assumed to be horizontal with a constant thickness, varying from 50 to 120 m.

The input parameters included

- ranges of vertical hydraulic conductivities and a transmissivity
- layer thicknesses
- recharge distribution and amounts
- elevations of streams and springs and their associated layers

A porosity of 0.1 was assumed for all layers. The rocks in the basin display vertical anisotropy and possibly also horizontal anisotropy. Ranges of values are given in Table 6.12. Darcy's law was supposed to be valid.

*Table 6.12. Ranges of the vertical hydraulic conductivities ($m \cdot s^{-1}$) estimated for the hydrostratigraphical units in the Piceance Basin.*

| Layer | Range |
|---|---|
| 5 | $4.6 \cdot 10^{-9}$ - $2.0 \cdot 10^{-6}$ |
| 4 | $6.0 \cdot 10^{-9}$ - $3.0 \cdot 10^{-6}$ |
| 3 | $1.0 \cdot 10^{-9}$ - $3.0 \cdot 10^{-7}$ |
| 1 | $3.0 \cdot 10^{-10}$ - $1.0 \cdot 10^{-7}$ |
| Transmissivity ($m^2 \cdot s^{-1}$): | |
| 3 | $4.9 \cdot 10^{-3}$ - $1.5 \cdot 10^{0}$ |

The objective of the case was to test methods of handling uncertainty and addressing model sensitivity for a large-scale three-dimensional flow in low permeability anisotropic rocks and the modelling approaches employed to simulate an incompletely defined system, where the input parameters are given only in terms of possible ranges.

The hydraulic parameters that control flow in the Piceance Basin were only known within a specified range. The use of the complete range of each variable would result in a large degree of uncertainty in the performance measure, e.g. the groundwater travel time. However, combinations of parameter values within the range of each variable might produce model results in the form of hydraulic heads that are inconsistent with the interpolated values. Therefore, in addressing uncertainty in hydraulic parameters the performance measure would be conditioned at the ability of the model to reproduce the measured heads. Interpolated heads, standard deviation from the kriging procedure and positions were provided, as well as location of the lines along which the values were to be calculated (Figure 6.32).

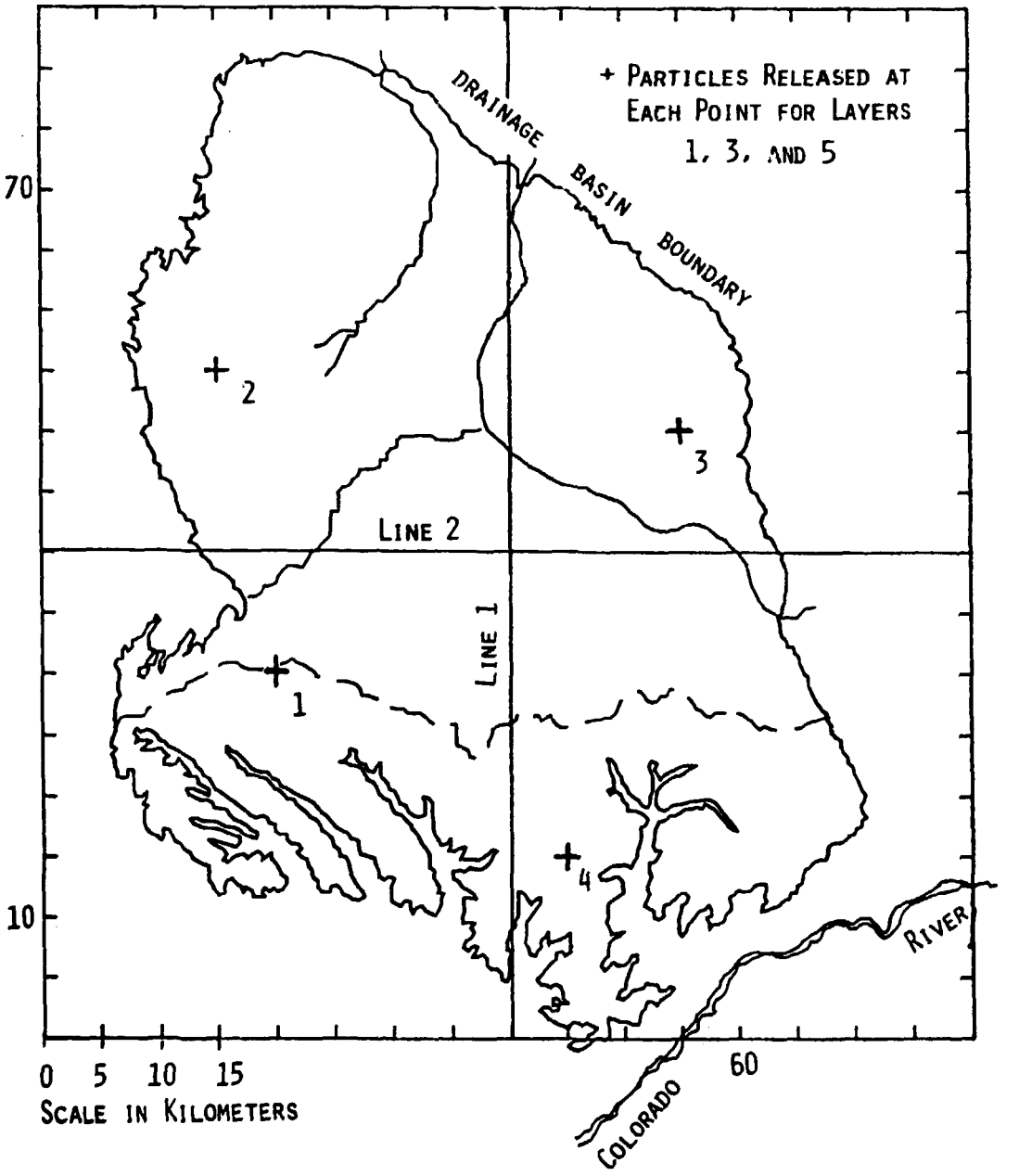


*Figure 6.32. Location of cross-section lines and particle release points for problem evaluation.*

***Results from Case 6***

Only the SAN-team using the USG-code tackled this case. Uncertainty and sensitivity analyses were performed, using Monte-Carlo simulations for uncertainty analysis and regression of the Monte-Carlo results against the sampled parameters for sensitivity analysis. The performance measure for both uncertainty and sensitivity analyses was the groundwater travel time for a particle released at the centre of the basin in the middle layer travelling to any discharge point.

For the *uncertainty analysis*, Latin Hypercube sampling was used to generate 90 sets of input data. Results from the simulations showed that predicted groundwater travel paths generally travelled initially downward to either layer 2 or all the way to layer 1 and then horizontally northward until they were forced upward at the edge of the model and discharged into Piceance Creek. Groundwater travel times ranged from 1700 to 87000 years with a median value of 18000 years. None of the 90 simulations produced hydraulic head surfaces in agreement with the measured surfaces, indicating that none of the sets of sampled values were in the range of the Level 2 calibrated values. Investigation disclosed that the cause of the error was probably the range of recharge specified in the problem definition.

The *sensitivity analysis* was performed by undertaking both stepwise and rank regression of the predicted groundwater travel times against the sampled parameter values. The parameters identified as most important are shown in Figure 6.33.

The porosity appeared to be the most important parameter. However, neither regression gave a very good fit. (The $R^2$ values were 0.63 and 0.59.) It was considered that the apparent importance of the porosity was due to the unrealistic choice of a common porosity for all the layers. It is doubtful that the porosity would have been the dominant parameter if a more realistic model had been used with a different porosity for each zone in each layer.

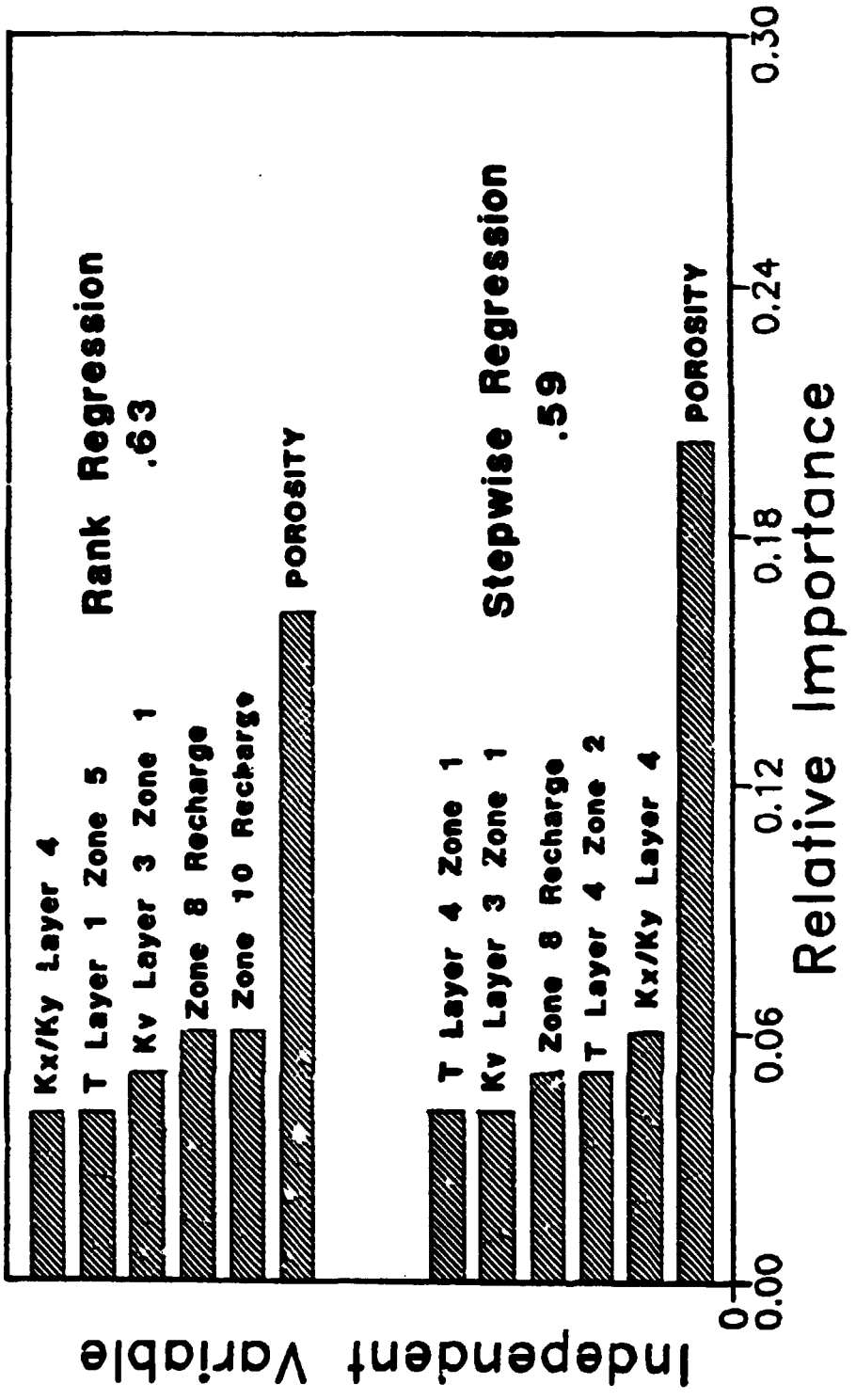


*Figure 6.33. Important variables as identified by the SAN-team.*

## 6.9 Case 7. Comparison of Calculated Flow Paths to Analytical Solutions

An important step in radionuclide transport analysis is to calculate pathlines using the results of a hydrological simulation. Regulatory bodies may require estimates of groundwater travel time in the evaluation of disposal sites. Most models are not devised to directly provide pathlines or stream function values. Consequently, transport paths must be obtained from calculations based on the calculated potential (or head). Approximations made in these calculations compound the uncertainty associated with the solution for the potential. In addition, the accuracy of the flow paths may exhibit sensitivity to certain features of the model, such as grid density, independent of the potential solution itself. Furthermore, particle tracking may depend on the methods used, as observed at Level 1.

This test case was designed to provide a means of comparing methods of trajectory calculation, independent of the model employed to estimate the potential surface. As the process of trajectory calculation can be conceived as being composed of two discrete steps, calculation of velocities from simulated potentials, followed by estimation of flow lines from the calculated velocities, the problem output called for both velocities estimated from samples of the potential field and flow paths calculated from the analytical expression for the velocity.

The formulation of this test case was oriented towards verification rather than sensitivity and uncertainty analysis. However, sensitivity analysis could be performed, to some extent, with respect to sensitivity certain parameters, such as grid density.

Test Case 7a concerned particle tracks in the flow field due to a single well discharging at a constant rate localised in a uniform flow field with homogeneous hydraulic properties (see Figure 6.34); while Case 7b dealt with particle tracks in a uniform flow field with a circular region in the middle of the domain having hydraulic properties differing from the rest of the domain.

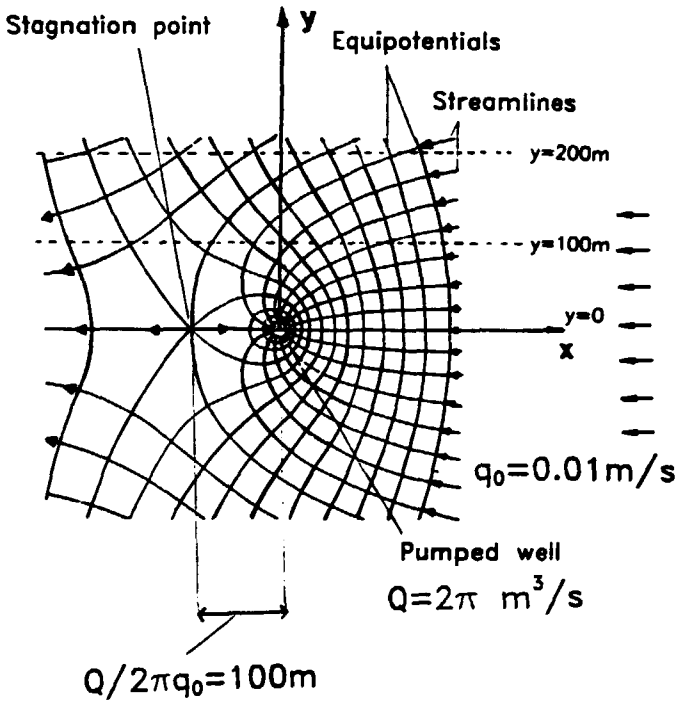


*Figure 6.34. Domain of interest for Case 7a. Flow field near a pumped well with uniform background velocity $v_x = -v^b$. Profile 1—3 correspond to velocity profiles.*

As shown in Figure 6.34 there is a groundwater divide in the flow field for Case 7a which defines two flow regions, one which converged to the well, and one which bypasses it. The potential or hydraulic head was assumed to obey the steady-state Poisson equation.

Boundary conditions as well as solutions for the potential and the velocity components in the x and y directions were provided based on the known analytical solution for the potential and stream function for flow in the combined flow field due to a pumping well in infinite confined aquifer. The specified values for the pumping rate of $2\pi$ $m^3 \cdot s^{-1}$ and background velocity 0.01 m/s resulted in a stagnation point at (-100.0) with the asymptotes of the groundwater divide at y =+100p. In order to provide a consistent velocity from the analytical solution, a subroutine was provided to find the average velocity normal to a directed line segment. An analytical solution for both the potential and stream-function was available for a pumping well in an infinite confined aquifer.

The Project Teams were requested to submit estimated trajectories of particles released at the points marked in Table 6.13, along with the associated path lengths and travel times.

*Table 6.13. Coordinates for release points of particles, Case 7a.*

| Point no | x (m) | y (m) |
|---|---|---|
| 1 | -110 | 0 |
| 2 | - 90 | 0 |
| 3 | - 50 | 150 |
| 4 | 100 | 200 |
| 5 | 400 | 250 |
| 6 | 400 | 260 |
| 7 | 400 | 100 |
| 8 | 400 | 0 |

The pathlines should be calculated with two sets of velocity values:

- Velocities calculated using analytical values for the potential as "model output" and a conductivity of 1 $m \cdot s^{-1}$; and
- Velocities obtained from either the analytical expression for velocity evaluated at the model nodes (in the case of most finite-element codes), or the average of the analytical velocity over the element or block boundaries (generally for finite-difference codes).

The analytical solutions to the requested pathlines are shown in Figure 6.35.

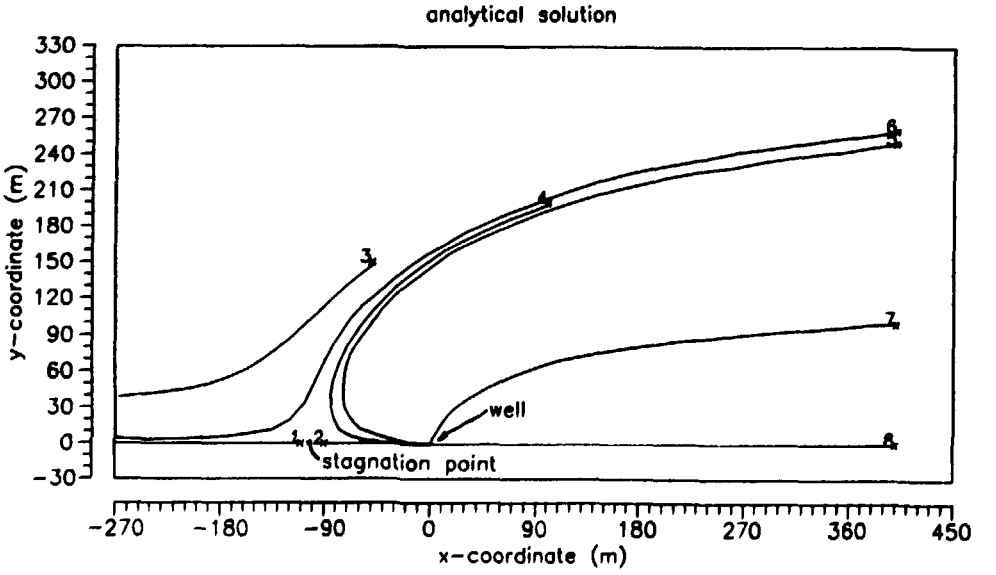


*Figure 6.35. Analytical solutions of the pathlines in the modelled domain for Case 7a. Only the upper part of the domain is plotted due to the symmetry of the domain.*

Three different gridding schemes should be used.

As an option the Project Teams were requested to report profiles for both the x and y components of velocity for both methods of velocity calculation for each gridding scheme along the sections specified in Table 6.14.

*Table 6.14. Velocity profile cross-section endpoint coordinates for Option 1 output.*

| Section no | $x_1$ (m) | $y_1$ (m) | $x_2$ (m) | $y_2$ (m) |
|---|---|---|---|---|
| 1 | -200 | 0 | 400 | 0 |
| 2 | -200 | 100 | 400 | 100 |
| 3 | -200 | 200 | 400 | 200 |

Analytical solutions to the velocities along the profiles were provided.

As a second option the requested output consisted of the error vs. the cumulative path length evaluated at each point in the flow path for release points 3, 4, 5, 6 and 7 and for each gridding scheme. Also a table of minimum distance vs. path length was requested along with the trajectories.

It contained a circular region which had properties that were different from those of the bulk of the domain. This could for example be regarded as a greatly idealised model of a repository. The origin of the coordinate system was taken at the centre of the circle. Uniform flow in the x-direction at large distances from the circle was assumed.

The domain for test case 7b is shown in Figure 6.36.

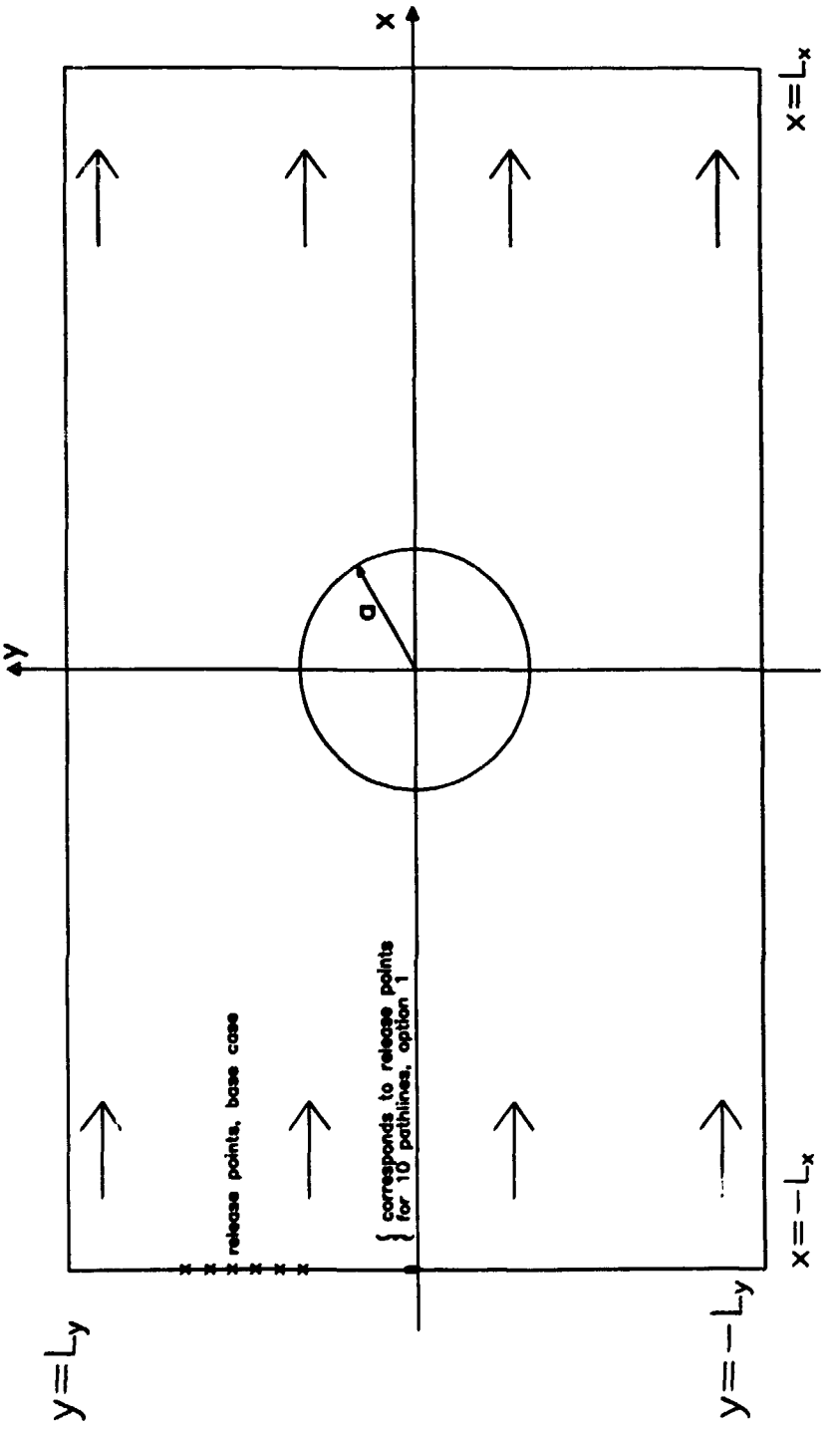


*Figure 6.36. Domain of interest for Case 7b. The circular inclusion is considered either as an intact concrete barrier with a lower hydraulic conductivity than the bulk of the domain or as a degraded concrete barrier with higher conductivity than the bulk of the domain.*

The base case concerned an inclusion with a conductivity higher than the bulk of the domain. This could for instance correspond to a repository with a weathered concrete barrier. Option 1 of Case 7b involved a situation with the concrete barrier intact, i.e. with a lower hydraulic conductivity than the bulk of the domain.

The objective of the case was to calculate pathlines using either

- the analytical field,
- a finite-element or finite-difference discretisation of the flow field,
- a flow field obtained from finite-element or finite discretisation of the analytical pressure (or head) field, or
- a flow field obtained from a numerically calculated finite-element or finite-difference pressure field.

The flow was taken to be steady-state, horizontal, incompressible, two-dimensional and the material properties were taken to be isotropic.

The requested output consisted of particle trajectories, errors defined below, and optionally errors in the velocities along the trajectories. Eight pathlines would be calculated starting from points on the left hand boundary of the domain. The analytical solutions are given in Figure 6.37. The errors in the calculated pathlines would be assessed using the following error measures:

$e_1$ = error in the y coordinate at $x = 0$,
$e_2$ = error in the y coordinate at $x = L_x$,
$e_3$ = error in the time to reach the line $x = 0$,
$e_4$ = error in the time to reach the line $x = L_x$.

The flow was taken to be steady-state, horizontal, incompressible, and two-dimensional and the material properties were taken to be isotropic.

The flow was assumed to obey Darcy's law. An analytical solution was provided for the pressure and stream function, the velocity field, and the pathlines. The travel time could not be expressed as a function of position using simple functions. However, it was easy to express the travel time to any position as an integral which could be evaluated numerically to any required accuracy.

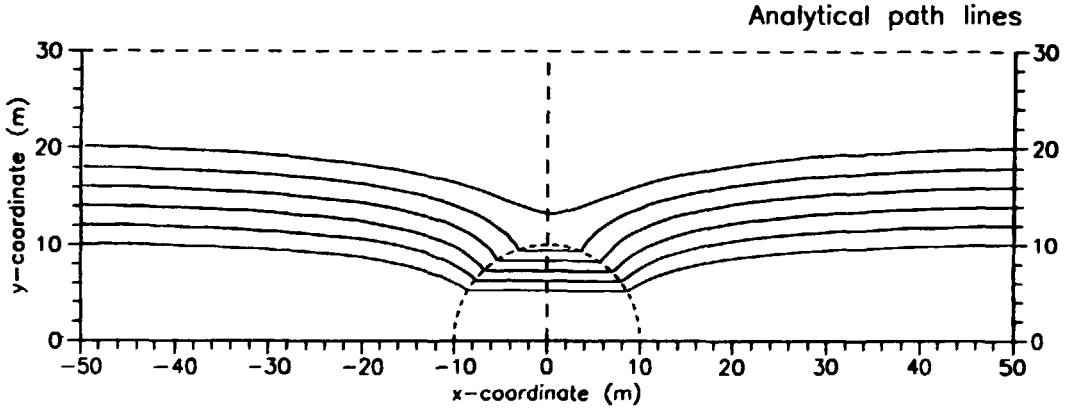


*Figure 6.37. Analytical solutions for the pathlines for Case 7b, Base Case.*

***Results from Test Case 7***

The Project Teams showed great interest in this case and the number of data files with particle tracks for different gridding schemes and types of solution algorithms on the base cases and the optional calculations amounted to more than 5000. It was decided to select a few typical results for presentation in the main report.

*The base case of Case 7a* was analysed by 11 Project Teams using various approaches, tracking routines and grid densities. The SAN-team used two tracking routines to the problem, the FLWPTH-routine and the TRACKU2-routine, the latter being designed for use with the finite-element code UNSAT2. They investigated the sensitivity of the tracking routines to different grid densities, different ways of calculating the velocities, and slight changes of the location of the well.

Their discretisation of the domain consisted of three grids with block sizes of 80 m, 40 m, and 20 m. They calculated the velocities from either analytically calculated nodal head values or from analytically calculated nodal velocity values. Using the coarse mesh with 80 m grid block for the cases with calculated head values, analytical velocity values, and with the well moved to the upper face of the grid block they found that the discretisation was too coarse to provide accurate pathways. The use of a fine grid with a 20 m grid block size improved the accuracy of the tracking substantially.

The NRC-team reported results for evaluating the flow field by applying the FEM-code to solve the flow field from the analytically calculated head values and also by evaluating the flow field from analytically calculated velocity values. For both cases they used the tracking routine that

is built into the FEM-code. They discretised the domain with grid blocks with the size of 120 m, 60 m, and 20 m. Furthermore, they analysed the travel times and travel lengths that were calculated and compared them to the analytical values. Figure 6.38 shows the pathlines as calculated with the FEM-code tracker with the use of analytical head values as an input. Results from two grid densities are shown. The coarsest grid did evidently not yield accurate pathlines. In comparison the finer grid gave results that agree well with the analytical solution. Both the well, the stagnation point and the water divide were detected by the tracking routine.

The results for analytically calculated velocities are shown in Figure 6.39. Also in this case particle-tracking using the coarse mesh failed to find the well, water divide, and stagnation point. The lower figure shows that it is possible with a fine enough grid to achieve accurate flowpaths.

The NRC-team also investigated the travel times and travel lengths of the generated particle tracks. The finest grid provided results that agree well with the analytical solution.

The JAE-team applied their tracking routine TRAC2D to *Case 7a, Option 1* and analysed the velocities along the profiles using either analytically calculated nodal head values or analytically calculated nodal velocity values as input. Figure 6.40 shows the velocity components along profile 1 calculated with the analytical pressure assigned to the nodal points.

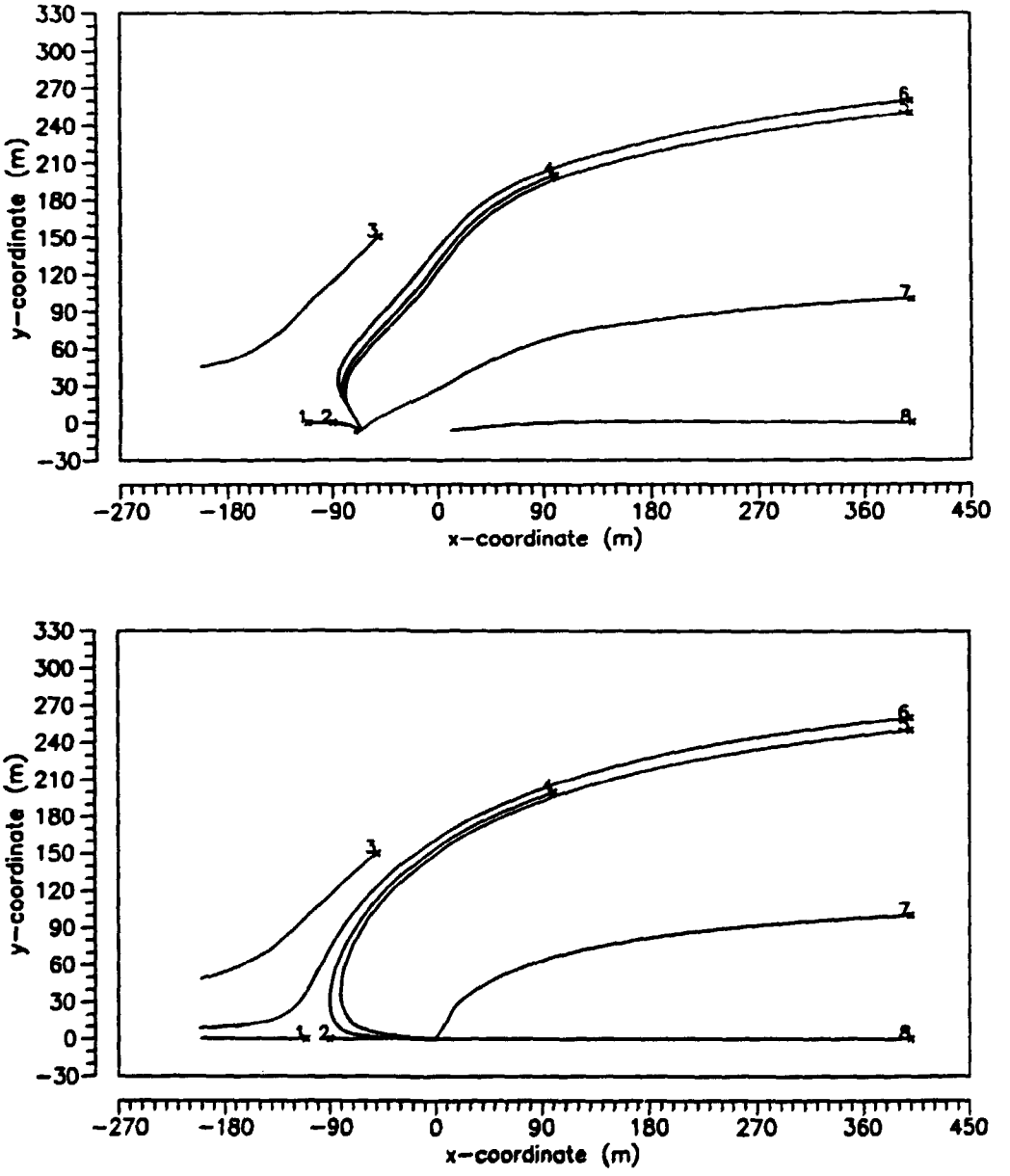


*Figure 6.38. Case 7a, Base Case. Pathlines 1—8 as reported by the NRC-team. Velocities calculated by the FEM-code. Upper: coarse mesh (120 m grid block size), lower: fine mesh (20 m grid block size).*

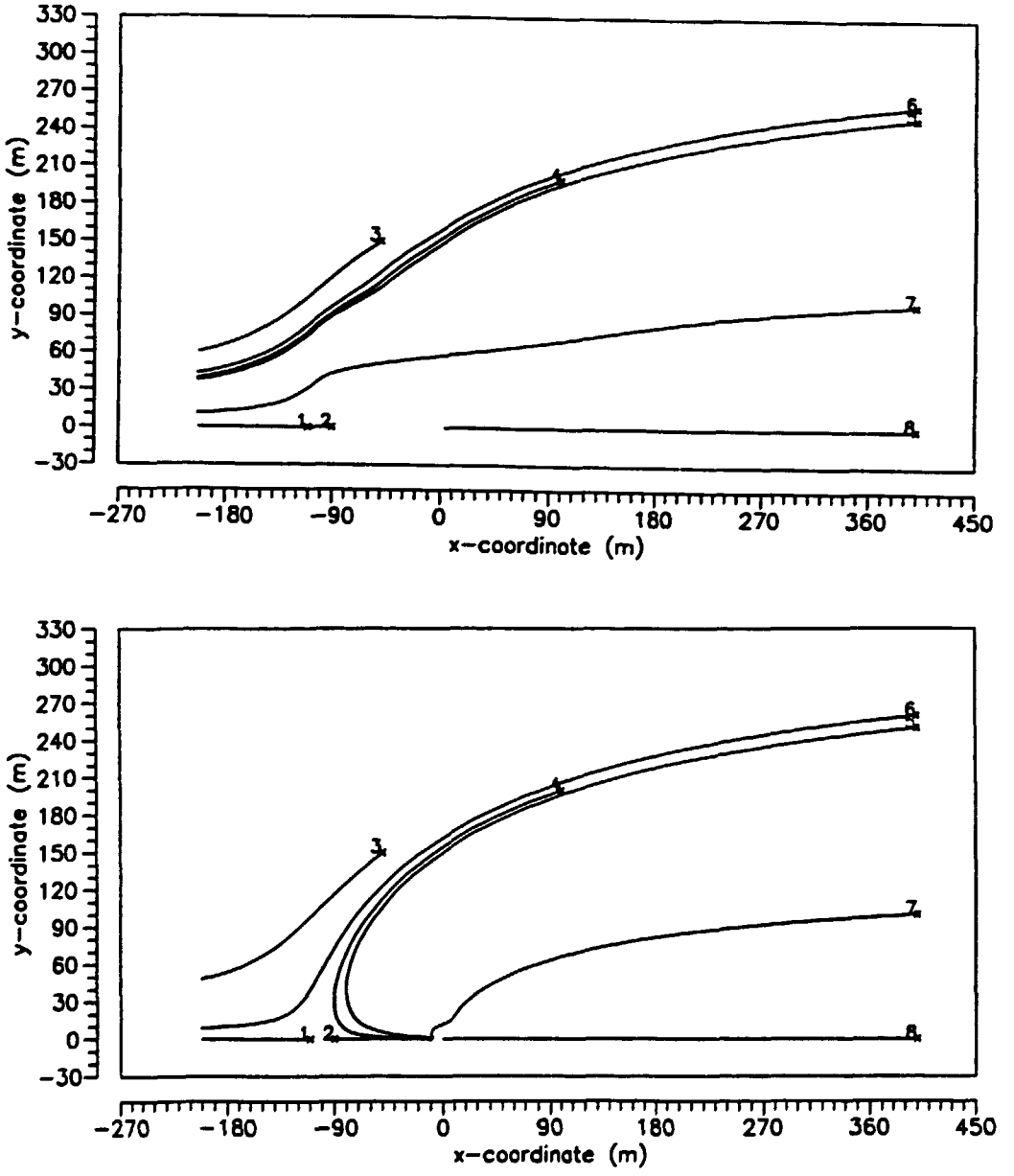


*Figure 6.39. Case 7a, Base Case. Pathlines 1—8 as reported by the NRC-team. Prescribed velocities. Upper: coarse mesh (120 m grid block size), lower: fine mesh (20 m grid block size).*

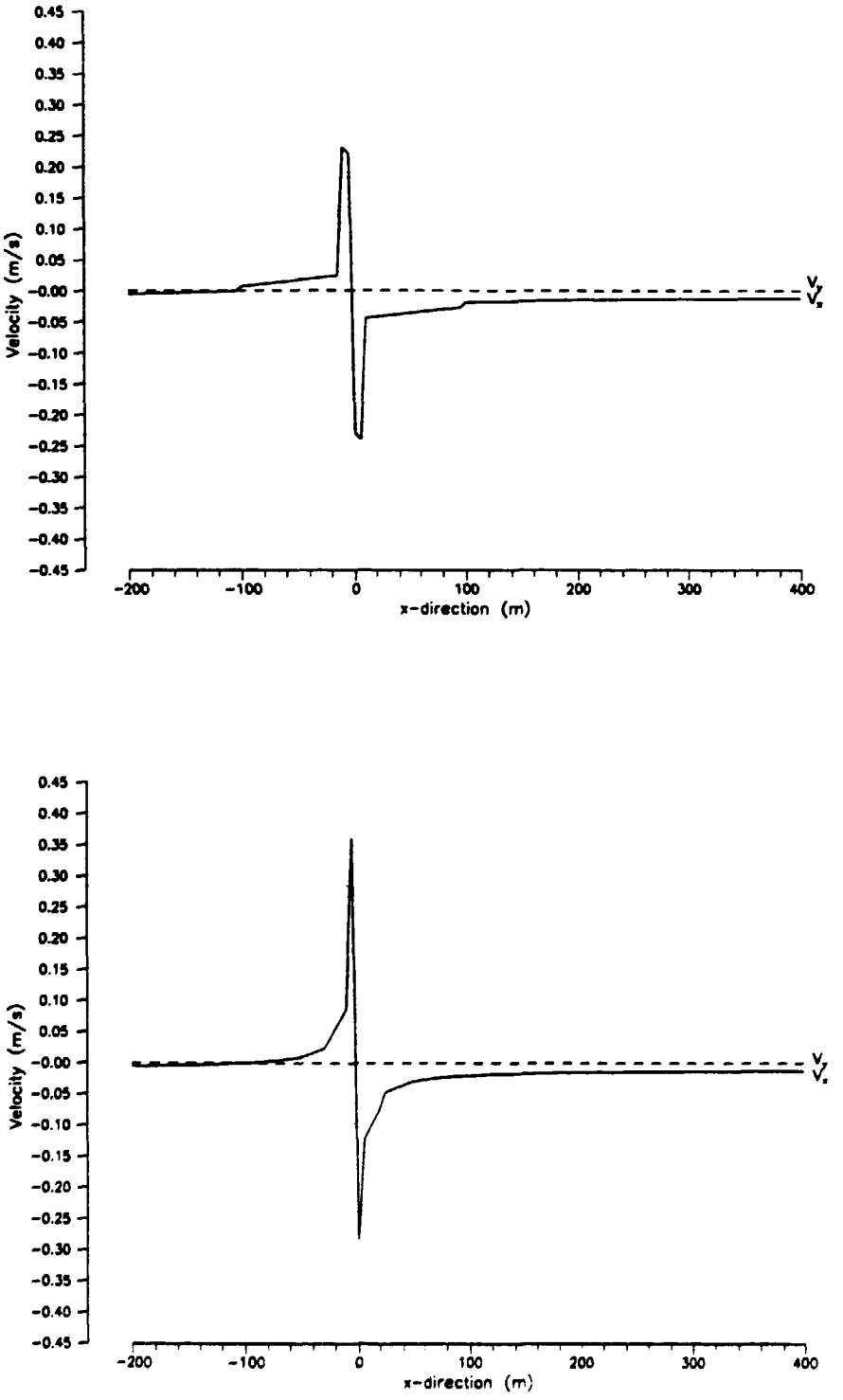


*Figure 6.40. Case 7a. Option 1. Velocity components along profile 1 as reported by the JAE-team. Flow field evaluated from prescribed nodal head values. Upper: coarse mesh (40 elements); lower: fine mesh (364 elements).*

For *Case 7a, Option 2*, the influence on the errors due to different gridding schemes on the calculated pathlines was investigated by the AEC-team for a coarse mesh (about 120 nodes) and a fine mesh (about 2250 nodes) using the analytical velocity field as an input to their tracking routine TRACK3DV. The errors for the pathlines 4, 5, and 6 were all less than 1 percent of the accumulated pathlength.

The NNW-team reported on the influence on the errors by the use of potentials or velocities. The results from the coarse grid were too poor to allow for an evaluation of different ways to calculate the velocity field. However, the results showed a tendency for the errors of pathlines associated with prescribed nodal head values to be somewhat larger than for the pathlines associated with prescribed velocity field.

The AEC-team analysed the difference in errors between pathlines for analytical and model computed velocities and found that for a fine grid the errors in both cases were similar.

The *Base Case of Case 7b* was analysed by eight Project Teams which examined a number of subcases and meshes. For example, the ETH-team considered all four ways of calculating the velocities according to the requirements. The meshes consisted of brick and pyramid elements with quadratic interpolation. Figure 6.41 shows the calculated pathlines, when the velocities were evaluated at nodal points using the FEM301-code.

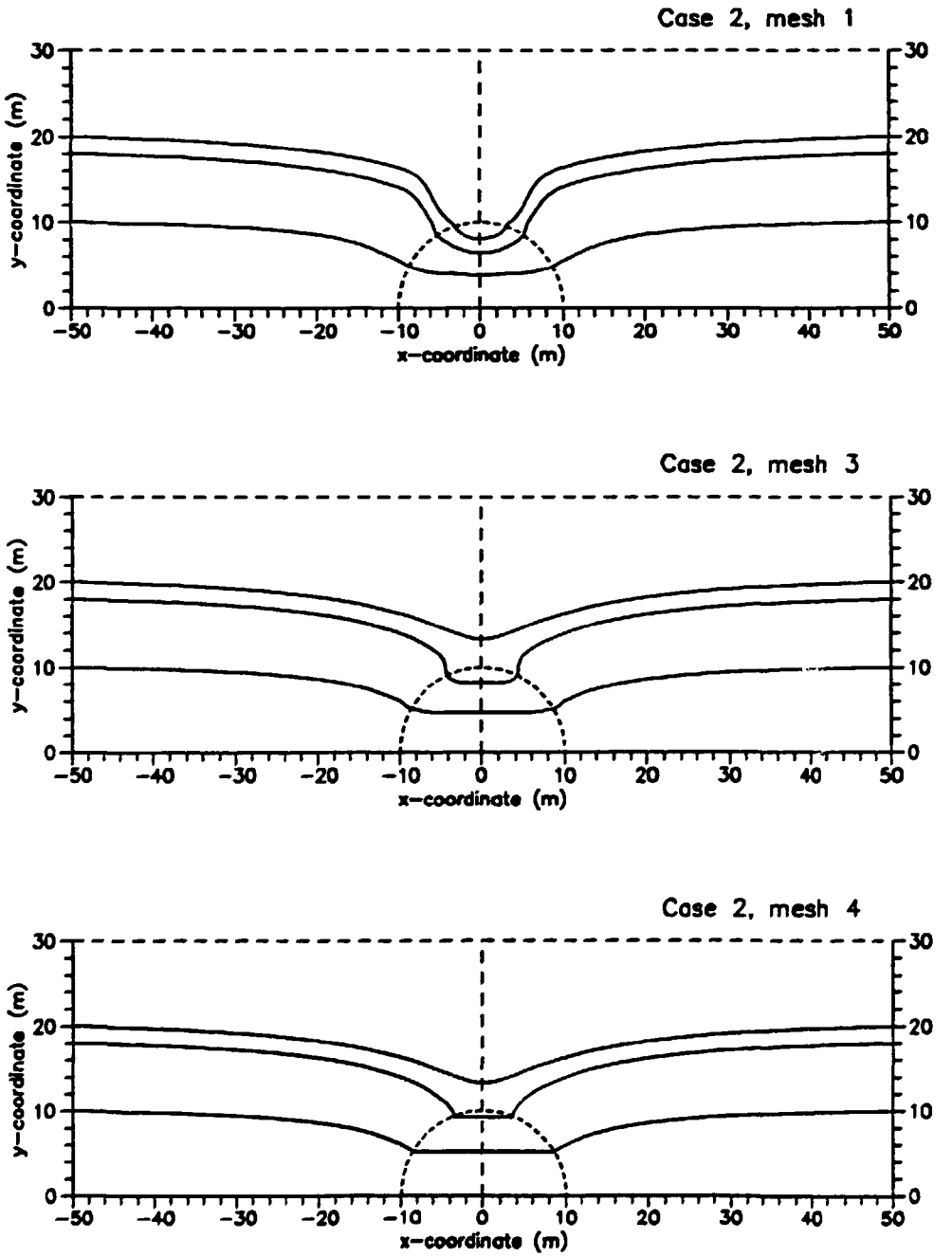


*Figure 6.41. Case 7b, Base Case. Pathlines 1, 5, and 6 as reported by the ETH-team using the flow field as evaluated by the FEM301-code. Upper: coarsest mesh; middle: finest mesh; lower: identical to finest mesh but with a refinement along the periphery of the inclusion.*

The tracking routine produced flow paths that agreed well with the analytical solution. However, there were difficulties in the vicinity of the inclusion when the flow field was calculated numerically, probably due to the coarse discretisation. With a modified grid, which was supposed to better represent the periphery of the inclusion, the tracking routine apparently works better. Calculations using the analytical or calculated potentials for evaluating the pathlines yielded results in good agreement with the analytical solutions.

The errors $e_3$ and $e_4$ deal with errors in space and time at $x = 50$ m at the right hand boundary of the domain. A source of error in this context is the stepping procedure in the tracking routine. The VTT-team investigated the sensitivity of the tracking to the specified step-length. Figure 6.42 shows the errors in space of particle tracks calculated at the right hand boundary of the domain using a fine mesh. The calculated errors were plotted as a function of the step-length, the flow field being represented either with prescribed analytical pressure or with the pressure being numerically calculated. From the results, it was clear that the way of calculating the velocity field has no major impact on the errors. The errors were strongly dependent on the step length, however. The sensitivity to the step-length seemed to be less pronounced for travel times than the errors in space.

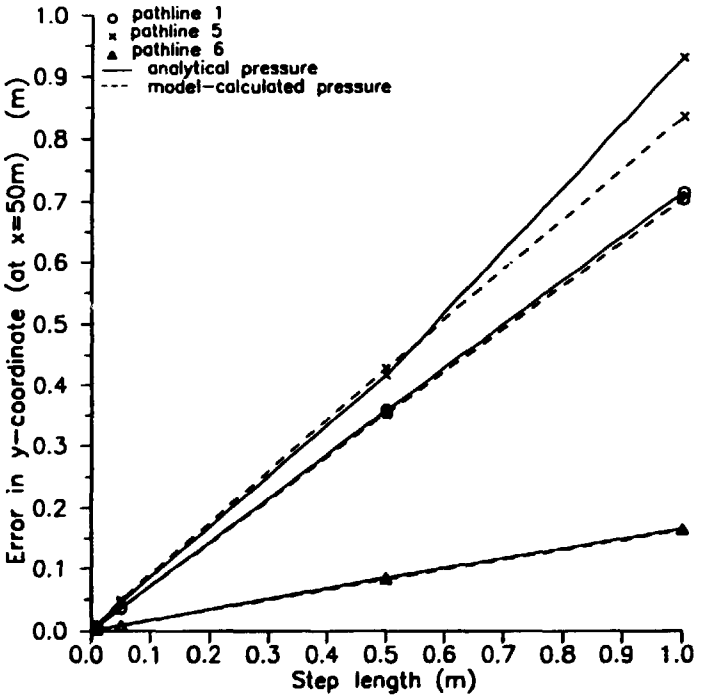


*Figure 6.42. Errors in the calculated particle tracks 1, 5 and 6 at x = 50 m for a fine mesh (102 eight-noded elements) using either prescribed analytical pressure (solid) or model-calculated pressure (dashed) results for Case 7b, Base Case as reported by VTT.*

Errors in velocities along the pathlines were calculated by the OWT-team using a relatively coarse mesh. Results indicated that the errors increased symmetrically around the inclusion. Peak values were obtained at the interface between the two material types, i.e. at the points of entrance into the inclusion.

*Case 7b, Option 1* was analysed by three Project Teams. The NNW-team and the ETH-team discussed three sources of error:

— the density of discretisation
— the four different ways of representing the flow field
— the orientation of the finite-elements

The NNW-team addressed the density of the discretisation and two different ways of representing the flow field. They had no problems in generating particle tracks that agreed well with the analytical solution even on the coarse mesh, when the analytical velocity field was prescribed to the grid points.

Calculation of the errors in the x-component of the velocity at different locations along the pathlines displayed very small deviations from the analytical values; most errors were between $10^{-14}$ and $10^{-12}$ m· $s^{-1}$ with the higher values mainly occurring at the interface between the two materials.

The ETH-team generated five different meshes and applied all four ways of evaluating the velocity field. When the pathlines were calculated using the analytical velocity field, the particle tracks were in good agreement with the analytical solutions for all the meshes used. Some discrepancies occurred when the velocity field was calculated in another way.

# 7. Summary and Conclusions

## 7.1 Level 1

Level 1 of the HYDROCOIN study aimed at verifying computer codes for groundwater flow calculations. This objective has been met by applying the codes to seven hypothetical test cases representing different physical situations. The test cases were primarily designed for testing the codes rather than as representations of realistic waste repository scenarios. In some of the test cases the verification was carried out by comparing the results with those from analytical solutions, whereas in the other cases the means of verification was intercomparison between numerical solutions. All test cases presumed that the conceptual porous medium model is valid.

The presented entities were primarily calculated entities such as groundwater pressures, salt concentrations and groundwater temperatures as well as properties evaluated from the gradients of the primary field entities, e.g. groundwater velocities and trajectories.

In the test cases giving rise to linear equations, the primarily calculated field entities have shown good agreement. The deviations observed have been satisfactorily explained in terms of different discretisations in space and time or other numerical characteristics of the solutions.

The velocity fields and trajectories also showed reasonable agreement. Since all models solve the flow equation for a scalar field, the vector fields are derived entities resulting from the application of post processing procedures. The results from HYDROCOIN Level 1 showed that these post-processing procedures should be selected with care. In order to test some of the procedures, a test case to compare and evaluate different strategies for particle tracking was included in HYDROCOIN Level 3.

Among the Level 1 test cases there are one mildly non-linear case and two strongly non-linear cases. The mildly non-linear case proved fairly easy to solve adequately for the primary scalar field, whereas the strongly non-linear cases were extremely difficult. In one of the latter cases, a coupled flow and brine transport problem, consensus about the solution was reached only after considerable discussions in the HYDROCOIN workshops and at an additional workshop devoted specifically to this problem. Substantial computer resources were required in order to arrive at a converged solution. The other strongly non-linear test case, an unsaturated flow problem with high permeability contrasts, turned out to be too difficult to solve in its initial formulation within the time available and the financial constraints on the project teams.

For the non-linear cases, the derivation of fluxes and trajectories proved to be at least as difficult as for the linear cases. In the mildly non-linear case, analytical solutions were available for the trajectories. The numerical solutions submitted by the project teams showed a substantial spread around these analytical solutions.

In order to save nodes, some of the project teams used one-dimensional finite elements to represent fracture zones in a two-dimensional model. This approach led to satisfactory solutions for the primary scalar field. Apparently there does not, however, exist a good particle tracking algorithm that can cope with such mixed dimensionality meshes.

The preliminary results presented at the early workshops were markedly further apart than those presented as final results. Many of the final results were obtained after several iterations including rediscretisation, change of interpolation order, up-dating of particle tracking algorithms, etc. The conclusion from this is that, although good solution methods are available for most of the problems tested in HYDROCOIN Level 1, independent checks of modelling results are important to ascertain that the methods are properly applied and that the results obtained could be relied upon. In this context there is a need to develop numerical quality criteria that can be used to check the solutions.

There is a consensus among the participants that HYDROCOIN Level 1 provided an efficient means for testing the strengths and weaknesses of various strategies for groundwater flow modelling and post processing. The objective of HYDROCOIN Level 1 was to test models and modelling strategies and not to select the best of codes, certify codes or to rank them. Nonetheless, the results do not indicate significant differences in accuracy or applicability of different algorithms or codes.

HYDROCOIN Level 1 met its objectives to test the numerical accuracy of the codes. The results indicate that appropriate numerical methods are available to solve linear or mildly non-linear problems. Some areas that should attract interest for future research and development have been identified, e.g. solution algorithms for strongly non-linear problems and particle tracking.

## 7.2 Level 2

HYDROCOIN Level 2 addressed the issue of validation of groundwater flow models to be used in performance assessments of radioactive waste repositories. In principle, validation involves calibration of the model against experimental data followed by predictions of independent data sets using the calibrated model. An ideal data set should thus contain independent subsets of data to be used for calibration and prediction. The data should also be sufficient to determine all model parameters in order to reduce the freedom of interpretation of the data.

The Level 2 exercise started with an extensive search for relevant experiments meeting the requirements just mentioned. The survey was constrained to experiments known by the HYDROCOIN participants and, because of the limited resources in terms of time and funds available to the participants, to experiments that did not require extensive work with data manipulation or model setup.

Five test cases were defined based on data sets that met the requirements to some extent. The data sets selected had in general not been generated for the purpose of model validation and, therefore, did not meet all the requirements. However, the data sets chosen were considered to be the most suitable available. They covered a number of processes relevant for the analysis of radioactive waste disposal in different media. In addition, the data sets spanned a variety of spatial and temporal scales. Table 7.1 shows some of the attributes of the five selected data bases.

*Table 7.1. Description of the attributes of Level 2 data bases.*

| Case | Transient data | Flux data | Data for calibration or identification of conceptual model structure | Data for a range of conditions to provide independent data for model validation | Judged quality of the data base |
|---|---|---|---|---|---|
| 1 | yes | no | limited | none | good for initial understanding |
| 2 | yes | no | none | none | poor |
| 3 | yes | no | limited | limited | good for initial understanding |
| 4 | no | no | very limited | none | poor but typical |
| 5 | yes | no | limited | none | good for initial understanding |

The conceptual models applied to the test cases were almost exclusively based on the equivalent porous medium approach. Only one analysis involved a fracture network model.

Validation involves evaluating the data, demonstrating the extent to which the model can represent the experimental results, and building confidence in the model. In order to validate a model of a particular system, the physics of the system, i.e. the important processes and their interactions, as well as the structure of the system, such as the geometry and boundary conditions, must be properly understood. It must also be recognised that there is no unique model of a particular system. The model adopted will depend on the purpose for which the model is intended. Processes and other attributes which are irrelevant for the usage intended are normally neglected. It is therefore unreasonable to expect exact matches between model predictions and experimental results. Instead, it is important to establish that the deviations observed are consistent with uncertainties in the data sets and those uncertainties imposed by neglecting physical processes.

It was concluded that the intended use of the model strongly affects the validation process. In particular it determines:

- the level of detail required in the model,
- the performance measure that should be correctly predicted by the model, and
- the criteria for the goodness-of-fit function or qualitative judgement used to assess whether the appropriate level of confidence or validation has been achieved.

Recognising this, a framework for the validation was developed during the course of the Level 2 work. The framework describes a normal scientific process and consists of the following ten steps:

- Formulation of conceptual models based on available data
- Translation of conceptual models and data into mathematical and numerical models
- Identification of appropriate goodness-of-fit functions for use in calibration and validation
- Calibration of models with observations and experimental data
- Development of model validation criteria based on the purpose of the model
- Goodness-of-fit function calculations based on model predictions for various conditions and data sets independent of calibration
- Assessment of acceptability of models using goodness-of-fit functions and other model results
- Analysis of model differences and discrepancies between model results and experimental observations
- Publication and presentation of the results to the scientific community and the public
- Conclusions on model validity and further validation efforts

The analyses performed and the consequent discussions between the participants in the HYDROCOIN workshops have given substantial experience in the application of the framework for validation. Some of these experiences and insights are summarised below.

It has been demonstrated that experiments for model validation need to be designed and conducted over a range of conditions that, when possible, brackets the expected conditions for which the model will be applied. In particular all processes that might be relevant need to be accounted for. A particular difficulty in the design of experiments is to provide means for distinguishing between alternative conceptual models. The difficulties involved in selecting the best of a suite of possible conceptual models and evaluating the associated uncertainties proved to be one of the major challenges to the participants. In general too many degrees of freedom were left to allow for a conclusive choice of model.

The formulation of mathematical and numerical models usually involves averaging, interpreting and interpolation of measurements made at small scale in order to obtain parameters for models applied at much larger scales. Experiments performed at a series of spatial and temporal scales are needed in order to demonstrate that we have an adequate understanding of this scaling and averaging process. The complexity of the natural flow system was found to be an important issue in this context. The complexity arises from the possibility of alternative processes, from the occurrence of heterogeneities, and from difficulties in the interpretation of experimental data.

The HYDROCOIN group recognised that the selection of an appropriate performance measure is an important part of model validation. The importance of the selection of performance measure reflects the fact that model validation is purpose specific. The selected measure should thus reflect the intended use of the model. It was, for instance, demonstrated in one of the test cases that different parameter sets were obtained if the maximum of a temperature profile along a borehole was to be simulated than if the model was tuned to match the observed skewness of

the same profile. In another case it was shown that the conclusions regarding the models ability to match the measured data were dependent on whether an arithmetic mean, a root-mean-square-error, or a kriged-weighted error was used in the comparison. It was also concluded that qualitative comparisons, e.g. visual comparisons of curves in a graph, were useful as a complement to more quantitative comparisons.

The validation process is iterative. In many of the analyses a need for further experiments to determine parameters or to investigate the cause of certain features of the data sets was identified. A particular point that was emphasised was that flux data are generally more informative than head data in the process of identifying and quantifying parameters and model structures. None of the data sets forming the basis for the test cases included measured data on fluxes.

Statistical methods and inverse modelling techniques proved beneficial in model calibration as well as in model validation. Inverse modelling greatly influenced the selection of model structure as well as the distribution and zonation of parameter values.

Setting up criteria for the acceptance of a model or a particular model result turned out to be a difficult issue. Again, sensitivity and uncertainty analysis methods and inverse modelling techniques provided significant guidance. In one analysis these techniques were used to show conclusively that steady-state data on the groundwater pressure contained insufficient information for determining the parameter distribution. Transient aquifer tests, however, provided an adequate statistical basis for this determination. The statistical analysis was also used to establish quantitative criteria for the acceptance of the match by investigating the consistency between observed deviations and estimated parameter uncertainties.

As can be seen in Table 5.1, only one of the test cases included data for model predictions that were independent of those used for the model calibration. The availability of such independent data was identified as a central point in the model validation procedure.

Analyses of the discrepancies obtained between the results of model calculations and measured data clearly showed that the match was better for simple and well characterised systems and deteriorated as the scale and complexity grew. The reason for this is that identifying the model structure properly becomes increasingly difficult as the scale and heterogeneity of the data set grows. Transient data was concluded to provide a more efficient means for identifying model structures than steady-state data.

Although none of the test cases provided a perfect model validation, the participants significantly increased their confidence in the models applied in HYDROCOIN Level 2. As mentioned, the project teams experienced difficulties in finding "the best conceptual model" in the validation process. This situation is normal in a scientific process and thus understandable in the scientific community. Because of the substantial attention that radioactive waste management obtains from the public, it is equally important, albeit more difficult, to explain the situation to a wider public. This task was identified as a future challenge.

HYDROCOIN Level 2 has contributed to an increased confidence in the applicability of groundwater flow models to situations relevant for radioactive waste disposal. The difficulties experienced in conclusively selecting from alternative conceptual models are similar to the experience from other validation exercises, e.g. the INTRACOIN study mentioned in Section

1.2. Before repositories can be evaluated with sufficient confidence, important uncertainties involved with the conceptual assumptions associated with the modelling of deep groundwater flow systems need to be further clarified. An important current line of development is the use of new model concepts such as different types of network models. It is important in the validation process to define what the roles of different model concepts should be in performance assessment.

Model validation is an interdisciplinary exercise. The process is clearly iterative and requires substantial interaction between experimentalists and modellers. It is strongly recommended that this is recognised when setting up future validation studies.

## 7.3 Level 3

Many complex physical and chemical processes acting over very long times affect the behaviour of a repository for radioactive waste. The overall safety of the repository is evaluated by making a performance assessment. In this process, it is ordinarily necessary to employ mathematical and numerical models. The parameters of these models are usually not well known. Sometimes the information available is insufficient to decide which of several mathematical models that should be used. The aim of HYDROCOIN Level 3 has been to address the problems caused by this lack of information. Although the difficulties in handling uncertainties and sensitivities in performance assessment are general for all scientific disciplines involved, HYDROCOIN Level 3 was limited in scope to address those sensitivities and uncertainties associated with groundwater hydrology. The reduction of uncertainties can only be achieved by gaining additional information, which requires additional measurements on the real physical system or closely related systems. This has been beyond the scope of HYDROCOIN Level 3.

Sensitivity analysis answers questions such as "What happens if such and such a parameter is changed by so much?" and "Which parameters are important?". The simplest approach is to vary the parameters and calculate the corresponding change in model output. Another approach is to calculate local sensitivities for the various parameters. This can be done either directly from the mathematical model or by fitting a response surface to the model and differentiating this.

The importance of a parameter can be evaluated e.g. by calculating measures of the correlation between the parameters and the model output. The adjoint technique can be used to reduce the computational work if local sensitivities are to be evaluated directly from the mathematical model.

Uncertainty can be described by probability density functions. Once the uncertainty in the parameters is known the probability density function of the model output can be calculated.

Both sensitivity and uncertainty analysis require the selection of combinations of parameter values from the parameter space. Various sampling approaches can be used, such as, Expert Choice, Point Estimate Sampling, Simple Random Sampling, Latin Hypercube Sampling, and Importance Sampling.

One major source of uncertainty in groundwater flow modelling is associated with the irregular and unpredictable spatial variation of properties such as the hydraulic conductivity. Whereas

one accurate measurement can be sufficient to determine a homogeneous parameter, many accurate measurements may be needed to significantly reduce the uncertainty of a partially varying parameter. Geostatistical methods can be applied to analyse the spatial variation of parameters. Kriging is often used for interpolation of a parameter from spatially varying measurements.

The Project Teams have applied a variety of the methods mentioned above to the seven test cases of HYDROCOIN Level 3. These test cases represent four different geological media that have been suggested as alternative choices for a nuclear waste repository: argillaceous, crystalline rock, tuff and salt. Both saturated and unsaturated flow are represented.

The analyses performed within Level 3 clearly demonstrate the importance of a good understanding of uncertainties and sensitivities in the performance assessment of nuclear waste repositories. It is obvious that the choice of conceptual model can greatly influence the outcome of the assessment. It has also been shown that the choice of performance measure in the sensitivity and uncertainty analysis can affect the conclusions, or even determine whether any conclusions can be drawn.

Some concluding remarks regarding the results from the individual test cases at HYDROCOIN Level 3 are given below.

### *Test Case 1*

The primary purpose of Test Case 1, near surface disposal in argillaceous media, was to determine the most important hydrogeological attributes and parameters. Saturated as well as undersaturated scenarios were analysed.

To a great extent the selected performance measure determined which of the parameters were judged to be the most important in the sensitivity analysis. Several performance measures should be used in order to obtain a full understanding of the system. It is also highly likely that different parameters would be most important in different positions in the parameter space for a realistic system with complicated hydrogeology. It was also shown that it is important that the numerical accuracy of the individual calculations is sufficiently high so that the evaluated uncertainties and sensitivities are not swamped by numerical errors.

### *Test Case 2*

Test Case 2 was set up to gain insight into the types of hydrologic behaviour that could affect the performance of a waste repository sited in unsaturated, layered and fractured tuff. Low and high flux as well as steady-state and transient flow were considered. At low flux the water transport was expected to be matrix dominated whereas at high flux the transport in fractures was expected to be predominant. The nonlinearities of the case were extreme and posed a very challenging numerical problem to the Project Teams.

For one-dimensional steady-state flow, the most dramatic change in water travel times was observed at the instance of transition from matrix to fracture flow. This transition resulted in a nonlinear behaviour in the performance measure. It was noted that sensitivity analysis methods

that could handle this situation are needed. It was also necessary to adjust the discretisation so that the rapid variations in the quantities of interest in some parts of the domain could be coped with.

It was suggested that using separate travel times for matrix flow and fracture flow would facilitate the sensitivity analysis. One Team used the parameter stepping technique to derive an accurate numerical solution and to gain information about the sensitivities of the system. It was commented that if automated procedures for sensitivity and uncertainty analysis were used to check the numerical accuracy of the solution, such procedures would be desirable.

*Test Case 3*

The objective of Test Case 3 was to examine sensitivity and uncertainty analysis techniques and other steps that are important for the estimation of performance measures for a hypothetical salt repository in a regional geological setting. Several uncertainty aspects including variable density flow and spatial variability were investigated. The analyses included the application of inverse modelling techniques, sampling schemes, as well as deterministic sensitivity and uncertainty analysis methods.

A general finding was that there is a strong coupling or correlation between hydraulic conductivity and recharge. These two parameters could not be independently estimated. It was also noted that flux measurements in addition to the head measurements given would have increased the sensitivity and thus the possibilities to draw conclusions about the system. Realisations in the sensitivity and uncertainty analysis that yield a model output that is inconsistent with the observed system behaviour should be discarded when evaluating the sensitivity and uncertainty of the system. It was shown that testing the parameter estimation for instability and insensitivity is extremely important. Even though a model may be calibrated, it may not be very close to reality, if there are problems in the parameter estimation.

*Test Case 4*

Results from HYDROCOIN Level 1 indicated that convection cells could arise from a salt source dissolving into the flowing groundwater. Test Case 4 was developed to investigate if these cells would be relevant for flow situations occurring above salt domes. The analysis was performed by carrying out a sensitivity analysis of the influence of hydrogeological parameters, boundary conditions and the conceptual model. The analysis made it possible to identify parameters with significant influence on the existence and development of convection cells.

All variations studied except two showed the presence of convection cells. It was therefore concluded that the appearance of convection cells is a real phenomenon and that the cells can form in systems where the brine concentration builds up to near full saturation and where relatively sharp brine-freshwater interfaces exist.

*Test Case 5*

Test Case 5 addressed the issue of sensitivity and uncertainty analysis of flow in crystalline rock. The case was based on measurements at the Chalk River Nuclear Laboratory (CRNL), Canada, and at the Swedish Fjällveden site. The objective was to analyse the sensitivity and uncertainty of performance measures, such as the flow rate at a defined point in space and the groundwater travel time along a flow path starting at the same point and ending in a defined recipient.

For CRNL sensitivity and uncertainty analysis was carried out as part of a model calibration and validation study. Sensitivity was studied by applying regression analysis. No particular predominant parameter was identified. In order to investigate the existence of predominant parameters with a nonlinear correlation to the performance measures, regression analysis of the ranks of the parameters was carried out. This analysis confirmed that there was no dominant parameter and that several parameters had a significant influence on the performance measures chosen.

In the uncertainty analysis the properties of the goodness-of-fit function used in the model calibration step were utilised. A Bayesian statistics analysis was applied to this goodness-of-fit function to a posteriori estimate the probability of a model run. These probabilities were then used to construct a cumulative probability distribution for the performance measure chosen. The results showed a rather sharp separation between probable, rather probable and highly unlikely parameter sets.

The analysis of the Fjällveden site consisted of extensive sets of model runs varying single parameters or sets of parameters. The performance measures chosen were more sensitive to the properties in the rock blocks than those in the fracture zones. It was also concluded that a flow path with its associated travel time gave a greater possibility to study the sensitivity of the system than did the flow rate at a point. This also applied to the statistical distribution of the flow rate at a given depth.

*Test Case 6*

The objective of Test Case 6 was to provide tests for methods of handling uncertainty and parameter sensitivity for a three-dimensional regional groundwater flow in low permeability rocks using Piceance Basin. Uncertainty and sensitivity analyses were performed applying Monte-Carlo simulations to address uncertainty and regression analysis of the Monte-Carlo runs with respect to the sampled parameters to investigate the sensitivity.

In the Monte-Carlo analysis only those runs that were in agreement with the hydraulic head surfaces interpolated from measured data were accepted. However, none of the simulations agreed with the interpolated heads. This was explained by probable deviations in the range of recharge specified. Thus, the simulated travel paths and times were not representative of the conditions within the Piceance Basin.

The regression analysis gave poor fits and only porosity could with certainty be identified as an important parameter for the travel times. The poor fits were attributed to variability in the

direction of the pathlines giving nonlinear and discontinuous behaviour of the performance measures.

*Test Case 7*

Test Case 7 was set up to investigate the calculation of flow trajectories independently from the model employed to calculate the distribution of the groundwater head. This was done by comparison with analytical solutions and by intercomparing numerical solutions. The case consisted of two subcases.

The first subcase can be described as a well with a constant pumping rate intersecting an aquifer with an originally uniform flow field. The resulting flow field consisted of two flow regions, one converging to the well and one bypassing the well. The requested output from this subcase was estimated trajectories starting at specified points with associated path lengths and travel times.

In the second subcase a circular region of contrasting permeability was included in an aquifer with a uniform flow field. The output requested from the second subcase was trajectories from specified points together with errors in position and travel time.

Test Case 7 gave rise to lively discussions in the workshops. It was pointed out that examination of the evaluated flow paths is an important part in getting an understanding of the hydrogeology of a nuclear waste repository. It appears that the accuracy of the evaluated trajectories is a function of the discretisation density used when solving for the groundwater head, as well as of the method used for calculating the velocity of the groundwater from the heads and the algorithm employed to integrate the flow paths from the velocity field. The results of Test Case 7 gave no single answer to which of these steps that is the most important. It appears though, that the discretisation density and evaluation of velocities have a greater influence on the accuracy than the integration method. Both subcases contained features that were difficult to evaluate correctly. In subcase 1 there was a water divide between the two flow regions, and in subcase 2 the accurate representation of flow paths around the circular inclusion, which was relatively impervious, required a fine discretisation.

## 7.4 Concluding Remarks

The HYDROCOIN study was set up to test and evaluate mathematical models describing groundwater flow in the context of performance assessment of nuclear waste disposal. The study has gained much interest both among the participants and externally. There is a consensus among the participating organisations that the cooperative study was very valuable. Much new information has been gained about the features of the groundwater flow models.

HYDROCOIN has contributed to demonstrating that appropriate numerical models exist for solving most groundwater flow problems and to pointing out areas where further work is needed in order to find appropriate methods. HYDROCOIN has greatly contributed to increasing the confidence of the participants in the models and to investigating the ranges of the applicability

of the models. In addition, some versatile and useful methods for sensitivity and uncertainty analysis have been applied.

The organisation of HYDROCOIN and the mode of international cooperation within the study has proved to be quite efficient. The discussions in the workshops have been very fruitful from a technical and scientific point of view. In numerous cases these discussions have led to the participants revisiting the problem in order to arrive at answers more in agreement with those of the other participants. The participants often referred to the prominent advantage of working together in a framework like HYDROCOIN.

Model validation has been identified as the perhaps most difficult issue addressed in HYDROCOIN. This issue is the main topic of the ongoing INTRAVAL study, which was started subsequent to the ending of HYDROCOIN.

# Appendix 1

## List of HYDROCOIN Participants

| Party | Project Team(s) |
|---|---|
| Atomic Energy of Canada Ltd. AECL | Atomic Energy of Canada Ltd. AECL |
| British Geological Survey BGS | British Geological Survey BGS |
| Commissariat à l'Energie Atomique/ Institut de Protection et de Sûreté Nucléaire CEA/IPSN | Commissariat à l'Energie Atomique, CEA/IPSN |
| | Ecole Nationale Supérieure des Mines de Paris EDM |
| Commissariat à l'Energie Atomique/ Agence Nationale pour la Gestion des Déchets Radioactifs (observer) CEA/ANDRA | Agence Nationale pour la Gestion des Déchets Radioactifs ANDRA |
| Gesellschaft für Strahlen- und Umweltforschung GSF | Gesellschaft für Strahlen- und Umweltforschung GSF |
| | Technical University of Berlin TUB |
| Japan Atomic Energy Research Institute JAERI | Japan Atomic Energy Research Institute JAERI |
| | Central Research Institute of Electric Power Industry CRIEPI |
| | University of Kyoto |
| | Okumura Corporation |
| | Hazama-Gumi Ltd. |
| Nationale Genossenschaft für die Lagerung radioaktiver Abfälle NAGRA | Colenco Ltd.[1] MCI |
| | ETH—Zürich ETH |
| | Polytechnical University of Catalunya UPC |
| | University of Neuchâtel |

| Party | | Project Team(s) | |
|---|---|---|---|
| Rijksinstituut voor Volksgezondheid en Milieuhygiëne | RIVM | Rijksinstituut voor Volksgezondheid en Milieuhygiëne | RIVM |
| Swedish Nuclear Fuel and Waste Management Co. | SKB | KEMAKTA Consultants Co./Swedish Geological Co.[1] | SGAB/KEM |
| | | Royal Institute of Technology | KTH |
| Swedish Nuclear Power Inspectorate | SKI | Managing Participant | |
| Technical Research Centre of Finland | VTT | Technical Research Centre of Finland | VTT |
| U.K. Atomic Energy Authority/ Harwell Laboratory | | Harwell Laboratory | HAR |
| | | Atkins Engineering Sciences | AES |
| U.S. Department of Energy | U.S. DOE | Salt Repository Project | SRP |
| | | Office of Waste Technology Development | OWTD |
| | | Nevada Nuclear Waste Storage Investigations | NNWSI |
| | | Basalt Waste Isolation Project | BWIP |
| U.S. Nuclear Regulatory Commission | U.S. NRC | U.S. Nuclear Regulatory Commission | U.S. NRC |
| | | Sandia National Laboratories | SANDIA |
| Organisation for Economic Co-operation and Development/ Nuclear Energy Agency (Observer) | OECD/NEA | Member of Secretariat | |
| Nordic Liaison Committee for AtomicEnergy/Institute for Energy Technology (Observer) | NKA/IFE | Member of Secretariat | |

[1] Former name Motor Columbus Consulting Engineers

# Appendix 2

## Abbreviations used for Codes and Project Teams in the Summary of HYDROCOIN Level 3

*Table 1. Abbreviations Used for Codes.*

| CODES | | | |
|---|---|---|---|
| CFE | CFEST | NAM | NAMMU |
| DLL | DLLUVIA | NAP | NAPSAC |
| FEG | FEGM | NOR | NORIA |
| FEM | FEMWATER | SAG | SAGUARO |
| FE2 | FEFLOW2 | STO | STOKES |
| FM3 | FEM301 | SUT | SUTRA |
| GWH | GWHRT | SW1 | SWIFT |
| INV4 | INVERT-4 | SW2 | SWIFT2 |
| LLU | LLUVIA | TRI | TRISEC |
| MAG | MAGUS | UNT | UNSAT2 |
| MET | METIS | USG | USGS3D |
| MOT | MOTIF | 2DS | 2DSEEP |
| MTR | METROPOL | 3DS | SDSEEP |

*Table 2. Abbreviations used for Project Teams.*

| PROJECT TEAMS | |
|---|---|
| AEC | Atomic Energy of Canada Limited, Canada |
| AES | Atkins Engineering Sciences, United Kingdom |
| AND[1] | Agence Nationale pour la Gestion des Déchets Radioactifs (Commissariat à l'Energie Atomique), France |
| BGS | British Geological Survey, United Kingdom |
| CRI | Central Research Institute of Electric Power Industry, Japan |
| EDM | Ecole Nationale Supérieure des Mines de Paris, France |
| ETH | Eidgenössige Technische Hochschule, Switzerland |
| GSF | Gesellschaft für Strahlen- und Umweltforschung, Federal Republic of Germany |
| HAR | Harwell Laboratory, United Kingdom |
| JAE | Japan Atomic Energy Research Institute, Japan |
| KEM/SGAB | Kemakta Consultants Co./Swedish Geological Co., Sweden |
| MCI[2] | Colenco Ltd., Switzerland |
| NNW | Nevada Nuclear Waste Storage Investigations, U.S.A. |
| NRC | U.S. Nuclear Regulatory Commission, U.S.A. |
| OWT | Office of Waste Technology Development, U.S.A. |
| RIV | Rijksinstituut voor Volksgezondheid en Milieuhygiëne, the Netherlands |
| SRP | Salt Repository Project, U.S.A. |
| SAN | Sandia National Laboratories/NRC, U.S.A. |
| UPC | Universidad Politécnica de Cataluña, Spain |
| VTT | Technical Research Centre of Finland, Finland |

1 The Project Team has acted as observer and has contributed calculational results.
2 Former name Motor Columbus Consulting Engineers.

# MAIN SALES OUTLETS OF OECD PUBLICATIONS – PRINCIPAUX POINTS DE VENTE DES PUBLICATIONS DE L'OCDE

**Argentina – Argentine**
Carlos Hirsch S.R.L.
Galería Güemes, Florida 165, 4° Piso
1333 Buenos Aires — Tel. (1) 331.1787 y 331.2391
Telefax: (1) 331.1787

**Australia – Australie**
D.A. Book (Aust.) Pty. Ltd.
648 Whitehorse Road, P.O.B 163
Mitcham, Victoria 3132 — Tel. (03) 873.4411
Telefax: (03) 873.5679

**Austria – Autriche**
OECD Publications and Information Centre
Schedestrasse 7
D-W 5300 Bonn 1 (Germany) — Tel. (49.228) 21.60.45
Telefax: (49.228) 26.11.04

Gerold & Co.
Graben 31
Wien I — Tel. (0222) 533.50.14

**Belgium – Belgique**
Jean De Lannoy
Avenue du Roi 202
B-1060 Bruxelles — Tel. (02) 538.51.69/538.08.41
Telefax: (02) 538.08.41

**Canada**
Renouf Publishing Company Ltd.
1294 Algoma Road
Ottawa, ON K1B 3W8 — Tel. (613) 741.4333
Telefax: (613) 741.5439

Stores:
61 Sparks Street
Ottawa, ON K1P 5R1 — Tel. (613) 238.8985
211 Yonge Street
Toronto, ON M5B 1M4 — Tel. (416) 363.3171

Federal Publications
165 University Avenue
Toronto, ON M5H 3B8 — Tel. (416) 581.1552
Telefax: (416)581.1743

Les Éditions La Liberté Inc.
3020 Chemin Sainte-Foy
Sainte-Foy, PQ G1X 3V6 — Tel. (418) 658.3763
Telefax: (418) 658.3763

**China – Chine**
China National Publications Import
Export Corporation (CNPIEC)
P.O. Box 88
Beijing — Tel. 44.0731
Telefax: 401.5661

**Denmark – Danemark**
Munksgaard Export and Subscription Service
35, Nørre Søgade, P.O. Box 2148
DK-1016 København K — Tel. (33) 12.85.70
Telefax: (33) 12.93.87

**Finland – Finlande**
Akateeminen Kirjakauppa
Keskuskatu 1, P.O. Box 128
00100 Helsinki — Tel. (358 0) 12141
Telefax: (358 0) 121.4441

**France**
OECD/OCDE
Mail Orders/Commandes par correspondance:
2, rue André-Pascal
75775 Paris Cédex 16 — Tel. (33-1) 45.24.82.00
Telefax: (33-1) 45.24.85.00
or (33-1) 45.24.81.76
Telex: 620 160 OCDE

Bookshop/Librairie:
33, rue Octave-Feuillet
75016 Paris — Tel. (33-1) 45.24.81.67
(33-1) 45.24.81.81

Librairie de l'Université
12a, rue Nazareth
13100 Aix-en-Provence — Tel. 42.26.18.08
Telefax: 42.26.63.26

**Germany – Allemagne**
OECD Publications and Information Centre
Schedestrasse 7
D-W 5300 Bonn 1 — Tel. (0228) 21.60.45
Telefax: (0228) 26.11.04

**Greece – Grèce**
Librairie Kauffmann
Mavrokordatou 9
106 78 Athens — Tel. 322.21.60
Telefax: 363.39.67

**Hong Kong**
Swindon Book Co. Ltd.
13 - 15 Lock Road
Kowloon, Hong Kong — Tel. 366.80.31
Telefax: 739.49.75

**Iceland – Islande**
Mál Mog Menning
Laugavegi 18, Pósthólf 392
121 Reykjavik — Tel. 162.35.23

**India – Inde**
Oxford Book and Stationery Co.
Scindia House
New Delhi 110001 — Tel.(11) 331.5896/5308
Telefax: (11) 332.5993

17 Park Street
Calcutta 700016 — Tel. 240832

**Indonesia – Indonésie**
Pdii-Lipi
P.O. Box 269/JKSMG/88
Jakarta 12790 — Tel. 583467
Telex: 62 875

**Ireland – Irlande**
TDC Publishers - Library Suppliers
12 North Frederick Street
Dublin 1 — Tel. 74.48.35/74.96.77
Telefax: 74.84.16

**Israel**
Electronic Publications only
Publications électroniques seulement
Sophist Systems Ltd.
71 Allenby Street
Tel-Aviv 65134 — Tel. 3-29.00.21
Telefax: 3-29.92.39

**Italy – Italie**
Libreria Commissionaria Sansoni
Via Duca di Calabria 1/1
50125 Firenze — Tel. (055) 64.54.15
Telefax: (055) 64.12.57

Via Bartolini 29
20155 Milano — Tel. (02) 36.50.83

Editrice e Libreria Herder
Piazza Montecitorio 120
00186 Roma — Tel. 679.46.28
Telex: NATEL I 621427

Libreria Hoepli
Via Hoepli 5
20121 Milano — Tel. (02) 86.54.46
Telefax: (02) 805.28.86

Libreria Scientifica
Dott. Lucio de Biasio 'Aeiou'
Via Meravigli 16
20123 Milano — Tel. (02) 805.68.98
Telefax: (02) 80.01.75

**Japan – Japon**
OECD Publications and Information Centre
Landic Akasaka Building
2-3-4 Akasaka, Minato-ku
Tokyo 107 — Tel. (81.3) 3586.2016
Telefax: (81.3) 3584.7929

**Korea – Corée**
Kyobo Book Centre Co. Ltd.
P.O. Box 1658, Kwang Hwa Moon
Seoul — Tel. 730.78.91
Telefax: 735.00.30

**Malaysia – Malaisie**
Co-operative Bookshop Ltd.
University of Malaya
P.O. Box 1127, Jalan Pantai Baru
59700 Kuala Lumpur
Malaysia — Tel. 756.5000/756.5425
Telefax: 757.3661

**Netherlands – Pays-Bas**
SDU Uitgeverij
Christoffel Plantijnstraat 2
Postbus 20014
2500 EA's-Gravenhage — Tel. (070 3) 78.99.11
Voor bestellingen: — Tel. (070 3) 78.98.80
Telefax: (070 3) 47.63.51

**New Zealand – Nouvelle-Zélande**
GP Publications Ltd.
Customer Services
33 The Esplanade - P.O. Box 38-900
Petone, Wellington — Tel. (04) 5685.555
Telefax: (04) 5685.333

**Norway – Norvège**
Narvesen Info Center - NIC
Bertrand Narvesens vei 2
P.O. Box 6125 Etterstad
0602 Oslo 6 — Tel. (02) 57.33.00
Telefax: (02) 68.19.01

**Pakistan**
Mirza Book Agency
65 Shahrah Quaid-E-Azam
Lahore 3 — Tel. 66.839
Telex: 44886 UBL PK. Attn: MIRZA BK

**Portugal**
Livraria Portugal
Rua do Carmo 70-74
Apart. 2681
1117 Lisboa Codex — Tel.: (01) 347.49.82/3/4/5
Telefax: (01) 347.02.64

**Singapore – Singapour**
Information Publications Pte. Ltd.
Pei-Fu Industrial Building
24 New Industrial Road No. 02-06
Singapore 1953 — Tel. 283.1786/283.1798
Telefax: 284.8875

**Spain – Espagne**
Mundi-Prensa Libros S.A.
Castelló 37, Apartado 1223
Madrid 28001 — Tel. (91) 431.33.99
Telefax: (91) 575.39.98

Libreria Internacional AEDOS
Consejo de Ciento 391
08009 - Barcelona — Tel. (93) 488.34.92
Telefax: (93) 487.76.59

Llibreria de la Generalitat
Palau Moja
Rambla dels Estudis, 118
08002 - Barcelona — Tel. (93) 318.80.12 (Subscripcions)
(93) 302.67.23 (Publicacions)
Telefax: (93) 412.18.54

**Sri Lanka**
Centre for Policy Research
c/o Colombo Agencies Ltd.
No. 300-304, Galle Road
Colombo 3 — Tel. (1) 574240, 573551-2
Telefax: (1) 575394, 510711

**Sweden – Suède**
Fritzes Fackboksföretaget
Box 16356
Regeringsgatan 12
103 27 Stockholm — Tel. (08) 23.89.00
Telefax: (08) 20.50.21

Subscription Agency/Abonnements:
Wennergren-Williams AB
Nordenflychtsvägen 74
Box 30004
104 25 Stockholm — Tel. (08) 13.67.00
Telefax: (08) 618.62.32

**Switzerland – Suisse**
OECD Publications and Information Centre
Schedestrasse 7
D-W 5300 Bonn 1 (Germany) — Tel. (49.228) 21.60.45
Telefax: (49.228) 26.11.04

Suisse romande
Maditec S.A.
Chemin des Palettes 4
1020 Renens/Lausanne — Tel. (021) 635.08.65
Telefax: (021) 635.07.80

Librairie Payot
6 rue Grenus
1211 Genève 11 — Tel. (022) 731.89.50
Telex: 28356

Subscription Agency – Service des Abonnements
Naville S.A.
7, rue Lévrier
1201 Genève — Tél.: (022) 732.24.00
Telefax: (022) 738.87.13

**Taiwan – Formose**
Good Faith Worldwide Int'l. Co. Ltd.
9th Floor, No. 118, Sec. 2
Chung Hsiao E. Road
Taipei — Tel. (02) 391.7396/391.7397
Telefax: (02) 394.9176

**Thailand – Thaïlande**
Suksit Siam Co. Ltd.
113, 115 Fuang Nakhon Rd.
Opp. Wat Rajbopith
Bangkok 10200 — Tel. (662) 251.1630
Telefax: (662) 236.7783

**Turkey – Turquie**
Kültur Yayinlari Is-Türk Ltd. Sti.
Atatürk Bulvari No. 191/Kat. 21
Kavaklidere/Ankara — Tel. 25.07.60
Dolmabahce Cad. No. 29
Besiktas/Istanbul — Tel. 160.71.88
Telex: 43482B

**United Kingdom – Royaume-Uni**
HMSO
Gen. enquiries — Tel. (071) 873 0011
Postal orders only:
P.O. Box 276, London SW8 5DT
Personal Callers HMSO Bookshop
49 High Holborn, London WC1V 6HB
Telefax: 071 873 2000
Branches at: Belfast, Birmingham, Bristol, Edinburgh, Manchester

**United States – États-Unis**
OECD Publications and Information Centre
2001 L Street N.W., Suite 700
Washington, D.C. 20036-4910 — Tel. (202) 785.6323
Telefax: (202) 785.0350

**Venezuela**
Libreria del Este
Avda F. Miranda 52, Aptdo. 60337
Edificio Galipán
Caracas 106 — Tel. 951.1705/951.2307/951.1297
Telegram: Libreste Caracas

**Yugoslavia – Yougoslavie**
Jugoslovenska Knjiga
Knez Mihajlova 2, P.O. Box 36
Beograd — Tel. (011) 621.992
Telefax: (011) 625.970

Orders and inquiries from countries where Distributors have not yet been appointed should be sent to: OECD Publications Service, 2 rue André-Pascal, 75775 Paris Cédex 16, France.

Les commandes provenant de pays où l'OCDE n'a pas encore désigné de distributeur devraient être adressées à : OCDE, Service des Publications, 2, rue André-Pascal, 75775 Paris Cédex 16, France.

OECD PUBLICATIONS, 2 rue André Pascal, 75775 PARIS CEDEX 16 - No. 76980 1992
PRINTED IN FRANCE

**HYDROCOIN Parties (in alphabetical order):**

**Atomic Energy of Canada Ltd. (Canada), British Geological Survey (UnitedKingdom), Commissariat à l'Energie Atomique / Institut de Protection et de Sûreté Nucléaire / Agence Nationale pour la Gestion des Déchets Radioactifs (France), Gesellschaft für Strahlen- und Umweltforschung (Federal Republic of Germany), Japan Atomic Energy Research Institute (Japan), Nationale Genossenschaft für die Lagerung Radioaktiver Abfälle (Switzerland), Organisation for Economic Co-operation and Development / Nuclear Energy Agency (observer), Rijksinstituut voor Volksgezondheid en Milieuhygiene (Netherlands), Swedish Nuclear Fuel and Waste Management Co. (Sweden), Swedish Nuclear Power Inspectorate (Sweden), Technical Research Centre of Finland (Finland), U.K. Atomic Energy Authority / Atomic Energy Research Establishment (United Kingdom), U.S. Department of Energy (USA), U.S. Nuclear Regulatory Commission (USA).**

**Project secretariat: Swedish Nuclear Power Inspectorate, Kemakta Consultants Co., U.K. Atomic Energy Authority / Atomic Energy Research Establishment, Organisation for Economic Co-operation and Development / Nuclear Energy Agency, Nordic Liaison Committee for Atomic Energy.**